



HAL
open science

Synthesis and investigation of new metallasesquioxanes based on transition metal ions and lanthanides : magnetic, optical properties and catalysis

Alena Kulakova

► **To cite this version:**

Alena Kulakova. Synthesis and investigation of new metallasesquioxanes based on transition metal ions and lanthanides : magnetic, optical properties and catalysis. Material chemistry. Université Montpellier; Rossijskij universitet družby narodov (Moskva), 2020. English. NNT : 2020MONTTS115 . tel-03349146

HAL Id: tel-03349146

<https://theses.hal.science/tel-03349146v1>

Submitted on 20 Sep 2021

HAL is a multi-disciplinary open access archive for the deposit and dissemination of scientific research documents, whether they are published or not. The documents may come from teaching and research institutions in France or abroad, or from public or private research centers.

L'archive ouverte pluridisciplinaire **HAL**, est destinée au dépôt et à la diffusion de documents scientifiques de niveau recherche, publiés ou non, émanant des établissements d'enseignement et de recherche français ou étrangers, des laboratoires publics ou privés.

THÈSE POUR OBTENIR LE GRADE DE DOCTEUR DE L'UNIVERSITÉ DE MONTPELLIER

École doctorale SCIENCES CHIMIQUES BALARD № 459

Unité de recherche: Institut Charles Gerhardt Montpellier

En partenariat international avec RUDN University, Moscow, Russia

**Synthesis and investigation of new metallasesquioxanes
based on transition metal ions and lanthanides: magnetic,
optical properties and catalysis**

Présentée par Alena KULAKOVA

Le 23/12/2020

**Sous la direction de Pr. Joulia Larionova
et Pr. Victor Khrustalev**

Devant le jury composé de

Pr. Dominique Luneau, Université Claude Bernard Lyon 1, Lyon, France	Rapporteur
Dr. Dmitry A. Valyaev, Laboratoire de Chimie de coordination, Toulouse, France	Rapporteur
Pr. Alexander A. Kirillov, University of Lisbon, Portugal	Examineur
Dr. Dmitry S. Perekalin, INEOS RAS, Moscou, Russia	Président du jury
Dr. Yannick Guari, Université de Montpellier, Montpellier, France	Examineur
Pr. Joulia Larionova, Université de Montpellier, Montpellier, France	Directeur de these
Pr. Victor N. Khrustalev, RUDN University, Moscou, Russia	Directeur de these
Dr. Alexey N. Bilyachenko, RUDN University, Moscou, Russia	Co-encadrant



**UNIVERSITÉ
DE MONTPELLIER**

ACKNOWLEDGMENTS

First and foremost, I want to thank my co-supervisors Pr. Joulia Larionova and Pr. Victor N. Khrustalev. I really appreciate all the hard work you've done to help me and thank you for your guidance and wisdom. I am so thankful to Dr. Alexey N. Bilyachenko for his useful ideas and great contribution to this work. I would like to thank Prof. Elena S. Shubina, Dr. Mikhail M. Levitsky and Dr. Yannick Guari for their advices and scientific discussions. I gratefully acknowledge Dr. Alexander A. Korlyukov and Dr. Anna V. Vologzhanina for their patience with crystals.

I am very thankful to the Institute of Charles Gerhardt Montpellier and people from The Molecular Engineering and Nano-Objects (IMNO) team and I am happy I was a part of this team.

I would also thank the staff and professors of the Department of Inorganic Chemistry from RUDN University (Peoples' Friendship University of Russia) for being patient and helping me improve my skills. I am also very grateful to the collective from the Laboratory of metal hydrides INEOS RAS for their friendship and understanding.

Thanks a lot to Lidia S. Shulpina (INEOS RAS), Georgiy B. Shulpin (Doctor of Chemical Sciences, ICP RAS), Yuriy N. Kozlov (Candidate of Chemical Sciences, ICP RAS), Pavel V. Dorovatovsky (Deputy Head of the Department of Synchrotron Experimental Stations KKSNI, Kurchatov Institute), Yan V. Zubavichus (Doctor of Physical and Mathematical Sciences, Institute of Catalysis SB RAS) and Prof. F. Lamaty (Montpellier University) and his scientific group for kind cooperation. I value your contribution to our successful collaboration.

I gratefully acknowledge the funding sources that made my PhD work possible. I was funded by Ministry of Science and Higher Education of the Russian Federation (project No. 075-03-2020-223 (FSSF-2020-0017)), RFBR (projects 16-03-00206, 16-03-00609, 16-29-05180-ofi_m, 16-53-150008, 17-03-00993, 19-03-00488, 19-53-15008, 20-03-00542), Russian Science Foundation (grant 17-73-30036). Lastly, I would like to thank the Embassy of France for a PhD grant (The Vernadski program aimed at supporting mobility for PhD students studying in a cooperative Franco-Russian graduate school).

I express my sincerest gratitude for the opportunities all of everybody provided. Many thanks for everything you have done for me.

RESUME EN FRANÇAIS

La conception et l'étude de composés moléculaires présentant diverses topologies structurales capables de présenter des propriétés physiques et chimiques intéressantes, telles que des propriétés catalytiques, magnétiques et optiques, constituent un des grands domaines en très fort développement de la science moderne. En particulier, les metasil- ou germesquioxanes contenant des ions de métaux de transition ou des lanthanides constituent une famille de composés moléculaires fascinante due à la diversité de leur organisation structurale et de leurs propriétés physiques. Le but de ce travail a été la synthèse de plusieurs familles de sil- and germesquioxanes contenant des métaux de transition ou des lanthanides et l'étude de leurs propriétés catalytique, magnétiques et optiques (luminescence).

Une approche basée sur une réaction d'auto-assemblage a été améliorée pour la synthèse de silsesquioxanes à base de Cu(II). Ainsi, 51 metasilsesquioxanes contenant de 2 à 11 ions de Cu(II) ont été synthétisés, caractérisés et étudiés. L'impact de divers paramètres, tels que la présence d'un substituant organique sur l'atome de silicium, la nature du solvant, l'utilisation de ligands additionnels, l'utilisation des ligands pontants sur l'organisation structurale a été démontré. L'approche employée pour la synthèse de metallasilsesquioxanes a été transposée aux germesquioxanes contenant des ions de Cu(II) avec la synthèse de cinq nouveaux composés polynucléaires. Les propriétés catalytiques et magnétiques de sil- et germesquioxanes de Cu(II) ont été étudiées.

La synthèse de sil- et germesquioxanes de Ni(II) a été réalisée et deux complexes Ni_4Na_2 -phenylgermesquioxane et Ni_4 -pyridine-carbonate ont été obtenus et étudiés. L'étude des propriétés magnétiques de ces composés montre la présence d'une relaxation lente de l'aimantation due au comportement de verre de spin.

Finalement, quatre nouveaux metallasilsesquioxanes tetranucléaires contenant Eu^{3+} et Tb^{3+} ont été synthétisés, caractérisés et leurs propriétés magnétiques et optiques (luminescence) ont été étudiées. Ces composés présentent une topologie de cage inhabituelle en forme de prisme. L'étude de leur propriété magnétique a révélé que le composé à base de Tb^{3+} présente une transition de spin-flip induite par le champ magnétique de l'état canté vers le régime paramagnétique. De façon remarquable, ces composés montrent une luminescence caractéristique de Eu^{3+} ou Tb^{3+} à basse température (77 K) ou à la température ambiante à l'état solide et peuvent être considérés comme les premiers lanthanide-silsesquioxanes luminescents.

Mots clés : metallasilsesquioxanes, metallagermesquioxanes, composés de coordination, catalyse, propriétés magnétiques, luminescence

SUMMARY IN ENGLISH

The design and study of molecular compounds exhibiting various structural topologies capable of exhibiting interesting physical and chemical properties, such as catalytic, magnetic, and optical ones, constitute one of the major fields in strong development. In particular, the metasil- or germesquioxanes containing transition metal ions or lanthanides represent a fascinating family of molecular compounds due to the diversity of their structural organization and their physical properties. The aim of this work was therefore the synthesis of several families of sil- and germesquioxanes containing transition metal ions or lanthanides and the study of their catalytic, magnetic, and optical (luminescence) properties.

A self-assembly reaction based approach has been improved for the synthesis of Cu(II)-containing silsesquioxanes. Thus, 51 metasilsesquioxanes containing from 2 to 11 Cu (II) ions have been synthesized, characterized, and investigated. The impact of various parameters, such as the presence of organic substituents on the silicon atom, the nature of the solvent, the use of additional ligands, the use of bridging ligands on the structural organization has been demonstrated. The approach used for the synthesis of metallasilsesquioxanes has also been transposed to germesquioxanes containing Cu (II) ions with the synthesis of five new polynuclear compounds. The catalytic and magnetic properties of Cu (II) sil- and germesquioxanes have been investigated.

The synthesis of sil- and germesquioxanes of Ni (II) was carried out and two complexes Ni₄Na₂-phenylgermesquioxane and Ni₄-pyridine-carbonate were obtained and studied. The study of the magnetic properties of these compounds shows the presence of slow relaxation of the magnetization due to the spin glass behavior.

Finally, four new tetranuclear metallasilsesquioxanes containing Eu³⁺ and Tb³⁺ were synthesized, characterized and their magnetic and optical properties (luminescence) were studied. These compounds exhibit an unusual prism-shaped cage topology. The study of their magnetic property revealed that the Tb³⁺-based compound exhibits a spin-flip transition induced by the magnetic field from the canted state to the paramagnetic regime. Remarkably, these compounds show a characteristic luminescence of Eu³⁺ or Tb³⁺ at low temperature (77 K) or at room temperature in the solid-state and can be considered as the first luminescent lanthanide-silsesquioxanes.

Key words: metallasilsesquioxanes, metallagermesquioxanes, coordination compounds, catalysis, magnetic properties, luminescence

ABBREVIATIONS

AC – alternating current;
bipy – 2,2'-bipyridine;
cy – cyclohexane;
3,5-Me₂Pz – dimethylpyrazole;
dppe – 1,2-bis(diphenylphosphino)ethane;
dppm – 1,2-bis(diphenylphosphino)methane;
FC – field-cooled;
HMPA – hexamethylphosphoric triamide;
HPLC – high performance liquid chromatography;
IBX – 2-iodoxybenzoic acid;
MTO – methyltrioxorhenium;
MS – metallaselquioxane;
NMR – nuclear magnetic resonance;
Phen – 1,10-phenanthroline;
POSS – polyhedral oligomeric silsesquioxane;
SMM – single molecule magnets;
SQUID – superconducting quantum interference device;
TBHP – *tert*-butyl hydroperoxide;
TON – turnover number;
TOF – turnover frequency;
TFA – trifluoroacetic acid;
ZFC – zerofield cooled;
FC – field-cooled.

SUMMARY

GENERAL INTRODUCTION	8
PART I. LITERATURE REVIEW	13
Catalytic properties of metallasesquioxanes	13
Oxidative amidation	13
Oxidative C-H activation	25
Magnetic properties of metallasesquioxanes	33
Magnetic properties of Cu(II)-containing sesquioxanes	35
Magnetic properties of Co(II)-containing sesquioxanes	45
Magnetic properties of Ni(II)-containing sesquioxanes	52
Synthesis, structures and properties of Ln(III)-containing sesquioxanes	60
PART II. RESULTS AND DISCUSSION	68
CHARTER 1. Cu(II)-silsesquioxanes: synthesis, structure and catalytic properties	68
1.1. Compounds based on structural fragment MeSiO _{1.5} .	68
1.1.1. Study of self-assembly reaction in solvating ligands (dimethyl sulfoxide and dimethylformamide)	68
1.1.2. Study of self-assembly reactions in the presence of chelating N,N-ligands (1,10-phenanthroline and 2,2'-bipyridine)	72
1.2. Synthesis of Cu(II) - silsesquioxanes containing the structural fragment PhSiO _{1.5}	76
1.2.1 Investigation of self-assembly reactions in different solvents	76
1.2.2 Investigation of self-assembly reactions in the presence of chelating N,N-ligands (1,10-phenanthroline, 2,2'-bipyridine, batophenanthroline)	79
1.2.3 Study of self-assembly reactions in the presence of chelating P,P-ligands (1,2-bis(diphenylphosphino)ethane, 1,2-bis(diphenylphosphino)methane)	85
1.2.4 Features of the synthesis and structure of Cu(II)-containing germesquioxanes	87
1.3 Investigation of catalytic properties of Cu(II)-sesquioxanes	94
1.3.1. Oxidative amidation	94
1.3.2 Oxidative C-H activation	97

CHARTER 2. Cu(II)-based silsesquioxanes: synthesis, structure and magnetic properties	104
2.1 Copperphenylsilsesquioxanes with a globular cage structure	104
2.2. Copperphenylsilsesquioxane with a "Cooling Tower" framework structure	108
2.3 Copperphenylsilsesquioxanes with a prismatic framework structure	108
2.4 Investigation of magnetic properties	109
CHARTER 3. Ni(II)-based silsesquioxanes: synthesis, structure and magnetic properties	112
3.1 Ni(II)-containing silsesquioxanes	112
3.2 Ni(II)-containing germesquioxanes	117
CHARTER 4. Tetranuclear Tb(III) and Eu(III)-containing silsesquioxanes: synthesis, structure and investigation of magnetic and luminescent properties	121
CONCLUSION	130
EXPERIMENTAL SECTION	133
Materials	133
Research methods and equipment	133
Synthesis	136
ANNEXES	148
REFERENCES	161

GENERAL INTRODUCTION

One of the most popular areas of modern chemical science is the study of molecular and supramolecular polynuclear architectures with various topologies capable of manifesting practically valuable properties including catalytic, magnetic, and optical ones. In recent years, significant progress has been made in the chemistry of multinuclear metal complexes due to the development of various types of building blocks or ligands capable of coordinating metal or lanthanide ions of various nature. Sil- and germsesquioxanes of the general formula $(\text{REO}_{1.5})_n$ ($E = \text{Si}, \text{Ge}$) represent one of these interesting families of universal ligands. The important feature of these compounds is the controlled formation of polyhedral (frame) isolated architectures of various structural organization and topology, which can contain controlled different number of 3d metal or lanthanide ions, which in some cases, may even be a combination of those. Firstly, regarding the properties of these architectures, there are prospects for the design of potential metal catalysts for demanded organic synthesis processes. Recently, it was shown that sesquioxane based frameworks containing transition metal ions (for instance Cu(II) or Fe(III)) exhibit high catalytic activity in the amidation reaction. The development of this direction is relevant due to the facts that: (i) amides are structural components of at least 25% of existing drugs, and (ii) previously proposed methods for obtaining an amide fragment were associated with the use of toxic reagents or catalysts based on expensive metals. In turn, it was noted that sesquioxane based frameworks containing Cu(II), Fe(III), Co(II), and Ni(II) ions are highly effective in homogeneous catalysis for oxidative functionalization of hydrocarbons. The development of this area is relevant for the creation of convenient methods for processing oil and gas hydrocarbons into chemical products with added value, including the processes of functionalization of low-activity alkanes. Note also that in previous studies, for both of the above-mentioned catalytic processes, the possibility of using MS catalysts containing simultaneously various transition metals ions, as well as metal complexes containing additional (to sesquioxane) organic ligands, has not been discussed.

Secondly, in the case of sesquioxanes containing metal ions with high magnetic anisotropy (Co(II), Ni(II), Fe(III), and others), the manifestation of effects of slow relaxation of the magnetization (behavior of a spin glass) has been observed. The development of this direction is relevant for potential applications in high-capacity information storage devices. In this line of thought, several examples of polynuclear isolated architectures containing Co(II) and Ni(II) mainly issue from the collaboration between the University of Montpellier and RUDN University have been published in the literature before that this work started. On the other hand, scientific literature completely lacked data on the properties of germsesquioxanes exhibiting similar properties.

Thirdly, the complexes containing lanthanide ions, assembled using siloxane ligands, are a promising area considering their exceptional magnetic and optical. The specific arrangement of

lanthanide spin carriers and the possibility of various exchange interactions in such compounds may allow achieving high spin values associated with a huge magnetic anisotropy leading to exceptional magnetic properties, as it has been demonstrated in the case of lanthanide ions based molecular magnets called Single Molecule Magnets (SMMs). However, surprisingly, there are no examples in the literature of a comprehensive study of the magnetic properties of sesquioxanes containing lanthanide ions. The exceptional emission properties of lanthanide ions are widely used in optical devices and molecular thermometry. However, only two works mentioned the investigations of optical properties of Eu(III)-based sesquioxanes, and even in these examples the crystal structures of these letters have not been reported.

Therefore, there is a lack of a regarding catalytic, magnetic, and optical properties of transition metal or lanthanide-based siloxane architectures and their relationship with the crystal structures. *The aim of this thesis work is to develop approaches to the synthesis of polynuclear metallasesquioxane complexes containing transition metal ions or lanthanides and study the structural aspects of these new obtained compounds, as well as their catalytic, magnetic, and optical properties.*

This manuscript is divided into two Parts. The first Part is devoted to the analysis of previously published in the literature works related to the topic of the dissertation. It consists of two sections, the first one deals with the catalytic properties of Cu(II)- and Fe(III)/(II)-containing silsesquioxanes, the second one describes the state-of-the-art on magnetic and optical properties of Cu(II)-, Co(II)-, Ni(II)-, and Ln(III)-containing silsesquioxanes. As a logic end of this state-of-the-art, the aim and the objectives of the dissertation work are formulated.

The Part II Results and Discussion is devoted to the presentation of the synthesis, structures, and investigations of the catalytic, magnetic, and optical properties of metallasilsesquioxanes and metallagermsesquioxanes. It includes four Chapters. Chapter 1 focuses on the synthesis of Cu(II)-containing silsesquioxanes (**1 – 36**) and germesquioxanes (**38 – 42**). Firstly, an effect of steric factors controlled by organic substituents at the silicon atoms on the complexes' topology was studied. It was obtained and characterized six complexes with Me- substituents at the silicon atom: [(MeSiO_{1.5})₁₈(CuO)₉] • DMSO **1**, [(MeSiO_{1.5})₁₂(CuO)₆] • 6DMF **2**, [(MeSiO_{1.5})₂₀(HO_{0.5})_{3.33}(CuO)₁₂(1,10-phen)₄(AcO_{0.5})_{0.67}] • 4DMSO • 4H₂O **3**, [(MeSiO_{1.5})₁₀(CuO)₆(MeO_{0.5})₂(1,10-phen)₂] • 0.5(1,4-diox) • 2.5MeOH **4**, [(MeSiO_{1.5})₁₀(CuO)₆(MeO_{0.5})₂(2,2'-bipy)₂] • 2MeOH **5**, and [(MeSiO_{1.5})₈(CuO)₃(2,2'-bipy)₂] • 3EtOH **6**. In this line of thought, the effect of solvents on the framework nuclearity with Ph- substituents at the silicon atom were investigated: [(PhSiO_{1.5})₁₂(CuO)₆] • EtOH • DMF **7**, [(PhSiO_{1.5})₁₂(CuO)₆] • DMF • THF **8**, [(PhSiO_{1.5})₁₂(CuO)₆] • DMSO **9**, [(PhSiO_{1.5})₁₂(CuO)₆] • MeCN **10**, [(PhSiO_{1.5})₁₂(CuO)₆] • PhCN • THF **11**, [(PhSiO_{1.5})₁₂(CuO)₆] • THF **12**, [(PhSiO_{1.5})₁₀(CuO)₅] • 5Py **13**, [(PhSiO_{1.5})₁₀(CuO)₅(DMF)₄] • H₂O **14**, [(PhSiO_{1.5})₁₂(CuO)₆] • DMF **15** and {[(PhSiO_{1.5})₁₀(CoO)₅(H₂O)₂]₂[(PhSiO_{1.5})₁₀(CuO)₅]} **16**. At the next stage, the effect of bidentate N-containing ligands on the formation of a supramolecular packing were studied, namely:

1) 2,2'-bipyridine [(PhSiO_{1.5})₁₀(CuO)₆(HO_{0.5})₂(2,2'-bipy)₂] • 2.5 DMSO **17**, [(PhSiO_{1.5})₁₀(CuO)₆(HO_{0.5})₂(2,2'-bipy)₂] • 2.5 MeCN • 2 H₂O **18**, [(PhSiO_{1.5})₁₀(CuO)₆(HO_{0.5})₂(2,2'-bipy)₂] • 4 MeCN **19**, [(PhSiO_{1.5})₁₀(CuO)₆(HO_{0.5})₂(2,2'-bipy)₂] • 3.5 PhCN • 0.5 H₂O **20**, [(PhSiO_{1.5})₁₀(CuO)₆(HO_{0.5})₂(2,2'-bipy)₂] • 3 PhCN **21**, [(PhSiO_{1.5})₁₀(CuO)₆(HO_{0.5})₂(2,2'-bipy)₂] • 1.5 THF **22** (48%), [(PhSiO_{1.5})₁₀(CuO)₆(HO_{0.5})₂(2,2'-bipy)₃] **23**, [(PhSiO_{1.5})₁₀(CuO)₆(MeO_{0.5})₂(2,2'-bipy)₂] **24**, [(PhSiO_{1.5})₁₀(CuO)₆(AcO_{0.5})₂(2,2'-bipy)₂] • MeCN **25**;

2) 1,10-phenanthroline [(PhSiO_{1.5})₁₀(CuO)₆(HO_{0.5})₂(1,10-phen)₂] • 4DMSO **26**, [(PhSiO_{1.5})₁₀(CuO)₆(HO_{0.5})₂(1,10-phen)₂] • 4.75DMSO **27**, [(PhSiO_{1.5})₁₀(CuO)₆(HO_{0.5})₂(1,10-phen)₂] • 4DMF **28**, [(PhSiO_{1.5})₁₀(CuO)₆(HO_{0.5})₂(1,10-phen)₂] • 4Py **29**;

3) 4,7-diphenyl-1,10-phenanthroline (bathophenanthroline) [(PhSiO_{1.5})₁₀(CuO)₆(HO_{0.5})₂(Bphen)₂] • MeCN **30**, [(PhSiO_{1.5})₁₀(CuO)₆(HO_{0.5})₂(Bphen)₂] • DMSO **31**, [(PhSiO_{1.5})₁₀(CuO)₆(HO_{0.5})₂(Bphen)₂] • Tol **32**.

Moreover the influence of bidentate P,P-ligands (1,2-bis(diphenylphosphino)ethane and 1,2-bis(diphenylphosphino)methane) on the architecture of Cu(II)-silsesquioxanes were investigated and three $[(\text{PhSiO}_{1.5})_{12}(\text{PhSiO}_{1.5})_8(\text{CuO})_8(\text{NaO}_{0.5})_4\{\text{Cu}(\text{O}_{0.5})_4\}] \cdot 2[\text{Cu}(\text{dppe})_2]$ **34**, $[(\text{PhSiO}_{1.5})_{12}(\text{CuO})_4(\text{NaO}_{0.5})_2] \cdot 2[\text{Cu}(\text{dppe})_2]$ **35** and $[(\text{PhSiO}_{1.5})_{12}(\text{CuO})_4(\text{NaO}_{0.5})_4(\text{dppmO}_2)_2]$ **36** was prepared.

Finally, using the previous published approach of original metallogermesquioxanes complexes' synthesis has been expanded the line of Cu(II)-germesquioxanes: $(\text{PhGeO})_{12}(\text{PhGe}_2\text{O})[\text{Fe}_5\text{O}_{17}(\text{OH})]\text{Cu}_2(2,2'\text{-bipy})_2$ **38**, $[\text{Na}_4\text{Cu}_{42}(\text{Ph}_2\text{Ge}_2\text{O}_5)_{12}(\text{OH})_{40}]$ **39**, $[(\text{PhGeO}_{1.5})_{10}(\text{CuO})_6(\text{HO}_{0.5})_2(1,10\text{-phen})_2] \cdot 2\text{H}_2\text{O}$ **40**, $[(\text{PhGeO}_{1.5})_{10}(\text{CuO})_6(\text{HO}_{0.5})_2(2,2'\text{-bipy})_2] \cdot 5\text{EtOH}$ **41** and $(\text{PhGeO}_2)_{10}\text{Cu}_6(2,2'\text{-bipy})_2(3,5\text{-Me}_2\text{Pz})_2$ **42**.

The catalytic tests of some Cu(II)-silsesquioxanes and germesquioxanes in the reactions of C-H functionalization (**1**, **13**, **16** – **17**, **22**, **33** – **36**, **38** – **39**, **41**) and oxidative amidation (**17**, **26**, **33** – **35**, **38** – **39**, **41**) are also described here. The mechanism of the reaction of oxidation of saturated hydrocarbons with peroxides in the presence of a catalyst is proposed on the basis of the studied selectivity parameters.

Chapter 2 is devoted to the preparation of new Cu(II)-containing silsesquioxanes and investigation of the influence of the bridging ligands (1,4-dioxane, acetonitrile) or alkali metal ions with a large ionic radius (K^+ , Cs^+) on the structural topology. The nine complexes were obtained: $[(\text{PhSiO}_{1.5})_{12}(\text{CuO})_4(\text{NaO}_{0.5})_4(\text{DMSO})_8]$ **44**, $[(\text{PhSiO}_{1.5})_{12}(\text{CuO})_4(\text{NaO}_{0.5})_4(\text{MeCN})_6(\text{H}_2\text{O})_2] \cdot 2\text{MeCN}$ **45**, (45%), $[(\text{PhSiO}_{1.5})_{12}(\text{CuO})_4(\text{NaO}_{0.5})_4(1,4\text{-diox})(\text{EtOH})_4] \cdot 0.5\text{EtOH}$ **46**, $[(\text{PhSiO}_{1.5})_{12}(\text{CuO})_4(\text{NaO}_{0.5})_4(1,4\text{-diox})_4(\text{H}_2\text{O})_3] \cdot 2\text{PhCN} \cdot 21,4\text{-diox} \cdot \text{H}_2\text{O}$ **47**, $[(\text{PhSiO}_{1.5})_{12}(\text{CuO})_4(\text{NaO}_{0.5})_2(\text{KO}_{0.5})_2(\text{DMF})_6]$ **48**, $[(\text{PhSiO}_{1.5})_{12}(\text{CuO})_4(\text{NaO}_{0.5})_3(\text{CsO}_{0.5})(\text{DMF})_4]$ **49**, $[(\text{PhSiO}_{1.5})_{12}(\text{CuO})_4(\text{NaO}_{0.5})(\text{CsO}_{0.5})_3(\text{DMF})_4(\text{DMSO} \cdot \text{H}_2\text{O})] \cdot 1.5\text{DMF}$ **50**, $[(\text{PhSiO}_{1.5})_{10}(\text{CuO})_2(\text{NaO}_{0.5})_2(\text{H}_2\text{O})_6]$ **51** and $(\text{PhSiO}_{1.5})_{12}(\text{CuO})_4(\text{NaO}_{0.5})_2(\text{CsO}_{0.5})_2(\text{DMF})_8] \cdot 0.5\text{H}_2\text{O}$ **52**. The magnetic properties of some selected compounds (**47**, **50**, **51**, **52**) have been studied. It was demonstrated the correlation of the exchange interaction strength for Cu(II)-containing compounds from the value of the Cu-O-Cu angle.

Chapter 3 focuses on the preparation of new Ni(II)-containing silsesquioxane $[\text{Ni}_4(\text{CO}_3)_4(\text{Py})_8\text{Na}] \cdot \text{Cl} \cdot \text{Py} \cdot \text{H}_2\text{O}$ **53** and germesquioxane $[(\text{PhGeO}_{1.5})_{10}(\text{NiO})_4(\text{NaO}_{0.5})_2] \cdot 9\text{EtOH} \cdot 4\text{H}_2\text{O}$ **54** and investigation of their magnetic properties. It was shown that a complex relaxation dynamic in **53** indicates the presence of the spin-glass behaviour, and the slow relaxation indicates **54** exhibits spin-glass properties.

Chapter 4 focuses on the preparation of Ln(III)-containing silsesquioxanes and investigation of their magnetic and luminescence properties. By using Tb(III) and Eu(III) ions in association with siloxane ligands four new complexes of a general formula

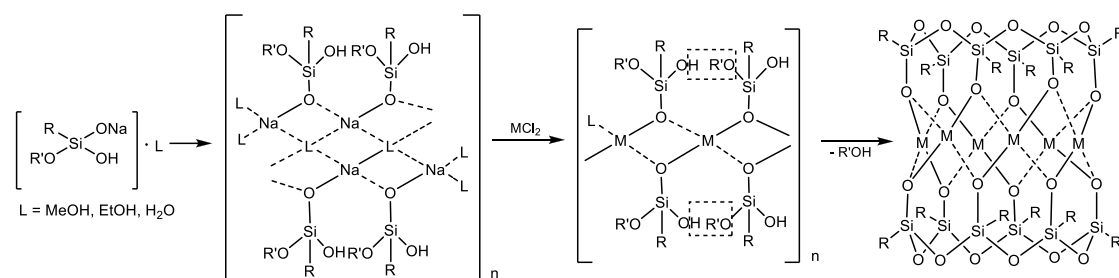
$(A)_2[(PhSiO_{1.5})_8(LnO_{1.5})_4(O)(NO_{2.5})_6(EtOH)_2(MeCN)_2]$ (where $A = Et_4N^+$ and Ph_4P^+) have been synthesized. They present similar crystal structure consisting of a tetranuclear lanthanide-based core surrounded/enwrapped by siloxane ligands. These compounds present characteristic Tb^{3+} and Eu^{3+} photoluminescence when excited in lanthanide-related bands and paramagnetic properties with a spin flip transition for the Tb^{3+} analogue.

The Experimental part describes the synthesis, physical methods for determining the composition and structure of the obtained compounds, as well as approaches for investigation of catalytic, magnetic, and photophysical properties obtained compounds.

Finally, the conclusions and outlooks about transition metal or lanthanide-based siloxanes and germanoxanes investigated in this work are given.

LITERATURE REVIEW

Metallasesquioxanes (MSs) are compounds that consist of metal oxide clusters containing transition metal or lanthanide ions embedded in an organosilicon or organogermanium matrix. The variety of their structures can be controlled using coordination chemistry methods by changing various parameters, including the nature of building blocks and metal ions, as well as organic ligands (Scheme 1) [1]. The peculiarity of sesquioxane ligands (the term sesquioxane indicates the index 1.5 of the oxygen atom in the $\text{RSiO}_{1.5}$ or $\text{RGeO}_{1.5}$) is the combination of organic and inorganic fragments. They can form cyclic, acyclic or polycyclic types of ligands that are capable to coordinate metal ions *via* oxygen atoms.



Scheme 1. General scheme for the synthesis of metallasesquioxanes (shown for the silicon-based complexes).

Various exchange interactions induced by specific arrangement of metal centers are possible in these cage-like structures. Beside interesting structural organization, metallasesquioxanes also present useful physical properties, such as magnetic and catalytic. The magnetic properties of cage-like Si-based MS are considered in the review [2]. Their catalytic potential is also quite significant, which is explainable by the possibility of introducing various metal ions into the framework structures, the diversity of the shape of crystalline structures, their dimensionality, and porosity. The catalytic properties of Si-based MS are described in detail in reviews [3, a-c].

This first Part of the manuscript presents a general state-of-the art on transition metal (Cu(II)-, Ni(II)-, Co(II)-) or lanthanide (Ln(III)) containing sesquioxane complexes, the strategies of their synthesis, their crystal structures and investigation of their catalytic, magnetic, and luminescent properties in order to give a general picture on the subject before description of the thesis's results.

Catalytic properties of metallasesquioxanes

Oxidative amidation

In organic chemistry, amides, also known as carboxamides, are derivatives of oxygen-containing acids where the hydroxyl group is substituted by an amino group with the general formula $\text{RC(O)NR}'\text{R}''$, where R, R'' are an organic groups or hydrogen atoms [4]. Amides are qualified as

primary, secondary, and tertiary according to whether the amine subgroup has the form $-NH_2$, $-NHR$, or $-NRR'$, where R and R' are groups other than hydrogen [5].

Amide fragments could be found in the composition of many important compounds, for example, proteins [6], pharmaceuticals such as palasimide (palasonin-N-phenylimide) [7, a-b], salfredin [8], thalidomide [9, a-c], julocrotine [10], lamprolobin [11], migrastatin [12] and phensuximide [13, a-b] (Fig. 1). In industry, amides are used as: (i) plasticizers for paper and artificial skin fabrication, (ii) starting reagents in production of polymers (for example, synthesis of nylons from caprolactam [14]), (iii) intermediates for dyes or sulfamide medicals preparation, (iv) for the disposal of radioactive metals [15].

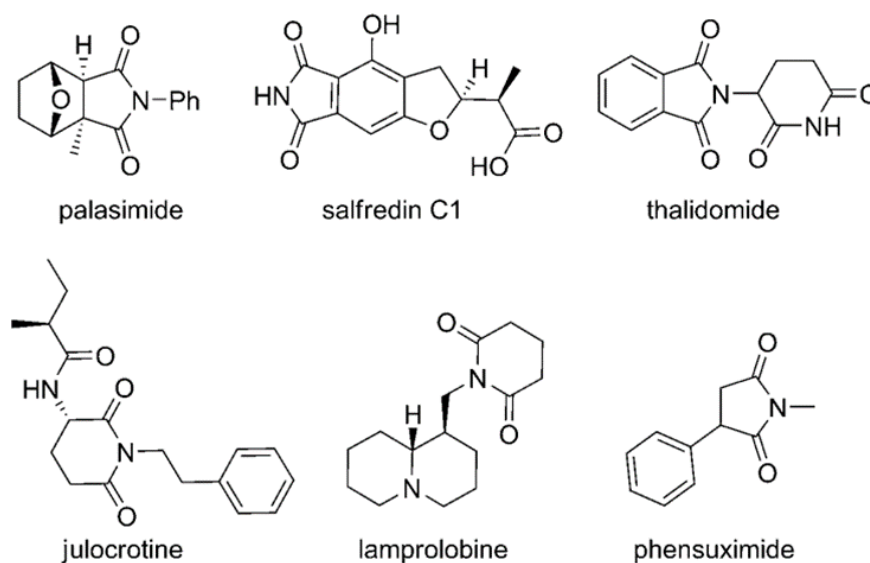


Figure 1. Examples of amides used in the pharmaceutical industry.

Amide production has been well studied. The basic methods of their synthesis are:

- The interaction between carboxylic acids and ammonia or primary and secondary amines is heated (Fig. 2) [16] (industrial production of succinimide and phthalimide) [17];

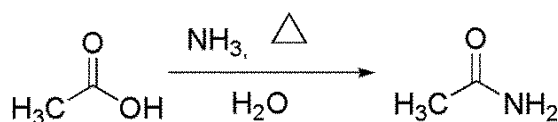


Figure 2. Scheme of the acetamide synthesis.

- Acylation reaction is the interaction of ammonia, primary and secondary amines with acid chlorides or anhydrides of carboxylic acids, ketones, esters [18]. The special cases are: (i) Schotten-Bauman reaction (the preparation of amides by the action of acid chlorides on amines in the presence of a base, Fig. 3) [19], (ii) Schmidt reaction (conversion of ketones to amides by reaction with NH_3), [20] and (iii) Haller-Bauer reaction (production of amides by cleavage of non-enolizable ketones under the action of the base) [21];

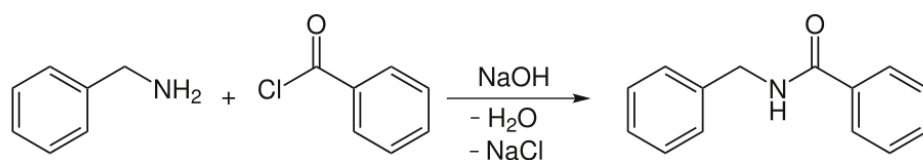


Figure 3. Scheme of the Schotten-Bauman reaction.

- Hydrolysis of nitriles (in an acidic or alkaline media) [22]. Sulfuric, hydrochloric, phosphoric acids and boron trifluoride are used as acid catalysts; hydrogen peroxide is used to provide an alkaline environment [23]. The Ritter reaction is the synthesis of N-substituted carboxylic acid amides by alkylation of nitriles with carbocations (Fig. 4) [24];

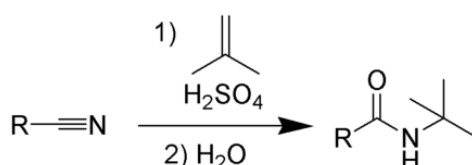


Figure 4. Scheme of the Ritter reaction.

- The rearrangements. The Beckman rearrangement is the conversion of oximes to amides by the action of Lewis acids [25]. This rearrangement is used in the industry to produce caprolactam [26]. Rearrangement proceeds in the presence of acid dehydrating agents: oleum, H₂SO₄, PCl₅. Chapman reaction is the rearrangement of O-arylamino esters to N, N-diarylamides of aromatic acids [27] (an important method for the synthesis of substituted diphenylamines and N-containing heterocycles). The Polonovsky rearrangement is a transformation of N-oxides of tertiary amines under the action of acetic anhydride [28].

Most of the methods described above use toxic (sometimes - commercially non-available) reagents and solvents. To circumvent these limitations, a direct method of direct reaction of alcohols and amines in the presence of metal-containing catalysts has been recently developed [29, a-d]. The general mechanism (Fig. 5) of the reaction is based on: (i) the oxidation of alcohol to the corresponding aldehyde, (ii) aldehyde interaction with amine, and (iii) formation of amide due to oxidation [30]. It is important to note that the aldehyde can be oxidized to undesirable by-product, carboxylic acid.

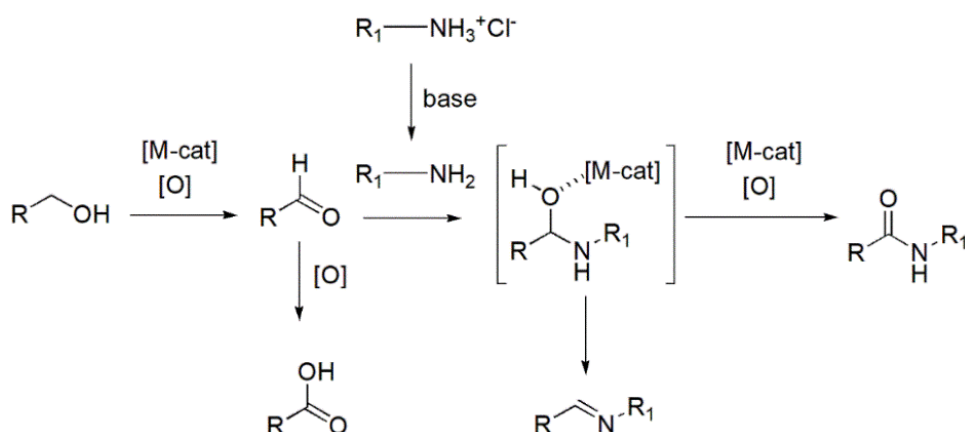
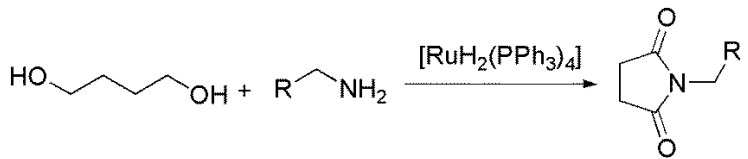
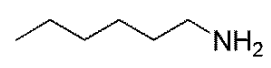
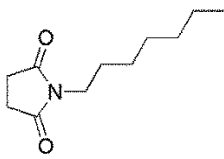
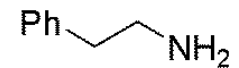
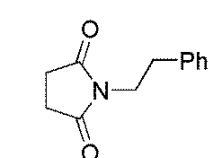

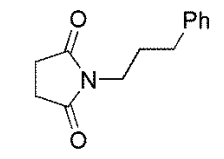
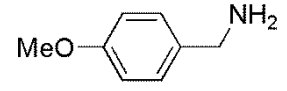
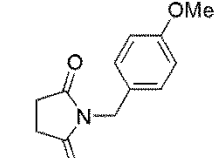
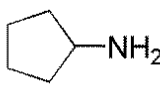
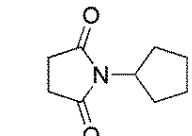
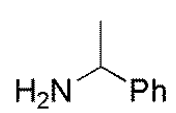
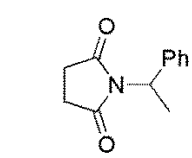


Figure 5. The reaction mechanism of amide synthesis from alcohols and amines.

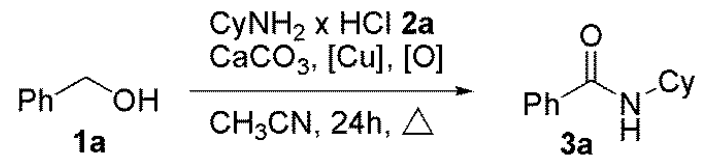
Currently, a great number of effective metal-containing catalysts for the preparation of amides from alcohols and amines, such as Ru [31, a-g], Rh [32, a-b] Ir [33], is known. For example, a method of synthesis of N-substituted succinimides by the reaction of 1,4-butanediol with primary amines in the presence of a [Ru] catalyst (Table 1) is described [34]. Reactions of 1,4-butanediol and amine required 24 hours at heating in a mixture of acetonitrile and toluene, in the presence of 5 mol% of the catalyst $[\text{RuH}_2(\text{PPh}_3)_4]$, 1,3-diisopropyl-imidazolium bromide and NaH (Table 1 shows the average yields based on 2-3 reaction runs).

Table 1. Synthesis of succinimides starting from 1,4-butanediol.

			
No	Amine	Amide	Yield, %
1.			81
2.			76
3.			88
4.			87
5.			68
6.			36

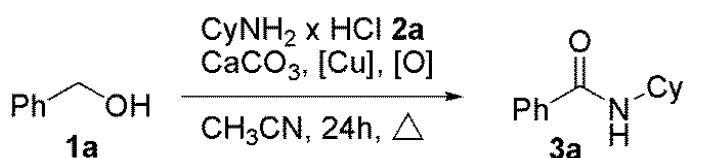
mmol), TBHP (70% in water, 4 equivalents), CH₃CN (1 ml), 80 °C, 4 hours. The best results were found for 5 mol% loading of FeCl₂ × 4H₂O or FeCl₃ (the yield of amide was 87%).

Table 2. Evaluation of the catalytic properties of iron salts in the model of amidation reaction.

			
Nº	[Fe] (mol.%)	[O] (equiv.)	Yield 3a , %
1.	FeSO ₄ × 7H ₂ O (5)	TBHP (4)	84
2.	FeCl ₂ × 4H ₂ O (5)	TBHP (4)	87
3.	K ₄ Fe(CN) ₆ × 3H ₂ O (5)	TBHP (4)	53
4.	Fe(acac) ₃ (5)	TBHP (4)	78
5.	Fe(NO ₃) ₃ × 9H ₂ O (5)	TBHP (4)	84
6.	FeCl ₃ (5)	TBHP (4)	87
7.	FeCl ₂ × 4H ₂ O (5)	H ₂ O ₂ (4)	<5

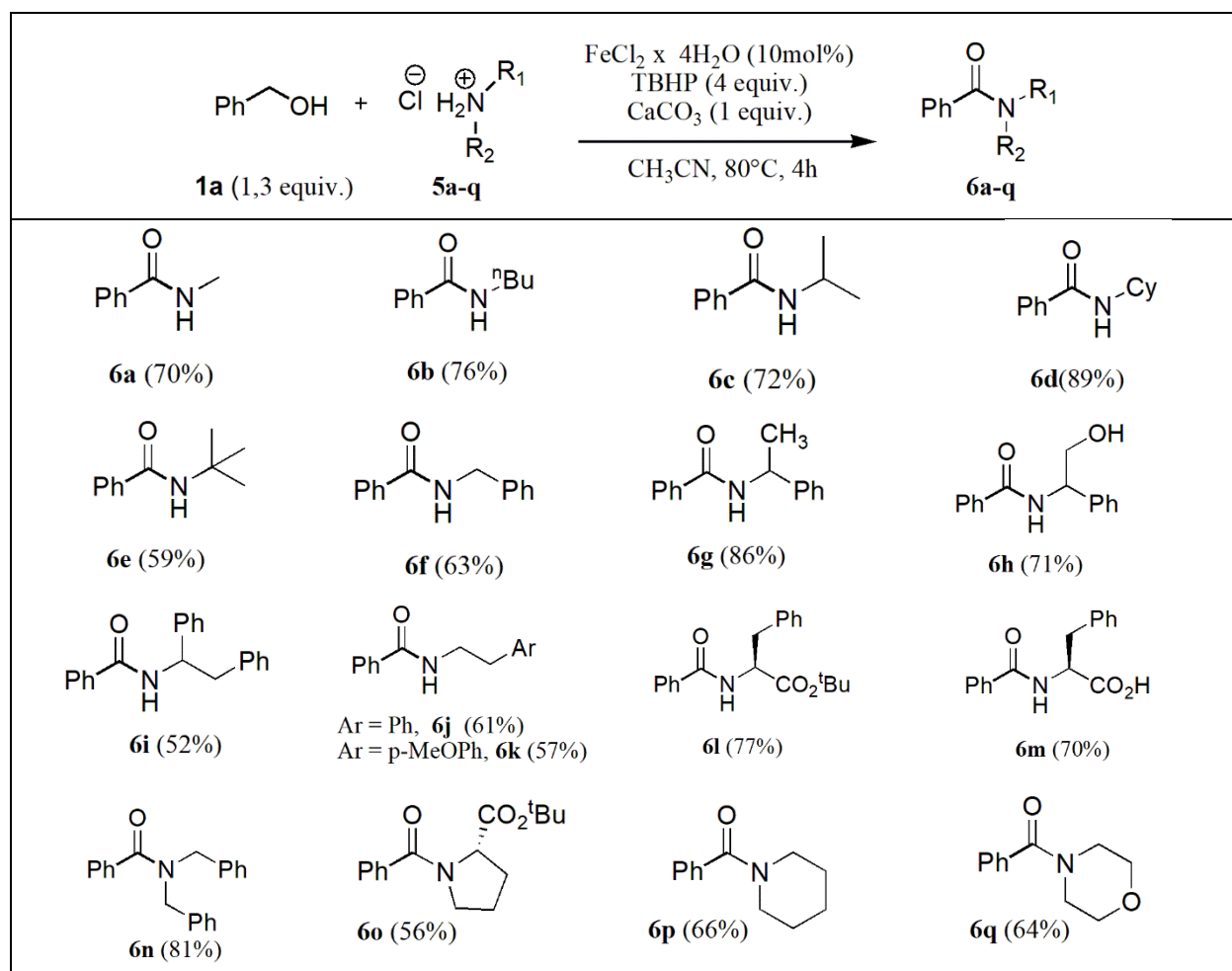
Then, the conditions of the reaction were optimized for the most active catalyst (FeCl₂ × 4H₂O) (Table 3). The highest yield of amide **3a** (89%) was achieved for the following conditions: ratio “amine × HCl: alcohol” = 1: 1.3, the quantity of FeCl₂ × 4H₂O = 10 mol% and 4 equivalents of TBHP.

Table 3. Optimization of the model amidation reaction for FeCl₂ × 4H₂O.

				
Nº	[Fe] (mol.%)	[O] (equiv.)	Ratio 2a / 1a	Yield 3a , %
1.	FeCl ₂ × 4H ₂ O (5)	TBHP (5)	1 : 1.3	72
2.	FeCl ₂ × 4H ₂ O (10)	TBHP (5)	1 : 1.3	89
3.	FeCl ₂ × 4H ₂ O (10)	TBHP (4)	1 : 1.3	89
4.	FeCl ₂ × 4H ₂ O (10)	TBHP (4)	1 : 1.3	82
5.	-	TBHP (4)	1 : 1.3	27

The efficiency of the FeCl₂ × 4H₂O catalyst was also proved for the scope of various primary and secondary amines **5a-q** (Table 4).

Table 4. The study of the effectiveness of catalysts $\text{FeCl}_2 \times 4\text{H}_2\text{O}$.



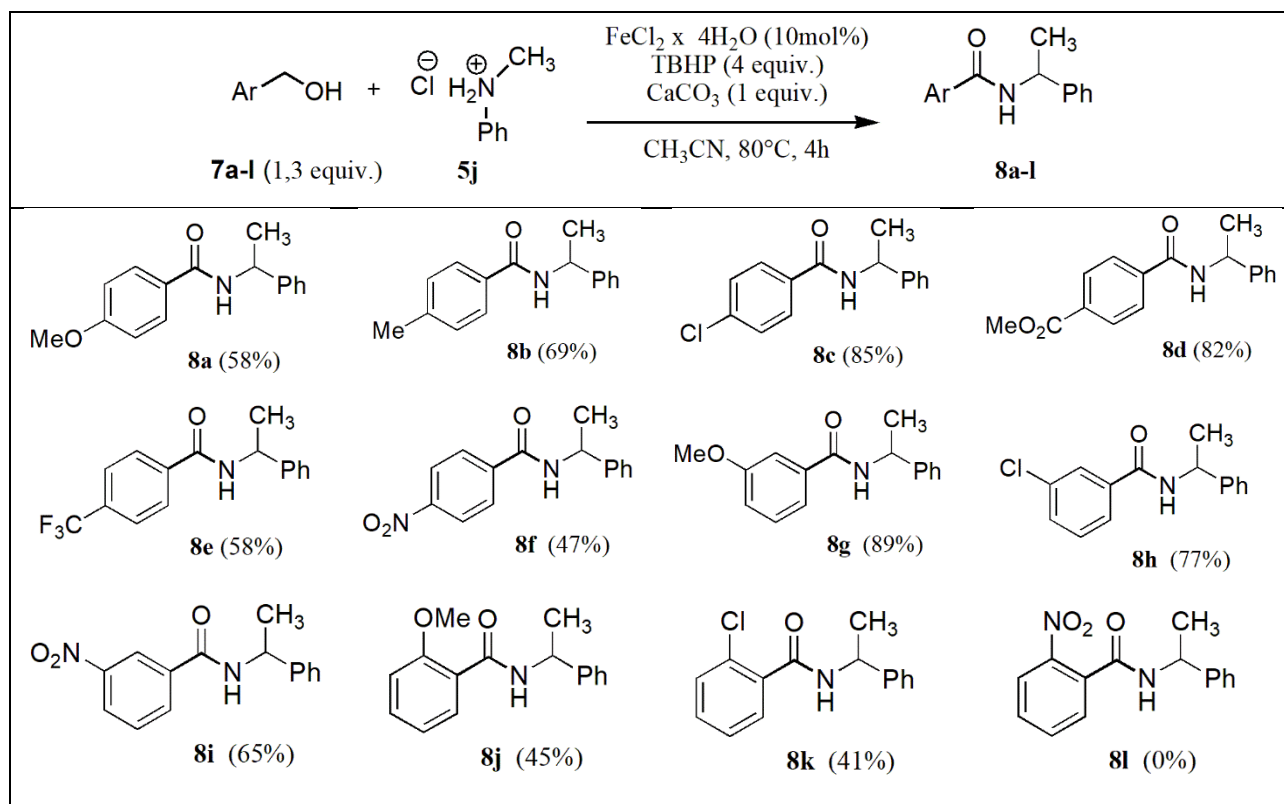
For the scope of primary amines **5a-m**, the corresponding amides were isolated in the following range of yields – from the lowest 59% (**6d**) to the highest 89% (**6g**). Substituted benzylamines **5e-o** give the corresponding amides **6e-o** in the yields ranging from 52% to 86%. Amine **5n** with an unprotected carbonyl group gives N-benzoylphenylalanine **6n** in 70 % yield, this indicates to a low sensitivity of functionality of the carboxylic acid to the reaction conditions.

Secondary amines have also been studied in the iron-catalyzed amidations. Cyclic amines (*tert*-butylpyrrolidine-2-carboxylate **5p**, piperidine **5p** and morpholine **5c**) being reacted to **1a**, gave amides in 55% (**6p**), 65% (**6p**) and 64% (**6c**) yields, respectively.

The catalytic efficiency of $\text{FeCl}_2 \times 4\text{H}_2\text{O}$ for the scope of alcohols in the reaction with α -methyl benzylamine **5g** has also been studied (Table 5). For the alcohols bearing electron-donating groups in *para* position, corresponding amides **8c**, **8e** were isolated in 85% and 82% yields, respectively. Unexpectedly, the *p*-NO₂ substituent, which provided the highest yield of amide in case of copper-catalyzed amidation, allowed amide **8e** in average 47% yield. *Meta*-substituted amines **7g**, **7h** and **7i** gave corresponding amides **8g** (89%), **8h** (77%) and **8i** (65%). Use of *ortho*-substituted benzylic

alcohols (providing steric and electronic effects) led to the lowest yields of corresponding amides **8j**, **8k** and **8l** (45%, 41% and 0%, respectively).

Table 5. Synthesis of amides from various alcohols.



Note, that other research teams also reported optimistic results for non-expensive catalytic systems, based on Zn- [41, a-c], Fe- [42, a-b] or Mn-based [43, a-b] complexes, which indicates the development and prospects of this “abundant metal” direction in amidation.

In the context of the further development of this topic, several Cu(II)-containing silsesquioxane complexes [(PhSiO_{1.5})₁₀(CuO)₂(NaO_{0.5})₂] **9**, [(PhSiO_{1.5})₁₂(CuO)₄(NaO_{0.5})₄] **10** and [(PhSiO_{1.5})₁₂(CuO)₆(1,4-diox)₄(PhCN)₂(MeOH)₄] **11**, were isolated and catalytically tested (Fig. 7) [44].

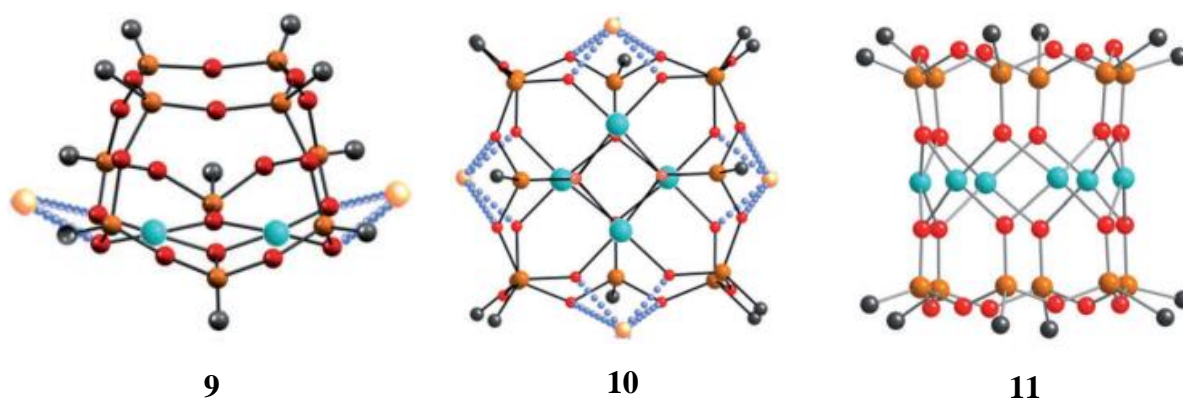


Figure 7. Simplified structures of Cu(II)-containing silsesquioxanes complexes **9-11**.

The self-assembly synthesis of complexes **9** – **10** is based on partial cleavage of oligomeric $[(\text{PhSiO}_{1.5})_2(\text{CuO})]_n$ MS by alkaline siloxanolate $[(\text{PhSiO}_{1.5})(\text{NaO})]_4$ in different conditions (varying of reactants ratio and/or reaction media) [45, a-b]. A common feature of complexes **9** – **10** is the availability of Na^+ ions of ionic silanolate fragments (RSiO^-Na^+). Sodium ions could be easily replaced by copper ones *via* transmetalation reaction (Fig. 8).

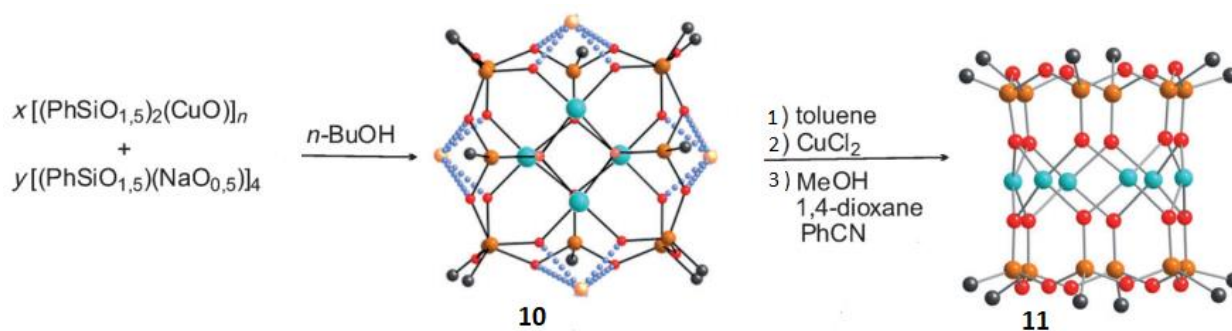


Figure 8. Synthesis of complexes **10** and **11**.

Complex **9** was tested as a catalyst in the reaction between benzylic alcohol (0.5 mmol) and α -methylbenzylamine (0.75 mmol), in the presence of CaCO_3 (99.995% pure; 0.5 mmol) as a base. Other reaction conditions are as follows: TBHP as oxidant (5.5M in nonane, 5 equivalents, 2.5 mmol), CH_3CN as solvent (1 ml), 80°C , 24 hours (Table 6).

The optimization of catalyst **9** loading has been performed. It was shown that even 0.01 mol % of **9** is sufficient for the 99% yield of amide (use of 2 mol% of CuO under identical conditions gave 87% yield).

Table 6. Optimization of the amidation reaction catalyzed by **9**.

No	Catalyst	[Cu], mol. %	Base	Yield, %	TOF, h^{-1}
1.	9	0.01	CaCO_3	99	413
2.	9	0.01	CaCO_3	72	300
3.	9	0.01	-	35	146
4.	-	-	CaCO_3	24	-
5.	9	0.005	CaCO_3	58	483
6.	9	0.01	CaCO_3	83	346
7.	9	1	CaCO_3	84	21
8.	CuO	2	CaCO_3	87	11

In summary, compounds **9**, **10**, and **11** exhibit very high catalytic activity in oxidation amidation (Table 7). The highest yield of amide was 94% with TOF value equal to 392 h⁻¹ (compare to best TOF value of 34 h⁻¹ found for CuO catalyst [46]).

Table 7. The study of the effectiveness of catalysts **9**, **10** and **11** at low loadings.

Amide	Catalyst	[Cu], mol %	Yield, %	TON / TOF, yr ⁻¹
	9	0.01	83	8300 / 346
	10	0.01	94	9400 / 392
	11	0.01	71	7100 / 296
	CuO	2	87	44 / 11
	9	0.01	83	8300 / 346
	10	0.01	83	8300 / 346
	11	0.01	87	8700 / 363
	CuO	2	80	40 / 10
	9	0.01	73	7300 / 304
	10	0.01	74	7400 / 308
	11	0.01	79	7900 / 329
	CuO	2	66	33 / 8
	9	0.01	75	7500 / 313
	10	0.01	93	9300 / 388
	11	0.01	85	8500 / 354
	CuO	2	87	44 / 11
	9	0.01	67	6700 / 279
	10	0.01	71	7100 / 296
	11	0.01	64	6400 / 267
	CuO	2	70	35 / 9
	9	0.01	71	7100 / 296
	10	0.01	76	7600 / 317
	11	0.01	66	6600 / 275
	CuO	2	62	31 / 8

Regarding the iron-based MS catalysts for amidation reactions, an article [47], describing the first example of germsilsesquioxane $[(\text{Ph}_5\text{Ge}_5\text{O}_{10})_3\text{Fe}_6(\text{OH})_3(\text{O})\text{Na}_2] \cdot (\text{EtOH})_2 \cdot \text{H}_2\text{O}$ **12**, could be mentioned. The complexation of **12** with 1,10-phenanthroline gave $[(\text{Ph}_5\text{Ge}_5\text{O}_{10})_3\text{Fe}_6(\text{OH})_3(\text{O})\text{Na}_2(\text{Phen})] \cdot (\text{EtOH})_4 \cdot (\text{H}_2\text{O})_{0.5}$ **13** (Fig. 9).

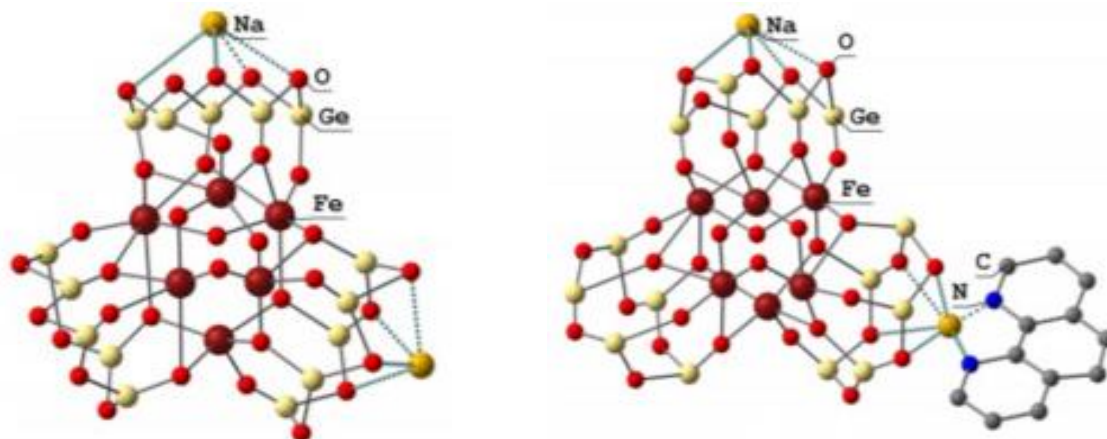


Figure 9. Structures of the complexes **12** (left), **13** (right).

The testing of complex **13'** activity revealed for the first time a potential of using microwave radiation for MS-catalyzed amidations (Table 8) [48]. An interaction between benzylic alcohol (2 equivalents) and (\pm)- α -methylbenzylammonium chloride (1 equivalent) in CH_3CN at 130°C during 45 minutes was chosen as a model reaction. This provided N-(1-phenylethyl)benzamide in 71% yield with complex **13** as a catalyst. The fact that reference catalyst $\text{FeCl}_2 \times 4\text{H}_2\text{O}$ gave only 51% yield is clearly pointing at a stabilizing effect of sesquioxane ligands, improving the stability of active metal centers.

Table 8. The amidation reaction under microwave radiation catalyzed by **13**.

$\text{Ph-CH}_2\text{-OH} + \text{Cl}^- \text{H}_3\text{N}^+\text{-CH(CH}_3\text{)-Ph} \xrightarrow[\text{CH}_3\text{CN, } 130^\circ\text{C, MW, 45 min}]{\text{TBHP (6 equiv.)}} \text{Ph-C(=O)-N(CH}_3\text{)-CH}_2\text{-Ph}$ <p style="text-align: center;">2 equiv. 1 equiv.</p>	
[Fe], мол. %	N-(1-phenylethyl)benzamide, %
$\text{FeCl}_2 \times 4\text{H}_2\text{O}$ (5)	51
13 (5)	71

In conclusion to this section, the oxidative amidation process is a promising alternative to the formation of the classic amide bond by the interaction between a carboxylic acid and amine with a stoichiometric quantity of the base/acid substrates, which are either toxic or generate toxic by-

products [49]. Furthermore, this is an atom-economical (using the terms “green” chemistry) reaction, since only by-products are water or *tert*-butanol.

Currently, catalysts based on expensive metals such as ruthenium and rhodium are widely used. However, study of catalysts including abundant metal ions, for example, copper or iron ones, is highly relevant.

Oxidative C-H activation

It is widely known that one of the most important process in modern organic chemistry is hydrocarbons' transformation to a variety of valuable compounds, such as alcohols, ketones, aldehydes, and carboxylic acids (so-called C–H functionalization [50, a-c]). However, transformations of saturated hydrocarbons to useful products usually require several reaction steps under harsh conditions (high temperature and pressure) due to inertness of alkanes [51, a-b]. Consequently, the development of new and effective methods of mild conditioned functionalization of saturated hydrocarbons is an actual purpose for catalysis as well as for organic and biomolecular chemistry [52].

Synthesis of alcohols and carbonyl compounds *via* oxidation of saturated hydrocarbons has been studied widely. One of the synthetic approaches implies oxidative ability of dioxiranes [53], e.g. dimethyldioxirane [54] or methyl(trifluoromethyl)dioxirane [55, a-b] (Fig. 10). Unfortunately, thermal and chemical lability of dioxiranes significantly limit the application of this approach. Some other reagents capable to oxidize alkanes to alcohols are: (i) oxaziridine [56, a-b], (ii) peroxyacids (*p*-nitronadbenzoic acid) [57], (iii) N-oxides (amine oxides) [58], or (iv) O₃ / IBX (IBX = 2-iodobenzoic acid) [59].

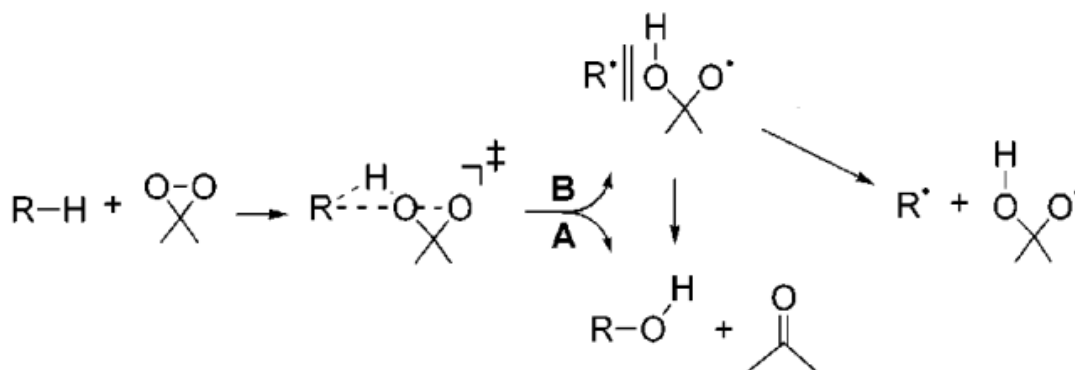


Figure 10. Mechanism of the oxidation of alkanes with dimethyldioxirane.

The oxidation of saturated hydrocarbons with 3d metal peroxocomplexes is also widely described in the literature. The most efficient systems are: VO(O₂)(pic)(H₂O) / H₂O₂ (pic - picolinic acid) [60], (NH₄)₄W₁₀O₃₂ / O₂, *hν* [61], CrO₂(OAc)₂ (CrO₃, CrO₂Cl₂) / H₅IO₆ (Bu₄NIO₄) [62, a - b], CH₃Re(O)₃ / H₂O₂ [63, a - b], RuCl₃ / KBrO₃ [64], [CoHB(3,5-*i*Pr₂pz)₃]₂(μ-O₂) / H₂O₂ (3,5-*i*Pr₂pz - 3,5-bis-isopropylpyrazole) [65]. CrO(O₂)HMPA / H₂O₂ (HMPA – hexamethylphosphorictriamide) [66, a-b], MoO(O₂)₂(H₂O)(HMPA) / H₂O₂ [67], WO(O₂)(H₂O)(HMPA) / H₂O₂ [68]. The efficiency of such complexes is due to high reactivity of corresponding peroxy or superperoxy complexes of 3d metal ions (Fig. 11). Limitations of this approach are: (i) reactive species are stable only at low temperatures and (ii) necessity of use of stoichiometric quantities of expensive reagents.

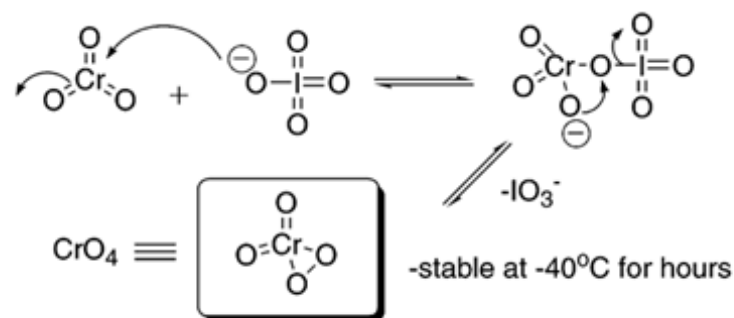


Figure 11. The mechanism of formation of reactive CrO_4 species.

Oxidations of saturated hydrocarbons with aqueous solutions of peroxides and organic cocatalysts are reported for the following systems: H_2O_2 , *t*-BuOOH / azobisisobutyronitrile [69] or H_2O_2 / 1,2,3-benzoxathiazine-2,2-dioxide (Fig. 12) [70]. This approach suffers from several drawbacks: non-selectivity of oxidations and impossibility of re-use of expensive co-catalysts.

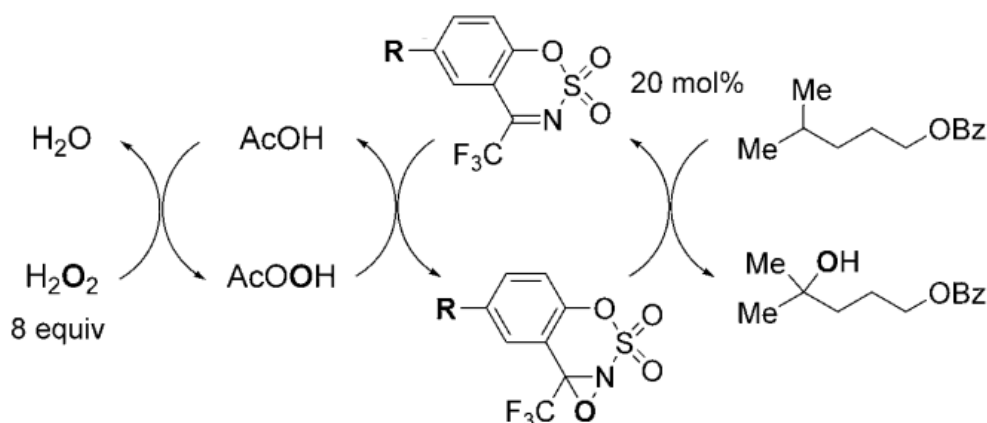


Figure 12. The mechanism of the oxidation reaction with the H_2O_2 / 1,2,3-benzoxathiazine-2,2-dioxide system.

Metalloporphyrin complexes applied as co-catalysts to hydrogen peroxide (in the oxidation of alkanes to alcohols or carboxylic compounds) have also been reported [71]. Most popular types of such cocatalysts are porphyrins complexed with Fe(III) [72, a-b] and Mn(II) [73] ions. The mechanism of their action is similar to the activity of cytochrome P-450 [74].

Several iron complexes were discussed as effective catalysts for C-H activation reactions with hydrogen peroxide as oxidant: $[\text{Fe}_2\text{O}(\text{TPA})_2(\text{H}_2\text{O})_2]^+ / \text{H}_2\text{O}_2$ (TPA - Tris(2-pyridylmethyl)amine) [75, a-b], $[\text{Fe}(\text{CF}_3\text{SO}_3)_2(\text{S,S,R})\text{-MCP}]\text{P} / \text{H}_2\text{O}_2$ [76, a-b], $[\text{Fe}(\text{S,S-PDP})(\text{CH}_3\text{CN})_2](\text{SbF}_6)_2 / \text{H}_2\text{O}_2$ (S,S-PDP-(2S,2'S-(-)-[N,N'-bis(2-pyridylmethyl)]-2,2'-bipyridine) [77, a-c] (Fig. 13). The advantages of this method are: (i) selectivity of oxidations and (ii) low loadings of iron complexes and peroxide. The disadvantage of the approach is the use of an equimolar amount of acid cocatalysts (AcOH).

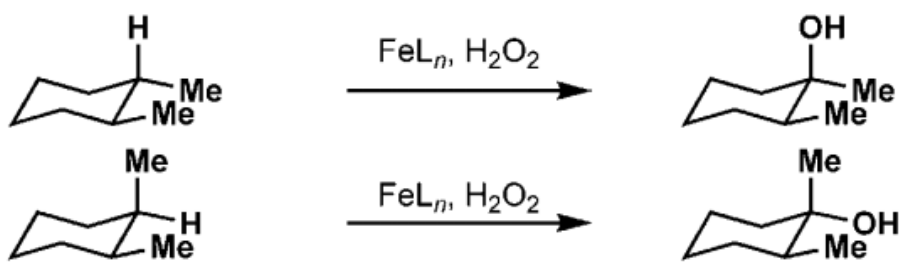


Figure 13. Scheme of alkane oxidation by the FeLn / H₂O₂ system.

In turn, using of catalytic system “copper-containing complex / hydrogen peroxide” is mentioned in literature as a “soft” method for the oxidation of saturated hydrocarbons [78]. The advantage of this method, in comparison to before mentioned Fe-based systems, is a lower (catalytic) amount of acid cocatalysts.

In the progress of this approach, some examples of Cu-containing silsesquioxanes, active in C-H compounds oxidations, have been recently suggested [79, a-b]. Firstly, the synthesis of the non-trivial “Cooling Tower” complex [(PhSiO_{1.5})₁₀(CuO)₂(NaO_{0.5})₂ • 4EtOH] **14** containing one four-membered and two five-membered condensed siloxane rings in the cage structure was described [80] (Fig. 14).

Catalytic properties of compound **14** were tested in the mild benzene oxidation with aqueous hydrogen peroxide (Fig. 14). The main oxygenate of this reaction is phenol, which could be partially (up to 20%) overoxidized into to *p*-quinone in case of longer reaction time.

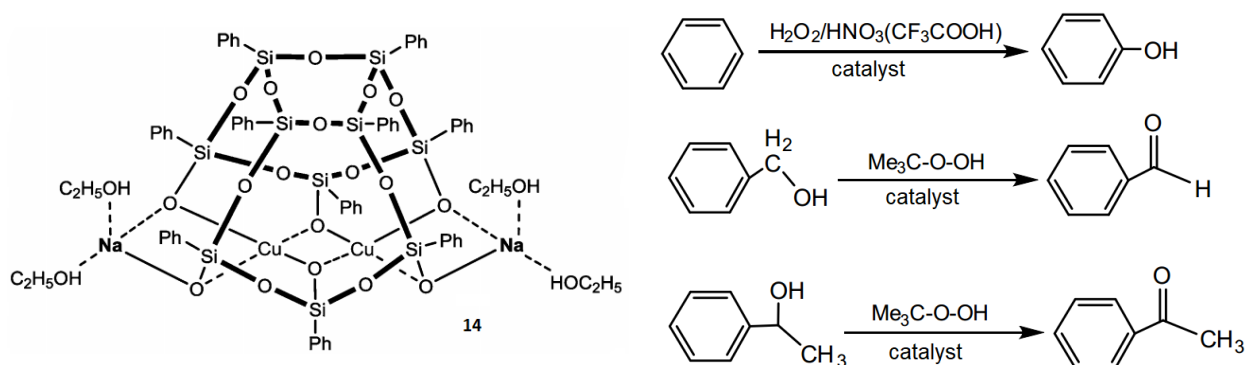


Figure 14. Structure of the complex **14** (left); oxidations catalyzed by **14** (right).

For this reaction, it was shown that the initial oxidation rate W_0 depends nonlinearly on concentration of **14** (Fig. 15). The reaction efficiency was estimated using the TON parameter: TON reaches 530 after 14 hours of reaction (an initial concentration of **14** was 1×10^{-4} M) (Fig. 15, curve 1).

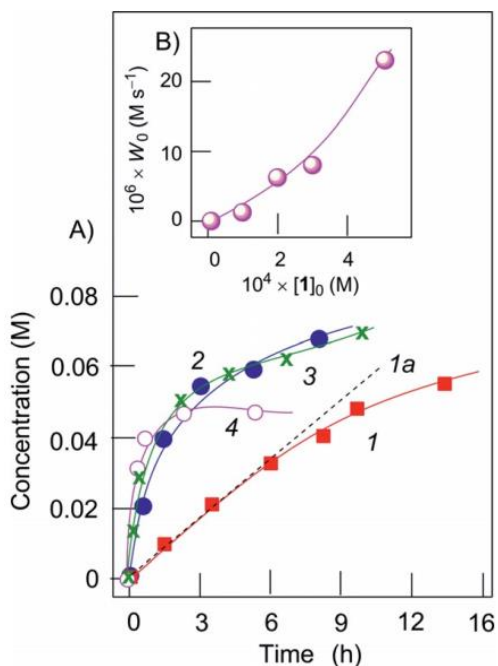


Figure 15. Graph A: the accumulation of phenol during the oxidation of benzene (0.45 m) H_2O_2 (1.35 m; 35% aqueous solution), at various concentrations of **14**: 1×10^{-4} M (curve 1), 2×10^{-4} M (curve 2), 3×10^{-4} M (curve 3) and 5×10^{-4} M (curve 4). The reaction was carried out in CH_3CN in the presence of HNO_3 (0.05 m, 65% aqueous solution) at 70°C .

Figure B: the dependence of the initial reaction rate W_0 on the initial concentration of **14**.

The oxidation of benzene (0.8 m) by hydrogen peroxide (2.56 m, 50% aq) catalyzed by **14** (5×10^{-4} M) in the presence of HNO_3 (0.4 M, 65% aq) after 6 hours of the reaction gave phenol in 41% yield. The reaction proceeds rapidly: TON reaches 420 after 2 hours, which corresponds to a very high TOF of 210 h^{-1} . Using of TFA in the benzene oxidation to phenol was also effective and allowed to decrease reaction temperature to 50°C .

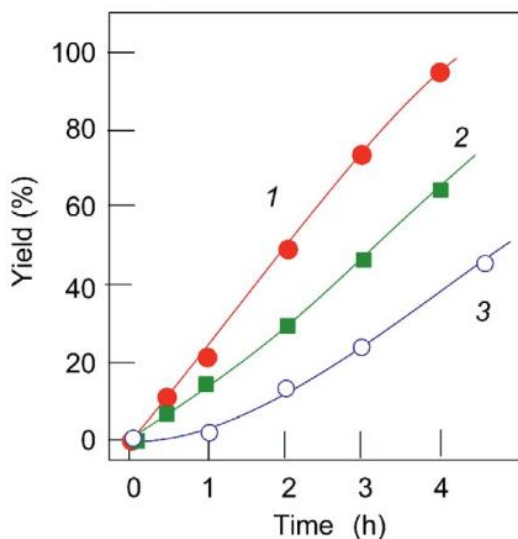


Figure 16. Curve 1: the oxidation of 1-phenylethanol to acetophenone by the TBHP-**14** system. Curve 2: the oxidation of benzyl alcohol to benzaldehyde by the TBHP-**14** system. Curve 3: the accumulation of benzaldehyde during the oxidation of styrene by the H_2O_2 - TFA system.

At the second stage, the complex **14** was evaluated as a catalyst for the oxidation of alcohols (Fig. 16). It has been shown that *tert*-butylhydroperoxide exhibits excellent efficacy even in the absence of acid cocatalyst. The oxidation of 1-phenylethanol (0.25 M) by TBHP (1.65 M, 70% aq) at 50 °C after 4 hours of the reaction gave acetophenone in almost quantitative yield (initial concentration of catalyst $[\mathbf{14}]_0$ was 5×10^{-4} M) (Fig. 16, curve 1). Oxidation of benzyl alcohol (0.39 M) to benzaldehyde by TBHP (0.6 M, 70% aq) catalyzed by **14** ($[\mathbf{14}]_0 = 5 \times 10^{-4}$ M, 60 °C, 4 hours) was less effective (Fig. 16, curve 2). The “**14** - TFA - H₂O₂” system oxidizes styrene to benzaldehyde in the moderate yield (Fig. 16, curve 3).

Tetranuclear complexes $[(\text{PhSiO}_{1.5})_{12}(\text{CuO})_4(\text{NaO}_{0.5})_4]$ **15** and $[(\text{PhSiO}_{1.5})_6(\text{CuO})_4(\text{NaO}_{0.5})_4(\text{PhSiO}_{1.5})_6]$ **16** (Fig. 17) were also evaluated as catalysts for mild oxidation of benzene and 1-phenylethanol by aqueous hydrogen peroxide or TBHP [81].

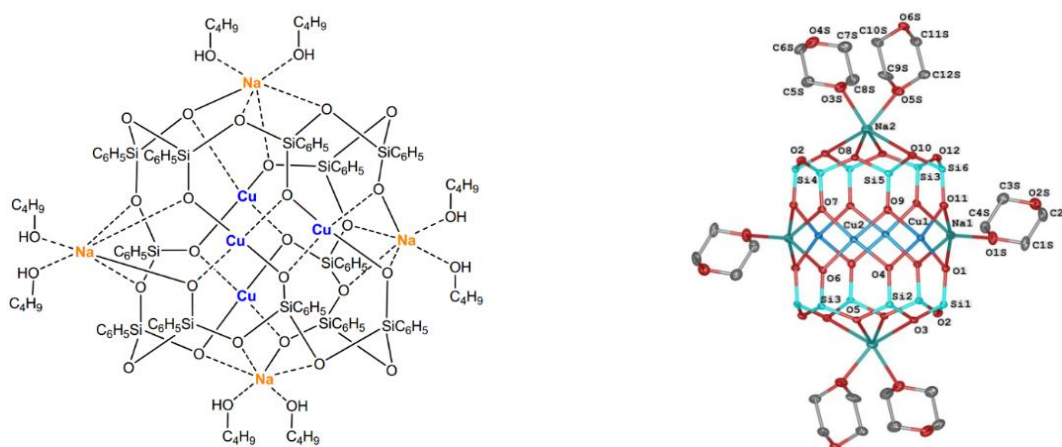


Figure 17. Structures of complexes **15** (left) and **16** (right).

Oxidation of benzene (0.45 M) by hydrogen peroxide (1.35 M; 35% aq) catalyzed by **15** (2×10^{-4} M) has been optimized varying the quantity of acid: $[\text{TFA}]_0 = 0$ M (Fig. 18, curve 1); $[\text{TFA}]_0 = 0.0025$ M (Fig. 18, curve 2); $[\text{TFA}]_0 = 0.01$ M (Fig. 18, curve 3).

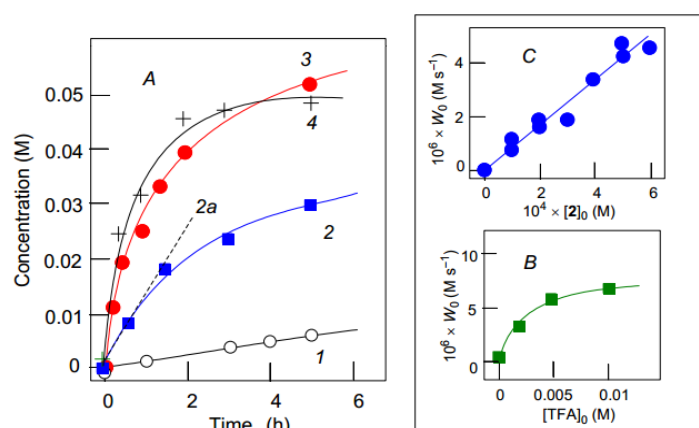


Figure 18. Graph A: Phenol accumulation during the oxidation of benzene **15** at various concentrations of TFA. Graph B: Dependence of the initial benzene oxidation rate W_0 on the concentration of added TFA. Graph C: Dependence of the rate of oxidation of benzene W_0 on the initial concentration of catalyst **16**.

A kinetic curve for the reaction ($[\mathbf{15}]_0 = 5 \times 10^{-4}$ M, $[\text{TFA}]_0 = 0.01$ M at 50°C) is shown on Fig. 18, C. The best result of the benzene oxidation catalyzed by complex **16** gave TON = 250 after 5 hours of reaction ($\text{TOF} = 240 \text{ h}^{-1}$). Authors suggested that TFA partially cleaved some bonds in the initial catalyst complex. It promotes potential contacts of copper ions with hydrogen peroxide and benzene.

Also, it was found that oxidation of 1-phenylethanol by TBHP catalyzed by complexes **15** and **16** is efficient even in the absence of acid promoters (Fig. 19).

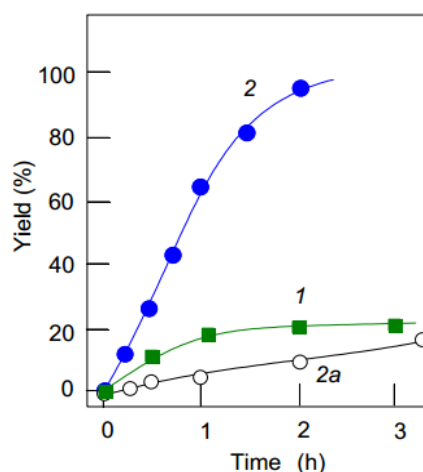


Figure 19. Accumulation of acetophenone during the oxidation of 1-phenylethanol by **15**.

Oxidation of 1-phenylethanol (0.25 M) by TBHP (1.65 M, 70% aq) catalyzed by **15** ($[\mathbf{15}]_0 = 5 \times 10^{-4}$ M, 60°C , in CH_3CN) gave acetophenone in a quantitative yield (Fig. 19, curve 2). TON reaches 475 after 2 hours of reaction (TOF was 280 h^{-1}). Observed lower activity of compound **16** (in comparison to **15**) was explained by the supramolecular structure of **16** leading to screening of copper ions.

The catalytic properties of complexes **11** and $[(\text{PhSiO}_{1.5})_{12}(\text{CuO})_6(\text{NaCl})(1,4\text{-diox})_{12}(\text{H}_2\text{O})_2]$ **17** (Fig. 20) were discussed in ref [45]. Complex **17** contains the central Cu_6O_6 fragment coordinated by two siloxanolate cycles. Additional feature of complex **17** is an encapsulation of Cl^- ion into the inner void of the cage.

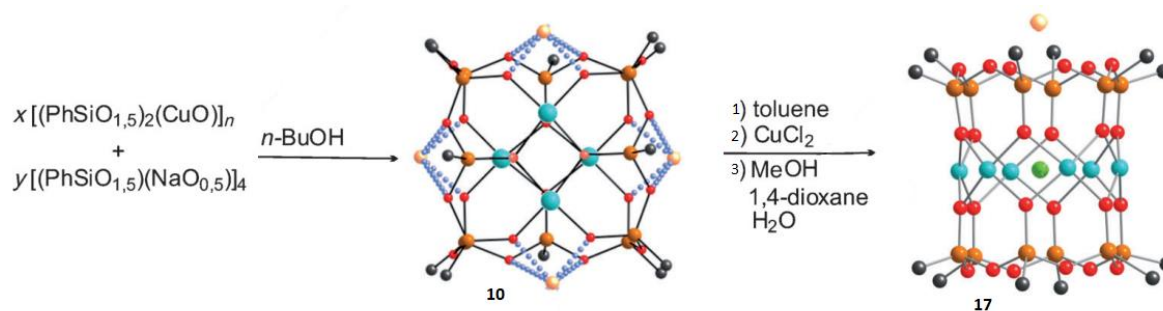


Figure 20. Synthesis of of the complex **17**.

Compounds **11** and **17** were tested in the oxidation reactions of benzene, hydroquinone or 1-phenylethanol by aqueous hydrogen peroxide. It was shown that nitric acid (cocatalyst for the benzene oxidation) caused decomposition of the catalysts **11**, which precipitates as a blue solid. However, the TFA does not decompose complex **11**.

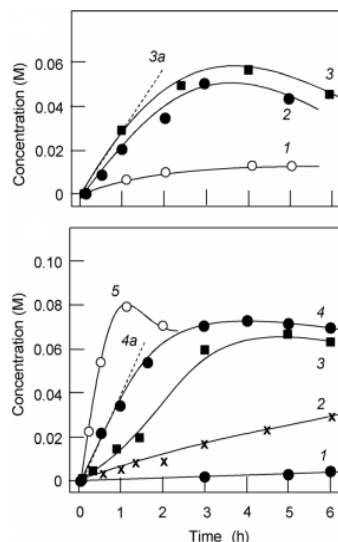


Figure 21. Oxidation of benzene to phenol, catalyzed by compounds **11** and **17**.

Complex **17** effectively catalyzes the oxidation of benzene in the presence of nitric acid (conditions: benzene (0.45 M), H_2O_2 (2.6 M; 35% aq), catalyst loadings were $[\mathbf{17}]_0 = 2 \times 10^{-4}$ M or $[\mathbf{17}]_0 = 1 \times 10^{-4}$ M). The best result achieved for **17** was the observed concentration of phenol equal to 0.05 M after 2.5 hours of reaction (Fig. 21, curve a).

It was shown that compound **11** efficiently catalyzed the oxidation of benzene by TFA, giving 0.08 M of phenol after 1 h (total yield 18%, $\text{TOF} = 160 \text{ h}^{-1}$) (Fig. 21 curve 5). For $[\mathbf{11}]_0 = 0.5 \times 10^{-4}$ M, TON reached 1510 after 13 h ($\text{TOF} = 116 \text{ h}^{-1}$) (Fig. 21, curve 2). Authors concluded that higher catalytic activity of **17** in comparison to **11** is due to the presence of the Cl^- anion in the center of cage structure **17**. Such additional coordination of copper ions stabilizes catalytic species.

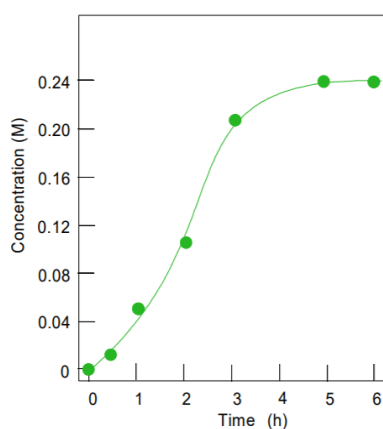


Figure 22. Oxidation of 1-phenylethanol to acetophenone, catalyzed by **17**.

The oxidation of 1-phenylethanol by TBHP was also studied (H_2O_2 was found less effective). The reaction does not require acid promoters. The optimal reaction conditions are as follows: 1-phenylethanol (0.25 M), TBHP (1.5 M, aq. 70%), catalyst **17** (5×10^{-4} M) in CH_3CN solution at 60 °C (Fig. 22). The yield of acetophenone reached 95% after 5 hours of reaction. Compound **11** does not catalyze the oxidation of 1-phenylethanol.

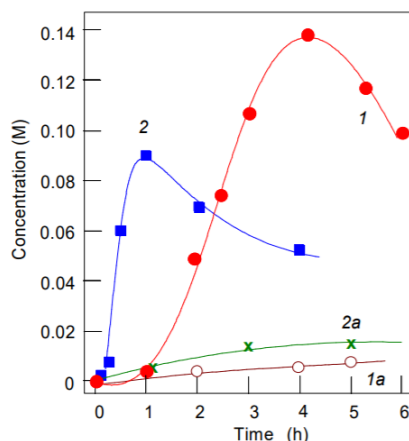
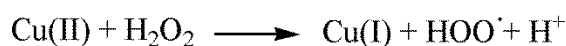


Figure 23. Oxidation of hydroquinone to *p*-quinone, catalyzed by **11** or **17**.

Oxidation of hydroquinone to *p*-quinone by TBHP has been performed under following conditions ($[\text{TFA}]_0 = 0.01$ M, $[\mathbf{11}]_0 = 1 \times 10^{-4}$ M or $[\mathbf{17}]_0 = 2 \times 10^{-4}$ M, CH_3CN , 20 °C) (Fig. 23). The best result achieved with **11** as catalyst was the 56% yield of *p*-quinone after 4.5 hours (Fig. 23, curve 1).

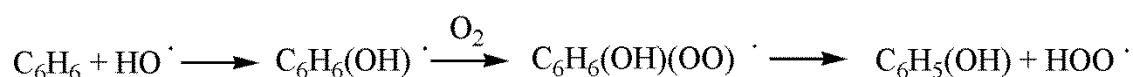
The analysis of the kinetic data obtained for **11**, **14** - **17** let authors to propose a general mechanism for the oxidation of phenol by hydrogen peroxide, catalyzed by Cu-silsesquioxanes. The mechanism is similar to one suggested for the oxidation catalyzed by vanadates [82, a- d]. In the first step, the catalyst interacts with hydrogen peroxide:



Thus formed Cu(I) species in turn react with hydrogen peroxide giving hydroxyl radicals and Cu(II) ions:



Hydroxyl species provokes chain radical reactions:



In conclusion to this section, it is worth to note that Cu(II)-containing silsesquioxanes are proved to be very effective catalysts for the oxidation of hydrocarbons by peroxides. Occasionally, the acid co-catalysts are not required. These results suggest that the development of this topic is a promising scientific task, deserving further investigation.

Magnetic properties of metallasiloxanes

Molecular magnets are isolated architectures or compounds with extended structure (1D, 2D or 3D) built by transition metal or lanthanide ions (spin carriers) connected through inorganic or organic ligands demonstrating interesting magnetic properties. They may exhibit different types of magnetic behavior, including an occurrence of a long-range magnetic ordering in extended structures, Single Molecule Magnetic (SMM) behavior in discrete architectures, spin-glass behavior, and others. Organic radicals may also present interesting magnetic behavior and they constitute a particular sub-family of molecular magnets. [83]. Note that whatever the type of the magnetic behavior, the magnetic interactions between the spin carriers may be operational through bridging ligands (exchange interactions) or through space (dipolar interactions).

The Single Molecule Magnets (SMMs) are one of the most famous families of molecular magnets investigated up to now. They exhibit a slow relaxation of the magnetization and a memory effect under a blocking temperature of a purely molecular origin [84]. The archetype of SMM is a famous polynuclear compound $[\text{Mn}_{12}\text{O}_{12}(\text{OAc})_{16}(\text{H}_2\text{O})_4]$, originally reported in 1980 by T. Lis, which is composed of twelve Mn ions with two different oxidation states (+2 and +3) coupled by superexchange interactions through oxygen bridges to give a large ground state $S = 10$, blocking of the magnetization at low temperature and a hysteresis effect [85]. The extensive investigation of this compound and understanding of its magnetic behavior open a tremendous way to numerous new discrete architectures with high spin state and larger energy barriers. Thus, up to day, numerous SMMs based on transition metal ions or lanthanides have been published including the recently discovered Dy^{3+} cyclopentadienyl family exhibiting a hysteresis effect up to 75 K [86]. Another interesting example of isolated magnetic architectures with remarkable properties is a polyoxometalate anion, $[\text{V}_{15}\text{As}_6\text{O}_{42}(\text{H}_2\text{O})]^{6-}$, containing fifteen antiferromagnetically coupled $S = \frac{1}{2}$ spins resulted in an $S = \frac{1}{2}$ ground state exhibiting a long-lived quantum coherence in a nonmagnetic environment, that suggesting that self-organized molecular qubit network with coherence times of the order of hundreds of fs is realistic [87, a-b]. The third example is a famous family of molecule-based magnets presenting extended three-dimensional structures, made by an assembly of metal ions and cyanometallate fragments, which is called Prussian Blue Analogous, $\text{A}_x\text{M}_y[\text{M}'(\text{CN})_6]_z$ (where M and M_0 are transition metal ions). In these compounds, the magnetic interactions propagate in three space directions conducting to an appearance of ferro- or ferrimagnetic ordering up to room temperature for some selected members of this family [88, a-b].

A spin glass behavior in molecule-based magnets is a relatively scarce phenomenon, but it is well known in other families of inorganic magnets. Given that in this manuscript we will consider several metallasiloxanes exhibiting this type of magnetic behavior, we wish to provide a brief

description of this phenomenon. Spin glasses are considered as a state of a magnetic system with a disordered position of magnetic atoms (and spins) in space. In such systems, ferromagnetic and antiferromagnetic interactions often coexist and compete with each other inducing a spin frustration phenomenon. Above the spin glass transition temperature (so-called freezing temperature), T_f , the spin glass exhibits a typical paramagnetic behaviour, but below reaching T_f , a short-range magnetic ordering occurs and the sample becomes a spin glass and further cooling caused little change in its magnetization. In the other words, compounds having the spin glass properties present a slow relaxation of the magnetization and a hysteresis effect below their freezing temperature. The canonical spin-glass behaviour is usually observed in inorganic dilute magnetic alloys or in amorphous materials containing randomly dispersed magnetic ions presenting structural disorder and spin frustration, but also in inorganic nanoparticles presenting surface or volume spin frustration. Such behavior has also been found in molecule-based magnets with extended structures or in polynuclear architectures, while the examples of such behavior are still scarce. We can cite an example of the coordination polymer $[\text{Co}(\text{C}_3\text{H}_3\text{N}_2)_2]_n$ (Co^{2+} , $S = 3/2$) exhibiting a low-field magnetic susceptibility with two maxima (T_f) at 8 and 4 K, which reflect the presence of a short-range low-dimensional antiferromagnetic behaviour and the existence of a spin-glass-like state, respectively [89]. Another example with magnetic properties is metal–organic frameworks, where the building blocks are nanoscale pseudospherical clusters. The complex $[\text{Fe}_8(\mu^4\text{-O})_4(\mu\text{-4-CH}_3\text{-pz})_{12}]$ (4-R-pz = 4-substituted pyrazolato anion) studied by the combination of Mössbauer spectroscopy and magnetism measurements reveals a spin-glass behavior with $T_f = 30$ K [90]. Other examples of Co(II) and Ni(II)-based siloxanes exhibiting this behavior are described in details in the following sections.

The particularity of magnetic metallasilsesquioxane in comparison to other molecule-based magnets consists in the use of silsesquioxane ligands able to form polynuclear cages. Advantages of the silsesquioxanes involve: (i) the possibility of several types of bridging coordination of metal ions, (ii) diversity of structural topology of metal – oxygen skeleton in the cage, (iii) formation of new type of polyhedral cages, which is different in comparison to the ones formed by other ligands and which are often referred to as small nanoparticles. At the same time, detailed investigations of magnetic properties of MS remained rare. In the following sections, we will summarize the description of the magnetic behavior of Cu(II)-, Ni(II)- and Co(II)-silsesquioxane in order to offer for a reader a representative image of works published before this thesis starts.

Magnetic properties of Cu(II)-containing metallasesquioxanes

To date, among various metallasesquioxanes, Cu(II)-based architectures are most often studied, probably due to the relative ease of their synthesis, and also due to the fact that copper (II) ions have $S = 1/2$, which makes them relatively easy to describe from both, experimental and theoretical points of view. However, it can be noted that among the various MSs synthesized to date based on Cu(II), having different topology and nuclearity (from 4 to 12), the magnetic properties have been investigated only for a relatively limited part of them.

Synthesis of complexes $[(\text{PhSiO}_2)_6\text{Cu}_6(\text{O}_2\text{SiPh})_6] \cdot 6\text{EtOH}$ **18**, $\text{Na}_4[(\text{PhSiO}_2)_{12}\text{Cu}_4] \cdot 8\text{BuOH}$ **19** and $\text{K}_4[(\text{C}_2\text{H}_3\text{SiO}_2)_{12}\text{Cu}_4] \cdot 6\text{BuOH}$ **20** and investigation of their magnetic behavior are presented in ref. [91]. The hexanuclear complex $[(\text{PhSiO}_2)_6\text{Cu}_6(\text{O}_2\text{SiPh})_6] \cdot 6\text{EtOH}$ **18** [92, a-b] is a compound of cylindrical form (Fig. 24, left). Each Cu ion is four-coordinated by oxygen atoms in a square planar geometry with bond lengths in the range 1.92 – 1.98 Å, which is comparable to the sum of the ionic radii O^{2-} and Cu^{2+} (1.93 Å). The Cu-O_{sol} distances are elongated (2.34 – 2.38 Å), forming distorted tetragonal pyramidal geometry of Cu^{2+} ions. The Cu-O-Cu angles are in the range 91.5 – 94.6°. Stacking interactions between phenyl rings with distances up to 3.38 Å were also observed. The magnetic behavior of **18** is shown in the graph $\chi T - T$ (χ is the magnetic susceptibility) (Fig. 24, right). The χT value increases upon cooling from 2.8 $\text{emu}\cdot\text{K}\cdot\text{mol}^{-1}$ at 260 K to a plateau of 5.80 $\text{emu}\cdot\text{K}\cdot\text{mol}^{-1}$ at 8 K. Mathematic model using the Weiss correction was calculated (Fig. 24, right), solid line with the best fit parameters $g = 2.14$, $J = -42.0 \text{ cm}^{-1}$ (g -factor is a dimensionless magnetic moment [93]; J is the exchange interaction potential [94]). This description corresponds to the ferromagnetic coupling model for the ground state $S = 3$, in which all six spins are parallel to each other.

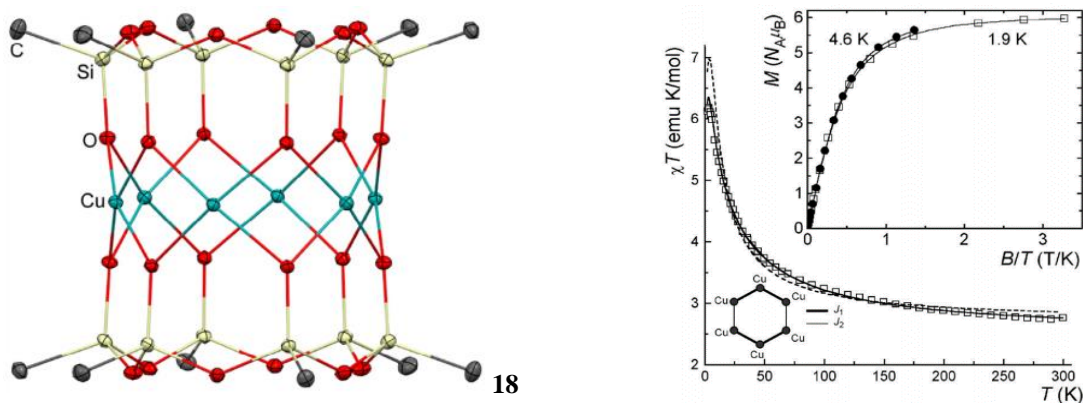


Figure 24. Structure of complex $[(\text{PhSiO}_2)_6\text{Cu}_6(\text{O}_2\text{SiPh})_6] \cdot 6\text{EtOH}$ **18** (left); the dependence of $\chi T - T$ for **18** (right).

$\text{Na}_4[(\text{PhSiO}_2)_{12}\text{Cu}_4] \cdot 8\text{BuOH}$ **19** and $\text{K}_4[(\text{C}_2\text{H}_3\text{SiO}_2)_{12}\text{Cu}_4] \cdot 6\text{BuOH}$ **20** complexes contain cyclohexasiloxanolate ligands ($L = -[\text{PhSiO}_2]^{6-}$ and $-[\text{C}_2\text{H}_2\text{SiO}_2]^{6-}$, respectively) (Fig. 25) [95]. These ligands are coordinated (via O_m atoms) to four Cu atoms, which are located at vertices of the elongated tetrahedron. Complex **19** is constructed of two almost parallel Cu_2O_2 blocks arranged in a cross-like

fashion. In contrast to the tetragonal-pyramidal coordination in **18**, the Cu atoms adopt square planar coordination in **19**. The average Cu-O distances (1.92 Å and 1.94 Å for **19** and **20**, respectively) correspond to the sum of ionic radii, the same as for **18** (2.03 Å). The bridging Cu-O-Cu angles in **19** and **20** are increased to values 101.7 and 101.2 °, respectively. It was found that the Cu-Cu distances inside the Cu₂O₆ units are 3.02 and 3.06 Å, while the Cu-Cu distances between these units are 3.899 Å for **19** and 3.386 Å for **20**. This excludes apical coordination of Cu atom to O atom of the neighboring Cu₂O₂ fragment.

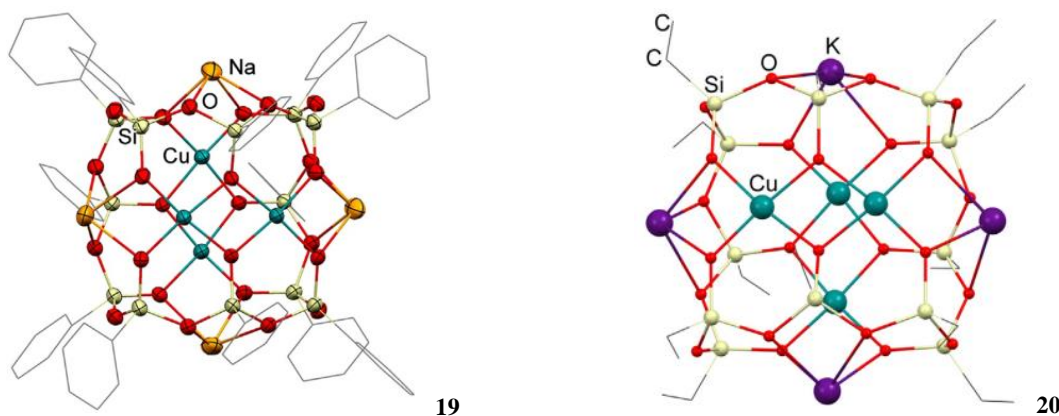


Figure 25. Structures of complexes Na₄[(PhSiO₂)₁₂Cu₄] · 8BuOH **19** (left) and K₄[(C₂H₃SiO₂)₁₂Cu₄] · 6BuOH **20** (right).

Temperature dependencies of magnetic susceptibility for **19** and **20** complexes (Fig. 26) revealed the maximum near 170 K and 175 K (**19** and **20** respectively), then sharp decrease of χ upon cooling, reaching minimum values at 25 K and 30 K. This behavior could be explained by antiferromagnetic interactions between atoms Cu of Cu₂O₆ fragment. Further cooling of the samples from 30 K to 1.8 K revealed an increase of χ values due to the presence of a small number of non-interacting particles in the samples. To estimate the molar fraction of these particles, authors suggested the presence of “paramagnetic impurity” which follows the Curie law and has the same g -factor as the main compound. Using that assumption, authors calculated the ρ -parameter.

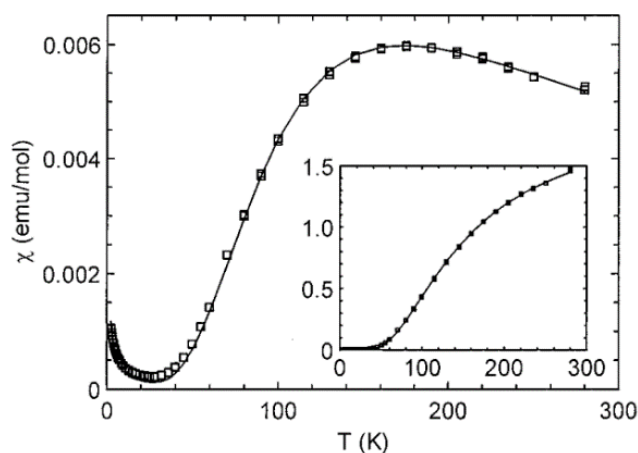


Figure 26. The dependences $\chi - T$ for **19** Inset: the dependence $\chi T - T$.

Using the least squares method, the following parameters were calculated: $g = 2.35$, $J = 193.0 \text{ cm}^{-1}$ and $\rho = 2.07 \times 10^{-3}$, $R = 6.3 \times 10^{-5}$ for **19** and $g = 2.43$, $J = 210.0 \text{ cm}^{-1}$ and $\rho = 7.62 \times 10^{-2}$, $R = 9.8 \times 10^{-5}$ for **20**. High values of g parameter reflect some systematic error in the data. However, unlike compound **18**, obtained exchange interaction constants are completely consistent with the values predicted by Hatfield and Hodgson [96]. In this case, values of $J = 255 \text{ cm}^{-1}$ for **19** and $J = 219 \text{ cm}^{-1}$ for **20** should be expected. Satisfactory concordance of results allowed to conclude the similarity between siloxanolate and hydroxo linkers.

Cylindrical complex $[\text{Cu}_6\{(\text{MeSiO}_2)_6\}_2] \cdot 6\text{DMF}$ **21** was described in ref. [97]. Framework of product consists of two *cis*-methylcyclohexasiloxanolate ligands $[(\text{MeSiO}_2)_6]^{6-}$ located between six Cu^{2+} ions. Neighboring Cu^{2+} ions are bonded by two siloxanolate oxygen atoms, which provide the main pathway of magnetic exchange of copper ions spins with $S = 1/2$. The length of Si-O (Si) bonds varies in the range $1.624 - 1.636 \text{ \AA}$, while Si-O-Si angles vary in the range of $133.98 - 136.64^\circ$, which is usual for this class of compounds. The lengths of Si-O-Cu bonds are much shorter ($1.609 - 1.613 \text{ \AA}$) than the corresponding lengths of Si-O (Si) bonds. The Cu-Cu distances are 2.816 , 2.841 , and 2.861 \AA . Distance between opposite copper atoms varies between 5.495 and 5.820 \AA . The Cu- O_m bond lengths lay in the range $1.946 - 1.974 \text{ \AA}$, which is close to the values for copper atoms with square-pyramidal geometry (SP). The angles Cu- O_m -Cu including linking oxygen atoms, which primarily determine the magnetochemical behavior of multinuclear clusters, vary in the range of $91.26 - 94.59^\circ$.

Based on study of low-temperature magnetic behavior of the **21** (Fig. 27), it was concluded that compound consists of two Cu(II) trimers, with a strong exchange interaction inside the trimers with $J = -72.5 \text{ K}$ (exchange interaction between the trimers showed $J = -7.0 \text{ K}$). In addition, the experimentally observed magnetization $M(B)$ of the complex at $T = 2 \text{ K}$ can be adequately reproduced by the Brillouin function for the effective spin $S = 3$ and $g = 2.00$.

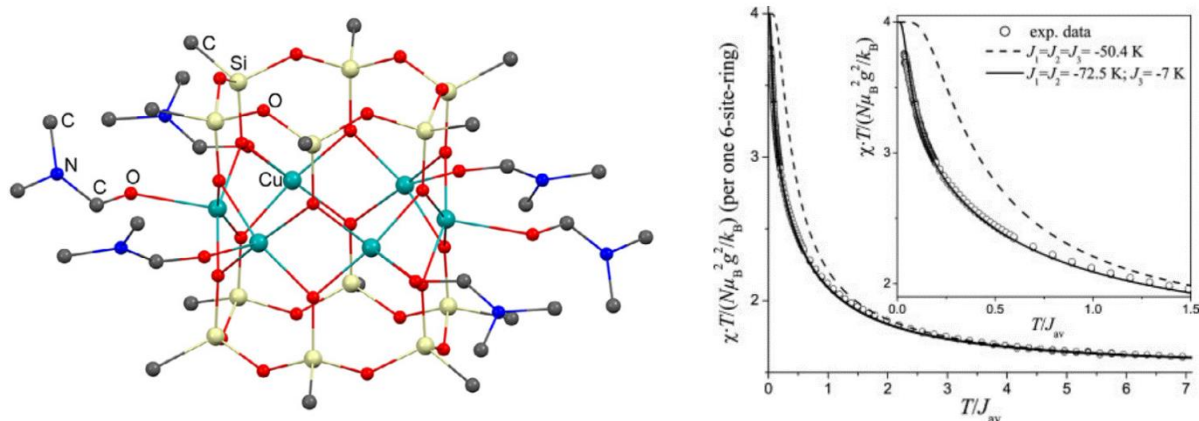


Figure 27. $\chi T / (N\mu_B^2 g^2 / k_B)$ as a function of normalized temperature T / J_{av} . The dashed line represents theoretical calculation of the ferromagnetic interactions inside the cluster, the solid line corresponds to the exchange interaction model.

The work of Abbati and colleagues [98] described the synthesis of $[\text{Cu}_6\{(\text{PhSiO}_2)_6\}_2\{\text{NCCu}(\text{tmpa})\}_4](\text{PF}_6)_4$ **22** by the interaction of two Cu-containing complexes: $[\text{Cu}_6\{(\text{PhSiO}_2)_6\}_2(\text{BuOH})_{6-x}(\text{H}_2\text{O})_x]$ and $[\text{Cu}(\text{tmpa})\text{NC}]_4(\text{PF}_6)_4$ (tmpa = $[\text{NC}_5\text{H}_4\text{CH}_2]_3\text{N}$).

The architecture of complex **22** is a hexagonal cage fragment of Cu_6 nuclearity connected through cyanide bridges to four peripheral $\text{Cu}(\text{tmpa})$ units (Fig. 28). The trigonal bipyramidal (TB) geometry of Cu(II) ions in the complex is slightly distorted to $0.843 \pm 0.902 \text{ \AA}$ (compare to 0.943 \AA reported for $[\text{Cu}(\text{tmpa})\text{NC}]_4(\text{PF}_6)_4$ [99, a-b]). The $\text{CuNC-Cu}(\text{tmpa})$ fragments possess a *cis*-conformation, with angles $\text{NC-Cu}(\text{tmpa})$ vary in the range $168.8 \pm 173.5^\circ$ (for Cu-NC angles - $153.0 \pm 159.9^\circ$). The distances between opposite copper ions lay in the range $5.4164 - 5.7408 \text{ \AA}$.

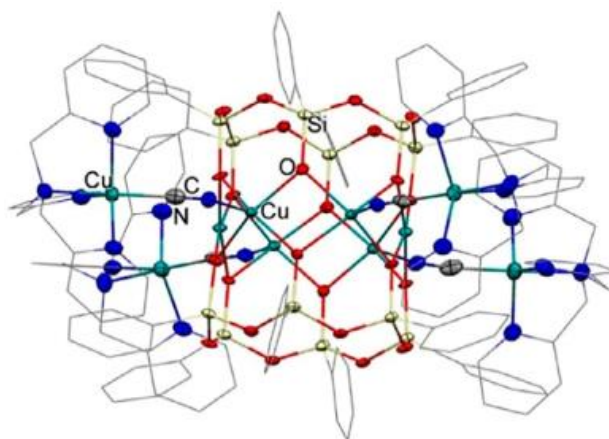


Figure 28. Structure of $[\text{Cu}_6\{(\text{PhSiO}_2)_6\}_2\{\text{NCCu}(\text{tmpa})\}_4](\text{PF}_6)_4$ complex.

For complex **22**, temperature dependence of the molar magnetic susceptibility $\chi T - T$ at 1 T, as well as magnetic properties as a function of temperature (T) and of applied magnetic field (B) (Fig. 29) were investigated. It allowed to conclude ferromagnetic interaction between Cu-Cu ions located in the framework unit of complex (bold lines in Fig. 31). The peripheral copper ions interact with the framework copper ions in antiferromagnetic manner (dashed lines in the Fig. 31). The calculated parameters are as follows: $g = 2.25$, $J_1 = -47 \text{ cm}^{-1}$, $J_2 = 0 \text{ cm}^{-1}$, $J_3 = 1.7 \text{ cm}^{-1}$. The ground state of the molecule is $S = 5$.

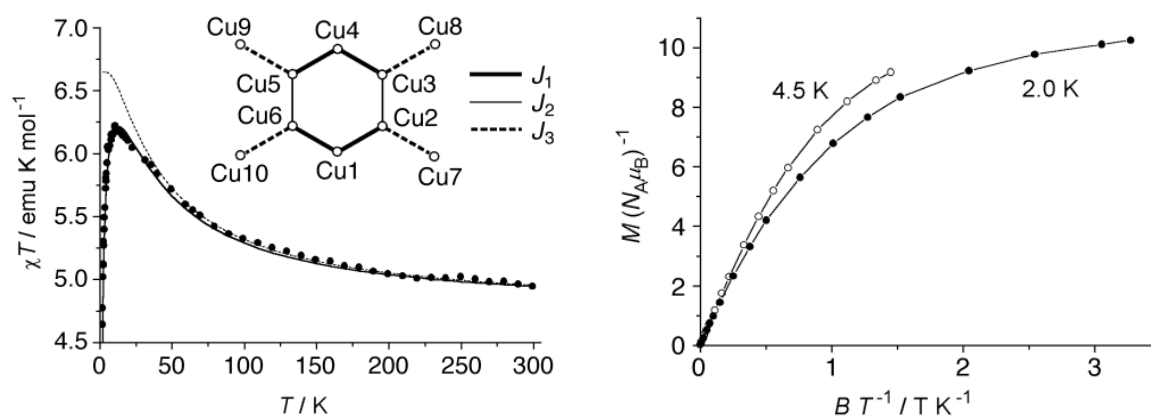


Figure 29. Graph of the dependence $\chi T - T$ (left); $M - B / T$ plot for compound **22** (right).

Using the same synthetic method [100], scientific group of Abbati synthesized compound $[\text{Cu}_6\{(\text{PhSiO}_2)_6\}_2\{\text{NCCu}(\text{Me}_6\text{tren})\}_2(\text{MeOH})_4](\text{ClO}_4)_2$ **23**, $\text{Me}_6\text{tren} = \text{tris-[2-(dimethylamino)ethyl]amine}$ (Fig. 30). Structure **23** includes an almost planar hexagonal lattice of six quadratically pyramidal (QP) Cu(II) ions. This central core is connected through cyanide bridges to two $[\text{Cu}(\text{Me}_6\text{tren})]$ fragments, containing Cu(II) ions of trigonal bipyramidal (TB) geometry. This coordination significantly distorts the central unit $[\text{Cu}_6\{(\text{PhSiO}_2)_6\}_2]$. The nonlinear structure of the Cu-C-N-Cu linker characterizes by angles N-C-Cu(TB) and Cu(QP)-N-C of 176.9° and 169.28° values, respectively.

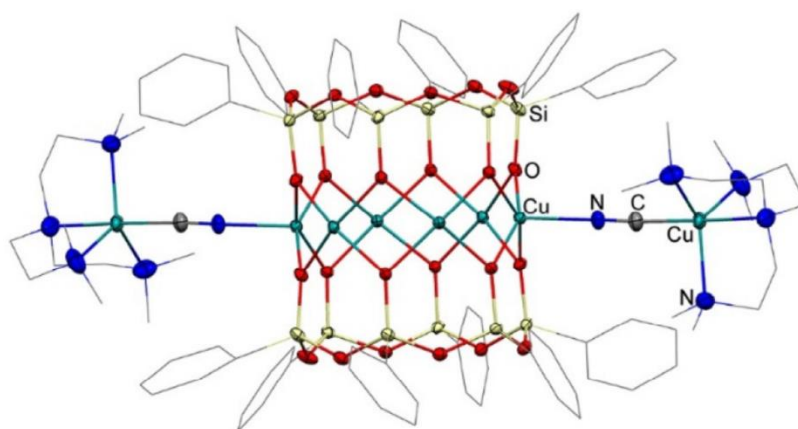


Figure 30. Structure of compound $[\text{Cu}_6\{(\text{PhSiO}_2)_6\}_2\{\text{NCCu}(\text{Me}_6\text{tren})\}_2(\text{MeOH})_4](\text{ClO}_4)_2$ **23**.

The magnetic properties of complex **23** have also been studied. The molar magnetic susceptibility of **23** was measured in the range 5.0 – 300.0 K. The magnetic susceptibility of compound **23** is $\chi T = 3.82 \text{ emu}\cdot\text{K}\cdot\text{mol}^{-1}$ at 300 K and slowly increases upon cooling, reaching a maximum of $\chi T = 4.56 \text{ emu}\cdot\text{K}\cdot\text{mol}^{-1}$ at 16 K, and then rapidly decreases to $\chi T = 3.52 \text{ emu}\cdot\text{K}\cdot\text{mol}^{-1}$ at 5.0 K (fig. 31).

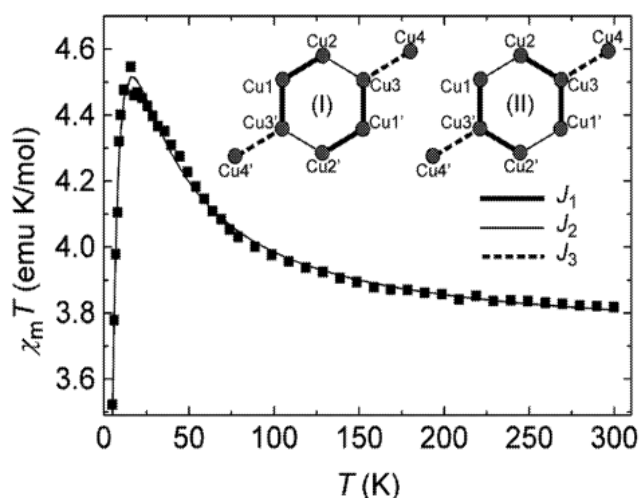


Figure 31. Experimental $\chi T - T$ curve for **23** with exchange schemes I and II.

Two options of the exchange interaction were studied (Fig. 31 (I) and (II)). The calculated parameters for scheme (I) are: $g = 2.224$, $J_1 = J_2 = -19.7 \text{ cm}^{-1}$, $J_3 = 15.2 \text{ cm}^{-1}$ while for scheme (II) $g = 2.225$, $J_1 = -24.4 \text{ cm}^{-1}$, $J_2 = 5.9 \text{ cm}^{-1}$, $J_3 = -1.2 \text{ cm}^{-1}$. Both schemes are consistent with experimental results and demonstrate the presence of ferro- and antiferromagnetic exchange interactions. The Cu_6 core has the ground spin state $S = 3$; after the insertion of $[\text{Cu}(\text{Me}_6\text{tren})]$ fragments, it decreases to $S = 0$.

The article [101] describes a hexanuclear sandwich complex $\{\text{Cu}_6[(\text{PhSiO}_2)_5]_2(\text{OH})_2(2,2'\text{-bipy})_2\} \cdot 4\text{DMF} \cdot 3\text{H}_2\text{O}$ **24** containing two siloxanolate and two 2,2'-bipyridine (bipy) ligands (Fig. 32). Complex **24** contains six Cu(II) ions, forming $\text{Cu}_6\text{O}_{10}(\text{OH})_2$ fragment, consisting of two parallel layers $\text{Cu}-\text{O}_2-\text{Cu}-\text{O}_2-\text{Cu}-(\text{O}, \text{OH})$. The value of angle formed by three copper ions Cu-Cu-Cu is 173.5° . The Cu-Cu distances lay in the range $2.9931 - 3.0310 \text{ \AA}$. The central metal-containing fragment is coordinated by two pentaphenylcyclopentasiloxanolate ligands. The Si-O bond length varies in the range $1.591 - 1.652 \text{ \AA}$, which is usual for this class of compounds [102]. Two copper ions Cu (1) and Cu (4) are additionally coordinated by two 2,2'-bipyridine moieties, with the Cu-N bond distances equal to $1.999 - 2.015 \text{ \AA}$. The Cu-O-Cu angles formed by copper atoms of different layers have values close to 90° , while for the angles formed by copper ions from the same layer these values are $93.13 - 100.7^\circ$. The angles formed by copper ions and hydroxy-oxygen atoms are varying in the range $108.59 - 110.94^\circ$.

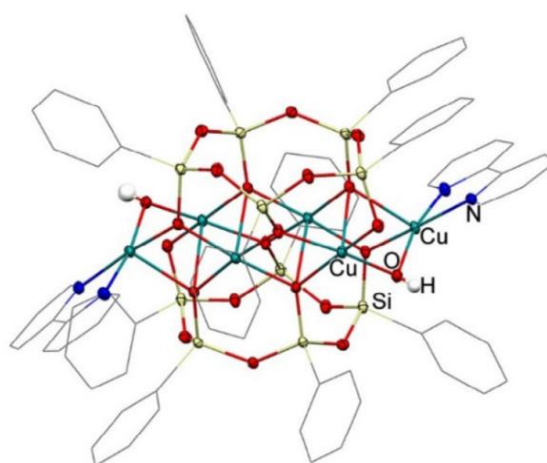


Figure 32. The structure of $\{\text{Cu}_6[(\text{PhSiO}_2)_5]_2(\text{OH})_2(2,2'\text{-bipy})_2\} \cdot 4\text{DMF} \cdot 3\text{H}_2\text{O}$ **24**.

The bipyridine ligands favor the π - π stacking interactions between neighboring molecules with an interplanar distance equal to 3.43 and 3.22 \AA [103].

Approximating the experimental data on measurements of χT vs T at 0.05 T for compound **24** (Fig. 33), authors obtained a theoretical model corresponding to the Curie - Weiss law. The low-temperature part of the model describes the formation of an effective isolated linear trimeric state $S = 1/2$ with an isotropic antiferromagnetic exchange coupling $J / k_B = 85 \text{ K}$ (k_B is the Boltzmann constant). With the antiferromagnetic intertrimer interaction $J / k_B = 3.5 \text{ K}$, a singlet ($S = 0$) ground

state and an excited triplet ($S = 1$) state appeared. This allows to adequately describe magnetic behavior of this complex at low temperatures.

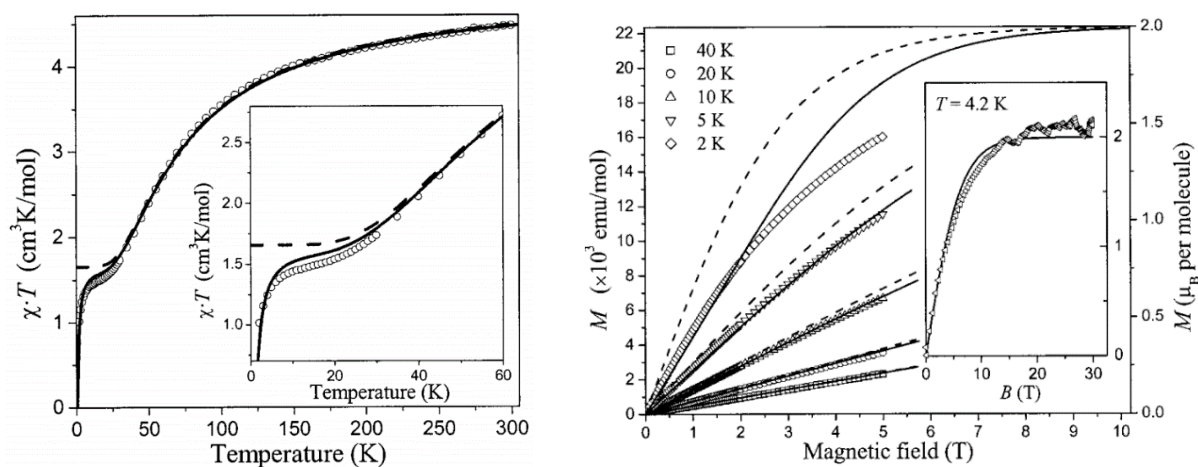


Figure 33. The dependence $\chi T - T$ of complex **24** at 0.05 T (left); Measurements of isothermal magnetization in DC fields from 0 to 5 T (main panel) and pulsed fields from 0 to 30 T (inset) at various temperatures (right).

A comparative study of magnetic properties in dependence to the diameter of cylindrical cage complexes was given in ref. [104]. This work describes the structural and magnetic properties of a Cu(II)-based complexes containing 6, 8, or 10 copper atoms in the central cyclic part: $\text{Cu}_6[(\text{MeSiO}_2)_6]_2 \cdot 6\text{DMF}$ **21**, $[\text{Cu}_8[(\text{MeSiO}_2)_8]_2 \cdot 8\text{DMF}] \cdot \text{EtOH}$ **25**, $[\text{Cu}_{10}[(\text{MeSiO}_2)_{10}]_2 \cdot 10\text{DMF}] \cdot 6\text{DMF}$ **26** (Fig. 34).

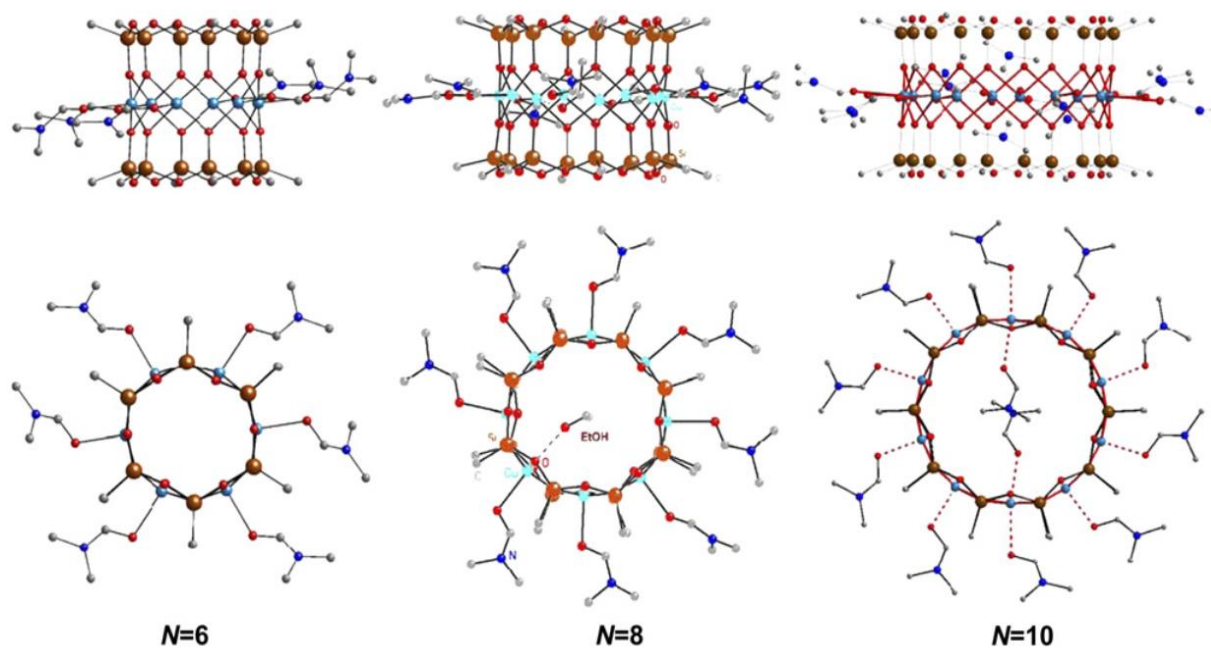


Figure 34. Structures of the complexes $\text{Cu}_6[(\text{MeSiO}_2)_6]_2 \cdot 6\text{DMF}$ **21**, $[\text{Cu}_8[(\text{MeSiO}_2)_8]_2 \cdot 8\text{DMF}] \cdot \text{EtOH}$ **25**, $[\text{Cu}_{10}[(\text{MeSiO}_2)_{10}]_2 \cdot 10\text{DMF}] \cdot 6\text{DMF}$ **26**.

Structurally, each Cu^{2+} ion is bonded to four oxygen atoms, that provides magnetic exchange interactions between Cu(II) centers with $S = 1/2$. The lengths of equatorial Cu-O bonds vary in the range 1.928 – 1.985 Å (1.957 Å for **21**, 1.951 Å for **25**, 1.960 Å for **26**). The average Cu-O-Cu angles vary between 91.2 – 97.7 ° (93.02 ° for **21**, 95.26 ° for **25**, 96.50 ° for **26**) (Table 9).

Table 9. Comparison of the structural and magnetic parameters of multinuclear Cu (II) complexes.

Structure Cu-MOS	Distance Cu-Cu, Å	Angle Cu-O-Cu	Molecule diameter, Å	$2J / k_B$, (K)
$\text{Cu}_6[(\text{PhSiO}_2)_6]_2 \cdot 6\text{EtOH}$ 18	2.807	92.25 °	5.614	-60 (FM)
$\text{Cu}_6[(\text{MeSiO}_2)_6]_2 \cdot 6\text{DMF}$ 21	2.839	93.02 °	5.677	-50.4 (FM)
$\text{Cu}_8[(\text{MeSiO}_2)_8]_2 \cdot 8\text{DMF} \cdot \text{EtOH}$ 25	2.882	95.26 °	7.575	-27.6 (FM)
$\text{Cu}_{10}[(\text{MeSiO}_2)_{10}]_2 \cdot 10\text{DMF} \cdot 6\text{DMF}$ 26	2.911	96.50 °	9.410	+17.2 (AFM)

A detailed analysis of the magnetic properties of **21**, **25**, **26** demonstrates: (i) a strong ferromagnetic exchange interaction Cu-Cu ($2J / k_B = - 50.4$ K) for Cu_6 complex with a high-spin ground state $S = 3$, (ii) a moderately strong ferromagnetic interaction ($2J / k_B = - 27.6$ K) for Cu_8 complex with ground state $S = 4$ and antiferromagnetic interaction ($2J / k_B = + 17.2$ K) with a nonmagnetic ground state $S = 0$ for Cu_{10} complex (Fig. 35).

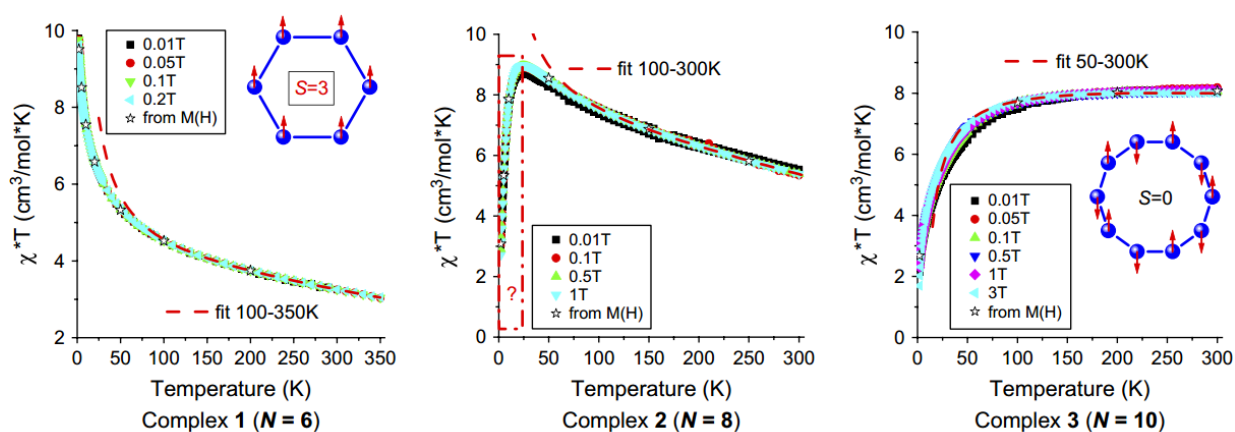


Figure 35. Temperature dependence of χT for **21**, **25** and **26** complexes. Asterisks denote susceptibility data obtained by measuring isothermal magnetization.

The dependence of the $2J / k_B$ values on the structural data of the complexes was analyzed. Notably, the parameters of the transition from ferromagnetic interaction to antiferromagnetic were found, namely, the critical distance Cu-Cu ~ 2.903 Å, the critical angle of Cu-O-Cu ~ 96.04 °, and the critical diameter of the molecule 8.686 Å [105].

Cu(II)-containing silsesquioxane, including two nonequivalent cage fragments bearing different ligand environments, $\{[\mu^6 - (\text{PhSiO}_2)_6]_2\text{Cu}_6(\text{MeOH})_6\} \cdot \{[\mu^6 - (\text{PhSiO}_2)_6]_2\text{Cu}_6(\text{C}_3\text{H}_5\text{N}_2\text{O}_2)_2\} \cdot (\text{NEt}_4)_2 \cdot 5\text{MeOH} \cdot \text{CHCl}_3$ **27** was described in ref. [106].

One of these cages, with $\{[\mu^6 - (\text{PhSiO}_2)_6]_2\text{Cu}_6(\text{C}_3\text{H}_5\text{N}_2\text{O}_2)_2\} \cdot (\text{NEt}_4)_2$ composition, includes two Cu(II) ions coordinating $\text{C}_3\text{H}_5\text{N}_2\text{O}_2$ (2-amino-2-oxoethanimidic acid methyl ester monoanion) ligand (Fig. 36) [107]. N-ligands coordinate Cu atoms (distances are 1.991 and 1.968 Å) thus distorting hexanuclear ring. Cu(II) ions form two symmetrical trimers. Interdimer distance $\text{Cu}_1\text{-Cu}_3$ is equal to 3.7181 Å which is much larger than intradimer distances (2.9185 and 2.9636 Å). Tetracoordinated Cu(II) ions are surrounded by siloxane oxygen atoms (distances in the range 1.903 – 1.975 Å). Pentacoordinated ions Cu_2 и Cu_2^a exhibit more regular coordination geometry, with four siloxanolate oxygen atoms (Cu-O distance is 1.931 Å) and a fifth apical contact with a methanol molecule (2.541 Å).

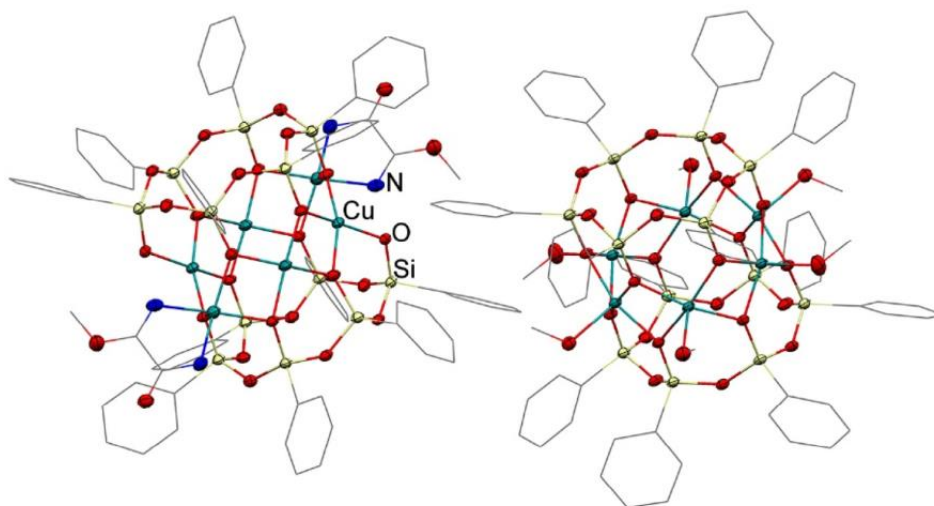


Figure 36. Structure of complex $\{[\mu^6 - (\text{PhSiO}_2)_6]_2\text{Cu}_6(\text{MeOH})_6\} \cdot \{[\mu^6 - (\text{PhSiO}_2)_6]_2\text{Cu}_6(\text{C}_3\text{H}_5\text{N}_2\text{O}_2)_2\} \cdot (\text{NEt}_4)_2 \cdot 5\text{MeOH} \cdot \text{CHCl}_3$ **27**.

The second cage fragment of the complex **27**, with the $\{[\mu^6 - (\text{PhSiO}_2)_6]_2\text{Cu}_6(\text{MeOH})_6\}$ composition, includes six pentacoordinated Cu(II) ions surrounded by oxygen atoms. Geometry of copper site is square pyramidal one (Cu-O distance is 1.970 Å). In case of coordination with methanol molecule, an axial geometry with a Cu-O_{sol} distance 2.218 Å is realized. Cu ions form a regular hexanuclear cluster with the neighboring Cu-Cu distances laying in the range 2.8275 – 2.8958 Å, while distances between opposite atoms are 5.5674 – 5.9115 Å.

The value $\chi_m T$ of **27** is equal to 5.5 $\text{emu}\cdot\text{K}\cdot\text{mol}^{-1}$ at room temperature, which is consistent with the parameters $S = 1/2$ and $g = 2.18$ for twelve Cu (II) ions. Upon cooling down to $T = 4$ K the $\chi_m T$ value increases to 7.5 $\text{emu}\cdot\text{K}\cdot\text{mol}^{-1}$. Further cooling lead to a $\chi_m T$ value decrease (Fig. 37). Increased magnetic moment at low temperatures could be explained by ferromagnetic contribution of the

$\{[\mu^6-(\text{PhSiO}_2)_6]_2\text{Cu}_6(\text{MeOH})_6\}$ cluster with average Cu-O-Cu angles of $91.4 - 94.8^\circ$ and the ground spin state $S = 3$. Higher observed magnetic moment of the complex is explained by the presence of a second cage $\{[\mu^6-(\text{PhSiO}_2)_6]_2\text{Cu}_6(\text{C}_3\text{H}_5\text{N}_2\text{O}_2)_2\} \cdot (\text{NEt}_4)_2$, with the larger Cu-O-Cu angles ($95.8 - 99.8^\circ$).

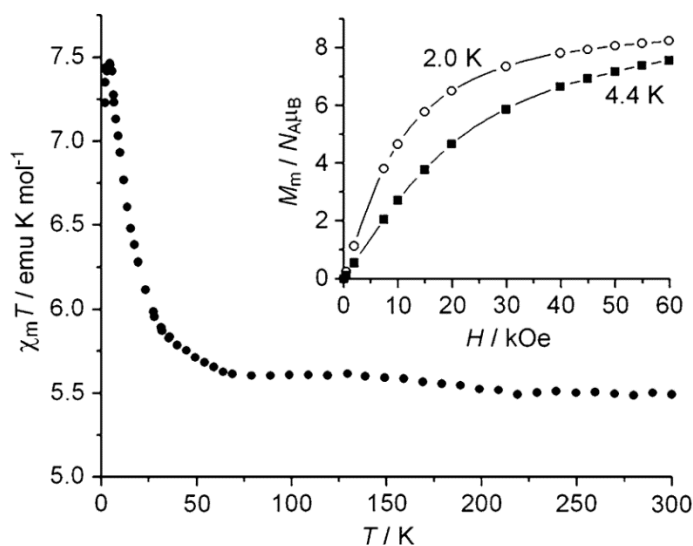


Figure 37. Measurement of molar magnetic susceptibility $\chi T - T$ for complex **27**.

In summary, the magnetic properties of numerous Cu(II)-containing metallasesquioxanes have been investigated [108]. A comparative characteristic of Cu(II) complexes from **18** to **27**, containing coordination cyclic fragments, shows that the exchange interactions are related to the Cu-O-Cu angle and can be described by a simple equation $-J (\text{K}) = -106.6 \alpha + 10468.8$ [109]. In the case of copper complexes, the small Cu-O-Cu angle $\alpha < 97.5^\circ$ leads to a triplet state of the molecule, due to the difficult overlap of the p -orbitals of oxygen and the d -orbitals of the metal, while the larger angle provides the stabilization of a single ground state and antiferromagnetic interactions.

Magnetic properties of Co(II) - containing metallasilsesquioxanes

Examples of Co(II)-containing silsesquioxanes are surprisingly scarce despite the promising potential of this paramagnetic ion to form molecular magnets with interesting properties, as it presents an association of a high magnetic anisotropy with a relatively high spin value ($S = 3/2$). In this line of thought, a few Co(II)-based silsesquioxanes have been reported around thirteen years ago mainly for their original structural organization and their catalytic properties, but their magnetism has not been investigated. Recently, two interesting examples of three- and pentanuclear Co(II)-based silsesquioxanes presenting a slow dynamic behaviour of the magnetization identified as spin-glass compartment has been reported by hosting laboratories. In this section, we describe a series of discrete Co(II)-based silsesquioxanes with different nuclearity and their magnetic studies.

Complex $[(\text{RSi}(\text{OH})\text{O}_2)\text{Co}(\text{OPMe}_3)]_4$, where $\text{R} = 2,6\text{-}i\text{Pr}_2\text{C}_6\text{H}_3\text{N}(\text{SiMe}_3)$ **28** (Fig. 38), was described in ref. [110]. Its established by X-ray diffraction studies, is a drumlike architecture containing a $\text{Co}_4\text{O}_8\text{Si}_4$ core with an oxo-ligands bridge. Cobalt and oxygen atoms form two planar four-membered Co_2O_2 rings. Each Co(II) ion is tetracoordinated by oxygen atoms (the fourth coordination site is occupied by OPMe_3 ligand). Both cobalt and silicon centers adopt almost tetrahedral coordination geometry. Co-O distances vary in range from 1.937 Å to 2.016 Å. Si-O bond lengths vary in 1.600 – 1.640 Å range. The Co-O-Co angles of Co_2O_2 structural units are close to 90° . That leads to the realization of almost ideal rectangular geometry of Co_2O_2 fragments. The Co-Co bond lengths are in the range of 2.890 – 2.889 Å. M: Si ratio is equal to 4: 4. The $1/\chi - T$ dependence measured in the temperature range 2 – 300 K, allowed authors to conclude the presence of the ferromagnetic interactions.

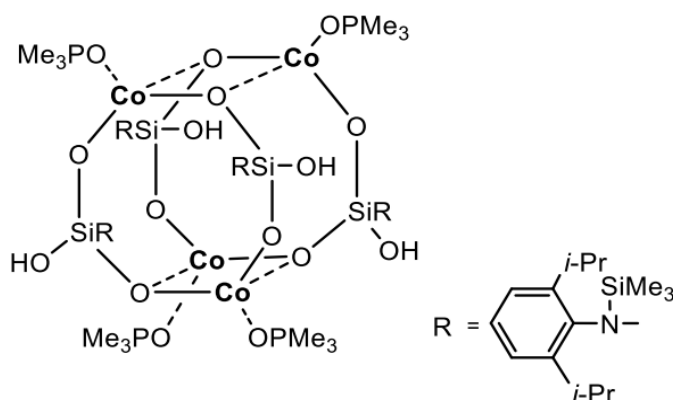


Figure 38. The structure of complex $[(\text{RSi}(\text{OH})\text{O}_2)\text{Co}(\text{OPMe}_3)]_4$ **28**.

Trinuclear cobalt-containing complex $[(\text{PhSiO}_{1.5})_{22}(\text{CoO})_3(\text{NaO}_{0.5})_6] \cdot 6\text{EtOH} \cdot \text{H}_2\text{O}$ **29** exhibits an unusual magnetic (spin glass) behavior [111]. X-ray diffraction studies reveal molecular structure of complex **29** with three peripheral fragments containing Co(II) ions connected by Co-O-

Na-O-Co links (Fig. 39). Each peripheral fragment contains seven silicon atoms, forming a distorted cubane-like architecture. These fragments are linked to the central silicon atom, which leads to the formation of an anisotropic triangular cluster molecule. Six Na^+ ions and three Co^{2+} ions ensure the electroneutrality of the cluster. The Co(II) ions have tetrahedral geometry with Co-Co distance vary in the range 6.679 – 6.869 Å (Co-O bond lengths vary from 1.927 to 1.976 Å). Cage-like molecules are well isolated in the crystal phase due to the presence of bulky phenyl groups at silicon atoms. EXAFS analysis confirmed the oxidation state of cobalt ions as +2.

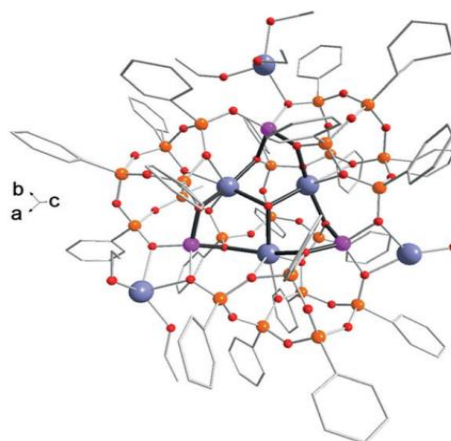


Figure 39. The structure of complex $[(\text{PhSiO}_{1.5})_{22}(\text{CoO})_3(\text{NaO}_{0.5})_6] \cdot 6\text{EtOH} \cdot \text{H}_2\text{O}$ **29**.

The temperature dependence of molar magnetic susceptibility for complex **29** reaches $11.09 \text{ cm}^3 \cdot \text{K} \cdot \text{mol}^{-1}$ at 300 K, which corresponds to the presence of three isolated Co(II) ions with $S = 3/2$ and $g_{iso} = 2.81$ [112]. Upon cooling down to 7 K, the χT value decreases to a maximum point of $10.47 \text{ cm}^3 \cdot \text{K} \cdot \text{mol}^{-1}$, and at 2 K the value becomes equal to $7.84 \text{ cm}^3 \cdot \text{K} \cdot \text{mol}^{-1}$ (Fig. 40). Weak ferromagnetic interactions between Co(II) ions *via* diamagnetic Co-O-Na-O-Co bridges explains the presence of a maximum of the χT value at low temperature.

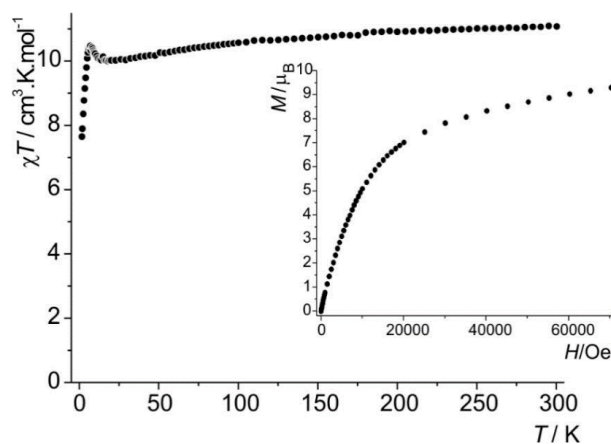


Figure 40. The temperature dependence of χT for **29** at 1000 Oe. Insert: the field dependence of magnetization for **29** at 1.8 K.

The temperature dependence of the alternative current (AC) susceptibility, its in-phase (χ'), and out-of-phase (χ'') components, measured in the zero-DC magnetic field in the 1 to 1500 Hz frequency range, shows a series of frequency-dependent peaks (Fig. 41, left). Given that the shortest Co^{II}-Co^{II} intercluster distances are quite large (>14.46 Å), we assumed that the presence of the magnetic transition is caused either by a superparamagnetic behavior of each metallasesquioxanes molecule or by a spin-glass behavior due to an intrinsic spin frustration of the individual MS. Furthermore, the memory effect experiments show a sharp jump in the magnetization versus time curve with the temperature change, proving the presence of a distribution of the relaxation times incompatible with superparamagnetic behavior (Fig. 41, right).

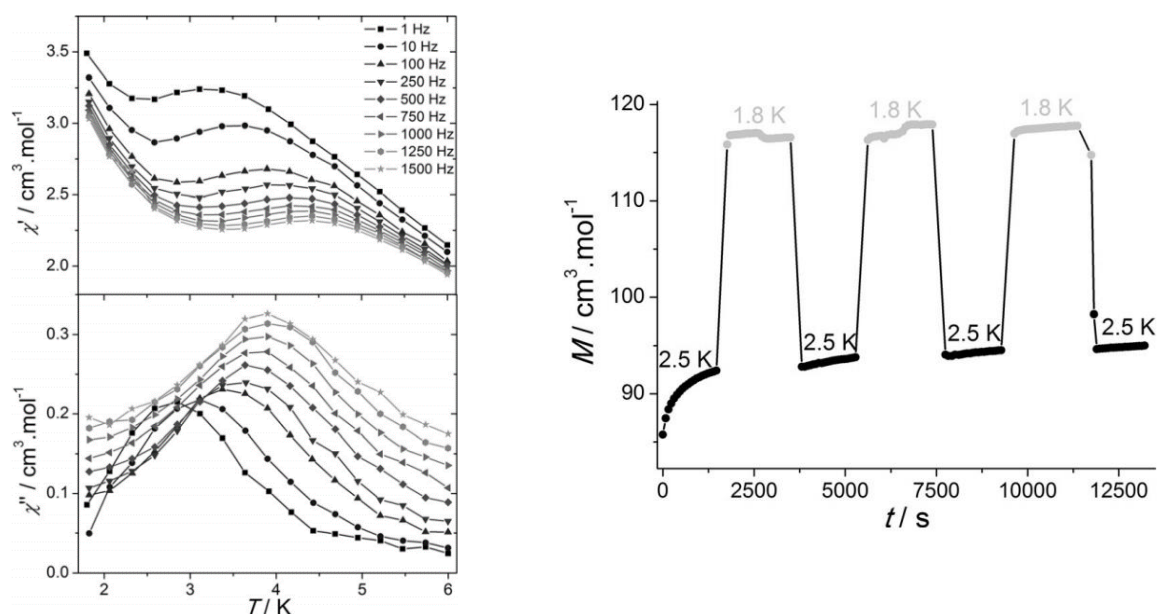


Figure 41. Left) Temperature dependence of the in-phase, χ' , and out-of-phase, χ'' susceptibilities with a zero DC magnetic field for **29**; right) Zero-field cooled (ZFC) relaxation curves ($H=20$ Oe) with temporary cooling. Solid lines are a guide for the eye.

The complex of $[(\text{PhSiO}_{1.5})_{10}(\text{CoO})_5(\text{NaOH})]$ composition **30** (Fig. 42) was described in [113]. Complex represents a cylindrical geometry with two siloxanolate $[\text{PhSi}(\text{O})\text{O}]_5$ cycles containing five Co(II) ions, adopting a distorted octahedral geometry. Cage encapsulates hydroxyl group in its cavity, while Na^+ ion, located outside the framework, ensures the electroneutrality of the complex. The central oxygen atom coordinates cobalt ions of the ring. The shortest Co-Co distance is equal to 2.77 Å (Fig. 42, right). For the central $[\text{CoO}]_5$ ring, Co-O bond lengths vary in the range 2.017 – 2.163 Å, Co-O-Co angles vary between 81.0 – 88.4 °. Molecules are well isolated from each other in crystal lattice, with the shortest intermolecular Co-Co distance being 11.30 Å.

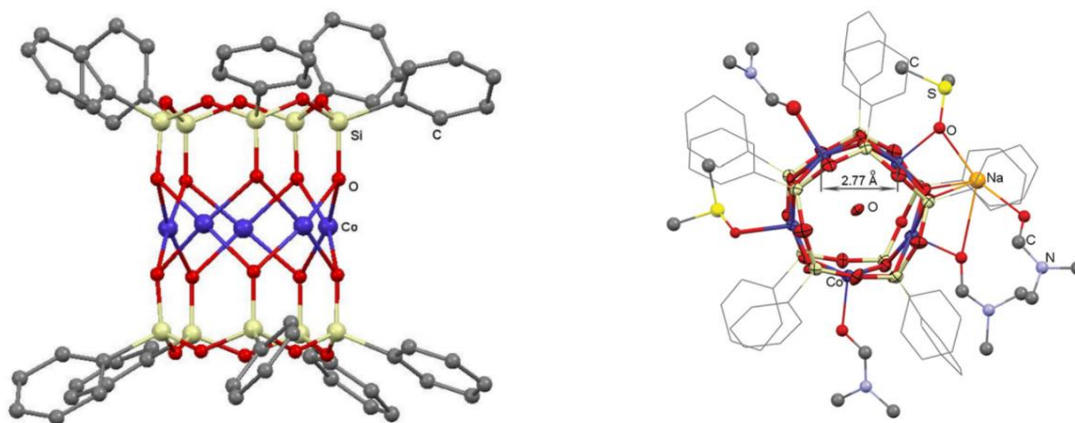


Figure 42. Structure of complex $[(\text{PhSiO}_{1.5})_{10}(\text{CoO})_5(\text{NaOH})]$ **30**.

The χT value of complex **30** reaches $19.08 \text{ cm}^3 \cdot \text{K} \cdot \text{mol}^{-1}$ at 300 K, which corresponds to the presence of five isolated Co(II) ions with $S = 3/2$ and $g_{\text{iso}} = 2.81$. Upon cooling, the χT value decreases demonstrating a plateau at 10 K ($\chi T = 3.71 \text{ cm}^3 \cdot \text{K} \cdot \text{mol}^{-1}$), then decreases to reach the value of $2.16 \text{ cm}^3 \cdot \text{K} \cdot \text{mol}^{-1}$ at 1.8 K (Fig. 43). The χT value of the plateau is in agreement with the ground state $S = 3/2$, while the strong decrease at low temperature can be imputed to a zero-field splitting phenomenon and antiferromagnetic interactions between Co(II) ions. The field dependence of the magnetization at 7 T yields a value of $M = 3.16 \mu_B$ at 1.8 K, without saturation, confirming the presence of magnetic anisotropy (Fig. 43, insert).

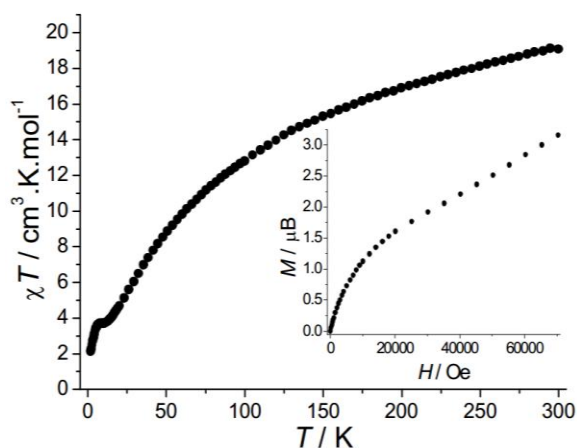


Figure 43. The temperature dependence of χT under 1000 Oe for **30**. Insert: the field dependence of M **30** at 1.8 K.

The temperature dependence of **30** of the in-phase (χ') and out-of-phase (χ'') ac components shows frequency dependent peaks (Fig. 44, left), indicating the occurrence of a short-range magnetic ordering arising from the slow dynamics of the magnetization. Such dynamics may arise from either the superparamagnetic behavior of each polynuclear complex or a spin-glass compartment induced by an intrinsic spin frustration and/or intermolecular interactions. At 1.8 K, a clear open hysteresis (memory) loop can be observed with a small coercive field of 65 Oe, which indicates the presence of blocking of

the magnetization. The magnetic irreversibility was additionally confirmed by the monitoring of magnetization following the ZeroField Cooled / Field-Cooled procedure (Fig. 44, right).

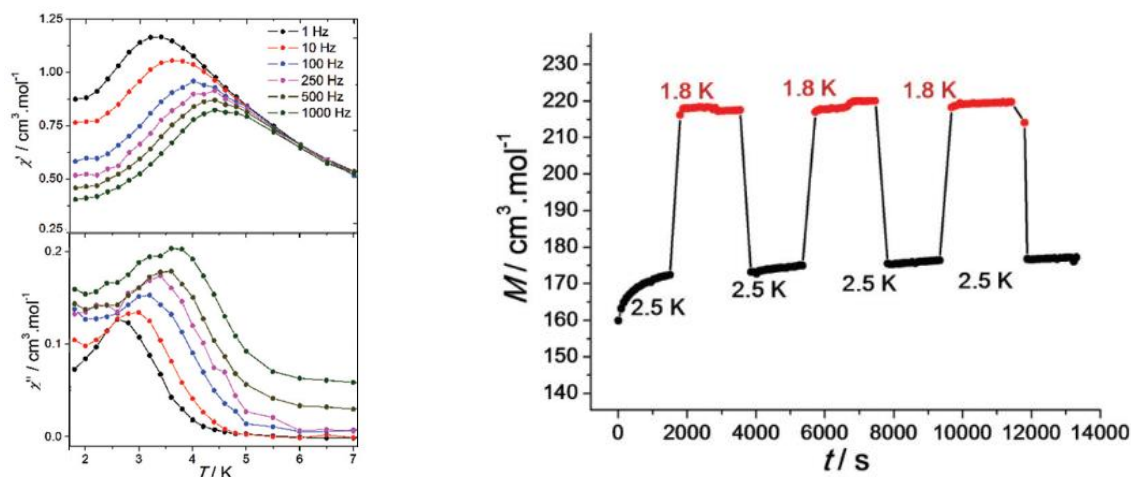


Figure 44. Left) Temperature dependence of the in-phase, χ' , and the out-of-phase, χ'' , susceptibilities with zero DC magnetic field for **30**; right) ZFC relaxation curve with temporary cooling (measured at 2.5 K and at 1.8 K) with an applied magnetic field of 100 Oe for **30**. Solid lines are the guide for the eye (right).

Two complexes $\{\text{Co}_8[(\text{MeSiO}_2)_4]_2(3,5\text{-Me}_2\text{Pz})_8\}$ **31** and $\{\text{Co}_8[(\text{PhSiO}_2)_4]_2(3,5\text{-Me}_2\text{Pz})_8\}$ **32**, where 3,5-Me₂Pz = 3,5-dimethylpyrazole (dimethylpyrazole) are discussed in [114]. Molecular structures of both products were revealed by X-ray diffraction analysis. Each compound contains eight cobalt atoms, four 3,5-Me₂Pz -ligands and two silsesquioxane ligands staggered with a rotation angle of 45.7 and 45.1 ° for **31** and **32** respectively (Fig. 45). Complexes exhibit a ring-like topology composed of two types of bridges: Co-O-Co and Co-N-N-Co. The Co-Co distances are in the range 3.13 – 3.18 Å and 3.11 – 3.18 Å for **31** and **32**, respectively. Eight Co(II) ions possess the same tetracoordinate tetrahedral geometry by coordinating two oxygen atoms from two silsesquioxane ligands and two nitrogen atoms from two 3,5-Me₂Pz -ligands with Co-O and Co-N bond lengths vary between 1.966 – 1.992 Å and 1.957 – 1.984 Å, respectively for **31**, and Co-N in the range 1.333 – 1.355 Å for **32**.

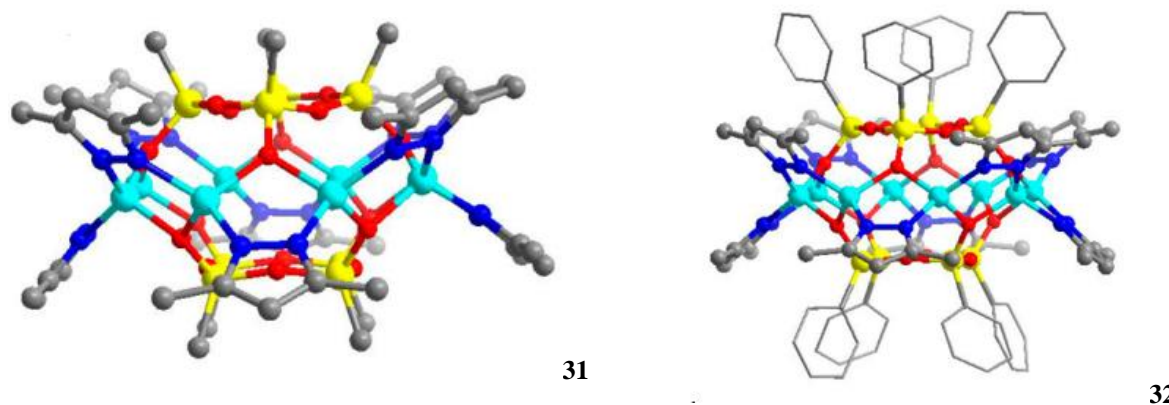


Figure 45. The structure of complexes $\{\text{Co}_8[(\text{MeSiO}_2)_4]_2(3,5\text{-Me}_2\text{Pz})_8\}$ **31** and $\{\text{Co}_8[(\text{PhSiO}_2)_4]_2(3,5\text{-Me}_2\text{Pz})_8\}$ **32**.

The magnetic susceptibility of **31** at 1 kOe increases monotonically from $\chi = 0.062 \text{ emu}\cdot\text{mol}^{-1}$ at 300 K to a local maximum of $\chi = 0.256 \text{ emu}\cdot\text{mol}^{-1}$ at 9.4 K, indicating antiferromagnetic interactions between Co(II) ions in a molecule (Fig. 46). However, dynamic magnetic measurements of **31** have not been mentioned in the articles.

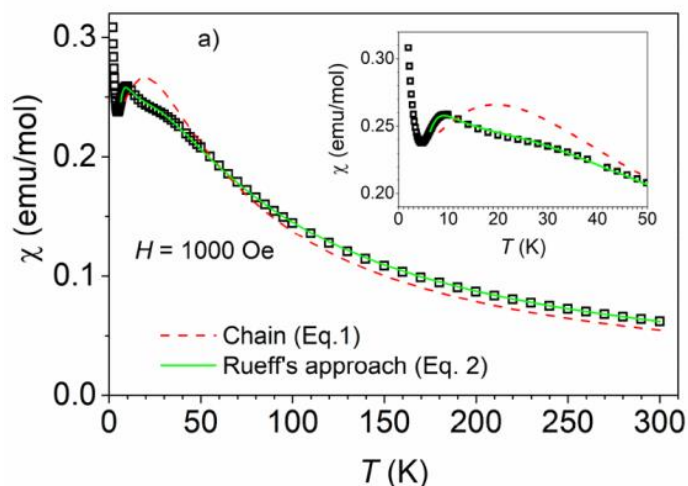


Figure 46. The dependences $\chi - T$ for **31**, the inset: the maximum susceptibility.

Complex $[\text{Co}_8(\text{OH})_2\{(\text{MeSiO}_2)_6\}_2(2,2'\text{-bipy})_2(3\text{-}O\text{-}2,2'\text{-bipy})_2]$ **33** which contains eight cobalt atoms, two hexameric silsesquioxane ligands $(\text{MeSiO}_2)_6^{6-}$, two 2,2'-bipyridine, two 3-*O*-2,2'-bipyridine and two $\mu^3\text{-OH}^-$ groups was described in [115] (Fig. 47). The metal-containing layer $\{\text{Co}_8\text{O}_{12}(\text{OH})_2\}$ located in the center of the complex is coordinated by two silsesquioxane ligands which are offset to each other. 12 siloxanolate oxygen atoms are not enough to satisfy the coordination of eight Co(II) ions. This provokes Co(II) ions to coordinate with additional 2,2'-bipy, 3-*O*-2,2'-bipy, and OH^- ligands to compensate charge of the whole cluster. Two $\mu_3\text{-OH}^-$ anions, located in the molecule center, act as bridging ligands to coordinate four cobalt atoms. Complex **33** includes four five-coordinated and four six-coordinated cobalt atoms. The Co-Co distances vary between 2.822 – 3.299 Å. The length of Co-O and Co-N bonds varies in the range 1.990 – 2.314 and 2.052 – 2.130 Å, respectively.

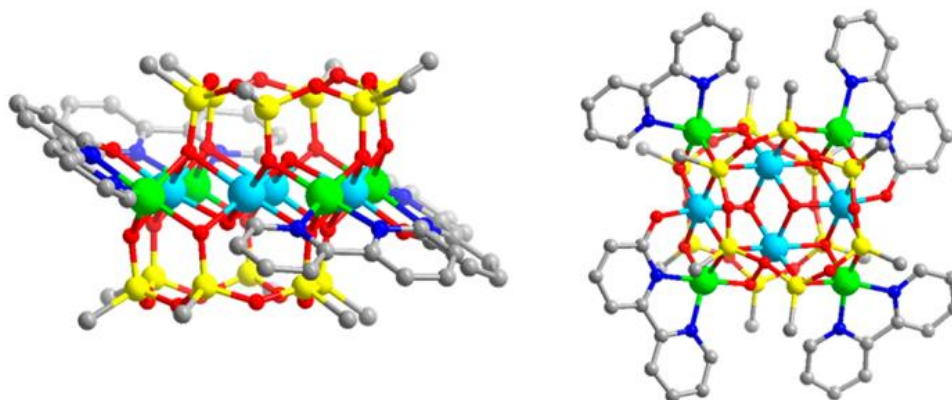


Figure 47. The structure of complex $[\text{Co}_8(\text{OH})_2\{(\text{MeSiO}_2)_6\}_2(2,2'\text{-bipy})_2(3\text{-}O\text{-}2,2'\text{-bipy})_2]$ **33**.

The magnetic analysis of complex $\{\text{Co}_8[(\text{MeSiO}_2)_4]_2(3,5\text{-Me}_2\text{Pz})_8\}$ showed antiferromagnetic interactions in complex **33**. The profile of the χT curve indicates the occurrence of dominant ferromagnetic interactions between Co(II) ions inside the cluster, mediated by oxygen bridges (the χT value equal to $23 \text{ emu}\cdot\text{K}\cdot\text{mol}^{-1}$ at 50 K and $72 \text{ emu}\cdot\text{K}\cdot\text{mol}^{-1}$ at 3.8 K) (Fig. 48, left). A peak occurs at 3.8 K, the experimental values of the magnetic susceptibility correspond to the ground spin state of $S = 12$. The temperature dependences of the out-of-phase susceptibilities χ'' measured in zero dc magnetic field are shown as full lines in Fig. 48 (right). The shift of the peak in χ'' was evaluated with the parameter $(\Delta T/T)/\Delta \log f = 0.11$, which is of the order typical for superparamagnetic systems. This suggests the occurrence of a slow relaxation of magnetization characteristic for SMMs rather than a spin-glass behavior.

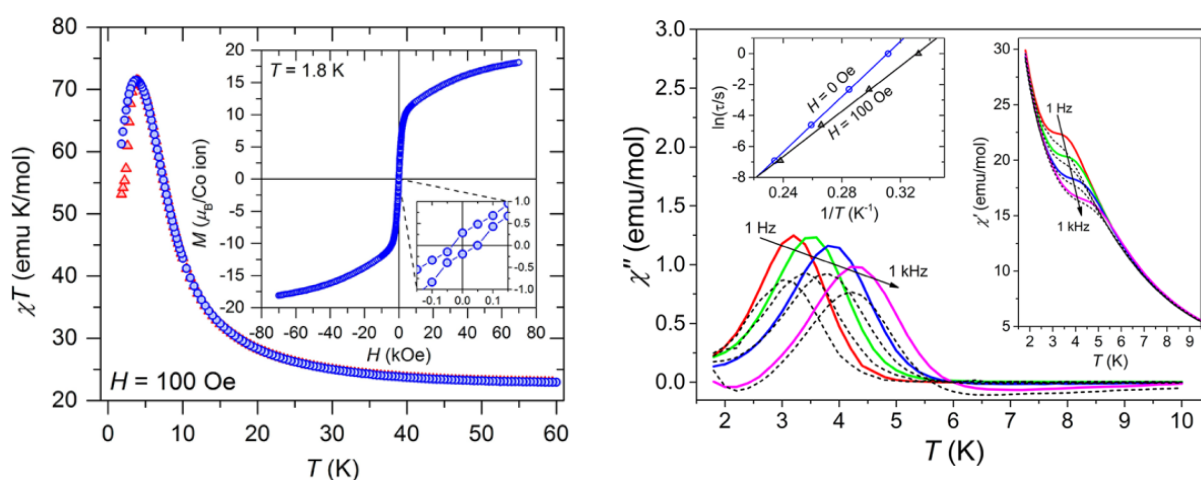


Figure 48. Left) The temperature dependence of χT of **33** is under 100 Oe. Inset: field dependence of the magnetization measured at 1.8 K; right) The temperature dependences of χ'' measured at 1 Hz (red), 10 Hz (green), 100 Hz (blue) and 1 kHz (violet) with zero permanent magnetic field (dashed black line - constant magnetic field 100 Oe).

To summary, Co(II)-containing magnetic silsesquioxanes are relatively rare despite promising features of this ion for magnetic architectures' design, probably due to the synthetic difficulties. The classical geometrical spin frustration, as well as the presence of competitive ferromagnetic and antiferromagnetic exchange interactions, conduct to the appearance of a spin-glass behaviour for a few of them.

Magnetic properties of Ni(II) - containing metallasilsesquioxanes

Polynuclear Ni(II)-containing silsesquioxanes constitute probably the most investigated family after the Cu(II)-based architectures. Nickel (II) has a $S = 1$ in the most usual octahedral environment. The anisotropy of Ni(II) ion is originated from the lift of the degeneracy of the spin triplet ground state induced by a small distortion of the ion geometry from a perfect octahedral crystal field [116]. Due to these interesting properties, Ni(II) ion has been widely used to design polynuclear magnetic architectures in association with various ligands [117]. The employment of the siloxane ligands permits the design of a large variety of polynuclear MS with different number of Ni(II) ions connected through oxygen atoms, in which different parameters governing magnetic interactions may be modified depending on the architecture's topology.

In this section, we describe a series of discrete Ni(II)-based silsesquioxanes with different nuclearity. In all these architectures, the magnetic properties are mainly governed by the environment and geometry of the nickel sites, Ni-O-Ni angles in the oxometallic core and Ni-O and Ni-Ni distances, as it was observed for their counterparts with classical coordination chemistry ligands.

Synthesis and magnetic properties of complex $\text{Na}[(\text{PhSiO}_2)_6\text{Ni}_6[(\text{PhSiO}_2)_6\text{Cl}]] \cdot 14\text{BuOH}$ **34** were described in refs [118] and [119]. Complex adopts a sandwich-like structure, with six Ni(II) ions coordinated by two $[\text{PhSiO}_2]_n$ ligands and BuOH solvent molecules (Fig. 49). Encapsulated Cl^- ion, located in the center void of the molecule, is compensated by Na^+ ion located outside of the cage. Ni-Cl bond lengths are equivalent and equal to 2.819 Å. All Ni(II) ions adopt tetragonal bipyramidal symmetry due to coordination with the four oxygen atoms of the silsesquioxane ligand, the oxygen atom from BuOH, and the central chloride ion. The Ni-O distances vary between 1.999 – 2.093 Å, Na-Cl = 5.28 Å, Ni-Ni = 2.845 – 2.863 Å. The O-Ni-O angle values vary in the range 79.9 – 170.7 °.

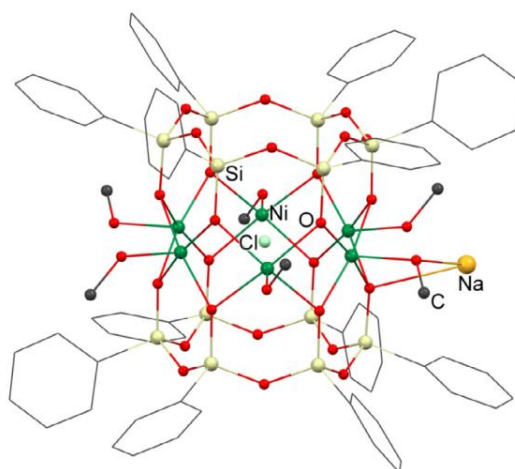


Figure 49. Structure of complex $\text{Na}[(\text{PhSiO}_2)_6\text{Ni}_6[(\text{PhSiO}_2)_6\text{Cl}]] \cdot 14\text{BuOH}$ **34**.

The value of magnetic susceptibility of **34** χT was found equal $8.4 \text{ emu}\cdot\text{K}\cdot\text{mol}^{-1}$ at room temperature, which is consistent with a system of six non-interacting spins ($\chi T = 8.64 \text{ emu}\cdot\text{K}\cdot\text{mol}^{-1}$ for $g = 2.2$). Upon cooling, the χT constantly decreases to zero value (Fig. 50). Upon decreasing of temperature, the molar susceptibility increases, reaching the peak value at 32 K, and then rapidly decreases, indicating the predominant antiferromagnetic interactions ($J = -18.6 \text{ K}$, $R = 2.63 \times 10^{-4}$). The authors attribute this behavior to the presence of independent exchange interactions between the central $\mu^6\text{-Cl}$ ion and six Ni ions.

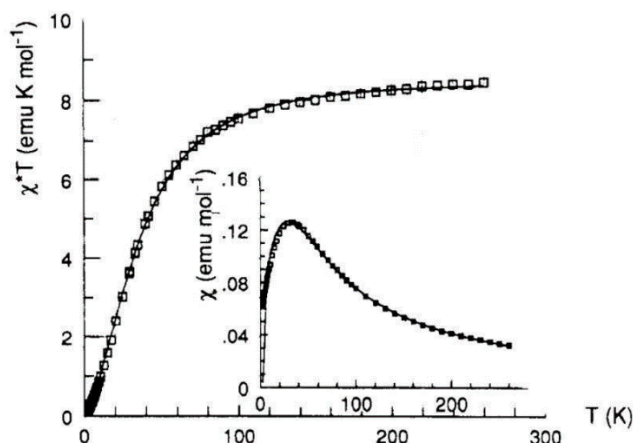


Figure 50. The $\chi T - T$ and $\chi - T$ dependences, experimental and calculated (solid lines) results of **34**.

Complex $\text{Na}_2[(\text{PhSiO}_2)_6\text{Na}_4\text{Ni}_4(\text{OH})_2(\text{O}_2\text{SiPh}_2)_6] \cdot 16\text{BuOH}$ **35** containing four Ni^{2+} ions and two Na^+ ions was reported in [120]. Metal-containing core of compound is sandwiched by two hexasilsesquioxane ligands displaced from the center by $54 - 56^\circ$ (Fig. 51). Electroneutrality of complex **35** is maintained by three $\mu^3\text{-OH}^-$ groups. Two Na^+ ions are located outside the complex and are coordinated by silsesquioxane ligands in “crown ether” manner. The Ni(II) ions adopt an octagonal coordination geometry. X-ray diffraction analysis revealed the following parameters of compound: $\text{Ni-O(H)} = 2.083 - 2.099 \text{ \AA}$, $\text{Ni-O(Si)} = 2.060 - 2.158 \text{ \AA}$, the Ni-Ni bond length is approximately 1.6 \AA , the angle Ni-O-Ni is in the range $94.8 - 95.8^\circ$.

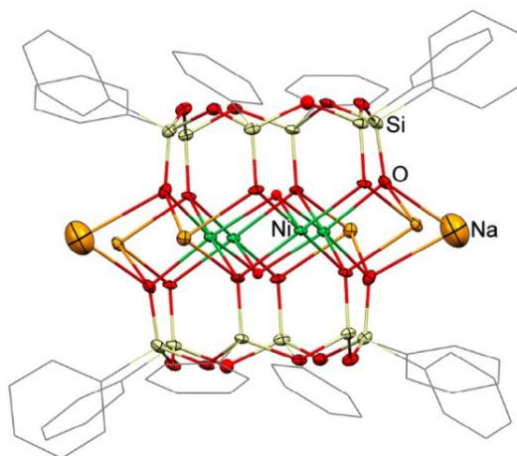


Figure 51. Structure of complex $\text{Na}_2[(\text{PhSiO}_2)_6\text{Na}_4\text{Ni}_4(\text{OH})_2(\text{O}_2\text{SiPh}_2)_6] \cdot 16\text{BuOH}$ **35**.

Upon cooling of complex **35** to 160 K the χT value reaches $5.7 \text{ emu}\cdot\text{K}\cdot\text{mol}^{-1}$ and then increases to a maximum value of $12.5 \text{ emu}\cdot\text{K}\cdot\text{mol}^{-1}$ at 8 K (Fig. 52). This data corresponds to the model of ferromagnetic coupling of moderate strength resulting from intramolecular interactions between four Ni(II) ions. At 2.3 K, value of χT reaches $11.7 \text{ emu}\cdot\text{K}\cdot\text{mol}^{-1}$, which corresponds to the spin state $S = 4$. Values of Ni-O-Ni angle ($94.8 - 95.8^\circ$) and the ferromagnetic properties in the complex **35** are consistent with published data on the dependence of the magnetic properties for Ni-containing complexes (e.g. β -NiO exhibiting Ni-O-Ni angle = 90°) [121].

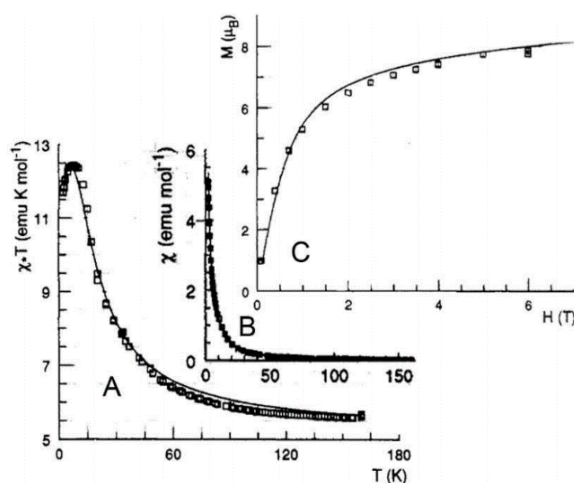


Figure 52. Magnetic behavior of **35**: **A** — χT - T dependence; **B** — χ - T dependence, **C** - magnetic field dependence.

Complex $\text{Na}\{[\eta^6\text{-(PhSiO}_2)_6]_2[\text{Fe(OR)}]_2\text{Ni}_4(\mu^6\text{-Cl})\}$ ($\text{R} = \text{H, Me}$) **36** was discussed in ref. [122]. Complex **36** represents a prismatic structure with an encapsulated Cl^- ion in the cage void (Fig. 53). The bond lengths for the Fe(III) and Ni(II) ions are significantly different: $\text{Fe-O} = 1.973 \text{ \AA}$, $\text{Ni-O} = 1.989 - 2.009 \text{ \AA}$, angle $\text{Ni-Fe-Ni} = 116.27^\circ$ (average values are given).

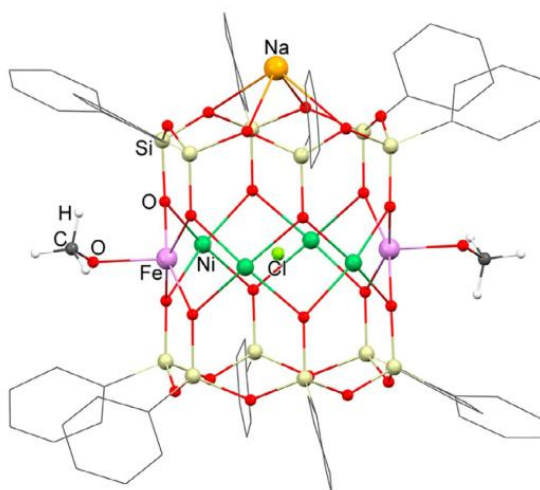


Figure 53. The structure of the complex $\text{Na}\{[\eta^6\text{-(PhSiO}_2)_6]_2[\text{Fe(OR)}]_2\text{Ni}_4(\mu^6\text{-Cl})\}$ **36**.

At $80 - 270 \text{ K}$, the molar magnetic susceptibility χ_M of complex **36** follows the Curie – Weiss law with constant $C = 14.5 \text{ emu}\cdot\text{K}\cdot\text{mol}^{-1}$ and the Weiss temperature $\theta = -15.3 \text{ K}$ (Fig. 54). The constant

C is consistent with an expected value for four high-spin Ni(II) ions ($S = 1$) and two high-spin ions Fe(III) ions ($S = 5/2$) [$14.3 \text{ emu}\cdot\text{K}\cdot\text{mol}^{-1}$ with $g(\text{Ni}) = 2.35$ and $g(\text{Fe}) = 2.00$].

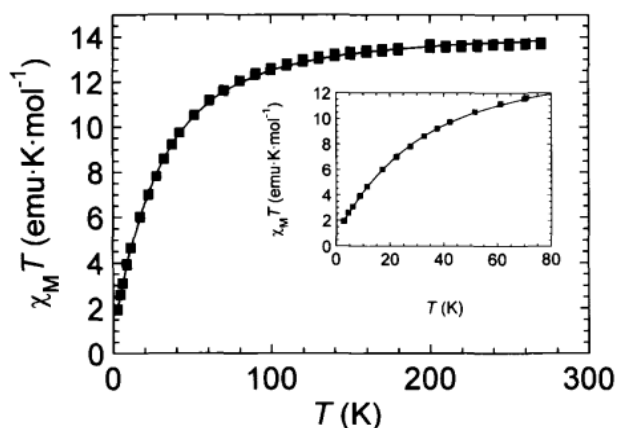


Figure 54. Magnetic behavior of complex **36**: Graph of $\chi_M T$ versus T in magnetic field of 1 T (calculated data presented as a solid line). The low temperature region is shown in more detail in the inset.

Approximation of the data of the dependence $\chi_M T - T$ at a low temperature ($T < 80 \text{ K}$) gave the exchange interactions between metal ions: $J_{\text{Ni-Ni}}^1 = -30.6 \text{ cm}^{-1}$, $J_{\text{Ni-Ni}}^2 = 3.9 \text{ cm}^{-1}$, $J_{\text{Ni-Fe}}^1 = 0 \text{ cm}^{-1}$, $J_{\text{Ni-Fe}}^2 = 5.5 \text{ cm}^{-1}$ and $J_{\text{Fe-Fe}} = 1.0 \text{ cm}^{-1}$ with $g = 2.13$. The resulting ground state of rotation possesses $S = 1$. Thus, the magnetic behavior of **36** is consistent with the presence of Ni-Ni ferromagnetic contributions mediated by bridging siloxanolate ligands and antiferromagnetic interactions of Ni-Ni, Ni-Fe, and Fe-Fe through the encapsulated Cl^- ion.

Complex $\text{Na}\{[\eta^6\text{-(PhSiO}_2)_6]_2\text{Co}_2\text{Ni}_4(\mu^6\text{-Cl})\}$ **37** was described in ref. [123] (fig. 55). Compound **37** characterizes by symmetrical hexagonal structure with the encapsulated Cl^- ion ($\text{M-Cl} \sim 2.880 \text{ \AA}$). The negative charge of the Cl^- ion is compensated by the presence of Na^+ cation located outside the cage (Fig. 58). Six metal ions adopt an octahedral coordination with (i) four oxygen atoms of silsesquioxane ligands, (ii) bridging Cl^- ligand, (iii) solvating DMF molecule (bond length $\text{M-O} \sim 2.035 \text{ \AA}$). Ni-O-Ni angles vary from 80.5 to 168.8° . The magnetic properties have not been measured in details [124].

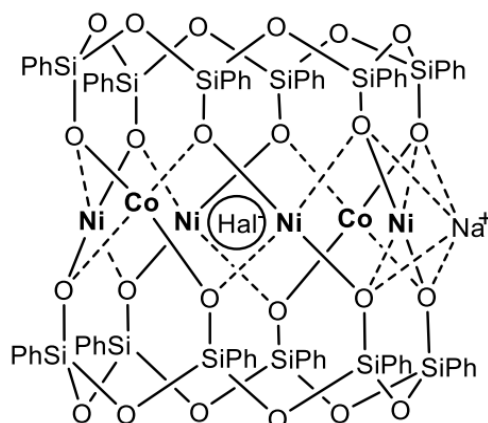


Figure 55. Structure of $\text{Na}\{[\eta^6\text{-(PhSiO}_2)_6]_2\text{Co}_2\text{Ni}_4(\mu^6\text{-Cl})\}$ **37**.

Two Ni(II)-containing complexes $[(\text{PhSiO}_{1.5})_{12}(\text{NiO})_6(\text{H}_2\text{O})(\text{DMSO})_9]$ **38** and $[(\text{PhSiO}_{1.5})_{10}(\text{NiO})_5(\text{NaOH})(\text{DMF})_7]$ **39** were reported in [125] (Fig. 56). The hexanuclear complex **38** has a cylindrical structure with an encapsulated water molecule in the center of the cage. The shortest intramolecular distances are Ni-Ni = 2.92 Å, Ni-O(Si) = 2.016 Å, Ni-O(H) = 2.938 Å. The architecture of complex **39** differs from **38** and contains five nickel(II) atoms. The encapsulated OH⁻ ligand is compensated by a presence of Na⁺ ion outside the framework. The smallest intramolecular distances are Ni-Ni = 2.70 Å, Ni-O(Si) = 2.0329 Å, Ni-O(H) = 2.061 Å.

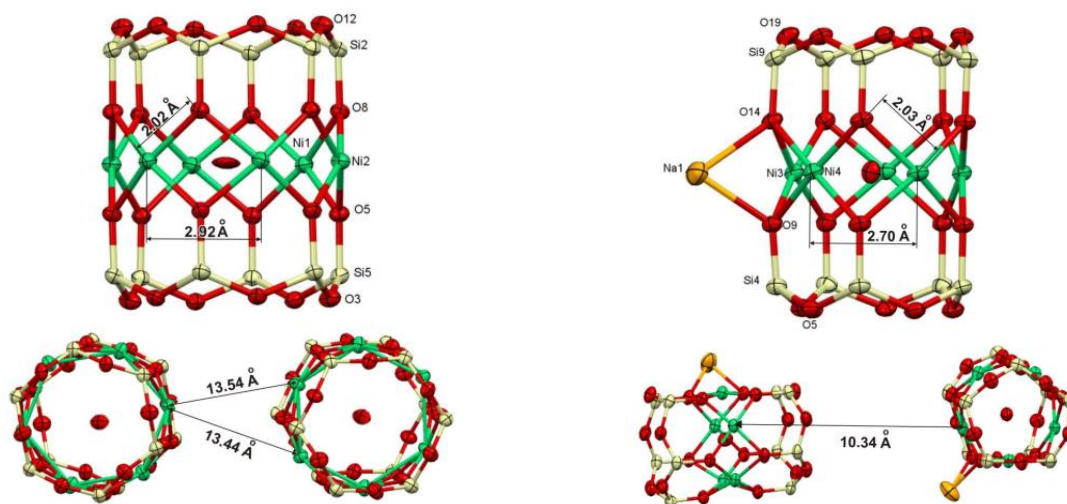


Figure 56. Structure of $[(\text{PhSiO}_{1.5})_{12}(\text{NiO})_6(\text{H}_2\text{O})(\text{DMSO})_9]$ **38** (left) and $[(\text{PhSiO}_{1.5})_{10}(\text{NiO})_5(\text{NaOH})(\text{DMF})_7]$ **39** (right).

The magnetic susceptibility of **38** and **39** was studied (Fig. 57). At 300 K, the value of **38**'s χT reaches $11.06 \text{ cm}^3 \cdot \text{K} \cdot \text{mol}^{-1}$ (theoretically calculated value of $8.26 \text{ cm}^3 \cdot \text{K} \cdot \text{mol}^{-1}$), which corresponds to six non-interacting high-spin Ni(II) ions. Upon cooling to 10 K, a maximum of the value $\chi T = 45.00 \text{ cm}^3 \cdot \text{K} \cdot \text{mol}^{-1}$ was observed. The obtained data confirm the presence of ferromagnetic interactions between all Ni²⁺ ions. The value $\chi T = 6.02 \text{ cm}^3 \cdot \text{K} \cdot \text{mol}^{-1}$, found for complex **39** at 300 K, is slightly higher than the value $5.51 \text{ cm}^3 \cdot \text{K} \cdot \text{mol}^{-1}$, expected for five non-interacting Ni(II). Upon cooling, χT continuously decreases, reaching a plateau at 12 K ($1.63 \text{ cm}^3 \cdot \text{K} \cdot \text{mol}^{-1}$), and then decreases strongly to $\chi T = 1.00 \text{ cm}^3 \cdot \text{K} \cdot \text{mol}^{-1}$ at 1.8 K. The presence of a nonzero plateau of χT may indicate the appearance of a spin frustrated system of a polynuclear complex. Upon heating, dominant antiferromagnetic interactions between metal ions are observed.

The studies of the magnetic properties of complexes **38** and **39** revealed a slow relaxation of magnetization induced by a similar spin-glass behavior, which is a consequence of spin frustrations in polynuclear complex and dipole interactions between metallasesquioxane molecules (the shortest Ni-Ni intermolecular distances are 13.54 and 10.34 Å for **38** and **39**, respectively).

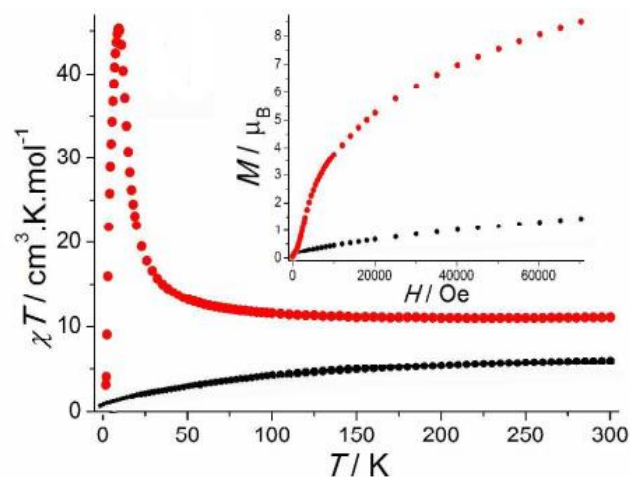


Figure 57. Temperature dependence of χT under a 1000 Oe DC magnetic field for **38** (black line) and **39** (red line).
Inset: field dependence of magnetization at 1.8 K.

The family of Ni(II)-containing complexes $[(\text{PhSiO}_2)_6]_2\text{Ni}_4\text{Na}_8(\text{O})_2$ **40**, $[(\text{PhSiO}_2)_5]_2\text{Ni}_5(\text{NaOH})$ **41**, $[(\text{PhSiO}_2)_7]_2\text{Ni}_2\text{Na}_{12}(\text{CO}_3)$ **42**, $[(\text{PhSiO}_2)_6]_2\text{Ni}_6$ **43**, $[(\text{PhSiO}_2)_6]_2\text{Ni}_4\text{Na}_4\text{K}_2(\text{OH})_2$ **44** and $[(\text{PhSiO}_2)_6]_2\text{Ni}_6\text{K}_{1.5}\text{Cs}_{0.5}\text{Cl}(\text{OH})$ **45** (Fig. 58) was reported in ref. [126]. The structural analysis of $[(\text{PhSiO}_2)_6]_2\text{Ni}_4\text{Na}_8(\text{O})_2$ showed that the compound may be described as a prismatic polyhedron with a metal center Ni_4 and two hexagonal ligands $[\text{PhSi}(\text{O})\text{O}]_6$. Sodium ions (in the composition of silanolate Si-O-Na fragments) compensate the charge of the whole complex. In principle, they also could participate in the formation of the metallasilsesquioxane coordination polymer structure [127]. Complex $[(\text{PhSiO}_2)_5]_2\text{Ni}_5(\text{NaOH})$ **41** possesses a cylinder shape of a cage with metal-containing Ni_5 layer. The presence of OH^- ligand, encapsulated in the center of cage' void, is compensated by the Na^+ ion located outside the structure. The architecture of **42** consists of two Ni^{2+} ions and two heptameric ligands $[\text{PhSi}(\text{O})\text{O}]_7$. The structure adopts a distorted prismatic geometry. Ten Na^+ ions, serving for the compensation of complex charge, are involved in the siloxanolate SiONa fragments. In addition, two sodium ions are found in composition sodium carbonate specie encapsulated in the inner void of cage. Six Ni(II) ions in complex **43** favors the organization of regular prismatic cage structure with two phenylsilsesquioxane $(\text{PhSiO}_2)_6$ ligands. Structure of complex **44** is similar to the type of the complex **40** and contains two $[\text{PhSi}(\text{O})\text{O}]_6$ ligands coordinating the central metal Ni_4 center and two potassium ions. External location of K^+ ions favors the assembly of 1D coordination polymer of **44** in crystal lattice. Complex **45**, containing six nickel ions (in the composition of cage) as well as external K^+ and Cs^+ ions, also aggregates into 1D coordination polymer structure.

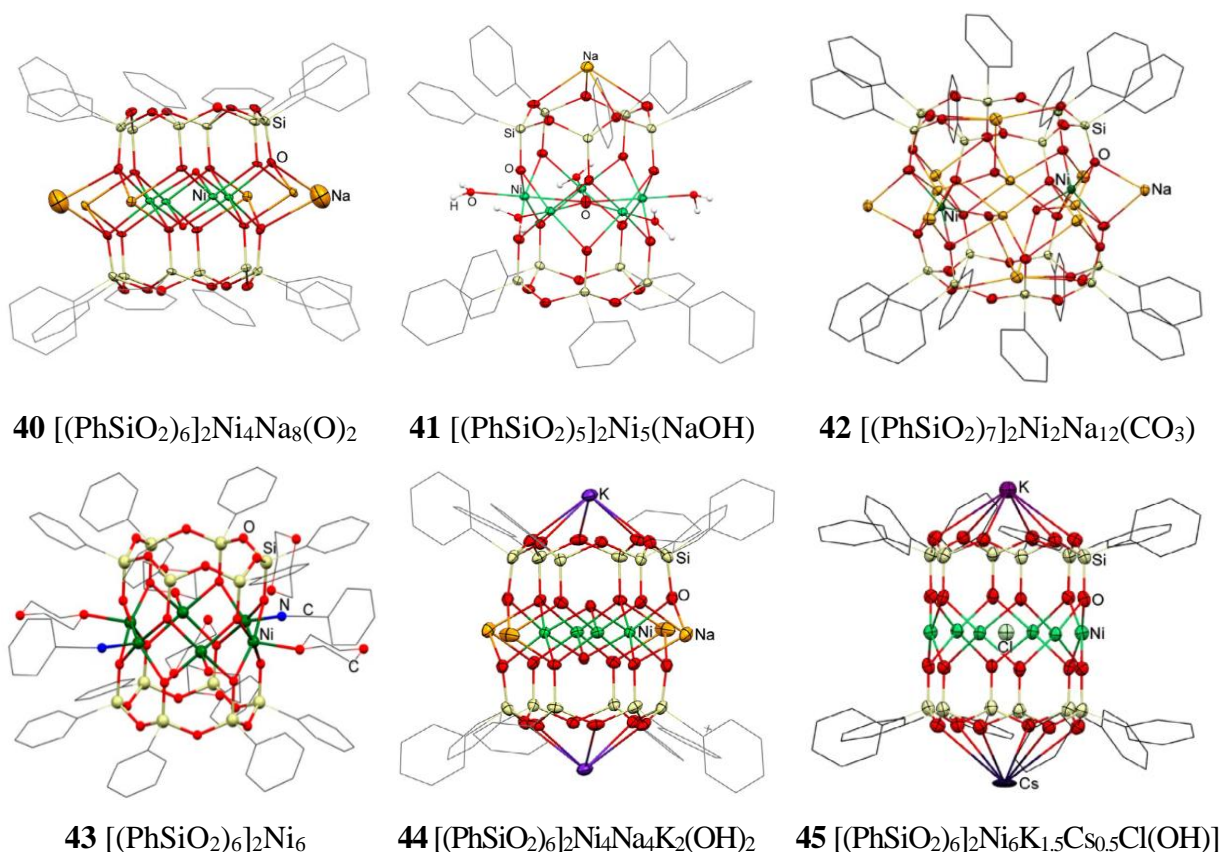


Figure 58. Structure of complexes **40** - **45**.

Magnetic susceptibilities of compounds **40** – **45** were also investigated (Fig. 59). The room-temperature values of χT for **40** – **44** correspond to those expected for corresponding quantity of isolated Ni^{2+} octahedral ions. Upon cooling to 150 K, samples **40**, **42**, and **43** demonstrate a plateau of χT values, and deviations from the Curie law upon further cooling. The observed positive deviations indicate the dominant ferromagnetic interactions between Ni^{2+} ions and show maximum $\chi T = 9.23$ (6 K), 3.68 (8 K), and 13.91 (8.5 K) $\text{cm}^3 \cdot \text{K} \cdot \text{mol}^{-1}$ for **40**, **42**, and **43**, respectively. The maximum χT values are lower than the theoretically calculated 11.02 $\text{cm}^3 \cdot \text{K} \cdot \text{mol}^{-1}$ ($S = 4$, $g = 2.1$) and 23.1 $\text{cm}^3 \cdot \text{K} \cdot \text{mol}^{-1}$ ($S = 6$, $g = 2.1$) for **40** and **43**, assuming ferromagnetic interactions between all nickel ions. The sharp decrease χT at lower temperatures for **40**, **42**, and **43** induced by splitting in the zero-field and/or intermolecular interactions.

At room temperature, χT for compound **44** reaches 4.04 $\text{cm}^3 \cdot \text{K} \cdot \text{mol}^{-1}$, which is slightly lower than the value 4.40 $\text{cm}^3 \cdot \text{K} \cdot \text{mol}^{-1}$ expected for four noninteracting Ni^{2+} octahedral ions with $g = 2.1$. The minimum value $\chi T = 3.25$ $\text{cm}^3 \cdot \text{K} \cdot \text{mol}^{-1}$ was observed at 60 K. The further cooling causes sharp increase of χT value (5.87 $\text{cm}^3 \cdot \text{K} \cdot \text{mol}^{-1}$ at 8 K). This shape of the $\chi T - T$ curve reflects the appearance of competitive antiferromagnetic and ferromagnetic interactions inside the tetranuclear complex mediated by various magnetic pathways.

At room temperature, compounds **41** and **45** demonstrate χT values much lower than expected for isolated Ni^{2+} ions, indicating antiferromagnetic interactions. Upon cooling, the χT continuously

decreases, reaching a plateau at 14 K for both compounds, and then sharply decreases at a low temperature. All studied compounds, except for the binuclear compound **42**, exhibit a slow relaxation of magnetization. Nuclearity as well as structural arrangement of Ni(II) ions in the cage framework play an important role in magnetic properties.

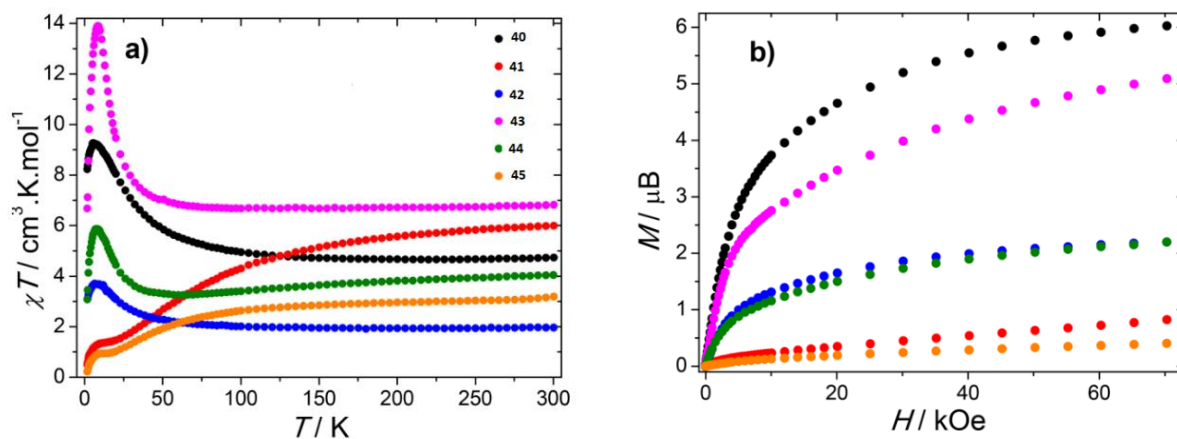


Figure 59. The temperature dependence of χT in a direct current field of 1000 Oe (left); the field dependence of magnetization at 1.8 K (right).

In summary, Ni(II)-based cage like siloxanes present a wide family of interesting molecule-based architectures, as well as interesting magnetic properties. The most interesting feature considering their magnetic properties consists in the appearance of a slow relaxation of the magnetization, which has been observed not only for crown type of topology with an odd number of spin carriers, but also in the case of six numbered oxo-nickel rings. Indeed, the important quantity of magnetic exchange pathways with different Ni(II)-L-Ni(II) angles through the peripheral siloxanates and through the central O or Cl⁻ creates a competition between ferromagnetic and antiferromagnetic interactions leading to the appearance of slow relaxation of the magnetization and a spin glass-like behaviour.

Synthesis, structures and properties of Ln(III) - containing sesquioxanes

Polynuclear silsesquioxanes architectures containing Ln³⁺ ions are relatively scarce, which is surprising considering a great interest in lanthanide(III) ion-containing polynuclear architectures. Surprisingly, the number of works devoted to the design of MS involving lanthanide ions are relatively scarce despite the great interest in their employment in molecule-based materials. Indeed, lanthanide-based complexes of different nuclearity and their extended structures saw a huge development in recent years owing to exceptional magnetic and optical properties. Regarding the topologies of siloxane ligands, two groups of compounds, namely, macrocyclic [RSiO_{1.5}]_n and incompletely condensed silsesquioxanes would be considered in this chapter [128].

The Zhdanov group reported a family of compounds based on macrocyclic ligands with the general composition Na₆{[PhSiO₂]₈Ln₄(μ⁴-O)[O₂SiPh]₈} • 10 EtOH • 8 H₂O for Ln = Nd³⁺ **46**, Gd³⁺ **47**, Dy³⁺ **48** [129, a-b]. Sandwich-like geometry of these clusters consists of two phenylsiloxane ligands and four ions with flat square coordination: Nd³⁺ in **46**, Gd³⁺ in **47**, and Dy³⁺ in **48** (Fig. 60). Compounds encapsulate oxygen atom, playing a role of additional stabilizing μ⁴-O₂ bridge. Six Na⁺ ions locate in the external coordination sphere of complexes, four of them coordinate siloxane ligands in “crown ether” manner.

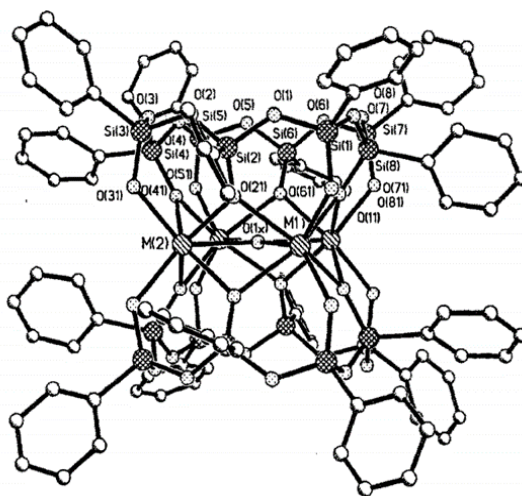


Figure 60. Molecular structure of complexes **46** - **48**.

The structure analysis of complexes **46** - **48** showed that the Ln-*t*-O_{Ln} bond lengths (*t*-O_{Ln} is the peripheral oxygen atom) vary in the range 2.328 – 2.359 Å for **46**, 2.26 – 2.33 Å for **47**, and 2.26 – 2.28 Å for **48**. Ln-μ⁴-O²⁻ bond length vary in the range 2.401 – 2.438 Å for **46**, 2.32 – 2.42 Å for **47** and 2.33 – 2.34 Å for **48**. The magnetic properties of these complexes were investigated, but not in details [130]. The authors mentioned about the measurements of the magnetic moment of Na₆{[PhSiO₂]₈Nd₄(μ⁴-O)[O₂SiPh]₈} • 10 EtOH • 8 H₂O **46**, which is equal to 6.42 μ_B and which is

close to the expected value for six unpaired electrons ($\mu_{eff} = 6.93$ mB) and corresponds at the possibility of indirect Nd-Nd interactions.

Complex of $K_5\{[ViSiO_2]_8La_4(\mu^4-OH)[O_2SiVin]_8\} \cdot 5BuOH \cdot 2H_2O$ composition **47** (Fig. 61), containing the central bridging ligand μ^4-OH^- , was also reported by Zhdanov group [131]. A feature of the complex is a three-dimensional structure assembled *via* external K^+ ions.

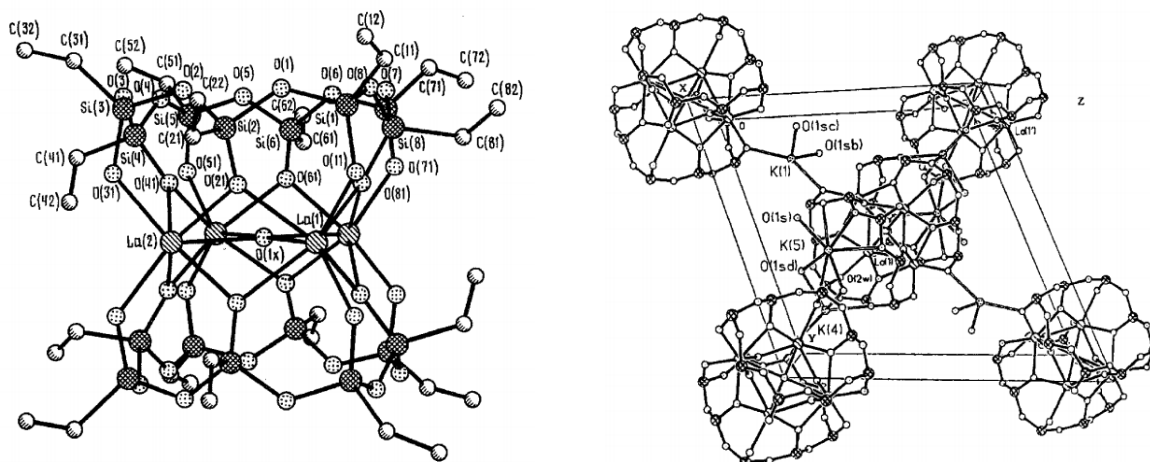


Figure 61. Structure and crystal packing of complex $K_5\{[ViSiO_2]_8La_4(\mu^4-OH)[O_2SiVin]_8\} \cdot 5BuOH \cdot 2H_2O$ **47**.

The central μ^4-OH ligand adopts unusual square-plane coordination (La-O(H) bond lengths vary in the range 2.62 – 2.73 Å, La-O(H)-La angles vary in the range 89.8 – 90.2°). The value of La-OLa bond corresponds to the sum of the ionic radii of La^{3+} and O^{2-} (an average value is 2.48 Å) [132]. Magnetic properties of this complex were not reported.

Another family of Ln(III)-containing compounds characterized by the presence of "partially condensed sesquioxane" [133]. In literature, such compounds are referenced as "smallest particles of silica possible" [134] or "small soluble chunks of silica" [135]. Incompletely condensed sesquioxanes, such as $Cy_7Si_7O_9(OH)_3$ (Fig. 62), have structural similarities with β -tridimite and β -cristobalite. They are convenient ligands for the formation of complexes with alkaline [136, a-e], transition [137, a-b] and rare earth [138, a-d] metals. However, the studies of rare earth metallasilsesquioxanes are limited due to the complexity of crystallization and characterization of these compounds [139].

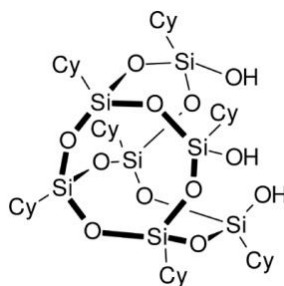


Figure 62. Incompletely condensed silsesquioxanes ligand (Cy - cyclohexane).

Some types of Ln(III)-based complex with incompletely condensed silsesquioxane were also reported. First type consists in the one Ln³⁺ and one siloxane ligand: [Cy₇Si₇O₁₂Ln(THF)_n] (Ln = La, Pr, Eu, and Yb) and [Cy₇Si₇O₁₂Ln(PMDTA)] (PMDTA = pentamethyldiethylenetriamine, Ln = La, Yb) [140]. The second one developed by Edelmann group consists on dimeric products [{"Cy₇Si₇O₁₂]₂Li₄}YbN(SiMe₃)₂ **48** [141], Cp*₂Sm[μ-Cy₇Si₈O₁₂O]₂Li • THF **49** [142], [Sm(OC₆H₃Bu^t_{2-2,6}){Cp₇Si₇O₉(OLi)(O)(OTBDMS)}₂] (TBDMS = *tert*-butyldimethylsilyl trifluoromethanesulfonate) **50** [143], [{"Yb(Cy₇Si₇O₁₁(OSiMe₃))(THF)₂]₂(PhNNPh) **51** [144], and two Nb(III) complexes [Cy₆Si₆O₁₁NbOEt]₂ **52** and [Cy₇Si₇O₁₂NbOEt(μ-OEt)]₂ **53** [145] (Fig. 63). All complexes were characterized by X-ray diffraction analysis, but their physical properties have not been studied.

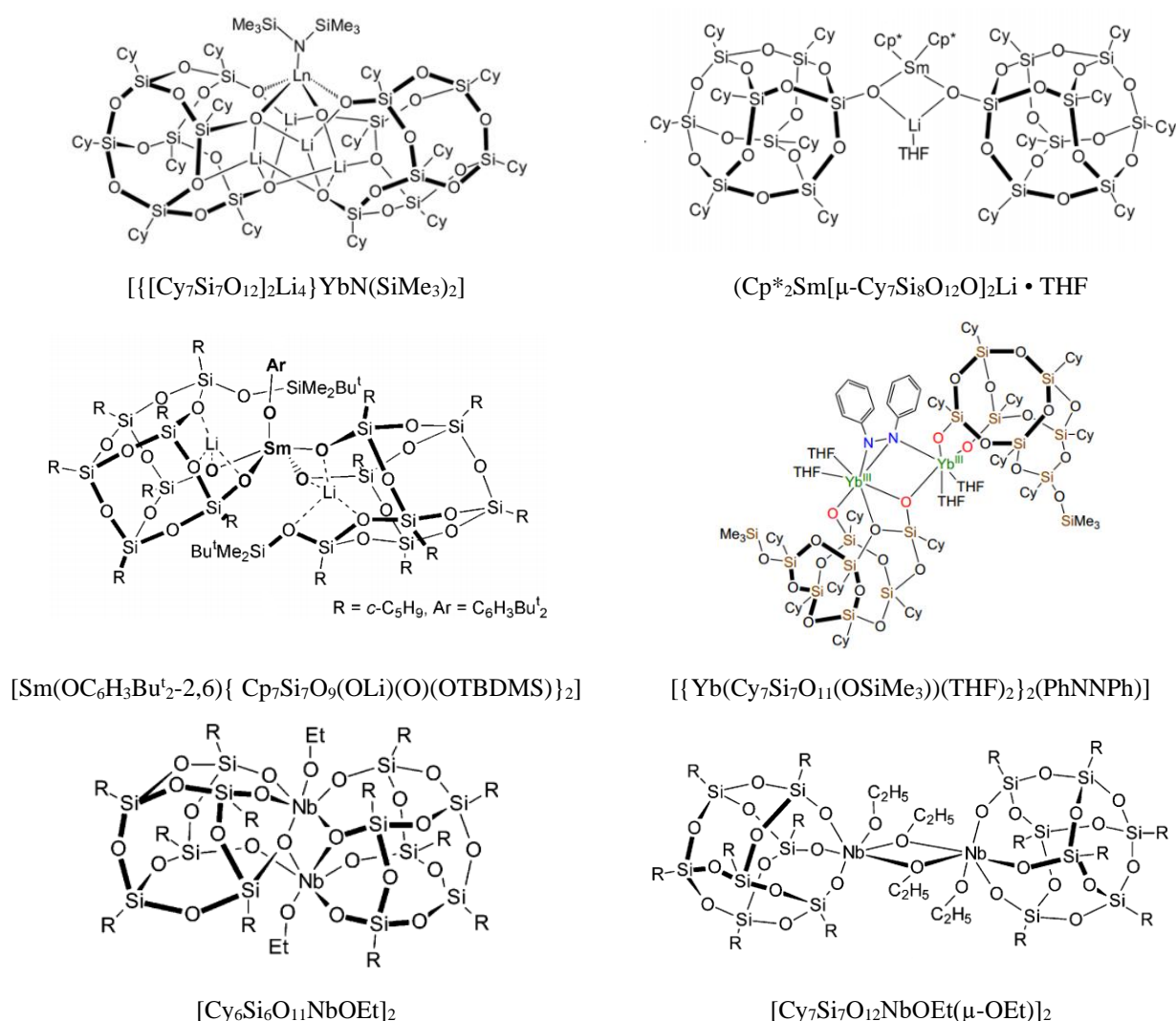


Figure 63. Structure of complexes **48** - **53**.

Tetranuclear complex [(Bu₇Si₇O₁₂Nd)₄NaCl] **54** (Fig. 64) was described in ref. [146]. X-ray diffraction analysis revealed that complex **54** includes four Nd atoms. Each Nd ion is coordinated by five oxygen atoms of Si-ligands. Cl⁻ ion, located in the center of the complex, coordinates all four Nd

ions (distance Nd- Cl = 2.5742 Å). As a result, each Nd ion is six-coordinated, forming a distorted octahedron. The Na⁺ counterion balances the sum charge of complex.

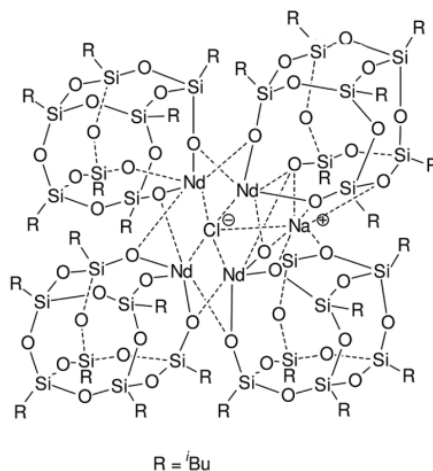


Figure 64. Structure of complex [(Bu₇Si₇O₁₂Nd)₄NaCl] **54**.

Asymmetric bimetallic complex Cy₂₁Si₂₁O₃₆(SiMe₃)Er₂(THF)₂Li₄Cl₂ **55** was reported in ref. [147]. Structure **55** consists of three Si-containing ligands, coordinating two Er³⁺ ions and four Li⁺ ions (Fig. 65). One of these Si ligands was accidentally functionalized by trimethylsilyl fragment attached to the one of Si-OH groups. Structural analysis of **55** revealed different coordination environment of lithium ions: two of them (LiO₄ and LiO₂Cl₂) are tetracoordinated, while the rest (LiO₅ and LiO₄Cl) are pentacoordinated.

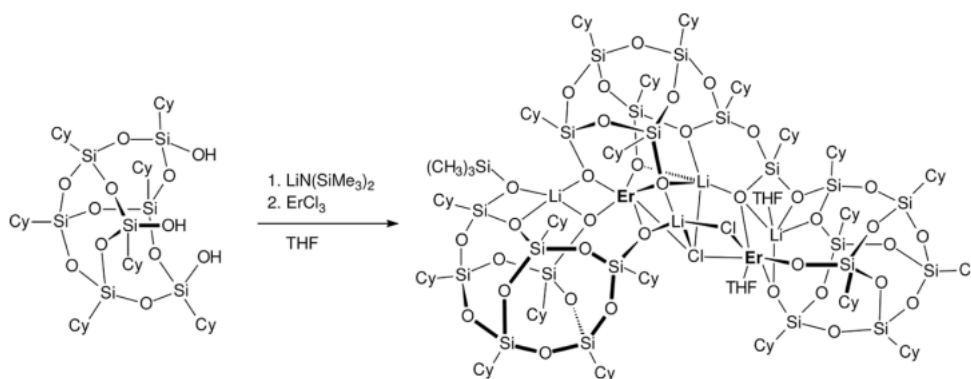


Figure 65. Synthesis of Cy₂₁Si₂₁O₃₆(SiMe₃)Er₂(THF)₂Li₄Cl₂ **55**.

For all these above described Ln³⁺-based siloxanes the photoluminescence properties have never been described. The emission spectra have been reported only for two Eu³⁺-based compounds, but their crystal structures have not been solved. The first example is complex **56** (Fig. 66), obtained by the reaction of anhydrous EuCl₃ and a solution of triethylamine and heptaisobutylsilanetriol, [148].

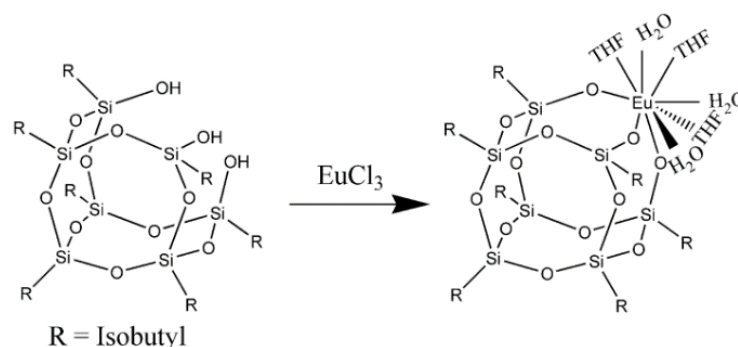


Figure 66. Synthesis of complex **56**.

Its photoluminescent properties were studied in chloroform solution (Fig. 67). Excitation spectrum registered for $\lambda_{em} = 615$ nm represents wide absorption band from 250 to 350 nm ($\lambda_{max} = 320$ nm) and narrow emission peaks relative to the intra- $4f_6$ electronic levels of Eu^{3+} (${}^5\text{D}_0 - {}^7\text{F}_j$ ($J = 0-4$)). Two absorption spectra were registered for $\lambda_{ex} = 320$ nm and 395 nm. Transitions characteristic of the Eu^{3+} ion was detected for two ${}^5\text{D}_0 - {}^7\text{F}_2$ excitation waves.

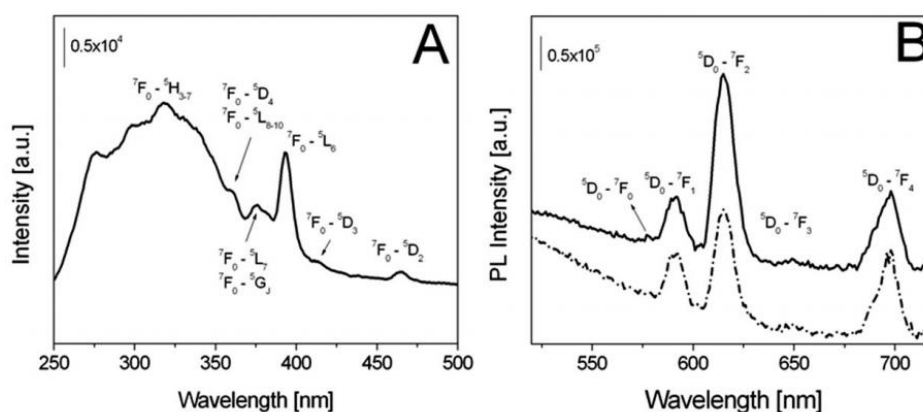


Figure 67. Excitation and emission spectra for **56**.

The second complex **57** built with $\text{Bu}_7\text{Si}_7\text{O}_9(\text{OH})_3$ ligand (Fig. 68) was reported in ref. [149].

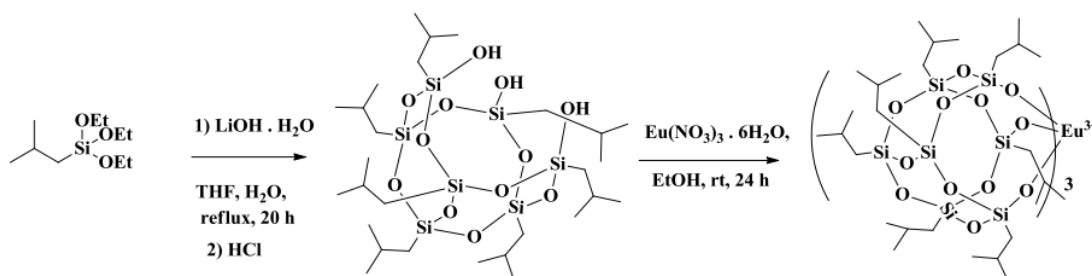


Figure 68. Synthesis of complex **57**.

Excitation spectrum (Fig. 69) of **57** at 618 nm represents set of wide bands (center is about 360 nm) [150]. The emission spectra registered for 466, 395 and 363 nm correlate with the characteristic

radiation of Eu^{3+} ion (558, 581, 592, 619 and 690 nm). The most sensitive transition is the ${}^5\text{D}_0 - {}^7\text{F}_2$ one, which indicates a low symmetry of the europium ion in the complex.

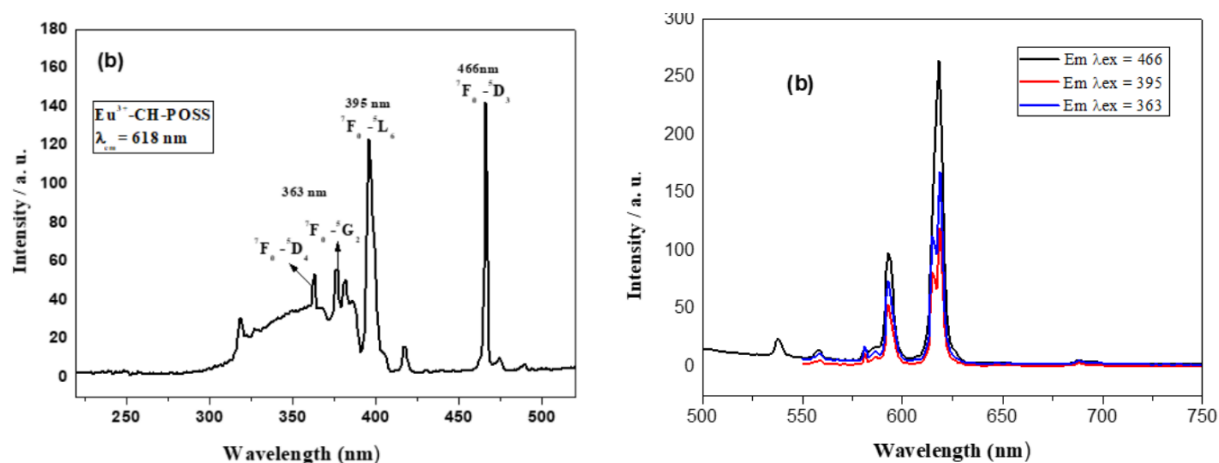


Figure 69. Excitation and emission spectra for Eu^{3+} -CH-POSS.

In summary, Ln(II)-containing silsesquioxanes are a quite perspective materials with potentially multifunctional properties such as magnetic and luminescent. However, to the best of our knowledge, the detailed investigations of magnetic properties have never been reported in the literature up to now and only two examples focus on investigation of photoluminescence, but the crystal structures of these complexes have not been reported. Note also that the Tb^{3+} -containing silsesquioxanes have never been synthesized up to now.

The aim and the objectives of this work

The sil- and germesquioxane ligands are an efficient and promising tool for design of metal ion or lanthanide-derived architectures, as shown in the literature review. It is important to note that the sesquioxanes containing transition metal ions (such as Cu(II) , Fe(III)) recently showed high catalytic activity in the reaction of amides (amides - structural components of $\sim 25\%$ of existing drugs). Moreover, the metallasesquioxanes are highly active in the homogeneous oxidative functionalization of hydrocarbons (alkanes, arenes, alcohols), representing both, high yields of oxidation products and good regioselectivity of reactions. Thus, the synthesis of new MSs and investigation of their catalytic activity constitutes the first direction of this work. On the other hand, metallasesquioxanes containing spin carriers with a relatively important magnetic anisotropy (Co(II) , Ni(II) , Fe(III) or some lanthanides) are capable to exhibit in certain structures interesting effects of slow relaxation of the magnetization, such as spin-glass or single-molecular magnetic behaviors.

Therefore, the synthesis of new molecule-based architectures with magnetic properties is the second direction of this PhD thesis.

Noteworthy that before we started this PhD thesis, cage-like metallagermaniumsesquioxanes were described in the literature only by a single publication. At the same time, a strong individuality bringing by germesquioxane ligands (in comparison to silsesquioxanes) points out their significant potential in design of metal or lanthanide-based architectures.

Secondly, the self-assembly of MSs in the presence of additional organic ligands were studied on only a few reported examples. At the same time, this approach is of utmost interest due to the opportunity to obtain principally new molecular architectures *via* interaction (or competition) of sesquioxanes and organic ligands. Moreover, the use of such heteroleptic metal complexes in catalysis is attractive due to the possible stabilization of the catalytically active species by additional organic ligands.

Another promising direction consists in the study of lanthanide derivatives of the metallasesquioxanes family due to the high magnetic anisotropy of lanthanide ions and their photoluminescence. Noteworthy, family of lanthanide-based sesquioxanes remained comparatively scarce and study of these objects was limited exclusively to a discussion of the peculiarities of synthesis and structure (without a detailed study of their properties). The study of the magnetic and photophysical properties of MS frameworks remained practically unexplored to date.

In this line of thought and taken into account the above presented state-of-the-art, **the aim of this PhD work consists in the synthesis of several families of sil- and germesquioxanes containing transition metals and lanthanides and investigation of their catalytic, magnetic and luminescent properties.**

We focused on following objectives:

1) To develop the synthetic methods for the preparation of Cu(II)-silsesquioxanes complexes founded on two independent synthetic routes: *i*) self-assembling reactions, based on excellent ability of alkoxysilanes to assembly into various (cyclic, acyclic, condensed) architectures with coordinate Cu²⁺ ions; and *ii*) transmetalation procedures consisting in replacement of metal ions in the polynuclear metallasiloxane based architectures by different metal ions. To investigate the steric factors organic substituent at the silicon atoms on the complex topology, the solvent effect on framework nuclearity (DMSO, DMF, pyridine), the effect of bidentate N-containing ligands (2,2'-bipyridine, 1,10-phenanthroline, bathophenanthroline, and 3,5-dimethylpyrazole) on the formation of supramolecular packing and the effect of bidentate P,P-ligands (1,2-bis(diphenylphosphino)ethane and 1,2-bis(diphenylphosphino)methane) on the architecture of Cu(II)-silsesquioxanes. The control of the geometry of polynuclear complexes will be provided by tuning the synthetic conditions including the proper choice of solvent systems, the temperature, and combinations of metal ions.

- 2) To synthesize Cu(II)-germsesquioxanes based on two independent synthetic routes: *i*) self-assembling reactions; and *ii*) transmetalation procedures. To investigate the influence the stoichiometric ratio of reagents to the geometry and nuclearity of polynuclear complexes.
- 3) To investigate the catalytic properties for Cu(II)-based siloxanes and germoxanes and their magnetic properties.
- 4) To synthesize Ni(II)-based siloxanes and germoxanes using self-assembling approach and investigate their magnetic properties.
- 5) To develop the synthetic methods for the preparation of Ln(III)-silsesquioxanes complexes by self-assembling reactions. To investigate their magnetic and optical properties.

RESULTS AND DISCUSSION

Chapter 1. Cu(II) - silsesquioxanes: synthesis, structure and catalytic properties

1.1. Compounds based on structural fragment MeSiO_{1.5}

A wide range of copper(II)-containing silsesquioxanes (these compounds possess high catalytic activity, as shown in the literature review) was of significant interest in the context of investigation of various factors influencing structure of products. At the first stage, an effect of steric factors (introduced by the different nature of the organic substituent at the silicon atoms) was studied. Methylsilsesquioxanes were chosen as objects with a lower steric hindrance (and then compared to bulkier phenylsilsesquioxanes).

It is worth mentioning that the number of known Cu(II)-based methylsilsesquioxanes was limited to a few examples [151, a-c]. Nevertheless, these results demonstrated significant prospects for the use of methylsilsesquioxane structural matrix for the assembly of unusual high-cluster compounds, in particular, octa- [151, a] or deca- [151, b] nuclear ones. The most interesting example is the octa-nuclear product [(MeSiO_{1.5})₈(CuO)₈(DMF)₉(pz)], containing an encapsulated pyrazine molecule [152] in the inner cavity of the prismatic product. The development of this approach (assembly of prismatic compounds with higher, in comparison to classical hexanuclear, nuclearity) due to the encapsulation effects is discussed in the next section. In the next sections, we will describe the results performed in the range of this PhD thesis on the synthesis, crystal structure analysis and catalytic activity investigations of a series of Cu(II)-based metasiloxanes **1** – **42**. We focus on the use these **1**, **13**, **16**, **17**, **26**, **32** – **36**, **38** – **39**, **41** complexes as catalysts for catalytic reactions on oxidation amidation and C-H activation. The details of the synthesis are described in Experimental Section on this manuscript and the details of the crystal structures are given in Annex 2 (Table 21 - 28).

1.1.1. Study of self-assembly reaction in solvating ligands (dimethyl sulfoxide and dimethylformamide)

The most probable mechanism for the formation of the high nuclear compound [(MeSiO_{1.5})₈(CuO)₈(DMF)₉] in the presence of pyrazine is the specific coordination of copper ions by the nitrogen centers of pyrazine in two metallasilsesquioxane “building blocks” (this compound has been obtained previously by [151] and we will use it as a comparison join). Thus, the distance between the coordinated copper ions (7.96 Å) determines the size of forming cage compound. It was noted that the value of the Si-Si-Si angle (calculated for three neighboring silicon atoms in the

1 in 44% yield. The obtaining compound is the first example of a prismatic silsesquioxane containing an odd amount of copper ions. In addition, this product is the first example of a nonanuclear metallasilsesquioxane (the crystal data are given in Annex 2, Table 21).

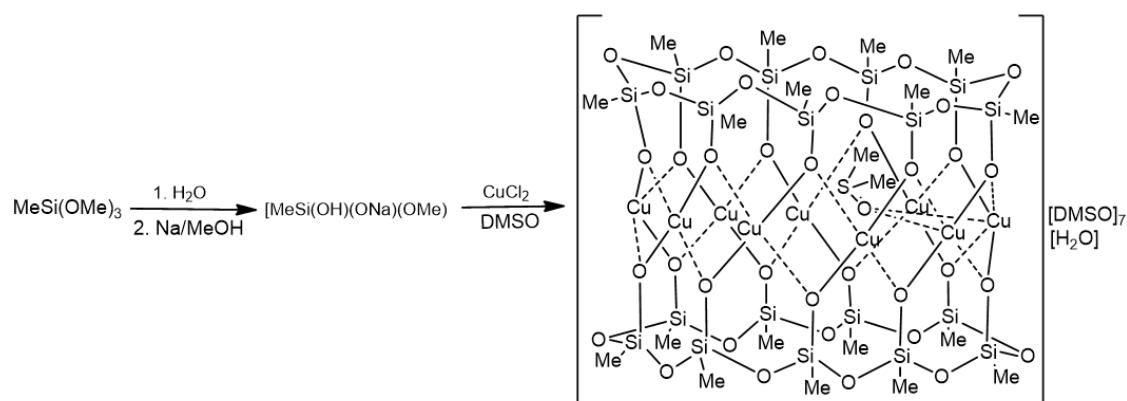


Figure 72. Synthesis of complex $[(\text{MeSiO}_{1.5})_{18}(\text{CuO})_9] \cdot \text{DMSO } \mathbf{1}$.

The investigation of **1** by X-ray diffraction analysis revealed its cage-like structure, coordinated by molecules of DMSO and water. The main feature of the structure is the encapsulation of the DMSO molecule into the internal cavity of the cage. In this case, DMSO coordinates two copper ions with both centers - oxygen and sulfur atoms (by analogy with Fig. 71, A). In turn, the oxygen atom is coordinately bounded to two neighboring copper ions (in accord to the mechanism shown in Figure 71, B). Such coordination of copper ions and DMSO promotes the specific orientation of two neighboring metallasiloxane fragments, which are located at an angle of 138.2° to each other. This value is close to the value of the internal angle of a regular nonagon (140°), which explains the formation of a nonanuclear product (Fig. 73).

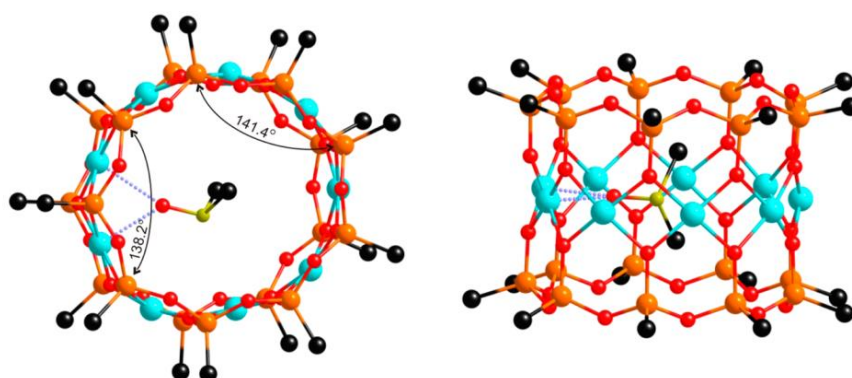


Figure 73. Coordination of the DMSO molecule in complex **1**: top view (left), side view (right).

The central (metal-containing) belt of complex **1** is of Cu_9O_{18} composition; each oxygen atom plays a role of μ^2 -bridge between two copper ions. Also, each copper atom coordinates one additional solvate molecule, with the realization of a square-pyramidal geometry. The average Cu-Cu distance in the compound **1** is 2.869, while the distance between the opposite copper atoms (the inner diameter of the

complex) is 8.229 Å. The Cu-S coordination bond is 3.412 Å. It is noteworthy that the coordination environment of copper ions is significantly different. Five copper atoms coordinate the outer-sphere solvate DMSO molecules, three copper atoms are bonded to the encapsulated DMSO molecule, and finally, the ninth ion atom coordinates the outer-sphere solvate water molecule. The copper ion, coordinating the water molecule, is located between the copper ions coordinating the encapsulated DMSO molecule. This feature leads to the crystal packing by the gear-wheel mechanism (Fig 74).

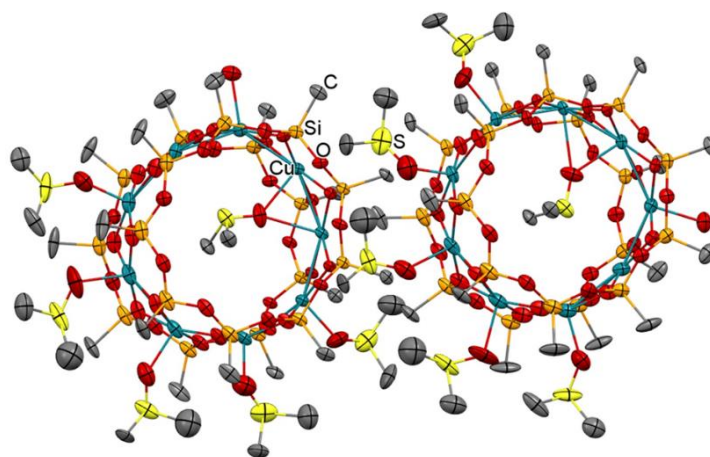


Figure 74. Arrangement of two neighboring Cu (II)-silsesquioxane molecules in a crystal **1**.

A similar synthesis, but with dimethylformamide instead of DMSO (DMF is a solvating ligand prone to coordination activity using only its oxygen atom), was carried out. The hexanuclear complex $[(\text{MeSiO}_{1.5})_{12}(\text{CuO})_6] \cdot 6\text{DMF}$ **2** was isolated in 50% yield (Fig. 75). Thus, it can be noted that synthesis in the presence of a potential linker significantly affects the architecture of metallasesquioxane complexes (the crystal data are given in Annex 2, Table 21).

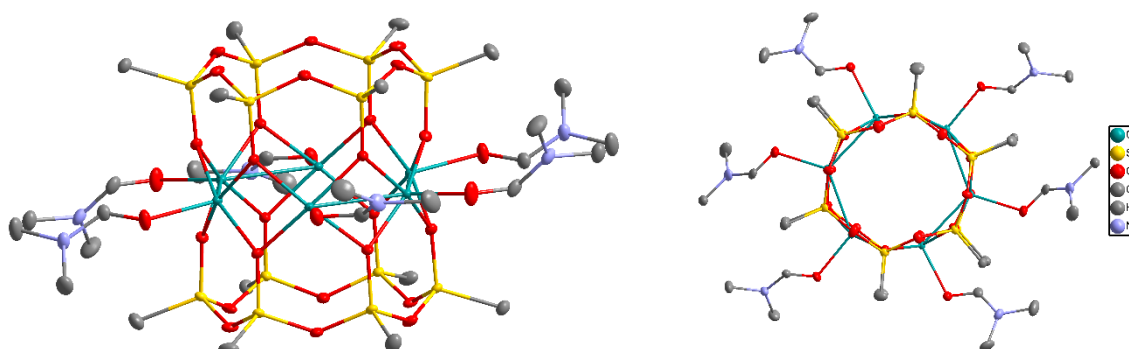


Figure 75. The structure of complex $[(\text{MeSiO}_{1.5})_{12}(\text{CuO})_6] \cdot 6\text{DMF}$ **2**.

The use of other types of bridging ligands (dicarboxylic acids, compounds of the 2,2'-bipyridine series) in the self-assembly of coppermethylsilsesquioxanes did not lead to the isolation of crystalline products. The bidentate N,N-ligands were used to prepare other examples of Cu(II)-containing silsesquioxanes. The results of this research are discussed in the next section.

1.1.2. Study of self-assembly reactions in the presence of chelating N,N-ligands (1,10-phenanthroline and 2,2'-bipyridine)

In the previous years, various scientific groups proved the effectiveness of using organic ligands (for example, carborane [154], acetylacetonate [155], tricyclohexylphosphine [156], cyclooctene [157], silylamide [158]) to obtain heteroleptic metallasilsesquioxane derivatives. The popular bidentate N,N-ligands (1,10-phenanthroline and 2,2'-bipyridine) were used to study the features of self-assembly of methyl-substituted copper silsesquioxanes.

At the first stage, we investigated the synthesis of Cu(II)-containing methylsilsesquioxane in condition of simultaneous presence of two different ligands in the reaction mixture (bridging DMSO and chelating 1,10-phenanthroline, Fig. 76). To this purpose, it was carried on the reaction between obtained $\text{MeSi}(\text{OH})(\text{ONa})(\text{OMe})$ (hydrolyzed $\text{MeSi}(\text{OMe})_3$ using NaOH) and CuCl_2 in the presence DMSO and 1,10-phenanthroline. The hexanuclear product with the composition $[(\text{MeSiO}_{1.5})_{10}(\text{HO}_{0.5})_{3.33}(\text{CuO})_6(1,10\text{-phen})_2(\text{MeSiO}_{1.5})_{10}(\text{AcO}_{0.5})_{0.67}(\text{CuO})_6(1,10\text{-phen})_2] \cdot 4\text{DMSO} \cdot 4\text{H}_2\text{O}$ **3** was isolated in 27% yield. The X-ray diffraction study of **3** shows that phenanthroline ligands, which directly coordinate two of the six ions of the product, are “directly” involved in the formation of the cage structure (the crystal data are given in Annex 2, Table 21). In turn, DMSO molecules only play a role of solvating ligands. Note, compound **3** is the first example of a metallasilsesquioxane containing phenanthroline ligands.

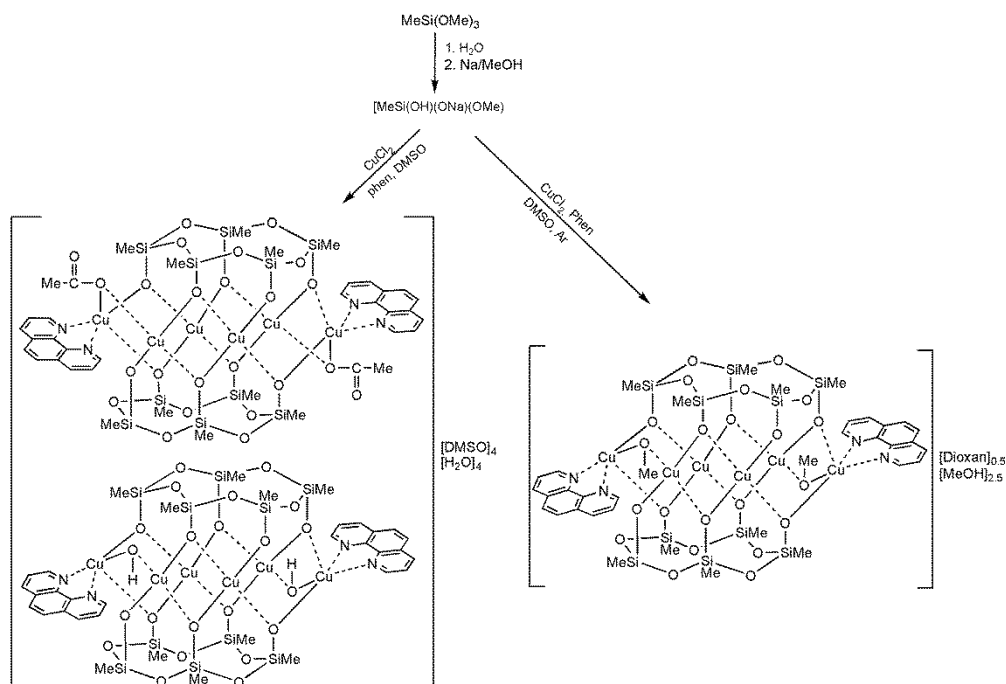


Figure 76. Synthesis of complexes

$[(\text{MeSiO}_{1.5})_{10}(\text{HO}_{0.5})_{3.33}(\text{CuO})_6(1,10\text{phen})_2(\text{MeSiO}_{1.5})_{10}(\text{AcO}_{0.5})_{0.67}(\text{CuO})_6(1,10\text{phen})_2] \cdot 4\text{DMSO} \cdot 4\text{H}_2\text{O}$ **3** (left)
and $[(\text{MeSiO}_{1.5})_{10}(\text{CuO})_6(\text{MeO}_{0.5})_2(1,10\text{-phen})_2] \cdot 0.5(1,4\text{-diox}) \cdot 2.5\text{MeOH}$ **4** (right).

The structure **3** contains two cyclic siloxanolate ligands $[(\text{MeSi}(\text{O})\text{O})]_5$ and metal oxide “belt” located between them. In turn, complex **3** contains two practically linear copper-containing trimeric fragments (the average Cu-Cu distance is 3.122 Å). It is noteworthy that twelve positive charges (from six Cu(II) ions in **3**) can't be compensated by ten negative charges bringing by two $[(\text{MeSi}(\text{O})\text{O})]_5$ pentameric ligands. Two types of charge-compensating groups could be found in the composition (this phenomenon is associated with the presence of two types of complexes in the composition of the crystal, **A** and **B**) (Fig. 77). The type **A** structure includes two hydroxyl groups, which compensate charges of compound and also coordinate two opposing copper ions. The structure of type **B** includes two acetoxy groups instead of hydroxyl fragments. It should be noted that acetate-containing components were not used in the synthesis of compound **3**. It may be concluded that acetoxy groups were formed during the oxidation of ethanol molecules in air, catalyzed by copper ions.

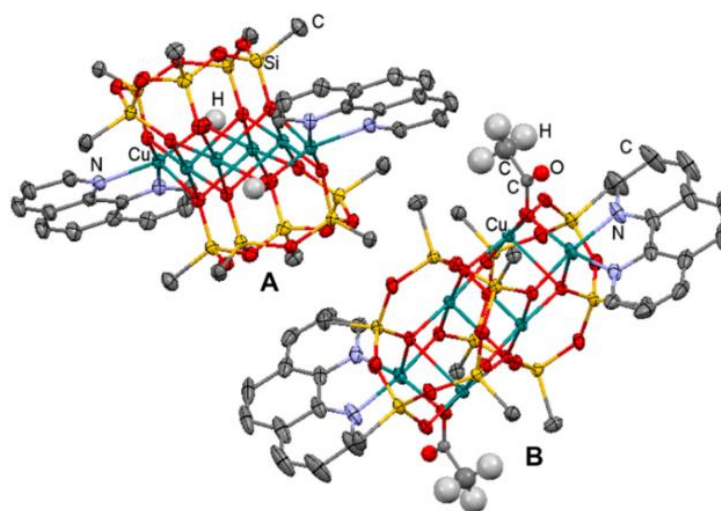


Figure 77. The structure of complex **3**.

To study the influence of the oxygen trace on the formation of cage-like coppersilsesquioxanes, several attempts were performed to reproduce the synthesis of complex **3** in an inert atmosphere. Crystalline product was not formed for the same solvent system (ethanol/DMSO), which was used for synthesis of **3**. However, with alternative (1,4-dioxane/methanol) system, a similar complex $[(\text{MeSiO}_{1.5})_{10}(\text{CuO})_6(\text{MeO}_{0.5})_2(1,10\text{-phen})_2] \cdot 0.5(1,4\text{-diox}) \cdot 2.5\text{MeOH}$ **4** was obtained in 82% yield (Fig. 78). It is worth noting, two charge-compensating methoxy fragments are found in composition of **4** (which is not surprising taking in mind the fact that methanol was used as a solvent). Thus, it was proved that synthesis in an inert atmosphere effectively suppresses oxidative side reactions.

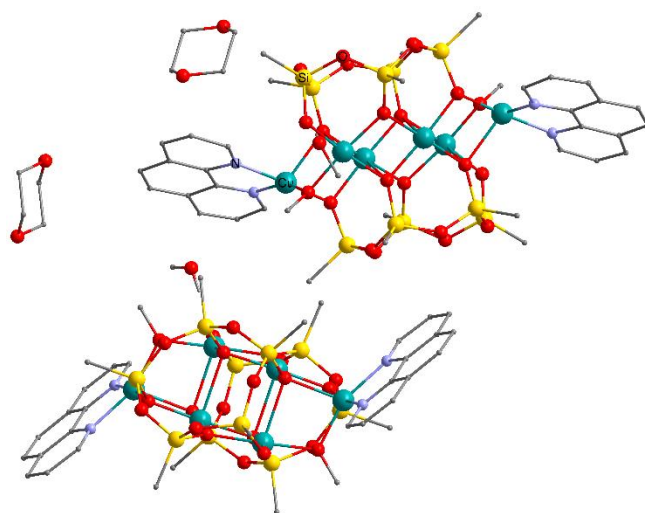


Figure 78. The structure of "inert" complex $[(\text{MeSiO}_{1.5})_{10}(\text{CuO})_6(\text{MeO}_{0.5})_2(1,10\text{-phen})_2] \cdot 0.5(1,4\text{-diox}) \cdot 2.5\text{MeOH } 4$.

At the second stage, additional syntheses of compound **3** analogs but in the absence of the highly coordinating DMSO were performed. This approach allowed to evaluate “metallasesquioxane self-assembly ability” of the bidentate nitrogen ligands themselves. Two parallel syntheses of copper methylsilsesquioxanes were carried out with different loadings of 2,2'-bipyridine. Two types of crystalline products $[(\text{MeSiO}_{1.5})_{10}(\text{CuO})_6(\text{MeO}_{0.5})_2(2,2'\text{-bipy})_2] \cdot 2\text{MeOH } 5$, and $[(\text{MeSiO}_{1.5})_8(\text{CuO})_3(2,2'\text{-bipy})_2] \cdot 3\text{EtOH } 6$, were isolated in 20% and 16% yields, respectively (fig. 79). The structures of the compounds were established using X-ray diffraction study (the crystal data are given in Annex 2, Table 21).

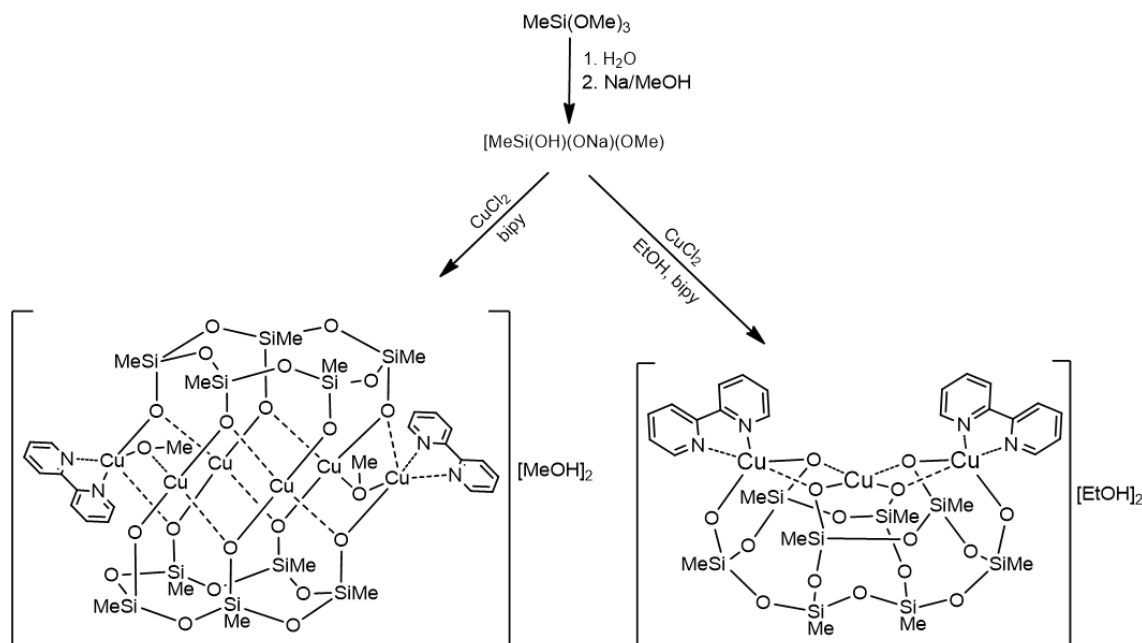


Figure 79. Synthesis of complexes $[(\text{MeSiO}_{1.5})_{10}(\text{CuO})_6(\text{MeO}_{0.5})_2(2,2'\text{-bipy})_2] \cdot 2\text{MeOH } 5$ (left) and $[(\text{MeSiO}_{1.5})_8(\text{CuO})_3(2,2'\text{-bipy})_2] \cdot 3\text{EtOH } 6$ (right).

The structure of hexanuclear complex **5** is completely similar to the molecular topology of compounds **3-4** (Fig. 88, left). Also, by an analogy to **3**, compound **5** includes two methoxy fragments as charge compensating groups.

The structure of trinuclear compound **6** is more remarkable (Fig. 80, right). This compound, as complex **1**, is the first example of a cage silsesquioxane with an odd number of copper ions. In addition, compound **6** exhibits an unprecedented eight-membered condensed ligand consisting of two five-membered rings (Fig. 81). Self-assembly of such unusual ligand can be compared only to condensed decamembered ligand in the structure of Cu_2Na_2 -phenylsilsesquioxane, comprising three cycles - one tetrameric and two pentameric ones [44].

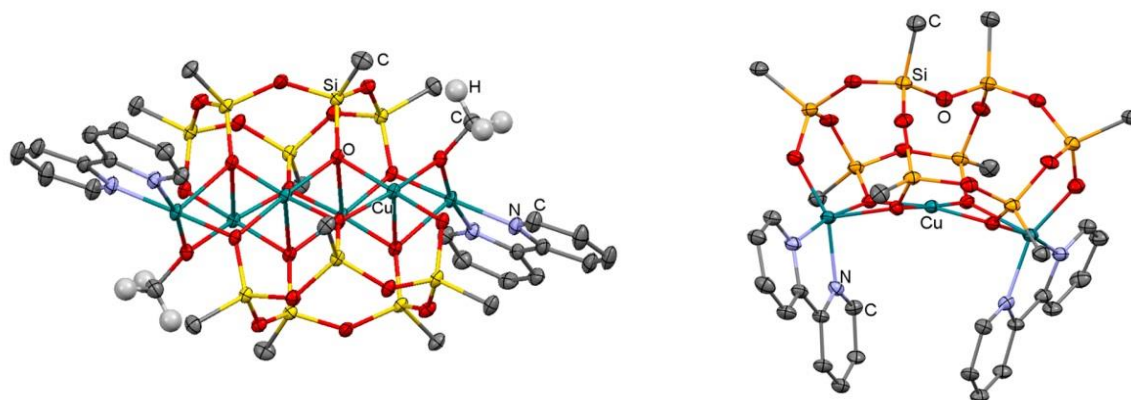


Figure 80. The structure of complexes $[(\text{MeSiO}_{1.5})_{10}(\text{CuO})_6(\text{MeO}_{0.5})_2(2,2'\text{-bipy})_2] \cdot 2\text{MeOH}$ **5** (left) and $[(\text{MeSiO}_{1.5})_8(\text{CuO})_3(2,2'\text{-bipy})_2] \cdot 3\text{EtOH}$ **6** (right).

Three copper atoms form an almost linear trimeric fragment in **6**, where the coordination site of the two terminal copper atoms corresponds to a distorted square pyramid, while central copper atom adopts plane-square coordination. The Cu-Cu distance in **6** is equal to 2.997 Å, the Cu-O distances are in the range 1.905 – 2.186 Å.

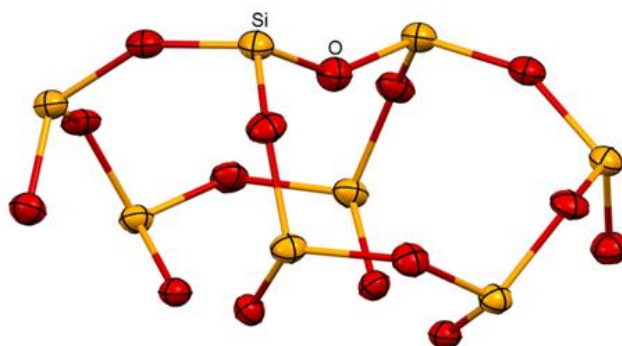


Figure 81. Condensed eight-membered complex ligand **6**.

Finally, compound **6** joins a small family of tri-nuclear cage metallasilsesquioxanes, mainly constructed on cubane silsesquioxane synthon [159, a-c].

The preparation of metal derivatives based on methylsilsesquioxane ligands (in the form of crystalline products) is significantly limited by the strong interchain interaction of the metallasiloxane fragments arising during the synthesis. This is easily explained by the small screening effects from methyl groups at silicon atoms. Since we were interested in studying the solid structures of compounds, the subsequent sections discuss phenylsilsesquioxane derivatives, which are more convenient in the context of single crystals' preparation.

1.2. Synthesis of Cu(II) - silsesquioxanes containing the structural fragment

PhSiO_{1.5}

1.2.1 Investigation of self-assembly reactions in different solvents

Copperphenylsilsesquioxane cages tend to form hexanuclear compounds with prismatic geometry, which differs in nature of the solvating ligands. Moreover, we carried out a series of exchange reactions between *in situ* obtained sodium phenylsiloxanolate [(PhSiO_{1.5})(NaO_{0.5})]_n and copper(II) chloride.

To determine an influence of solvent ligands on a structural formation, we used solvents of various natures, as well as their pair combinations: EtOH / DMF, DMF / THF, DMSO, MeCN, PhCN / THF and THF. Six crystalline products were isolated, namely: [(PhSiO_{1.5})₁₂(CuO)₆] • EtOH • DMF **7** (44% yield), [(PhSiO_{1.5})₁₂(CuO)₆] • DMF • THF **8** (64% yield), [(PhSiO_{1.5})₁₂(CuO)₆] • DMSO **9** (53% yield), [(PhSiO_{1.5})₁₂(CuO)₆] • MeCN **10** (40% yield), [(PhSiO_{1.5})₁₂(CuO)₆] • PhCN • THF **11** (15% yield) and [(PhSiO_{1.5})₁₂(CuO)₆] • THF **12** (50% yield) (Fig. 82). X-ray diffraction analysis revealed that compounds **7** – **12** belong to the classical hexanuclear type, confirming the most common of such compounds (the crystal data are given in Annex 2, Table 22 – 23).

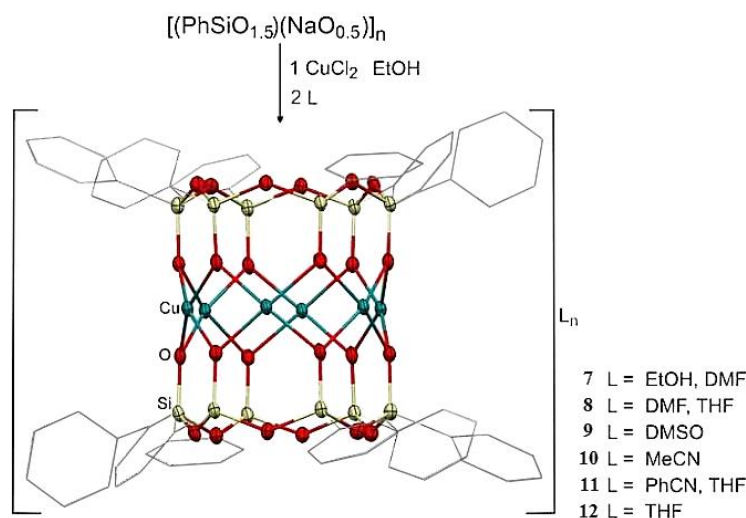


Figure 82. Synthesis of complexes **7** – **12**.

However, the use of pyridine as a specific solvate for the formation of cage products in the self-assembling reaction between $[(\text{PhSiO}_{1.5})(\text{NaO}_{0.5})]_n$ and copper(II) chloride allowed to change the nuclearity of the product. In this case, a rare (pentanuclear) type of prismatic metallasilsesquioxane, the complex $[(\text{PhSiO}_{1.5})_{10}(\text{CuO})_5(\text{Py})_5]$ **13**, was obtained in 66% yield (the crystal data are given in Annex 2, Table 23) (Fig. 83). Similar structure, obtained by *in situ* oxidation of Cu(I) into Cu (II) ions during the copperphenylsilsesquioxane synthesis, was published in the recent work [160].

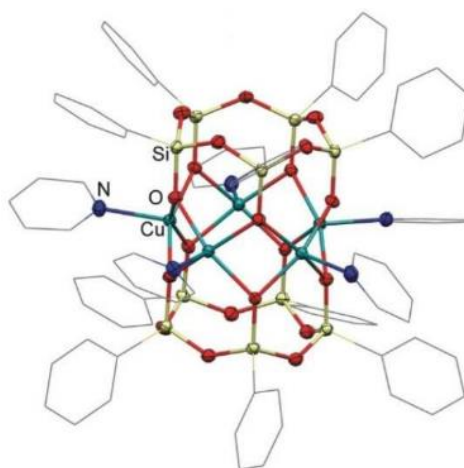


Figure 83. The structure of complex $[(\text{PhSiO}_{1.5})_{10}(\text{CuO})_5(\text{Py})_5]$ **13**.

Complex **13** contains a pentagonal oxometallic layer where each copper(II) ion coordinates a pyridine molecule. It was shown that the presence of pyridine in the system is the driving force for the selective formation of the pentanuclear compound, since for the Si-Si-Si angle corresponding to the regular pentagon (108.5°) pyridine molecules coordinating neighboring metal ions perfectly occupy available space (Fig. 84). For the Si-Si-Si angle corresponding to the hexagon structure, this location of pyridine molecules is not sterically favorable. The Cu-Cu distances in **13** range from 2.81 to 2.84 Å, while the Cu-O-Cu angle vary from 90.8 to 92.2 °.

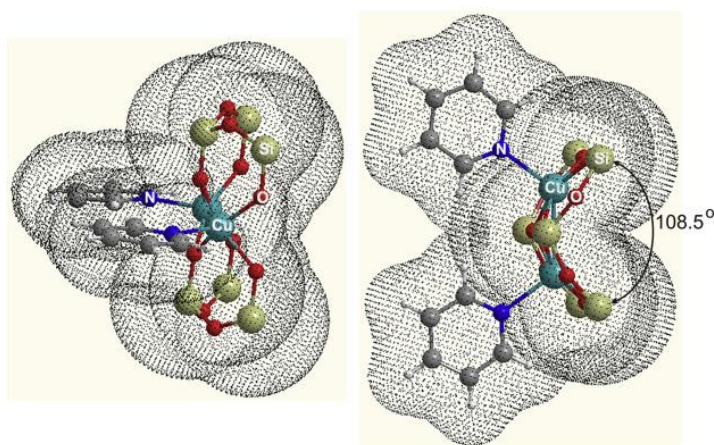


Figure 84. The theoretical calculated model of neighboring copper ions coordinating pyridine in **13** (front and top views), obtaining the ChemCraft program.

In addition, we were able to confirm that obtained pentanuclear geometry is rather stable and retained upon recrystallization of compound **13** from a DMF solution. In this case, the formation of a pentanuclear complex $[(\text{PhSiO}_{1.5})_{10}(\text{CuO})_5(\text{DMF})_4] \cdot \text{H}_2\text{O}$ **14** coordinated by DMF solvates was observed (the crystal data are given in Annex 2, Table 23) (Fig. 85).

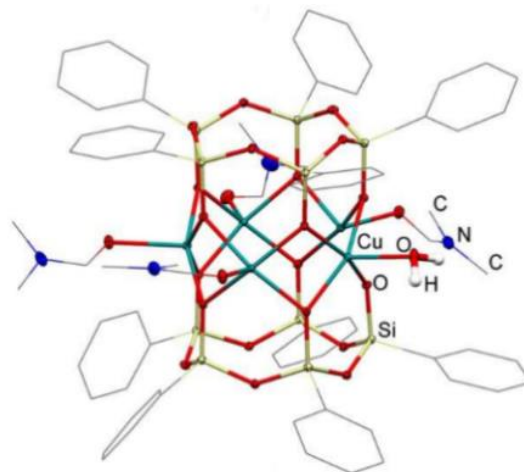


Figure 85. Structure of complex $[(\text{PhSiO}_{1.5})_{10}(\text{CuO})_5(\text{DMF})_4] \cdot \text{H}_2\text{O}$ **14**.

It is important to compare this result with the self-assembly of copper phenylsilsesquioxane from phenylsiloxanolate and copper (II) chloride in DMF media, which led to the formation of the classical hexanuclear compound $[(\text{PhSiO}_{1.5})_{12}(\text{CuO})_6] \cdot \text{DMF}$ **15** (the crystal data are given in Annex 2, Table 23) (Fig. 86).

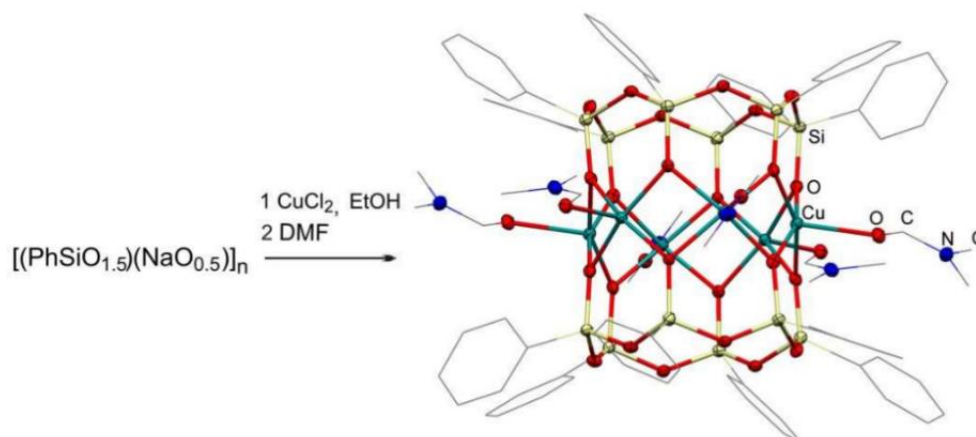


Figure 86. Synthesis scheme of complex $[(\text{PhSiO}_{1.5})_{12}(\text{CuO})_6] \cdot 6\text{DMF}$ **15**.

To confirm additionally the governing role of pyridine in the synthesis of metallasilsesquioxanes, a reaction between phenylsiloxanolate $[(\text{PhSiO}_{1.5})(\text{NaO}_{0.5})]_x$ and a mixture of copper(II) and cobalt(II) chlorides in ration Cu : Co = 2 : 1 in pyridine was performed. Noteworthy that product, $\{[(\text{PhSiO}_{1.5})_{10}(\text{CoO})_5(\text{H}_2\text{O})_2]_2[(\text{PhSiO}_{1.5})_{10}(\text{CuO})_5]\}$ **16**, is a mixed crystal including two types of pentanuclear cage compounds (Co_5 and Cu_5) in a 2 : 1 ratio (the crystal data are given in

Annex 2, Table 23) (Fig. 87). Average bond length Cu-Cu is 2.884 Å, the shortest Co-Co distance is 2.831 Å. This contraction can be explained by the presence of the hydroxyl anion encapsulated in the metallasilsesquioxane fragment.

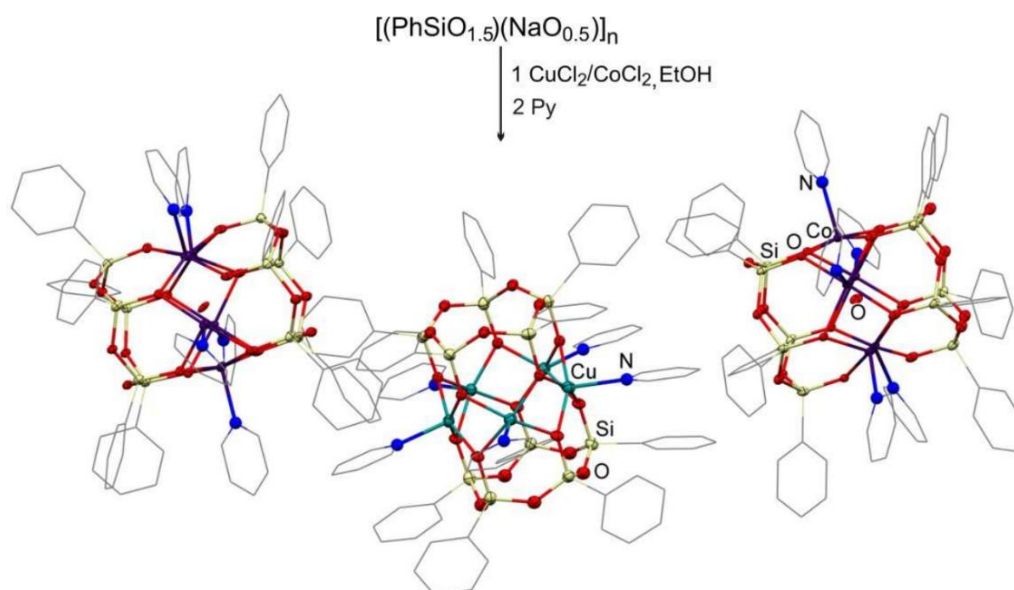


Figure 87. Synthesis of complex $\{[(\text{PhSiO}_{1.5})_{10}(\text{CoO})_5(\text{H}_2\text{O})_2]_2[(\text{PhSiO}_{1.5})_{10}(\text{CuO})_5]\}$ **16**.

Thus, it is obvious that pyridine (N-ligand) can be applied for the directed synthesis of cage metallasilsesquioxanes of lower nuclearity (M_5 instead of M_6). Considering this fact, it was of interest to study the formation of the corresponding complexes in the presence of chelating N,N-ligands. Results of this investigation are discussed in the next section.

1.2.2 Investigation of self-assembly reactions in the presence of chelating N, N-ligands (1,10-phenanthroline, 2,2'-bipyridine, bathophenanthroline)

The use of various additional organic ligands is widely used to obtain new types of metallasilsesquioxanes. The most popular method is post-synthetic functionalization of the resulting cage structure with an auxiliary ligand, for example, N,N-dimethylhydroxylamine or acetylacetonone [161], tris(2-pyridylmethyl) amine [101], 2,2'-bipyridine [162]. The introduction of an additional organic ligand before the stage of obtaining the framework metallamethylsilsesquioxane is not so well explored. Several parallel reactions of self-assembly of copper-containing phenylsilsesquioxanes in the presence of three types of N,N-ligands were performed. Chosen ligands (2,2'-bipyridine, 1,10-phenanthroline, and 4,7-diphenyl-1,10-phenanthroline (bathophenanthroline)) belong to the same family, but exhibit different steric features. This process leads to the preparation of a large group of compounds (16 examples) with a number of structural analogies. The reactions with 2,2'-bipyridine allowed to isolate nine Cu_6 complexes: $[(\text{PhSiO}_{1.5})_{10}(\text{CuO})_6(\text{HO}_{0.5})_2(2,2'\text{-bipy})_2] \cdot 2.5 \text{ DMSO}$ **17**

(61% yield), $[(\text{PhSiO}_{1.5})_{10}(\text{CuO})_6(\text{HO}_{0.5})_2(2,2'\text{-bipy})_2] \cdot 2.5 \text{ MeCN} \cdot 2 \text{ H}_2\text{O}$ **18** (40% yield), $[(\text{PhSiO}_{1.5})_{10}(\text{CuO})_6(\text{HO}_{0.5})_2(2,2'\text{-bipy})_2] \cdot 4 \text{ MeCN}$ **19** (20% yield), $[(\text{PhSiO}_{1.5})_{10}(\text{CuO})_6(\text{HO}_{0.5})_2(2,2'\text{-bipy})_2] \cdot 3.5 \text{ PhCN} \cdot 0.5 \text{ H}_2\text{O}$ **20** (10% yield), $[(\text{PhSiO}_{1.5})_{10}(\text{CuO})_6(\text{HO}_{0.5})_2(2,2'\text{-bipy})_2] \cdot 3 \text{ PhCN}$ **21** (14% yield), $[(\text{PhSiO}_{1.5})_{10}(\text{CuO})_6(\text{HO}_{0.5})_2(2,2'\text{-bipy})_3]$ **23** (12% yield), $[(\text{PhSiO}_{1.5})_{10}(\text{CuO})_6(\text{CH}_3\text{O}_{0.5})_2(2,2'\text{-bipy})_2]$ **24** (27% yield), $[(\text{PhSiO}_{1.5})_{10}(\text{CuO})_6(\text{AcO}_{0.5})_2(2,2'\text{-bipy})_2] \cdot \text{MeCN}$ **25** (25% yield). In all of them, the metal-containing layer is coordinated in the sandwich fashion by two cisoid silsesquioxane cycles $[(\text{PhSiO}_{1.5})_5]$, two N,N-ligand molecules coordinate opposing copper ions forming a skewed sandwich cage (the crystal data are given in Annex 2, Table 24 – 25) (Fig. 88).

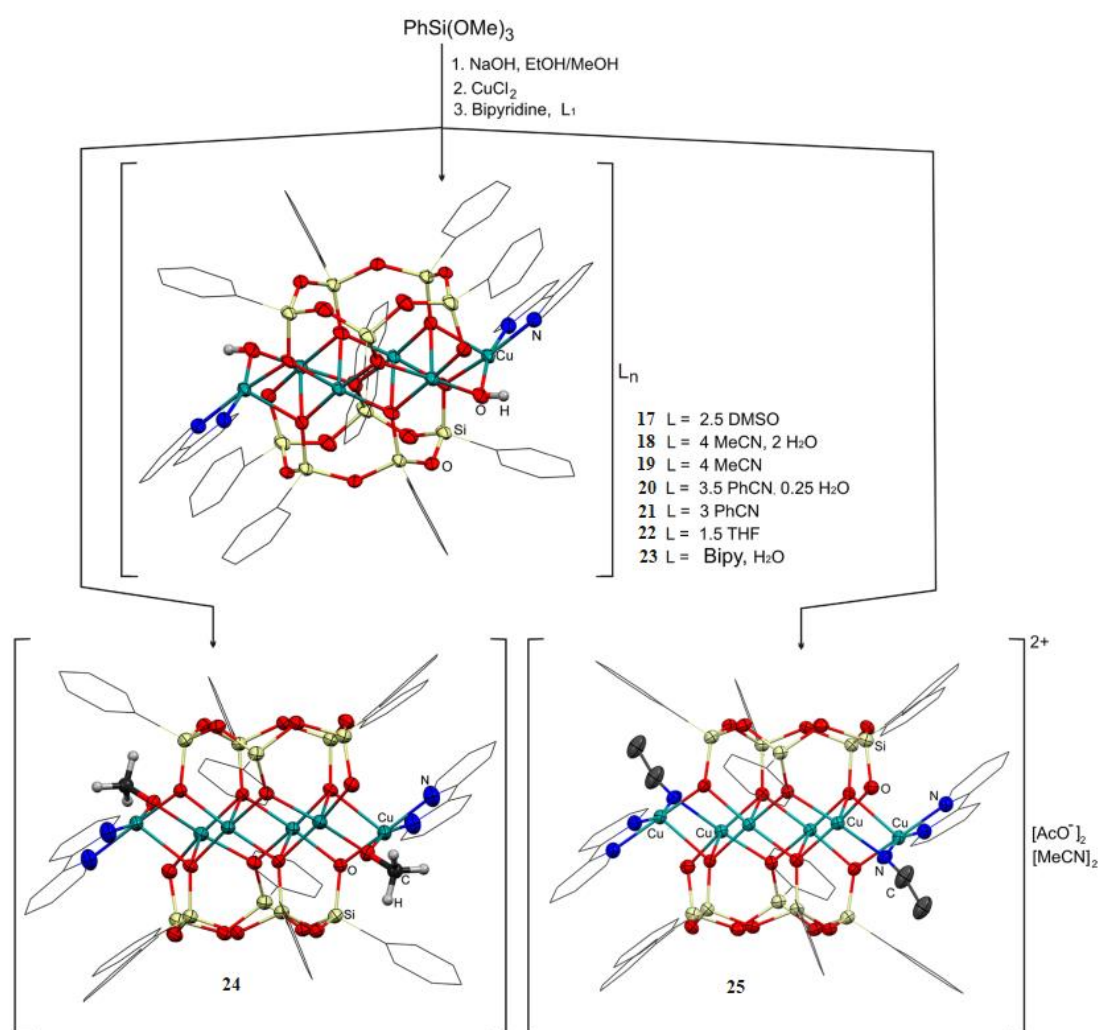


Figure 88. Synthesis of complexes **17** - **25**.

As in the case of compounds **3** – **4**, the balance of charges of compounds **17** – **25** (twelve positive charges from six Cu^{2+} ions vs ten negative charges from two pentameric silsesquioxane ligands) requires the presence of additional fragments with a negative charge. Such fragments are: hydroxyl **17** – **23**, methoxide **24** and acetate **25** anions. The appearance of hydroxyl groups in the composition of

the products **17** – **25** is easily explained by the presence of NaOH as a reagent in the reaction mixture. Similarly, the source of methoxy groups is methanol (solvent in the synthesis). However, the formation of acetate groups in **25** is not obvious. A possible mechanism for the formation of the acetate group was proposed by the homogeneous oxidation of primary alcohols in the presence of copper ions with the formation of the corresponding carboxylic acids (Fig. 89) [163].

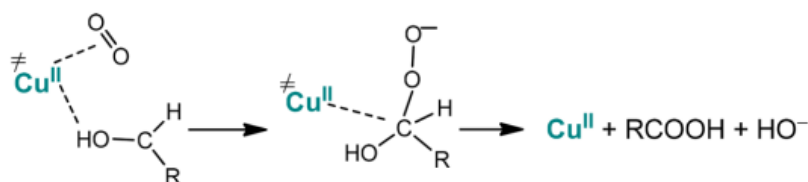


Figure 89. Mechanism of catalytic oxidation of primary alcohols.

Further, a remarkable feature of compound **21** (containing benzonitrile solvate molecules) is the implementation of an unusual triple π - π stacking due to contacts "phenyl group at the silicon atom - bipyridyl - benzonitrile" (Fig. 90). It is noteworthy that the presence of a solvate (water molecules), additional to benzonitrile, in the composition of complex **21** destroys this coordination, and stacking interactions do not occur.

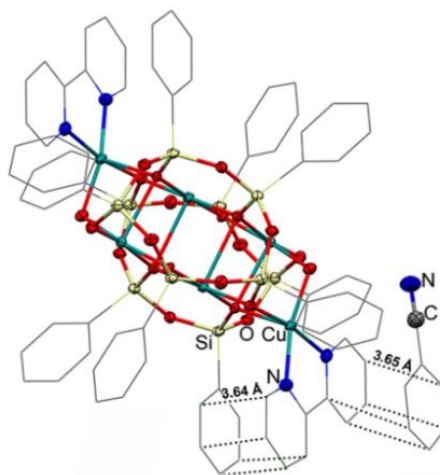


Figure 90. The structure of complex **21** with triple π - π -aromatic bond.

The similar self-assembly reactions were carried out in the presence of 1,10-phenanthroline. Four complexes $[(\text{PhSiO}_{1.5})_{10}(\text{CuO})_6(\text{HO}_{0.5})_2(1,10\text{-phen})_2] \cdot 4\text{DMSO}$ **26** (65% yield), $[(\text{PhSiO}_{1.5})_{10}(\text{CuO})_6(\text{HO}_{0.5})_2(1,10\text{-phen})_2] \cdot 4.75\text{DMSO}$ **27** (37% yield), $[(\text{PhSiO}_{1.5})_{10}(\text{CuO})_6(\text{HO}_{0.5})_2(1,10\text{-phen})_2] \cdot 4\text{DMF}$ **28** (47% yield), $[(\text{PhSiO}_{1.5})_{10}(\text{CuO})_6(\text{HO}_{0.5})_2(1,10\text{-phen})_2] \cdot 4\text{Py}$ **29** (31% yield) were isolated with a similar type of molecular architecture mentioned for compounds **17** - **24** (the crystal data are given in Annex 2, Table 25 – 26) (Fig. 91).

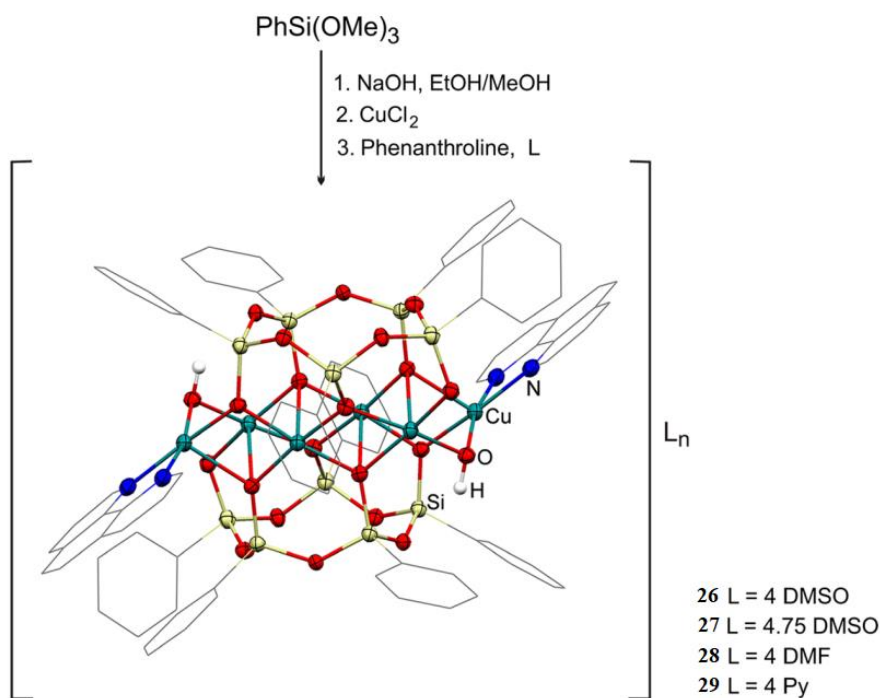


Figure 91. Synthesis of complexes **26** - **29**.

The hydroxyl OH⁻ fragments act as a “charge-compensating” group in all four compounds. Two compounds **26** and **27** form a supramolecular ladder structure due to π - π -stacking interactions of aromatic systems of phenanthroline ligands (Fig. 92).

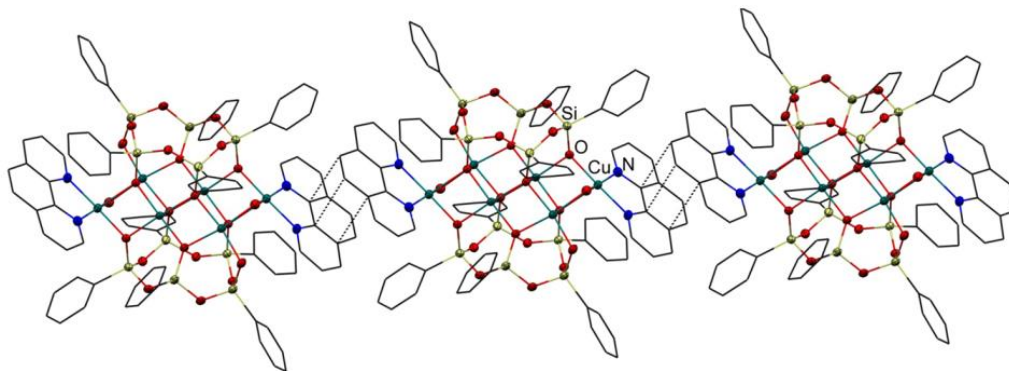


Figure 92. The structure of the crystal packing of the complex **27**.

Using bathophenanthroline, three compounds [(PhSiO_{1.5})₁₀(CuO)₆(HO_{0.5})₂(Bphen)₂] • MeCN **30**, [(PhSiO_{1.5})₁₀(CuO)₆(HO_{0.5})₂(Bphen)₂] • DMSO **31**, [(PhSiO_{1.5})₁₀(CuO)₆(HO_{0.5})₂(Bphen)₂] • Tol **32** were isolated in 41%, 30% and 22% yields, respectively (the first examples of metallasilsesquioxanes incorporating such ligands) (Fig. 93). The molecular geometries of products are similar to complexes **17** – **29**, and all compounds include hydroxyl groups as charge compensating ones (the crystal data are given in Annex 2, Table 26 – 27). Finally, the characteristic structure of bathophenanthroline (the absence of planarity in the aromatic system) leads to the fact that compounds **30** – **32** do not realize stacking interactions.

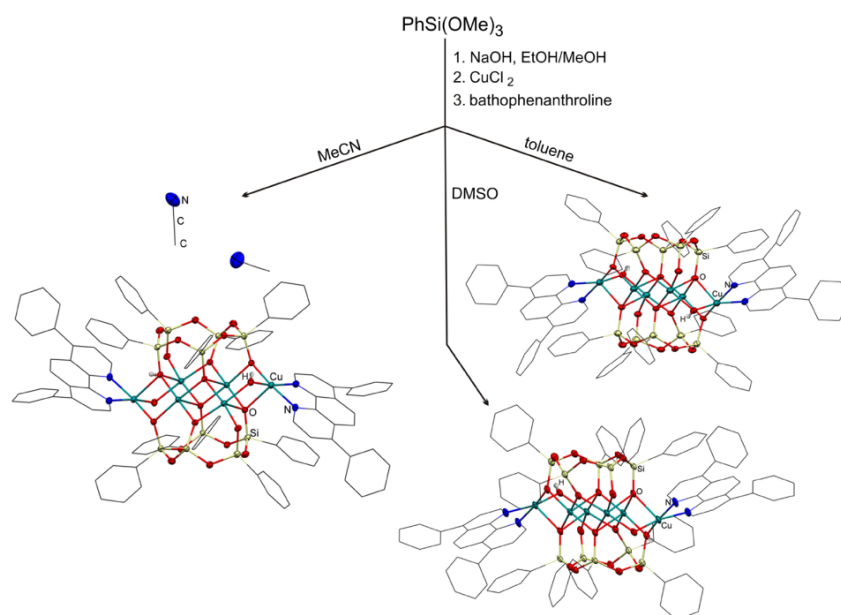


Figure 93. Synthesis of complexes **30** - **32**.

The wide variation of the solvents and ligands used in the synthesis of complexes **17** – **32**, leading to the one type of product, certainly indicates the high stability of such hexanuclear architecture. Nevertheless, the use of additional techniques (varying the ratio between the reaction components and the preservation of some of the sodium ions in the product) made it possible to isolate a new structural type. A complex with an unusual architecture in the form of a "bicycle helmet", $[\text{Ph}_{12}\text{Si}_{12}\text{O}_{12}(\text{OH})(\text{O}^-)_{11}\text{Cu}_5\text{Na}(\text{bipy})_3(\text{H}_2\text{O})(\text{THF})_7]$ **33** was obtained in 24% yield (the crystal data are given in Annex 2, Table 27) (Fig. 94). The specific features of compound **33** are as follows: (i) unprecedented type of nuclearity (Cu_5Na), (ii) an anomalously small number of sodium atoms in comparison to the content of the transition metal ($\text{Na} / \text{Cu} = 1/5$, compare e.g. to $\text{Na} / \text{Co} = 6/3$ [106], $\text{Na} / \text{Ni} = 5/1$ [164], $\text{Na} / \text{Cu} = 4/4$ [81], $\text{Na} / \text{Fe} = 6/6$ or $7/6$ [165]).

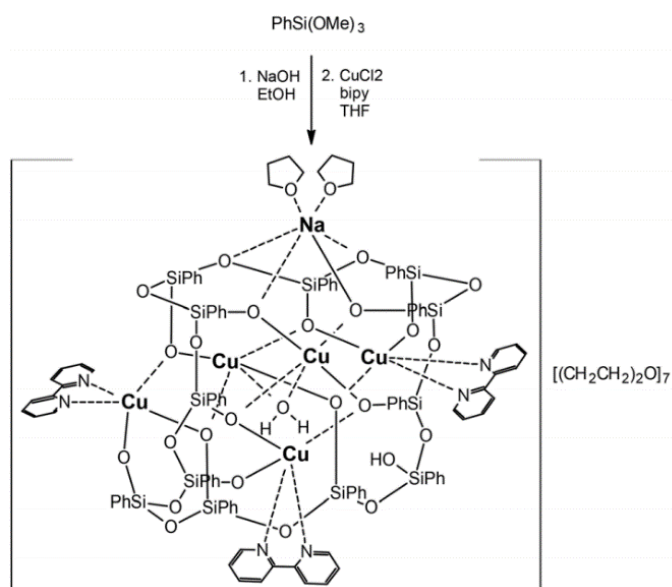


Figure 94. Synthesis of complex $[\text{Ph}_{12}\text{Si}_{12}\text{O}_{12}(\text{OH})(\text{O}^-)_{11}\text{Cu}_5\text{Na}(\text{bipy})_3(\text{H}_2\text{O})(\text{THF})_7]$ **33**.

It should be noted that 11 positive charges from metal ions (five Cu(II) ions, one Na(I)) are insufficient to compensate for the 12 negative charges bringing by the cyclic Si₁₂ ligand. This difficulty was overcome by protonation of one of the SiO fragments of the siloxanolate fragment, with the formation of a ligand of unusual composition Ph₁₂Si₁₂(O)₁₂(OH)(O⁻)₁₁ (Fig. 95, right). Additional stabilization of the structure occurs due to the system of hydrogen bonds between hydroxyl groups and a water molecule encapsulated in the inner cavity of the complex (Fig. 95, left).

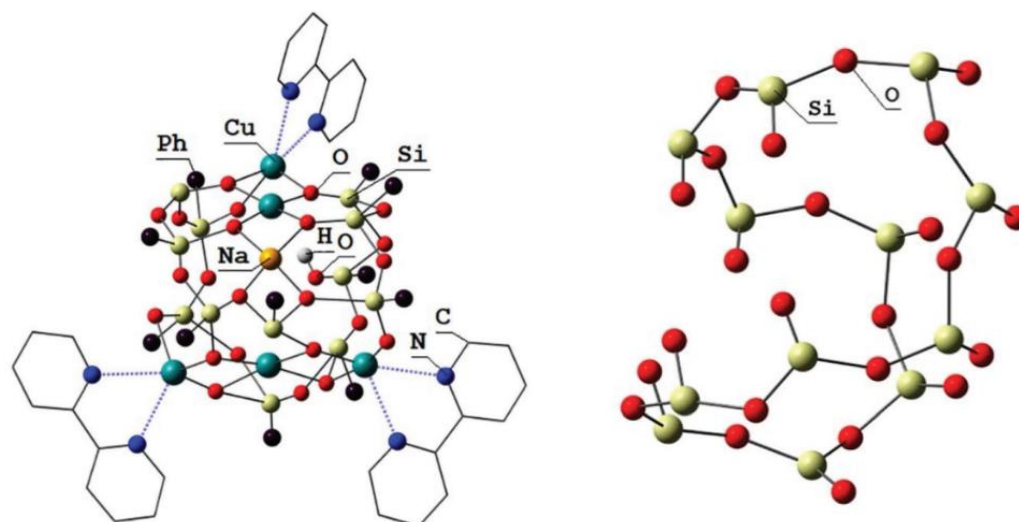


Figure 95. The structure of complex **33** (left) and the structure of dodecatesquioxane ligand (right).

The bipyridyl ligands of compound **33** promote the formation of supramolecular packing due to π - π stacking interactions of aromatic systems of nitrogen ligands and phenyl groups at silicon atoms (Fig. 96). It is noteworthy that only two of the three bipyridine ligands of complex **33** are involved in these interactions. The Cu-N bond length is in the range 1.996 – 2.214 Å, while the Cu-O bond length is 1.919 – 2.782 Å. Coordination of copper ions to oxygen atom of the encapsulated water molecule is characterized by the longest Cu-O contacts (2.523 and 2.782 Å).

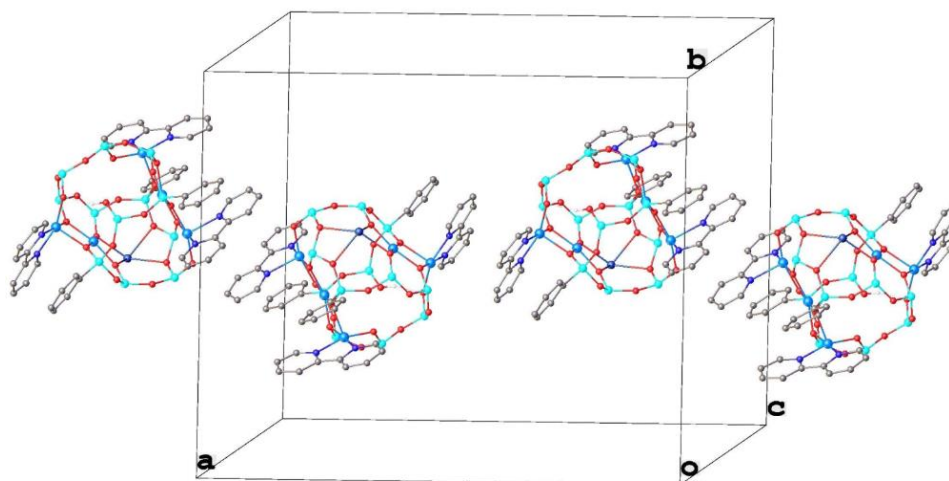


Figure 96. The structure of the crystal packing of the complex **33**.

Taking in mind the results of using additional N,N-ligands for the construction of copper-phenylsilsesquioxanes, it was of interest to investigate synthetic potential of bidentate ligands of other type, P,P-. The results of this study are summarized in the next section.

1.2.3 Study of self-assembly reactions in the presence of chelating P,P-ligands (1,2-bis(diphenylphosphino)ethane, 1,2-bis(diphenylphosphino)methane)

This section presents the results of a study of the self-assembly reaction of copper-containing phenylsilsesquioxanes in the presence of two types of P,P-ligands: 1,2-bis(diphenylphosphino)ethane (dppe), 1,2-bis(diphenylphosphino)methane (dppm). At the beginning of this research, the metallasilsesquioxane complexes containing dppm ligands were not known. On the other hand, previously described examples of metallasilsesquioxane complexes containing dppe ligands belong exclusively to the cubane type [166, a-b]. They were synthesized by post-functionalization of the corresponding metal complex using dppe. In our approach, we used, as in the case of nitrogen-containing ligands, a self-assembly reaction with dppe and dppm as “independent synthetic players”.

It was found that synthesis with phenylsilanolate $[(\text{PhSiO}_{1.5})(\text{NaO}_{0.5})]_x$, copper (II) chloride and 1,2-bis(diphenylphosphino)ethane leads to the formation of complexes with an unusual redistribution of ions copper between silsesquioxane and phosphorus ligands. The variations of the ratio between reagents allowed to isolate two types of products $[(\text{PhSiO}_{1.5})_{12}(\text{PhSiO}_{1.5})_8(\text{CuO})_8(\text{NaO}_{0.5})_4\{\text{Cu}(\text{O}_{0.5})_4\}] \cdot 2[\text{Cu}(\text{dppe})_2]$ **34** (42% yield) and $[(\text{PhSiO}_{1.5})_{12}(\text{CuO})_4(\text{NaO}_{0.5})_2] \cdot 2[\text{Cu}(\text{dppe})_2]$ **35** (46% yield) (the crystal data are given in Annex 2, Table 27) (Fig. 97).

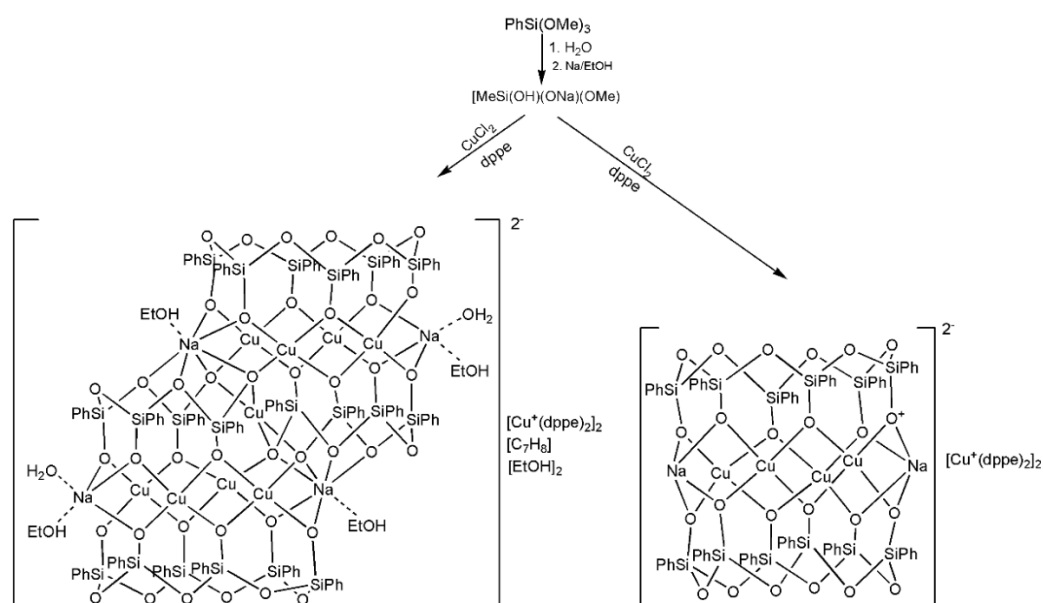


Figure 97. Synthesis of complexes $[(\text{PhSiO}_{1.5})_{12}(\text{PhSiO}_{1.5})_8(\text{CuO})_8(\text{NaO}_{0.5})_4\{\text{Cu}(\text{O}_{0.5})_4\}] \cdot 2[\text{Cu}(\text{dppe})_2]$ **34** (left) and $[(\text{PhSiO}_{1.5})_{12}(\text{CuO})_4(\text{NaO}_{0.5})_2] \cdot 2[\text{Cu}(\text{dppe})_2]$ **35** (right).

A common feature of both complexes is the presence of two cationic fragments $\text{Cu}^{\text{I}}(\text{dppe})_2$. Thus, the central frameworks (with nuclearity Cu_9Na_4 and Cu_4Na_2 for **34** and **35**, respectively) play a role of unusual anions. Such effect (of redistribution of metal ions between ligands of different types) has not been previously reported in the chemistry of metallasilsesquioxanes - known examples of the use of additional organic ligands (for example, triphenylphosphine oxide [167], *N,N,N',N'*-tetramethyl-*p*-phenylenediamine [168], trimethylphosphine [169], tris[2-(dimethylamino)ethyl]amine [93]) led to the formation of products where silsesquioxane and organic ligands coordinate metal ions in a same complex without the formation of ionic components.

The structures of framework fragments in compounds **34** and **35** differ significantly. In the first case, an unprecedented molecular geometry was observed (Fig. 98). This cage fragment includes two sandwich-like fragments with Cu_4Na_2 nuclearity, connected by the central (ninth) $\text{Cu}(\text{II})$ ion. The structure contains two types of silsesquioxane ligands: two classical cyclic $(\text{PhSiO}_{1.5})_6$ and two acyclic $(\text{PhSiO}_{1.5})_4$ ligands. The latter is a very rare type of silsesquioxane fragment previously found only for the structure of Mn,Na -phenylsilsesquioxane [170]. The structure of the **35** cage includes one sandwich fragment with Cu_4Na_2 nuclearity and two cyclic $(\text{PhSiO}_{1.5})_6$ ligands.

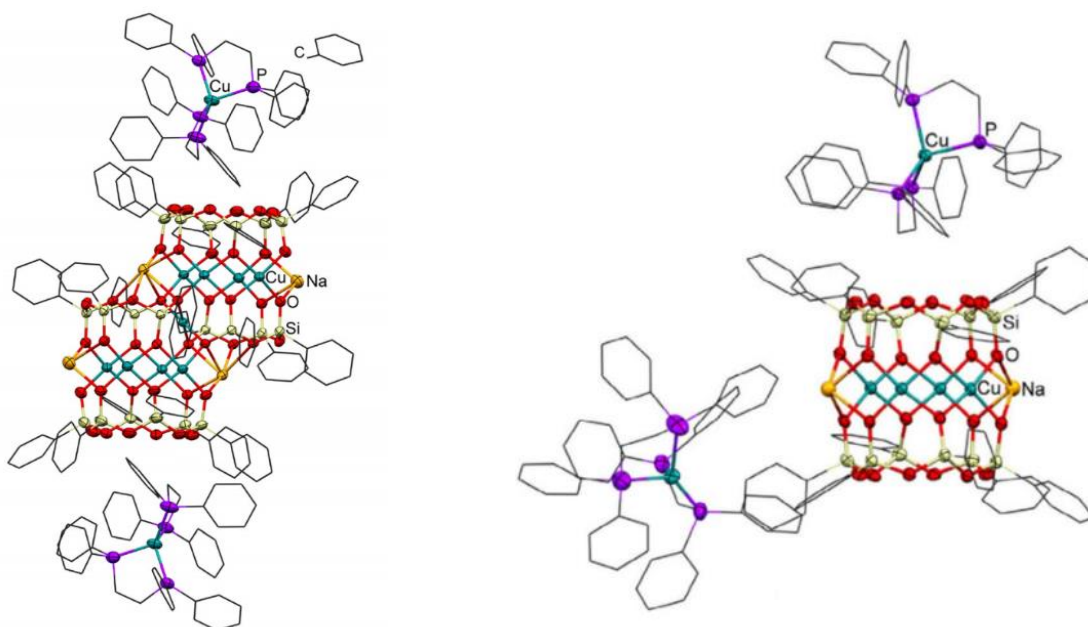


Figure 98. The structure of complexes $[(\text{PhSiO}_{1.5})_{12}(\text{PhSiO}_{1.5})_8(\text{CuO})_8(\text{NaO}_{0.5})_4\{\text{Cu}(\text{O}_{0.5})_4\}] \cdot 2[\text{Cu}(\text{dppe})_2]$ **34** (left) and $[(\text{PhSiO}_{1.5})_{12}(\text{CuO})_4(\text{NaO}_{0.5})_2] \cdot 2[\text{Cu}(\text{dppe})_2]$ **35** (right).

It is noteworthy that the use of another P,P-ligand (1,1-bis(diphenylphosphino)methane (dppm)) in a similar reaction leads to the formation of a principally different molecular architecture $[(\text{PhSiO}_{1.5})_{12}(\text{CuO})_4(\text{NaO}_{0.5})_4(\text{dppmO}_2)_2]$ **36** in 22% yield (the crystal data are given in Annex 2, Table 27) (Fig. 99).

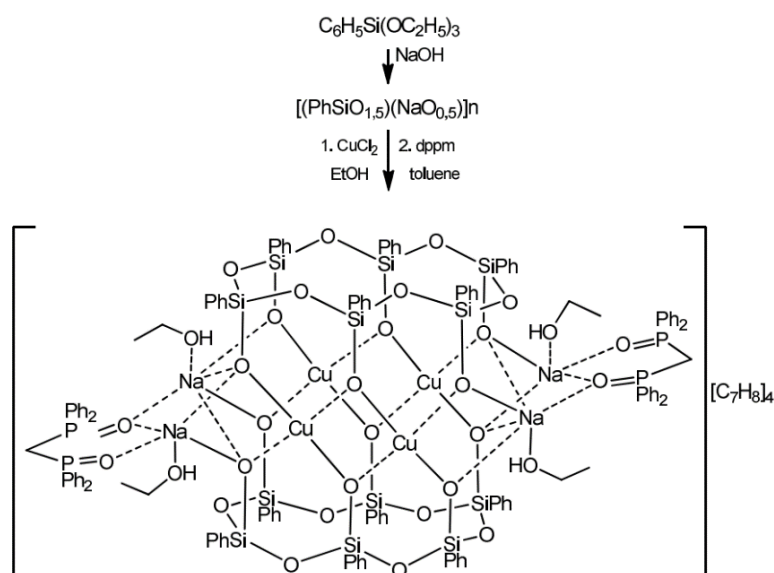


Figure 99. Synthesis of complex $[(\text{PhSiO}_{1.5})_{12}(\text{CuO})_4(\text{NaO}_{0.5})_4(\text{dppmO}_2)_2]$ **36**.

The compound **36** does not possess ionic components noted for complexes **34** and **35** (Fig. 100). The dppm ligand is subjected to *in situ* oxidation to the corresponding phosphine oxide. Also, a significant difference between compound **36** and complexes **34** - **35** is the coordination of the organic ligand to more sterically accessible sodium ions.

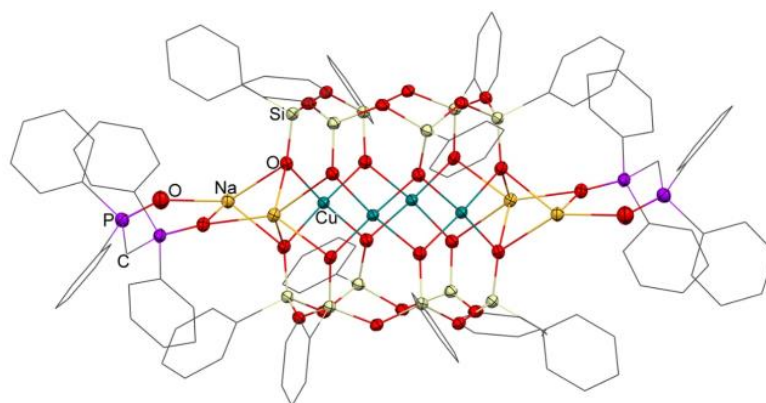


Figure 100. The structure of complex $[(\text{PhSiO}_{1.5})_{12}(\text{CuO})_4(\text{NaO}_{0.5})_4(\text{dppmO}_2)_2]$ **36**.

The studies of obtaining copper complexes containing organoelement sesquioxane ligands, we also carried out a series of works on the preparation of the corresponding derivatives, including rare germaniumsesquioxane ligands. The results of this investigation are presented in the next section.

1.2.4 Features of the synthesis and structure of Cu(II) - containing germsesquioxanes

The compounds containing Ge-O-Me fragments have been studied in details [171] and include various types of compounds: pure inorganic metallagermanates [172], "hybrid" (containing additional organic ligands) metallagermanates [173] and compounds obtained on the basis of germanium

sesquioxide. The latter group has been studied thoroughly; its synthesis is based on the hydrothermal approach, first proposed in 2009 [174]. The synthesis requires harsh conditions and a long reaction time (up to 10 days); products can incorporate metal ions in the Ge-O-M fragments and in salt fragments of carboxylic acids of the starting sesquioxide.

The last and most recently proposed (in 2016) series of compounds are metallagermsesquioxanes obtained under mild conditions of one-pot synthesis from $\text{PhGe}(\text{OMe})_3$. At the beginning of this dissertation, this method has been represented by only one publication describing Fe,Na-phenylgermsesquioxanes [47]. In this work, we describe the synthesis and crystal structures of a series of Cu(II) and Fe(III) based germanosesquioxane **37** – **42** obtained by described approach in ref. [47] from $\text{PhGe}(\text{OMe})_3$ or $[\text{PhSi}(\text{O})_{1.5}]$. The details of the synthesis are described in Experimental Section on this manuscript and the details of the crystal structures are given in Annex 2 (Table 28).

Using transmetallation of sodium ions of starting cage compound $[(\text{Ph}_5\text{Ge}_5\text{O}_{10})_3\text{Fe}_6(\text{OH})_3(\text{O})\text{Na}_2]$ **37** [47] *via* reaction with CuCl_2 followed by complexation with 2,2'-bipyridine, complex $(\text{PhGeO})_{12}(\text{PhGe}_2\text{O})[\text{Fe}_5\text{O}_{17}(\text{OH})]\text{Cu}_2(2,2'\text{-bipy})_2$ **38** was isolated in 9% yield (the crystal data are given in Annex 2, Table 28) (Fig. 101, method A).

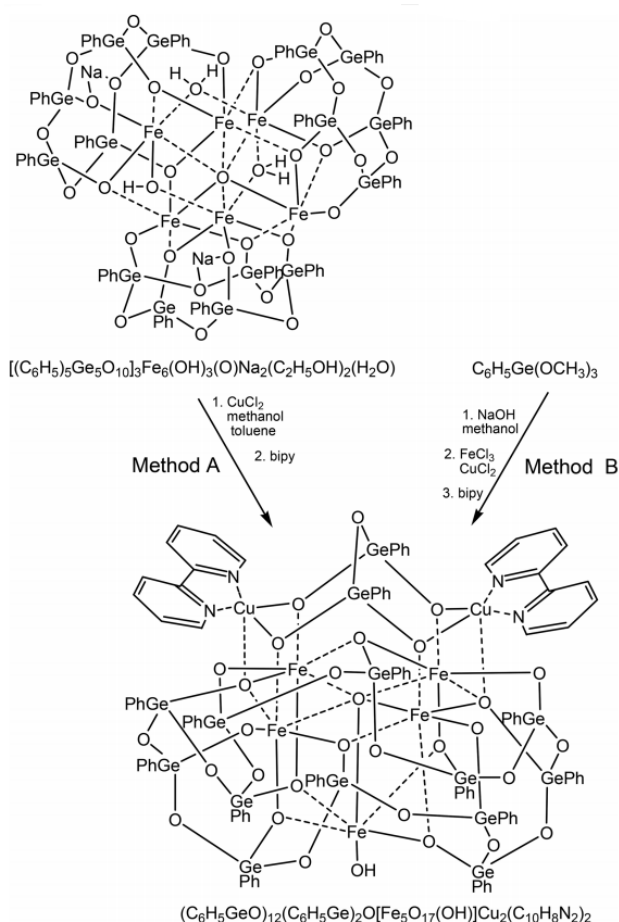


Figure 101. Synthesis of complex $(\text{PhGeO})_{12}(\text{PhGe}_2\text{O})[\text{Fe}_5\text{O}_{17}(\text{OH})]\text{Cu}_2(2,2'\text{-bipy})_2$ **38**.

Structure of **38** includes a mixed oxocluster with Cu_2Fe_5 core coordinated by ligands of two previously unknown types: cyclic twelve-membered $\text{Ph}_{12}\text{Ge}_{12}\text{O}_{24}$ and acyclic dimeric $\text{Ph}_2\text{Ge}_2\text{O}_5$ (Fig. 102). The formation of such structural fragments indicates a deep structural rearrangement since the initial compound **37** includes only cisoid pentameric ligands of the $[(\text{Ph}_5\text{Ge}_5\text{O}_{10})]$ composition. In addition, synthesis of **38** also caused the deep modification of the stable central site Fe_6O_{19} (Lindquist polyanion) of the initial compound **37**, with the elimination of the FeO group and the formation of the unusual Fe_5O_{18} oxocluster. The resulting vacant position is occupied by the bridging fragment $\text{Ph}_2\text{Ge}_2\text{O}_5$ also coordinating two copper(II) ions. The latter is additionally bound to two 2,2'-bipyridine molecules. This significant structural changes in comparison with the starting compound explain the low yield of product **38**. The alternative approach of its synthesis based on self-assembly from $\text{PhGe}(\text{OMe})_3$ was performed (Fig. 101, method B). Starting reagents (phenyltrimethoxygermane, 2,2'-bipyridine, copper (II) and iron (III) chlorides) were taken in an optimal ($\text{Ge}_{14} : \text{Cu}_2 : \text{Fe}_5 : \text{N}_4$) ratio to obtain the targeted product. Compound **38** was obtained with 21% yield.

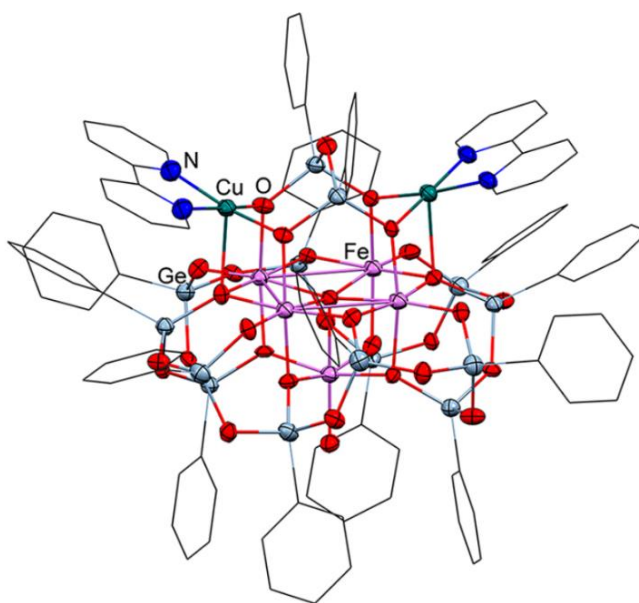


Figure 102. The structure of complex $(\text{PhGeO})_{12}(\text{PhGe}_2)\text{O}[\text{Fe}_5\text{O}_{17}(\text{OH})]\text{Cu}_2(2,2'\text{-bipy})_2$ **38**.

Germanium phenyltrichloride PhGeCl_3 , converted into the oligomeric compound $[\text{PhGeO}_{1.5}]_n$ (hydrolytic polycondensation) was tested as an alternative source of germesquioxane fragments. For this, an interaction between the oligomer $[\text{PhGeO}_{1.5}]_n$ and sodium hydroxide were carried out. Due to the low solubility of the oligomer under the reaction conditions, a large excess of alkali (Na / Ge ratio = 3/1) was used. On the other hand, such high concentration of reactive groups $\text{PhGe}(\text{O}^-\text{Na}^+)_3$ allowed to introduce a large amount of copper(II) ions into the germesquioxane matrix *via* the interaction with CuCl_2 . As a result, highnuclear complex $[\text{Na}_4\text{Cu}_{42}(\text{Ph}_2\text{Ge}_2\text{O}_5)_{12}(\text{OH})_{40}]$ **39** was obtained in 20% yield (the crystal data are given in Annex 2, Table 28) (Fig. 103).

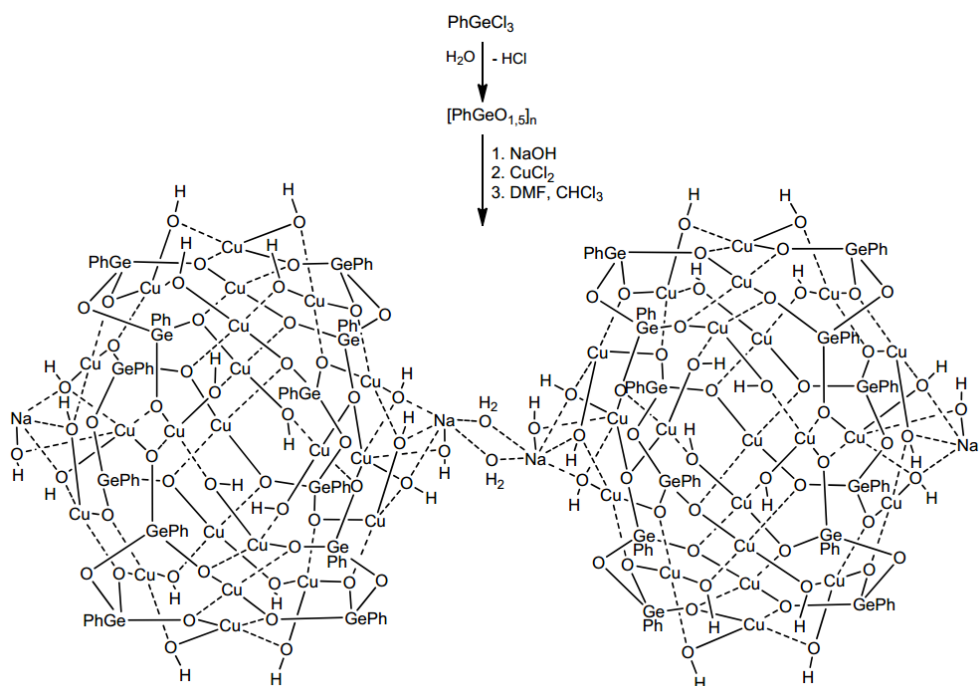


Figure 103. Synthesis of complex $[\text{Na}_4\text{Cu}_{42}(\text{Ph}_2\text{Ge}_2\text{O}_5)_{12}(\text{OH})_{40}]$ **39**.

It has a dimeric structure containing two cage fragments with unusually high nuclearity, $\text{Cu}_{21}\text{Ge}_{12}$ (Fig. 104). The connection of two framework components is realized *via* outer-sphere sodium ions coordinated by the oxygen centers of four hydroxyl groups and two water molecules. In turn, copper(II) ions are coordinated by various ligands : hydroxyl groups, solvating DMF molecules, and germsesquioxane ligands. Six germanium-containing fragments in structure **39** are bridge acyclic ligands of the $\text{Ph}_2\text{Ge}_2\text{O}_5$ composition. Thus, the product **39** becomes the first example of metallagermsesquioxane framework without cyclic Ge ligands.

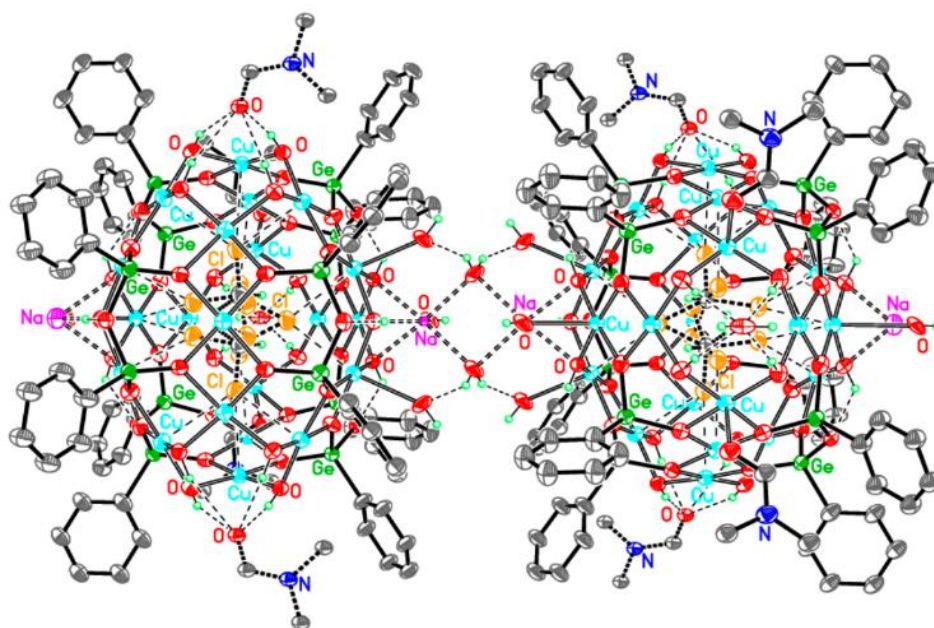


Figure 104. The structure of complex $[\text{Na}_4\text{Cu}_{42}(\text{Ph}_2\text{Ge}_2\text{O}_5)_{12}(\text{OH})_{40}]$ **39**.

Twenty-one copper ions of the framework fragments of complex **39** form almost planar fragments (three with the composition Cu_3O_8 and six with the composition Cu_2O_6), in which the four-coordinated metal atoms have a planar configuration. Six copper ions are additionally coordinated by two DMF and four OH ligands, while thirteen copper atoms coordinate the chlorine atom of the encapsulated chloroform molecule. Only two sterically screened copper(II) ions retain their four-coordinated geometry. It is noteworthy that examples of the encapsulation of chloroform by framework metallasesquioxanes have never been reported. Probably, the presence of chloroform in the reaction mixture contributes to the assembly of such multinuclear core architecture **39** due to a template effect.

The study of the self-assembly reaction of coppergermsesquioxanes from $\text{PhGe}(\text{OMe})_3$ led to the formation of crystalline products under conditions of additional complexation with 1,10-phenanthroline $[(\text{PhGeO}_{1.5})_{10}(\text{CuO})_6(\text{HO}_{0.5})_2(1,10\text{-phen})_2] \cdot 2\text{H}_2\text{O}$ **40** (in 21% yield) or 2,2'-bipyridine $[(\text{PhGeO}_{1.5})_{10}(\text{CuO})_6(\text{HO}_{0.5})_2(2,2'\text{-bipy})_2] \cdot 5\text{EtOH}$ **41** (in 39% yield) (the crystal data are given in Annex 2, Table 28) (Fig. 105).

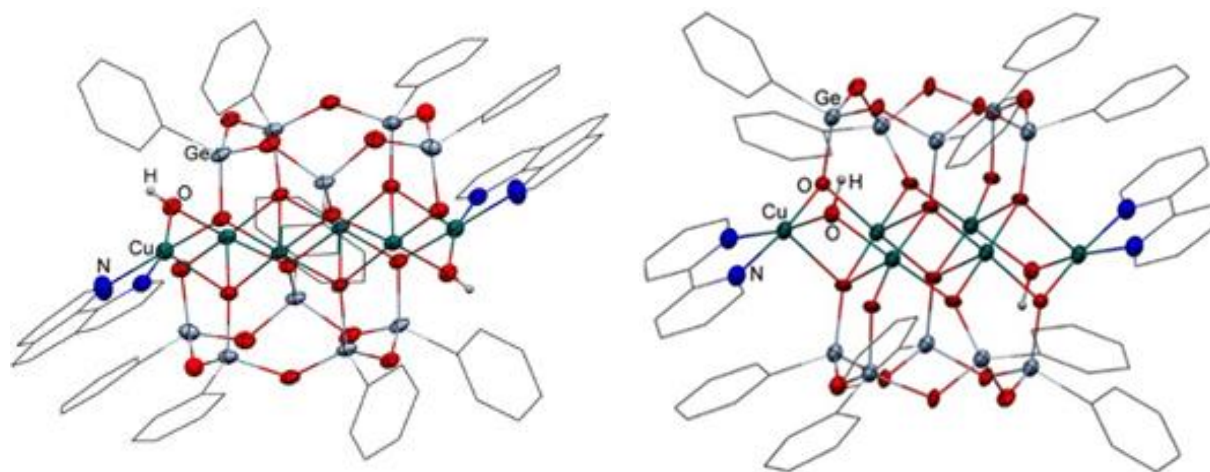


Figure 105. The structure of complexes $[(\text{PhGeO}_{1.5})_{10}(\text{CuO})_6(\text{HO}_{0.5})_2(1,10\text{-phen})_2] \cdot 2\text{H}_2\text{O}$ **40** (left) and $[(\text{PhGeO}_{1.5})_{10}(\text{CuO})_6(\text{HO}_{0.5})_2(2,2'\text{-bipy})_2] \cdot 5\text{EtOH}$ **41** (right).

Structures of complexes **40** – **41** are similar to silsesquioxane complexes **17** – **32**, they include two linear Cu_3 fragments coordinated by three pairs of ligands: cyclic pentameric phenylgermesquioxanes, bidentate N,N-ligands, and “charge-balancing” HO^- groups.

The self-assembly reaction of copper phenylhermsesioxane in the presence of two types of nitrogen ligands (2,2'-bipyridine and 3,5-dimethylpyrazole) lead to product $(\text{PhGeO}_2)_{10}\text{Cu}_6(2,2'\text{-bipy})_2(3,5\text{-Me}_2\text{Pz})_2$ **42**, isolated in 17% yield (Fig. 106) [175].

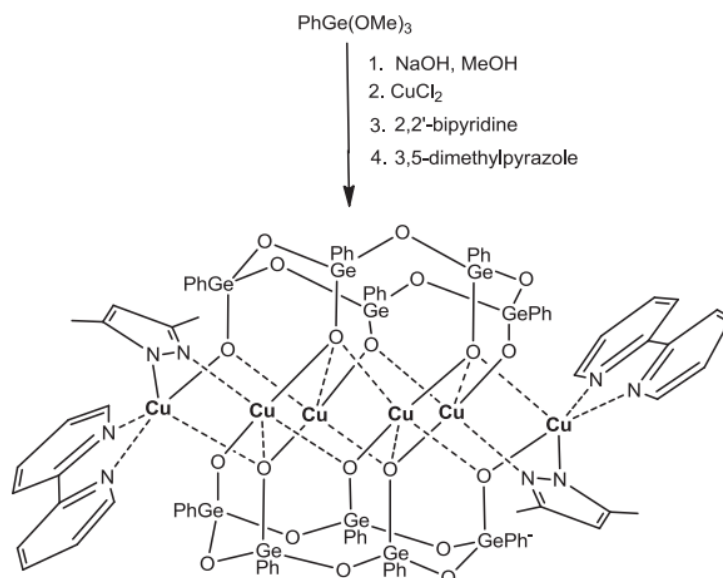


Figure 106 Synthesis of complex (PhGeO₂)₁₀Cu₆(2,2'-bipy)₂(3,5-Me₂Pz)₂ **42**.

The coordination of copper ions in one compound by three types of ligands (cyclic germsesquioxanes, bipy, 3,5-Me₂Pz) is an unusual feature of product **42**. Two cisoid sesquioxane ligands of composition (PhGeO_{1.5})₅ coordinate central layer of copper oxide forming two almost linear (171.10 °) Cu-Cu-Cu fragments. Some of the copper centers also coordinated by two additional N,N-ligands: 2,2'-bipyridine and 3,5-dimethylpyrazole (Fig. 107). The methods of coordination of nitrogen ligands differ significantly - nitrogen atoms of bipy moieties coordinate the same copper ion, while nitrogen atoms 3,5-Me₂Pz connect to neighboring copper atoms, acting as bridging ligand. [176]. In addition, due to the deprotonation of nitrogen atoms, pyrazolate fragments play the role of charge-balancing groups.

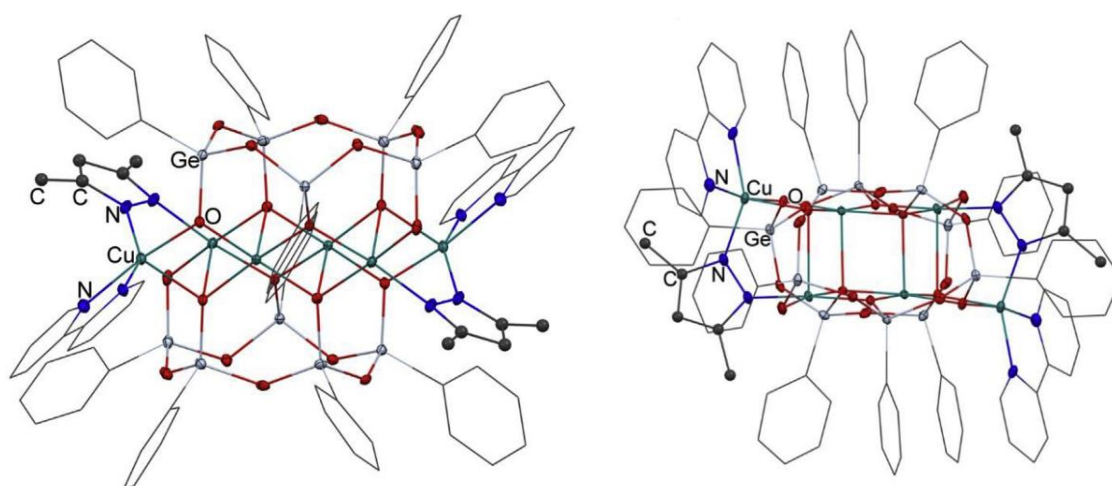


Figure 107. The structure of complex **42**: side view (left) and top view (right).

In summary, 36 complexes (**1** - **36**) of new polyhedral methyl and phenylsilsesquioxanes containing Cu(II), ions, characterized by different compositions and structures, depending on the

stoichiometric ratio of reagents, solvent systems, and type of ligands have been obtained. For the first time, new types of odd number nuclearity complexes as, 3, 5, 9 and 11 have been synthesized and characterized, namely, [(MeSiO_{1.5})₈(CuO)₃(2,2'-bipy)₂] • 3EtOH **6**, [(MeSiO_{1.5})₁₈(CuO)₉] • DMSO **1**, [(PhSiO_{1.5})₁₀(CuO)₅(Py)₅] **13** [(PhSiO_{1.5})₁₂(PhSiO_{1.5})₈(CuO)₈(NaO_{0.5})₄{Cu(O_{0.5})₄}] • 2[Cu(dppe)₂] **34**, respectively. An interesting impact of the solvent nature on the framework nuclearity has been evidenced. In fact, the use of DMSO promotes to increase the number of atoms in the cage (**1**), while the employment of pyridine helps to decrease it (**13**). An unusual structural feature of hexanuclear copper-silsesquioxanes complexes (2,2'-bipyridine, 1,10-phenanthroline, bathophenanthroline ligands) was observed. Namely, a presence of two pentameric sesquioxane ligands was not enough to maintain a charge balance for Cu₆²⁺ complexes. Due to this, several types of balancing anions (HO⁻, MeO⁻, Fm⁻, AcO⁻) were found in the composition of corresponding complexes. Appearance of formate and acetate groups is a consequence of mild oxidation of alcohol (methanol or ethanol) used as a reaction media. Moreover, the study of the effect of bidentate N-containing ligands on the structural topology demonstrated the formation of a supramolecular packing due to the π - π stacking interactions between the aromatic systems of nitrogen ligands (phenanthroline, [(PhSiO_{1.5})₁₀(CuO)₆(HO_{0.5})₂(C₁₂H₈N₂)₂] • 4.75DMSO **27**) of neighboring molecules (not observed for bipyridine, bathophenanthroline, and 3,5-dimethylpyrazole).

The effect of bidentate P,P-ligands on the architecture of the resulting complexes has been studied too. It was shown that dppe part of the cationic fragments Cu^I(dppe)₂ promotes the formation of unusual Cu₉Na₄ and Cu₄Na₂ cages. It was shown the versatility of the self-assembly reaction to obtaining Ge-containing complexes. It was described the example of the occurrence of oxidative processes dppm → dppmO₂, under mild conditions in the presence of copper ions (without the additional introduction of oxidizing reagents) during [(PhSiO_{1.5})₁₂(CuO)₄(NaO_{0.5})₄(dppmO₂)₂] **36** formation.

It was obtained and characterized five new polyhedral Cu(II)- or Cu(III)/Fe(III)-phenylsilsesquioxanes complexes (**38** – **42**) with different compositions and structures, depending on the stoichiometric ratio of reagents, solvent systems, and type of ligands. For the first time, the complexes containing 42 Cu(II) ions [Na₄Cu₄₂(Ph₂Ge₂O₅)₁₂(OH)₄₀] **39** was prepared.

The catalytic activity of Cu(II)-silsesquioxanes and Cu(II)-germanosequioxane in the reactions of C–H functionalization and oxidative amidation was conducted. The results of catalytic researches present in the next section.

1.3 Investigation of catalytic properties of Cu(II)-sesquioxanes

As was described in the literature review (Part I, Catalytic properties of metallasesquioxanes), Cu(II)-containing silsesquioxanes are proved to be very effective catalysts for the oxidation of hydrocarbons by peroxides and the oxidative amidation process. The catalytic potential of metallasilsesquioxanes and metallagermsesquioxanes attention due to their possibility to form a variety of polynuclear topologies containing Si- or Ge-matrixes, with transition metal ions combined *via* oxygen atoms. The addition of organic ligands to the structure of the complex is able to stabilize the active catalyst particles. Using the Cu-containing compounds as a catalyst makes the process cheaper comparing catalysts based on expensive metals such as ruthenium and rhodium saving the same efficiency. These results suggest that the search for new catalysts, including abundant metal ions, for example, copper or iron ones is a promising scientific task, deserving further investigation.

1.3.1. Oxidative amidation

As was described in literature review section (Part I, Catalytic properties of metallasesquioxanes), the use of sesquioxane derivatives of these metals is effective for homogeneous amidation reaction: metallasesquioxanes retain high activity down to 100 ppm for copper and down to 500 ppm for iron. In this line of thought, compounds **17**, **26**, **33** – **35**, **38** – **39**, **41** were tested in the oxidative amidation conditions (cooperation with Dr. F. Lamaty) (Fig. 108, Table 10).

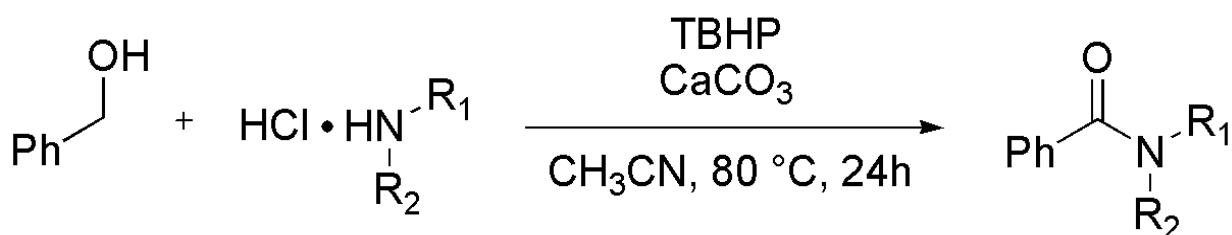


Figure 108. Synthesis of amides using oxidative amination reaction.

Testing the catalytic properties of $(\text{PhGeO})_{12}(\text{PhGe}_2)\text{O}[\text{Fe}_5\text{O}_{17}(\text{OH})]\text{Cu}_2(2,2'\text{-bipy})_2$ **38** was especially attractive because this complex contains both, copper(II) and iron(III) ions in the structure. Different amines (used in the form of ammonium salts) were reacted with benzyl alcohol in the presence of catalytic amounts of complex **38**. An additional base (high-purity 99.995% calcium carbonate) and *tert*-butyl hydroperoxide (used as terminal oxidant) were also used in the reaction. The optimization of the process showed that catalyst **38** demonstrates high yields and efficiency even at of 0.4 mol% loading. The difference in activity in comparison to the previously investigated copper- and iron-silsesquioxanes can be associated with the effect of the germesquioxane matrix in compound **38** (germanium can be

considered as an additional metal in the catalyst composition). Thus, secondary (\pm)-N-(α -methylbenzyl) benzamide was obtained in a very high yield of 93%. The use of cyclohexylamine and *n*-butylamine led to corresponding amides in 84 – 85% yields. It was found that the amidation reaction is also effective for secondary amines; corresponding amides (N-benzoylmorpholine and N,N-dibenzylbenzamide) were isolated in 82% and 71% yields, respectively. Moreover, found values of the turnover number (TON) and turnover frequency (TOF) of the catalyst - 232 and 9.7 h⁻¹, respectively, also indicate the high efficiency of catalyst **38** (TON = mmol of product / mmol of catalyst; TOF = TON / reaction time).

Testing of two similar in composition catalysts [(PhSiO_{1.5})₁₀(CuO)₆(HO_{0.5})₂(2,2'-bipy)₂] • 2.5 DMSO **17** and [(PhSiO_{1.5})₁₀(CuO)₆(HO_{0.5})₂(1,10-phen)₂] • 4DMSO **26**, logically, did not affect significantly on catalytic activity. Secondary and tertiary amides were obtained in yields 59 – 86%. It was found that even low catalyst loadings (100 ppm Cu) of **17** and **26** do not decrease yields of the target amides. Values of TON and TOF reached 8600 and 478 h⁻¹, respectively.

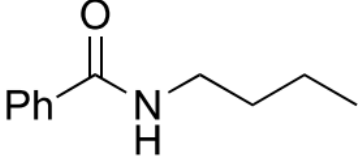
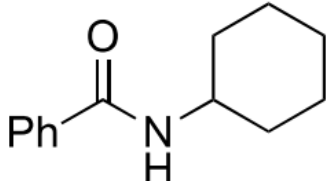
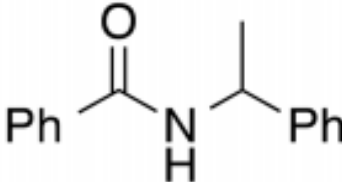
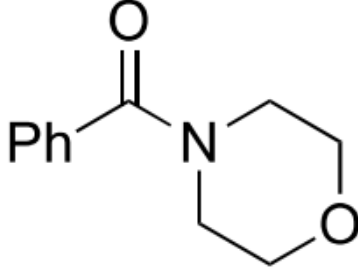
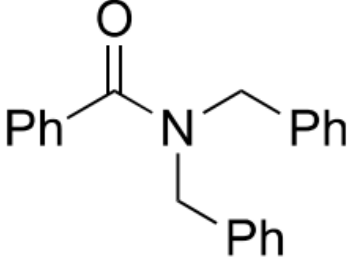
Complex Ph₁₂Si₁₂O₁₂(OH)(O⁻)₁₁Cu₅Na(2,2'-bipy)₃(H₂O)(THF)₇ **33** was tested as a catalyst at loading of 0.4 mol%; the secondary amides α -methylbenzylamine and cyclohexyls were obtained in 83 and 88% yields, respectively. The tertiary amines, the N-butylbenzamide and N-dibenzylbenzamide were isolated in good yields of 70% and 68%, respectively. TON and TOF were also calculated, giving values up to 220 and 9.2 h⁻¹, respectively.

Even low loadings of catalysts [(PhSiO_{1.5})₁₂(PhSiO_{1.5})₈(CuO)₈(NaO_{0.5})₄{Cu(O_{0.5})₄}] • 2[Cu(dppe)₂] **34** and [(PhSiO_{1.5})₁₂(CuO)₄(NaO_{0.5})₂] • 2[Cu(dppe)₂] **35** (100 ppm Cu), led to various amides in good yields (64 – 84%). It was found that primary amines are more reactive than secondary amines. Both complexes demonstrate high catalytic activity (excellent TON and TOF values were obtained, up to 8400 and 350 h⁻¹, respectively).

In turn, catalyst [Na₄Cu₄₂(Ph₂Ge₂O₅)₁₂(OH)₄₀] **39** at loading of 0.04 mol% allowed to transform the hydrochloride salts of α -methylbenzylamine and cyclohexylamine to the corresponding amides in 85% and 88% yields, respectively. Tertiary amides N-morpholinamide and N,N-dibenzylbenzamide were isolated in 71% and 86% yields, respectively. TON and TOF values were calculated and the best results are 2200 and 92 h⁻¹, respectively.

Complex [(PhGeO_{1.5})₁₀(CuO)₆(HO_{0.5})₂(2,2'-bipy)₂] • 5EtOH **41** was tested at a low loading 0.2 mol% Cu. Secondary amides, obtained from the corresponding hydrochloride salts (*n*-butyl, cyclohexyl, and (\pm)- α -methylbenzylamine), were isolated in yields range from 79 to 88%. The formation of tertiary amides was found to be less efficient (4-benzoylmorpholine and N,N-dibenzylbenzamide were obtained in 72 and 79% yields, respectively). TON and TOF values for this catalyst reach 220 and 9.2 h⁻¹, respectively.

Table 10. Results of catalytic studies of complexes **17**, **26**, **33** - **35**, **38** - **39**, **41**.

Amide	Catalyst	Yield, %	TON / TOF h ⁻¹
	17 . 0.01 mol. %	67	6700 / 279
	26 . 0.01 mol. %	68	6800 / 378
	33 . 0.4 mol. %	70	175 / 7.3
	34 . 0.01 mol. %	76	7600 / 317
	35 . 0.01 mol. %	77	7700 / 321
	38 . 0.4 mol. %	84	210 / 8.8
	39 . 0.04 mol. %	88	2200 / 92
	17 . 0.01 mol. %	78	7800 / 325
	26 . 0.01 mol. %	70	7000 / 389
	33 . 0.4 mol. %	88	220 / 9.2
	34 . 0.01 mol. %	74	7400 / 308
	35 . 0.01 mol. %	68	6800 / 283
	38 . 0.4 mol. %	85	213 / 8.9
	39 . 0.04 mol. %	85	2125 / 89
	17 . 0.01 mol. %	75	7500 / 313
	26 . 0.01 mol. %	84	8400 / 467
	33 . 0.4 mol. %	83	208 / 8.6
	34 . 0.01 mol. %	82	8200 / 342
	35 . 0.01 mol. %	83	8300 / 346
	38 . 0.4 mol. %	93	232 / 9.7
	41 . 0.2 mol. %	87	218 / 9.1
	17 . 0.01 mol. %	59	5900 / 246
	26 . 0.01 mol. %	61	6100 / 339
	34 . 0.01 mol. %	64	6400 / 267
	35 . 0.01 mol. %	86	6800 / 283
	38 . 0.4 mol. %	82	205 / 8.5
	39 . 0.04 mol. %	71	1775 / 74
	41 . 0.2 mol. %	72	180 / 7.5
	17 . 0.01 mol. %	86	8600 / 358
	26 . 0.01 mol. %	86	8600 / 478
	33 . 0.4 mol. %	68	170 / 7.1
	34 . 0.01 mol. %	77	7700 / 321
	35 . 0.01 mol. %	84	8400 / 350
	38 . 0.4 mol. %	71	178 / 7.4
	39 . 0.04 mol. %	86	2150 / 90
	41 . 0.2 mol. %	79	198 / 8.2

The data obtained were compared with the results of previous years, where the oxidative amidation was catalyzed by the reference catalyst CuO (TON and TOF values did not exceed 44 and 11 h⁻¹, respectively [39]).

1.3.2 Oxidative C–H activation

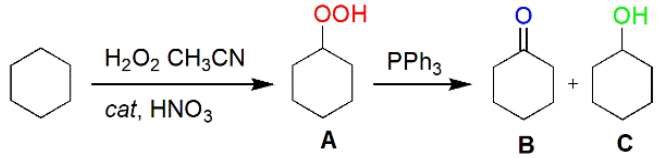
As was noted in the literature review section (Part I, Catalytic properties of metallasesquioxanes), the oxidation of hydrocarbons, alcohols, and other C–H compounds by peroxides in the presence of metal complexes is an important area of modern metal complex catalysis [177, a-b]. In particular, copper(II) ions are present in the active centers of various oxidizing enzymes [178, a-c], and a wide variety of bioinspired catalytic systems have been developed for the oxidation of C–H bonds by peroxides [179, a-e]. With previously reported results of high activity of Fe- and Cu-sesquioxanes in mind, we were interested in evaluation of copper and iron-containing cage complexes (obtained in the presenting dissertation) as catalysts in oxidation reactions (cooperation with Dr. Georgiy B. Shulpin).

Cyclohexane (0.46 M) was chosen as a model substrate for the oxidation of saturated hydrocarbons. Oxidation was carried out with aqueous hydrogen peroxide in the presence of a catalyst in CH₃CN solution. Product concentrations were measured by gas chromatography after the treatment of the reaction sample with solid PPh₃ [180]. The efficiency of the catalysts was compared to the literature data: under comparable conditions but in the presence of Cu(NO₃)₂, oxidation products were obtained in a yield of 3.5% [181].

It was shown that the use of complexes **1**, **13**, **36**, **38** – **39** as catalysts for the oxidation of cyclohexane did not lead to the formation of the products in the absence of the acid cocatalyst HNO₃ (Table 11). The efficiency of metallasesquioxanes as a catalyst increased with use of acid cocatalyst (0.05 M); so, it can be assumed that the acid cleaves part of the bonds between the sesquioxane ligands and copper and / or iron ions, facilitating the access of the substrate to the catalytic sites. It is most likely that on the first stage, the metallasesquioxanes' catalysts are structurally modified in the presence of an acid cocatalyst and thus plays the role of a precatalyst.

The oxidation of cyclohexane under the action of H₂O₂ (50% aqueous, 2M) in the presence of complex [(MeSiO_{1.5})₁₈(CuO)₉] • DMSO **1** leads to a total yield of oxidation products of 20% after five hours of the reaction. TON value reaches 184 (ketone: alcohol ratio = 0.084: 0.0008). The oxidation of cyclohexane by 70% aqueous hydrogen peroxide in the presence of **13** allowed to obtain cyclohexyl hydroperoxide in 18% yield after one hour of reaction.

Table 11. The efficiency of catalysts **1**, **13**, **36**, **38** – **39** in the oxidation reaction of cyclohexane with H₂O₂ in the presence of an acid.

		
The concentration of precatalyst, M	Temperature, °C	(Yield, TON)
1. 5×10^{-4}	50	20%, B : C = 0.084 : 0.008 TON = 184, after 5 h
13. 5×10^{-4}	60	18%, after 1 h
36. 5×10^{-4}	50	26% after 2 h, TON = 240
38. 5×10^{-4}	40	28%, after 2 h, TON = 260
39. 2.5×10^{-4}	40	22%, after 1 h, TON = 400

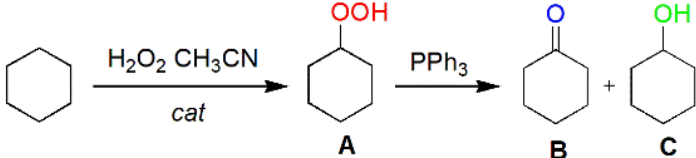
Oxidation of cyclohexane under the action of H₂O₂ (50% aqueous, 2M) in the presence of complex (PhGeO)₁₂(PhGe₂)O[Fe₅O₁₇(OH)]Cu₂(2,2'-bipy)₂ **38** leads to a total yield of oxidation products of 28% after two hours of reaction at 40 ° C (TON = 182). Oxidation of cyclohexane at lower loading of complex [Na₄Cu₄₂(Ph₂Ge₂O₅)₁₂(OH)₄₀] **39** (2.5×10^{-4} M) in the presence of nitric acid led to corresponding products of oxidation in 22% yield after 1 hour of the reaction (TON = 400).

Complexes [Ph₁₂Si₁₂O₁₂(OH)(O⁻)₁₁Cu₅Na(2,2'-bipy)₃(H₂O)(THF)₇] **33**, [(PhSiO_{1.5})₁₂(CuO)₄(NaO_{0.5})₂] • 2[Cu(dppe)₂] **35**, and [(PhGeO_{1.5})₁₀(CuO)₆(HO_{0.5})₂(1,10-phen)₂] • 2H₂O **41** were also tested as catalysts for the oxidation of cyclohexane with hydrogen peroxide in the absence of acid (Table 12). It was shown that catalysis by complex **33** leads to the formation of oxidation products in a total yield of 20% after two hours. TON reached 190.

The oxidation of cyclohexane in the presence of **35** led to the formation of cyclohexanol (0.039 M) and cyclohexanone (0.015 M) with TON = 108. It should be noted that presence of HNO₃ (0.05 M) led to decrease in the product yield (0.004 and 0.00027 M of cyclohexanol and cyclohexanone, respectively).

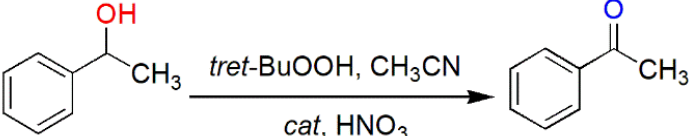
Complex **41** showed good catalytic activity in the oxidation reaction of cyclohexane with an aqueous solution of hydrogen peroxide at room temperature, leading to products with a yield of 29% after two hours of the reaction.

Table 12. The efficiency of catalysts **33**, **35** и **41** using oxidation reaction of cyclohexane H₂O₂ without acid.

		
The concentration of precatalyst, M	Temperature, °C	(Yield, TON)
33 , 5×10^{-4} M	50	20%, after 2 h, TON = 190
35 , 5×10^{-4} M	60	5.9%, B : C = 0.039 : 0.015 TON = 108, after 1 h
41 , 5×10^{-4} M	20	29%, after 2 h

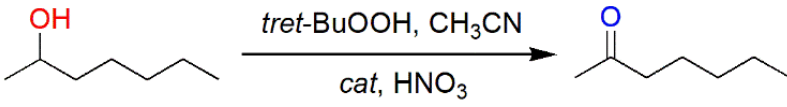
Another type of evaluation of the catalytic properties of Cu- and Fe-containing complexes **1**, **13**, **33**, **35** – **36**, **38**, **41** was the oxidation of alcohols to ketones using TBHP and H₂O₂ (Table 13). Oxidation of 1-phenylethanol with TBHP (70% aqueous) in acetonitrile in the presence of nitric acid (0.05 M) was chosen as a model. The best result was demonstrated by (PhGeO)₁₂(PhGe₂)O[Fe₅O₁₇(OH)]Cu₂(2,2'-bipy)₂ **38** – yield was 100% after five hours of reaction.

Table 13. The results of catalytic studies of complexes **1**, **13**, **33**, **35** - **36**, **38**, **41**.

				
The concentration of precatalyst, M	C(alcohol), M	C(acid), M	T, °C	(Yield, TON)
1 , 5×10^{-4} M	0.33	1.17	50	96% after 5 h
13 , 5×10^{-4} M	0.4	1.2	60	94% after 4 h
33 , 5×10^{-4} M	0.33	1.2	50	94%, after 14 h, TON = 600
35 , 5×10^{-4} M	0.5	1.2	60	94 % after 10 h
36 , 5×10^{-4} M	0.5	1.5	50	76% after 10 h
38 , 5×10^{-4} M	0.5	1.5	50	100 % after 5 h
41 , 5×10^{-4} M	0.16	1.2	50	98 % after 9 h

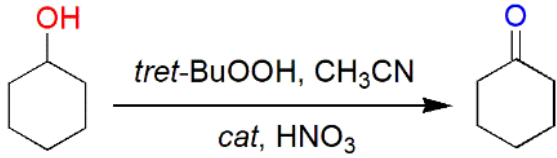
The oxidation reaction of 2-heptanol in the presence of nitrogen led to the formation of 2-heptanone in the presence of $[(\text{PhSiO}_{1.5})_{10}(\text{CuO})_5(\text{Py})_5]$ **32** in 50% yield and in the presence of $(\text{PhGeO})_{12}(\text{PhGe}_2)\text{O}[\text{Fe}_5\text{O}_{17}(\text{OH})]\text{Cu}_2(2,2'\text{-bipy})_2$ **38** - in 43% yield (Table 14).

Table 14. The results of catalytic studies of complexes **32**, **38**.

		
The concentration of precatalyst, M	Temperature, °C	Yield, TON
32 , $5 \times 10^{-4}\text{M}$	60	50% after 4 h
38 , $5 \times 10^{-4}\text{M}$	50	43%

For another model reaction, oxidation of cyclohexanol with *tert*-butyl hydroperoxide (70% aqueous, 1.2 M) in acetonitrile to form cyclohexanone (Table 15) was chosen. The following data were used for comparison of catalyst efficiency: the oxidation of cyclohexanol with TBHP, catalyzed by the Cu complex $[\text{Cu}_2(\text{L}-\kappa\text{ONO}')_2(\mu\text{-}4,4'\text{-bipy})(\text{DMF})_2]$ and $[\text{Cu}_2(\mu\text{-L-}1\kappa\text{ONO}':2\kappa\text{O})_2(\mu\text{-}4,4'\text{-bipy})]_n \cdot n\text{H}_2\text{O} \cdot n\text{DMF}$ leading to cyclohexanone in 55% yield [182]. The best results among metallasesquioxanes were demonstrated by $[(\text{PhSiO}_{1.5})_{12}(\text{CuO})_4(\text{NaO}_{0.5})_2] \cdot 2[\text{Cu}(\text{dppe})_2]$ **35**, giving cyclohexanone in 72% yield after five hours (TON = 550).

Table 15. The results of catalytic studies of complexes **1**, **26**, **34** - **36**, **38**.

			
The concentration of precatalyst, M	C(alcohol), M	T, °C	Yield, TON
1 , $5 \times 10^{-4}\text{M}$	0.38	50	77% after 24 h
26 , $5 \times 10^{-4}\text{M}$	0.4	60	83% after 16 h
34 , $5 \times 10^{-4}\text{M}$	0.38	60	70 % after 3 h
35 , $5 \times 10^{-4}\text{M}$	0.38	60	72% after 5 h TON = 550
36 , $5 \times 10^{-4}\text{M}$	0.46	50	76% after 10 h
38 , $5 \times 10^{-4}\text{M}$	0.38	50	60 % after 2 h

Oxidation of benzene with H₂O₂ (50%, 3M), catalyzed by [(PhSiO_{1.5})₁₀(CuO)₆(HO_{0.5})₂(1,10-phen)₂] • 2.5 DMSO **13** (5 × 10⁻⁴ M), in the presence of HNO₃ (0.05 M) at 60 ° C gave phenol in 15% yield after 2 hours of reaction. The efficiency of complex **35** turned out to be similar and leads to the formation of phenol (0.41 M) in 14% yield after 2 h along with overoxidation product (*p*-quinone, 0.008 M) (Fig. 109).

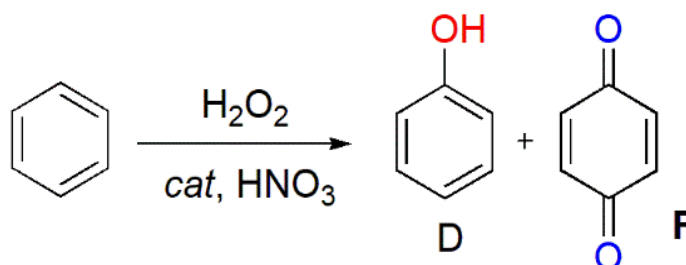


Figure 109. Synthesis of amides using oxidative amination reaction with H₂O₂.

For the investigation of the nature of the oxidizing particles, we studied the selectivity parameters of the process on the oxidation reactions of linear (*n*-heptane, Table 16), branched and cyclic (methylcyclohexane) saturated hydrocarbons with hydrogen peroxide for **1**, **13**, **17**, **26**, **33**, **38**, **39** and **41**. Obtaining results demonstrate that reaction proceeds *via* the intermediate formation of hydroxyl radicals, which then attack the C–H bonds of the substrate [183, a-c].

Table 16. The results from the study of regioselectivity in the oxidation reaction of *n*-heptane.

	Cat	Time(min)	C(1):C(2):C(3):C(4)
	1	60	1.0 : 6.0 : 6.5 : 6.0
	13	60	1.0 : 4.1 : 4.4 : 4.5
	17	60	1.0 : 5.2 : 5.2 : 4.7
	26	60	1.0 : 5.3 : 5.6 : 5.0
	33	60	1.0 : 5.5 : 5.0 : 4.5
	38	60	1.0 : 6.5 : 6.7 : 7.0
	39	60	1.0 : 7.4 : 7.2 : 7.9
	41	60	1.0 : 6.3 : 6.3 : 5.6

The oxidation of *cis*-1,2-dimethylcyclohexane in the presence of various metallasesquioxane catalysts led to the production of tertiary alcohols with a mutual configuration of methyl groups (*trans* / *cis*) with a ratio from 0.7 (**61**) to 0.9 (**33**). The selectivity parameters of methylcyclohexane oxidation catalyzed by **36** are 1: 2: 3 = 1.0: 5.4: 15.0, and for **41** complex 1: 2: 3 = 1.0: 5.4: 16.0.

The regioselectivity parameters of the oxidation of methylcyclohexane under the action of TBHP in the presence of complex $\{[(\text{PhSiO}_{1.5})_{10}(\text{CoO})_5(\text{H}_2\text{O})_2]_2[(\text{PhSiO}_{1.5})_{10}(\text{CuO})_5]\}$ **16** were studied. The possible structures of oxidation products (13 compounds) are shown in Fig. 110.

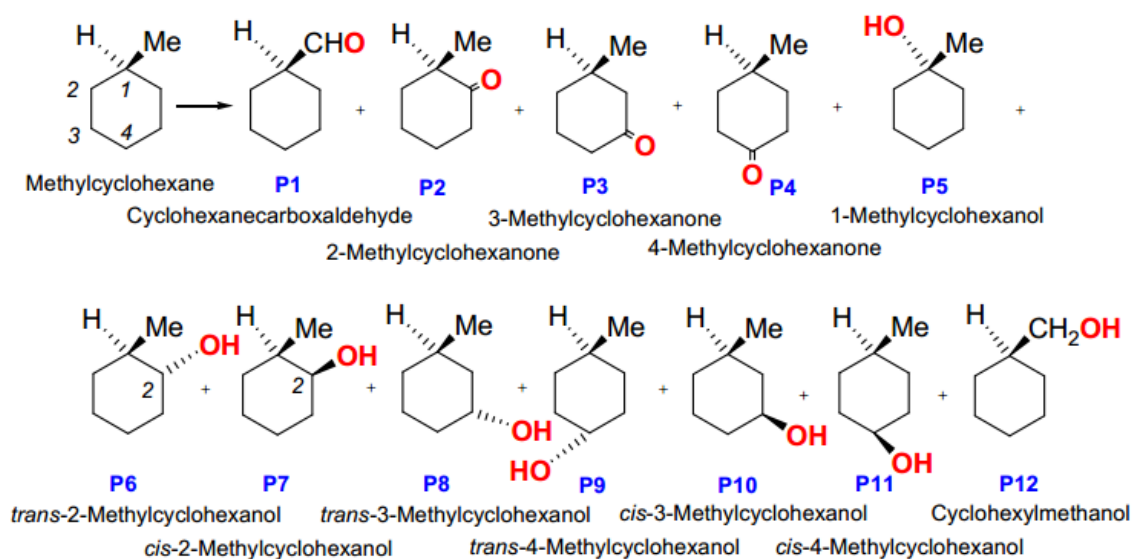


Figure 110. Oxidation products of methylcyclohexane H_2O_2 catalyzed by the complex **16**.

In table 17 shows the product yields of the oxidation of methylcyclohexane at various reaction times before and after the addition of PPh_3 . The obtaining data indicate that the oxidation of H_2O_2 occurs with the participation of hydroxyl radicals.

Table 17. Oxidation of methylcyclohexane H_2O_2 catalyzed by complex **16**.

№	Time, min	P2	P3	P4	P5	P6	P7	P8	P9	P10	P11	Sum
1.	10 before PPh_3	0.05	0.04	0.02	0.05	0.009	0.03	0.007	0.004	0.02	0.002	0.23
2.	10 after PPh_3	0.01	0.01	0.01	0.31	0.18	0.30	0.22	0.12	0.28	0.14	1.58
3.	20 before PPh_3	0.07	0.07	0.04	0.04	0.01	0.03	0.02	0.01	0.04	0.02	0.80
4.	20 after PPh_3	0.02	0.02	0.01	0.42	0.23	0.39	0.29	0.15	0.38	0.20	2.11
5.	60 before PPh_3	0.15	0.14	0.06	0.08	0.03	0.09	0.10	0.04	0.16	0.08	0.93
6.	60 after PPh_3	0.04	0.06	0.03	1.10	0.60	1.30	0.75	0.40	0.92	0.46	5.66
7.	120 before PPh_3	0.20	0.20	0.08	0.12	0.04	0.12	0.17	0.80	0.35	0.19	1.55
8.	120 after PPh_3	0.10	0.10	0.05	1.70	0.86	1.40	1.17	0.65	1.50	0.75	7.83
9.	180 before PPh_3	0.14	0.19	0.07	1.90	0.86	1.38	1.22	0.60	1.54	0.74	8.64

Based on the results of studied reactions of C–H functionalization catalyzed by Cu- and Fe-sesquioxane complexes, a reaction mechanism was proposed (Fig. 111).

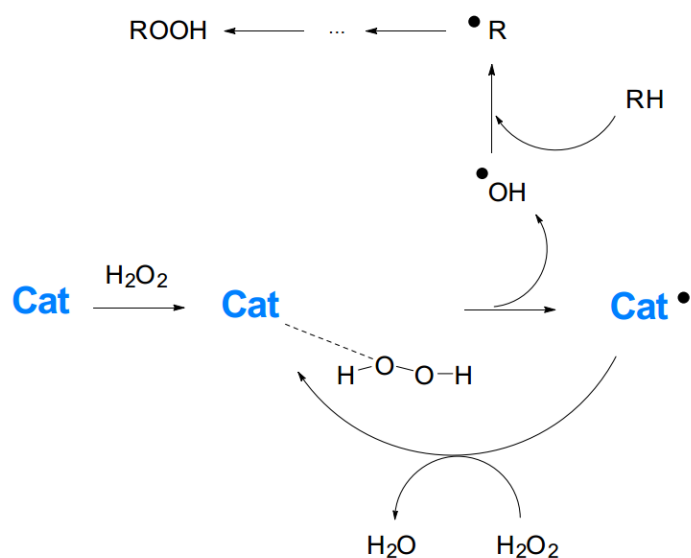


Figure 111. Supposed mechanism of catalytic oxidation of saturated hydrocarbons with peroxides in the presence of a catalyst.

The selectivity parameters of alkane oxidation let to conclude that peroxides H_2O_2 and *tert*-BuOOH under the action of metallasesquioxanes form radical $\text{HO}\bullet$ and *tert*-BuO \bullet species, which then attack the C–H bonds of substrates.

Chapter 2. Cu(II) - based silsesquioxanes: synthesis structure and magnetic properties

As we stated in section 1.2.1, copper(II)-based silsesquioxanes tend to form complexes of prismatic type crystal structure [184]. To study the possibility to achieve other types of molecular geometry based on coppersilsesquioxane unit, complex $[(\text{PhSiO}_{1.5})_{12}(\text{CuO})_4(\text{NaO}_{0.5})_4(\text{BuOH})_6]$ **42** of globular molecular architecture was chosen as the initial compound for further transformations [in ref 44]. This compound includes, in addition to copper ions, external sodium ions, which may easily be trasmetalated. In addition, the effect of replacing the solvating ligands (1- butanol) of compound **42** by other solvents was studied. This approach conducts to design of extended networks with 1D, 2D or 3D structures depending on the availability of the bridging ligands or the contacts «solvating ligand - M'» (M' stands for alkaline metal,). The details of the synthesis are described in the Experimental Section on this manuscript and the details of the crystal structures are given in Annex 2 (Table 29 - 30). Moreover, the magnetic properties of these networks have been investigated.

2.1 Copperphenylsilsesquioxanes with a globular framework structure

Good solubility of metallasilsesquioxanes (containing polar SiO^-M^+ fragments) in polar solvents makes it possible to replace the initial solvates (*n*-butanol) of compound **43** with a number of highly coordinating solvents of polar nature (acetonitrile, dioxane, DMSO) (Fig. 112).

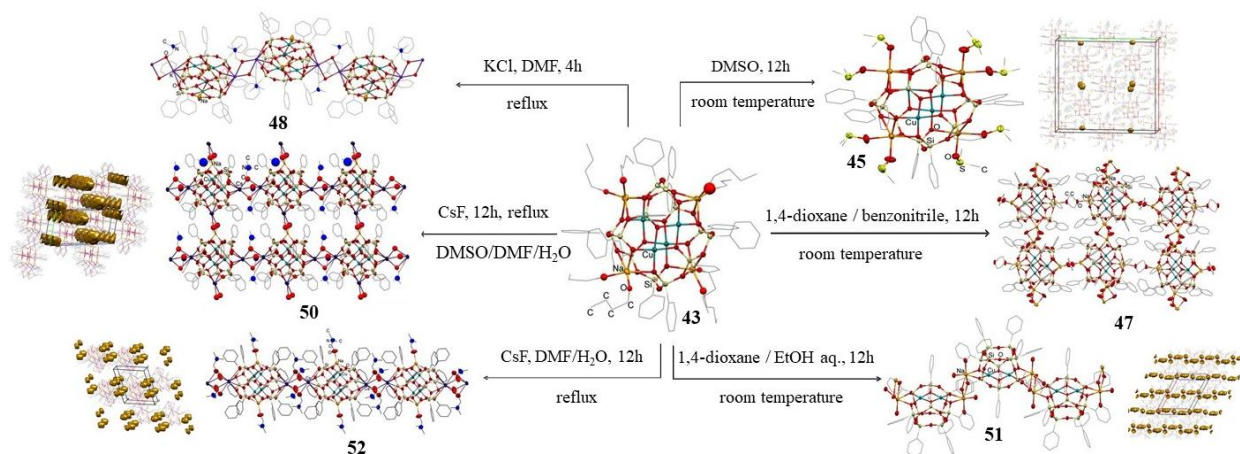


Figure 112. Synthesis of **45 – 52** from $(\text{PhSiO}_{1.5})_{12}(\text{CuO})_4(\text{NaO}_{0.5})_4 \cdot (\text{BuOH})_6$ **43**

On the one hand, the coordinating abilities of these solvents, which act as ligands in the formation of the crystal structure of the cage product, could contribute to a change in the type of molecular geometry of the product in comparison to globular type of the starting compound. Also, the possibilities of using these solvates for the design of supramolecular compositions are well known [185, a-b]. It

should be noted that before the start of presenting dissertation research, very limited number of directed designs of supramolecular derivatives of metallasilsesquioxanes was reported [186].

It was found that crystalline products of replacement butanol molecules of **43** by new solvates, namely, DMSO $[(\text{PhSiO}_{1.5})_{12}(\text{CuO})_4(\text{NaO}_{0.5})_4(\text{DMSO})_8]$ **44** (57% yield), acetonitrile $[(\text{PhSiO}_{1.5})_{12}(\text{CuO})_4(\text{NaO}_{0.5})_4(\text{MeCN})_6(\text{H}_2\text{O})_2] \cdot 2\text{MeCN}$ **45** (45% yield), dioxane / ethanol $[(\text{PhSiO}_{1.5})_{12}(\text{CuO})_4(\text{NaO}_{0.5})_4(1,4\text{-diox})(\text{EtOH})_4] \cdot 0.5\text{EtOH}$ **46** (39% yield) and dioxane / PhCN $[(\text{PhSiO}_{1.5})_{12}(\text{CuO})_4(\text{NaO}_{0.5})_4(1,4\text{-diox})_4(\text{H}_2\text{O})_3] \cdot 2\text{PhCN} \cdot 2(1,4\text{-diox}) \cdot \text{H}_2\text{O}$ **47** (55% yield) preserve the globular type geometry of initial complex **43**. At the same time, their ability to form supramolecular architectures is significantly different. The complex **44** coordinated by DMSO does not show a tendency towards inter-cage aggregation, while the complex **45** with acetonitrile demonstrates the formation of hydrogen-bonded layers through weak O-H \cdots N contacts between water molecules and MeCN ($r(\text{N} \cdots \text{O}) = 2.99 - 3.75 \text{ \AA}$ (Fig. 113).

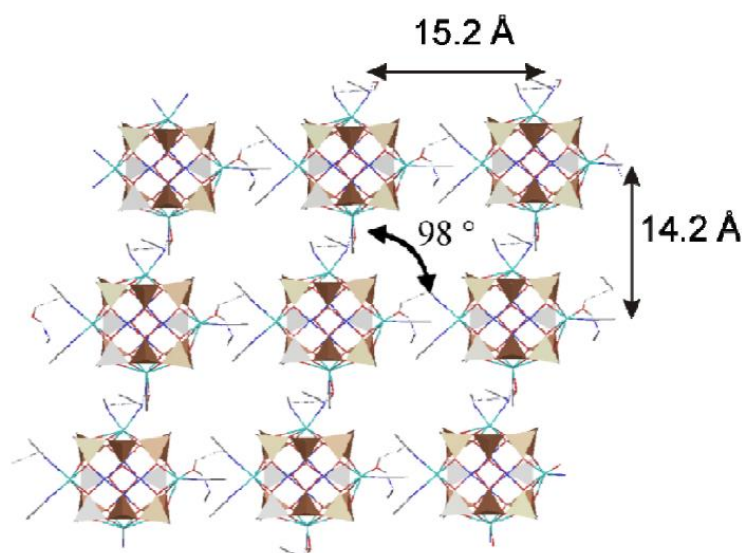


Figure 113. The structure of the crystal packing of the complex **45**.

In turn, the compounds coordinated by 1,4-dioxane molecules (**46** and **47**) demonstrate the efficient formation of the coordination polymer structure due to the coordination of neighboring cages with bridging dioxanes. It was noted that type of supramolecular product (1D or 2D) is determined by the choice of an additional solvate. Using the dioxane / ethanol combination (**46**), a one-dimensional zigzag product is formed, and the dioxane / benzonitrile combination (**47**) promotes the formation of a two-dimensional network compound (Fig. 114). The intramolecular Cu-O bonds are 3.9 – 4.1 Å for **44** – **45**, compared to 3.0 – 3.2 Å for **47**. Intramolecular bond in **46** is realized due to the interaction between two ethanol molecules O-H-O = 2.90 Å, (O-H-O angle = 137 °). The intramolecular OH-O hydrogen bond between the oxygen atoms of the siloxanolate anions in **47** is in the range of 3.12 – 3.65 Å.

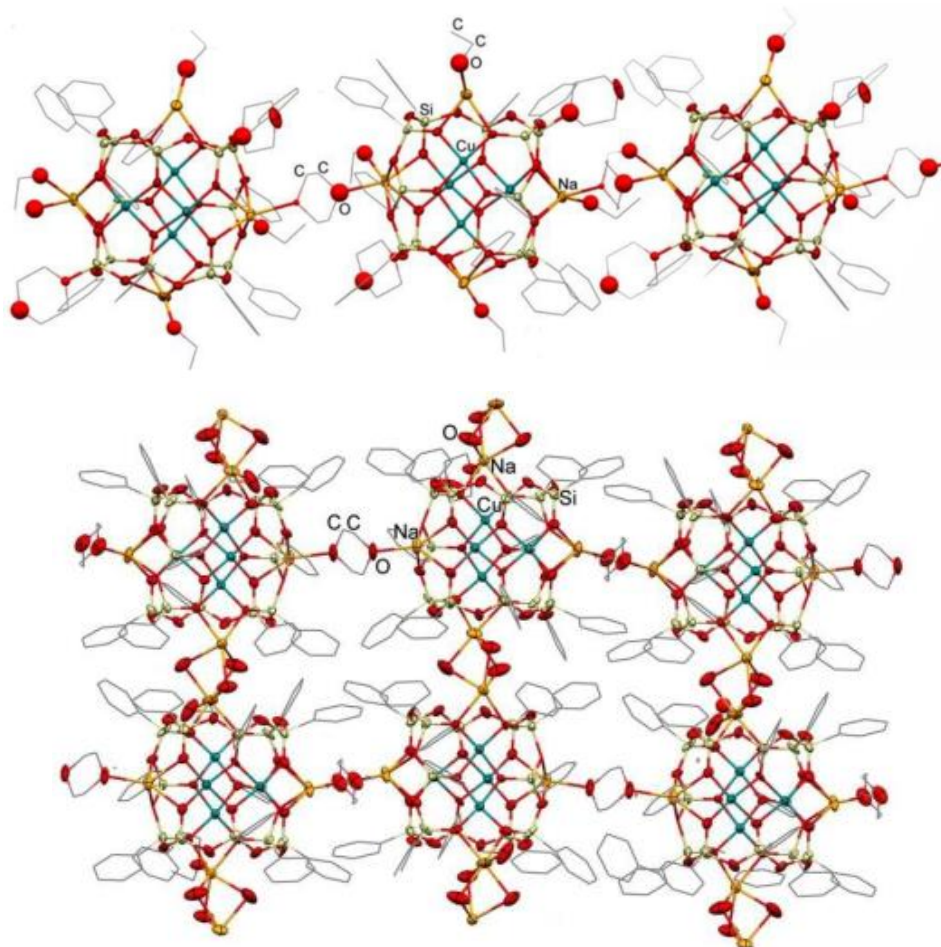


Figure 114. The structure of the crystal packing of the complex **46** (top) and **47** (bottom).

It is known from the literature that all coordination polymers based on cage metallasilsesquioxanes were connected with the participation of alkali metal ions [187]. On the other hand, the presence of sodium ions in the cage metallasilsesquioxane structure is often not enough to provide the formation of supramolecular structures. Thus, we were interested to investigate the effect of the insertion of alkali metal ions with larger ionic radius (potassium, cesium). It was suggested that the larger radius of the metal ion, the easier this ion could contact to potential binding linkers. Confirming this assumption, the derivative compound of **43** was obtained, with partial replacement of sodium ions. It was shown that mixed sodium / potassium product $[(\text{PhSiO}_{1.5})_{12}(\text{CuO})_4(\text{NaO}_{0.5})_2(\text{KO}_{0.5})_2(\text{DMF})_6]$ **48** forms a 1D coordination polymer *via* contacts of potassium centers (sodium ions are "inactive") (Fig. 115). The architecture of compound **48** is similar to that of compound **43**, and contains NaO_6 polyhedrons with a distorted trigonal prismatic geometry. Distances Na-O are in the range from 1.774 to 2.988 Å, which is comparable to the values observed for **44** – **47**.

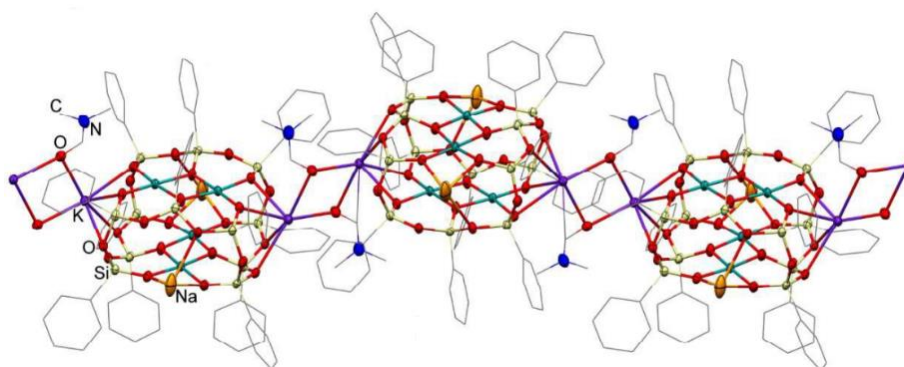


Figure 114. The structure of the crystal packing of the complex **48**.

The partial substitution of sodium ions by cesium led to 1D $[(\text{PhSiO}_{1.5})_{12}(\text{CuO})_4(\text{NaO}_{0.5})_3(\text{CsO}_{0.5})(\text{DMF})_4]$ **49** and 2D $[(\text{PhSiO}_{1.5})_{12}(\text{CuO})_4(\text{NaO}_{0.5})(\text{CsO}_{0.5})_3(\text{DMF})_4(\text{DMSO} \cdot \text{H}_2\text{O})] \cdot 1.5\text{DMF}$ **50** coordination polymer structures (Fig. 116). Compounds **49** – **50** also retain the globular geometry. In compound **49**, the NaO_5 coordination polyhedron takes on a square pyramidal geometry with a terminal DMF molecule. The sodium ion in **50** is part of NaO_4 , forming bonds with two oxygen atoms of the anion and two bridging solvent molecules at the vertices of the tetrahedron; it takes a tetrahedral geometry. The distances K-O and Cs-O are in the range from 2.712 to 2.939 and from 2.988 to 3.556 Å, respectively. In addition, potassium ions in **48** and cesium ions in **49** - **50** adopt high coordination numbers (≥ 7).

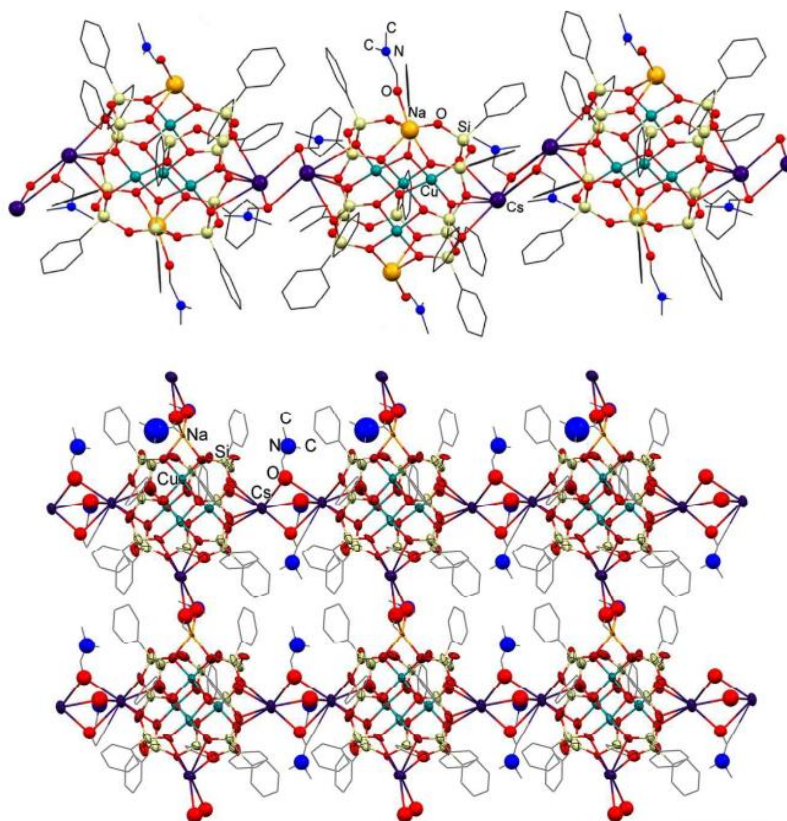


Figure 115. The structure of the crystal packing of the complex **49** (top) and **50** (bottom).

2.2. Copperphenylsilsesquioxane with a "Cooling Tower" framework structure

The complex **43** demonstrated an unexpected structural rearrangement in the case of ethanol / toluene solvent system. This results in isolation of compound $[(\text{PhSiO}_{1.5})_{10}(\text{CuO})_2(\text{NaO}_{0.5})_2(\text{H}_2\text{O})_6]$ **51** with the rare "Cooling Tower" type of architectural topology. Most probably that the driving force for formation of **51** is an organization of a stable condensed ligand $(\text{PhSiO}_{1.5})_{10}$, which includes two five-membered and one four-membered siloxane ring. Sodium ions of compound **51** take part in the formation of one-dimensional bent-shafted polymer chain (Fig. 117). In this case, the NaO_6 coordination polyhedron is formed from two oxygen atoms of phenylsilsesquioxane and four water molecules, two of them are bridging linkers, and two are terminal ligands. The smallest distance between neighboring Cu-Cu molecules is 12.217 Å.

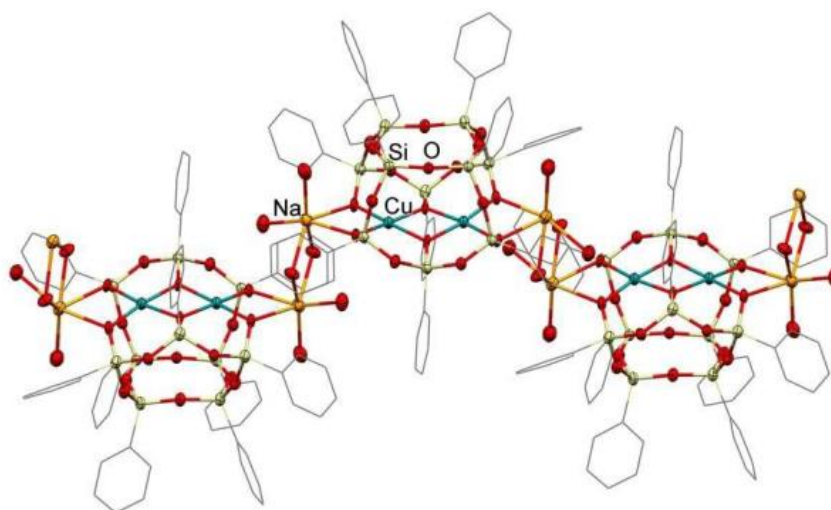


Figure 116. The structure of the crystal packing of the complex **51**.

It is worth mentioning that in principle structural rearrangements of metallasilsesquioxanes are described in detail [188], e.g. effects of oxidation of metal ions [189], elimination of an organic group from a silicon atom [190], and dimerization of framework fragments [191].

2.3 Copperphenylsilsesquioxanes with a prismatic framework structure

Further investigation of the transmetallation reaction of globular Cu,Na-phenylsilsesquioxane **43** using cesium ions (the compounds **48** - **50** described in Section 2. 2.1.) led to the formation of a prismatic complex $[(\text{PhSiO}_{1.5})_{12}(\text{CuO})_4(\text{NaO}_{0.5})_2(\text{CsO}_{0.5})_2(\text{DMF})_8] \cdot 0.5\text{H}_2\text{O}$ **52** (Fig. 118). As noted in Section 2.2., structural rearrangements are not rare in metallasilsesquioxanes chemistry. The formation of a prismatic form of cage fragment instead of a globular one (both forms are characterized by an identical ratio of "key" elements $\text{Si} : \text{Cu} = 12 : 4$) can be associated with almost equal enthalpies

of formation of these cage types and, consequently, the strong influence of the choice of solvents on the formation of one of them, discussed in [192].

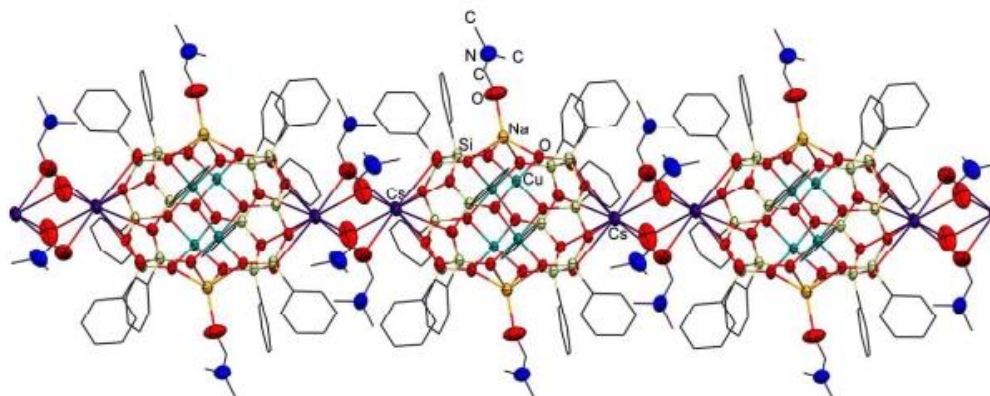


Figure 117. The structure of the crystal packing of the complex **52**.

Metal oxide Cu_2O_2 units of compound **52** are linked by the oxygen atoms of silsesquioxane, and by direct Cu-Cu interactions, while the Cu-O bonds between the atoms of neighboring Cu_2O_2 clusters and the Cu-Na bonds are absent. The NaO_5 coordination polyhedron adopts a square-pyramidal geometry. The distances Na-O in the complex **52** are in range from 1.774 to 2.988 Å.

2.4 Investigation of magnetic properties

The magnetic properties of Cu(II)-containing phenylsilsesquioxanes (1D coordination polymers with a linear chain $[(\text{PhSiO}_{1.5})_{12}(\text{CuO})_4(\text{NaO}_{0.5})(\text{CsO}_{0.5})_3(\text{DMF})_4(\text{DMSO} \cdot \text{H}_2\text{O})] \cdot 1.5\text{DMF}$ **50** zigzag chain $[(\text{PhSiO}_{1.5})_{10}(\text{CuO})_2(\text{NaO}_{0.5})_2(\text{H}_2\text{O})_6]$ **51**, and 2D coordination polymers $[(\text{PhSiO}_{1.5})_{12}(\text{CuO})_4(\text{NaO}_{0.5})_4(1,4\text{-diox})_4(\text{H}_2\text{O})_3] \cdot 2\text{PhCN} \cdot 2(1,4\text{-diox}) \cdot \text{H}_2\text{O}$ **47** and $[(\text{PhSiO}_{1.5})_{12}(\text{CuO})_4(\text{NaO}_{0.5})_2(\text{CsO}_{0.5})_2(\text{DMF})_8]$ **52** were investigated by using SQUID-MPMS magnetometer by Dr. J. Long (University of Montpellier) (Fig. 119).

At room temperature, the χT value ($0.81 \text{ cm}^3 \cdot \text{K} \cdot \text{mol}^{-1}$) for **50** is in close agreement with the expected value of $0.83 \text{ cm}^3 \cdot \text{K} \cdot \text{mol}^{-1}$ for two non-interacting copper ions ($S = 1/2$, $g = 2.1$). Upon cooling temperature, the decrease of value χT was observed, which indicates antiferromagnetic interactions between copper ions. At temperatures below 30 K, the χT is almost zero, which indicates a singlet diamagnetic ground state with $S = 0$. Using the Bleaney - Bowers equation [193] and in consideration of the additional intermolecular interaction between binuclear units, it was estimated value of the exchange interaction between the spin carriers: $J_{\text{Cu-Cu}} = -189.8 \pm 0.6 \text{ cm}^{-1}$, $g = 2.08 \pm 0.02$, intermolecular interaction $zJ' = -24 \pm 9 \text{ cm}^{-1}$.

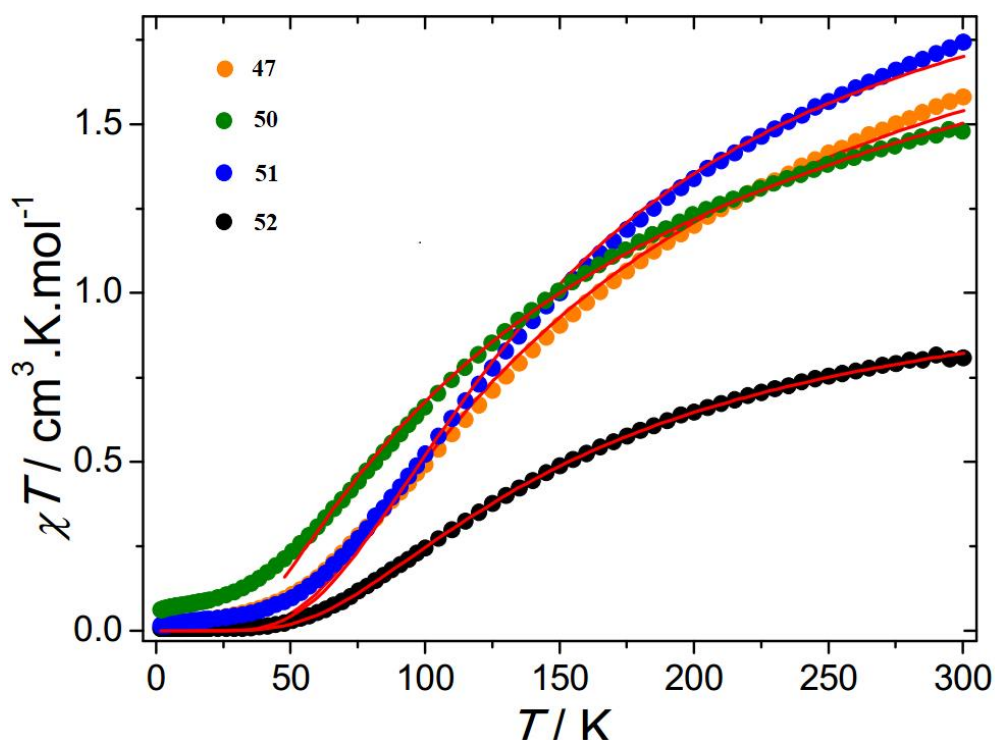


Figure 118. Temperature dependence of χT measured under a 1000 Oe DC field for compounds **47**, **50** - **52**. The red solid lines correspond to the fit.

The coordination silsesquioxane polymers containing central Cu_4 fragments in the cage have (**47**, **51**, and **52**), the χT values at 300 K equal $1.58 \text{ cm}^3 \cdot \text{K} \cdot \text{mol}^{-1}$, 1.74 , and $1.49 \text{ cm}^3 \cdot \text{K} \cdot \text{mol}^{-1}$, respectively. These values are close to the expected value of $1.65 \text{ cm}^3 \cdot \text{K} \cdot \text{mol}^{-1}$ corresponding to four independent copper ions $S = \frac{1}{2}$, $g = 2.1$. Upon cooling, the χT value decreases due to the appearance of antiferromagnetic interactions between metal ions. The values of exchange interactions for compounds **47** and **52** were determined using the model of a binuclear copper complex with introduction of intermolecular interactions. The following parameters were obtained: for **47**: $J_{\text{Cu-Cu}} = -181 \pm 2 \text{ cm}^{-1}$ and $zJ' = -83 \pm 4 \text{ cm}^{-1}$; for **52**: $J_{\text{Cu-Cu}} = -187 \pm 2 \text{ cm}^{-1}$ and $g = 2.073 \pm 0.007$ (Table 18). The χT value is not zero at low temperatures in the case of **51**, which indicates the presence of non-coupled metal atoms. The data were approximated by the molar fraction of unbound ions ρ in the Bleaney - Bowers equation, which allowed receiving the following parameters: $J_{\text{Cu-Cu}} = -126 \pm 2 \text{ cm}^{-1}$ and $g = 1.63 \pm 0.05$ and $\rho = 0.0017 \pm 0.0002$. The relatively low value of the gyromagnetic factor indicates the presence of dimer-dimer interactions in the last case. To further confirm this assumption, an approximation of the temperature dependence of the susceptibility in the range of 50 - 300 K was performed with considering intermolecular interactions. The following parameters have been obtained: $J_{\text{Cu-Cu}} = -128 \pm 1 \text{ cm}^{-1}$, $g = 2.14 \pm 0.02$, and $zJ' = -181 \pm 1 \text{ cm}^{-1}$, confirming the presence of strong intermolecular interactions in the system.

Table 18. Selected parameters of the exchange interaction in **47**, **51**, **52**.

Compound	Angle Cu-O-Cu (°)	Average distance Cu-O-Cu (°)	J_{Cu-Cu} (cm ⁻¹)
47	98.86 -102.40	100.66	-181
51	96.53-98.46	97.78	-126
52	98.27 - 101.90	100.33	-187

The differences of the exchange interaction strength for three compounds **47**, **51**, and **52** can be explained by the correlation of the value of the Cu-O-Cu angle (Table 18). The obtained values J_{Cu-Cu} for compounds **47** and **52** are a good agreement to other compounds having a Cu-O-Cu angle close to 100 ° [194]. In contrast, the exchange interaction values by **51** correspond to other binuclear frameworks with Cu-O-Cu angles are in the range from 98.51 to 98.80 ° [195].

Chapter 3. Ni(II) - based silsesquioxanes: synthesis, structure and magnetic properties

In addition to the investigation of copper(II)-containing sesquioxane complexes, we were also interested in the study of compounds containing metal ions with higher magnetic anisotropy. This section will present and discuss the synthesis, structures, and magnetic investigations of two Ni(II) compounds presenting polynuclear discrete architecture: Ni(II)-silsesquioxane and Ni(II)-germsesquioxane. Both of them exhibit a slow relaxation of the magnetization due to a spin glass behavior. The details of the synthesis are described in the Experimental Section on this manuscript and the details of the crystal structures are given in Annex 2 (Table 31).

3.1. Ni(II) - containing silsesquioxanes

In the literature review section (Part I, Magnetic properties of Ni(II)-containing sesquioxanes), numerous nickel(II)-containing phenylsilsesquioxanes (with nuclearity from Ni₂ to Ni₆) [129 - 137] exhibiting paramagnetic behavior or a spin glass behavior were described. Thus, further investigation of the nickelsilsesquioxanes was of great interest. Early, synthesis of cage silsesquioxanes with high nuclearity (Cu₇ or Cu₁₁) by the reactions involving bridging ligands - 4,4'-bipyridine and pyrazine [196], or terephthalic and 2,6-naphthalenedicarboxylic acids [197] was reported. By analogy with these results, interaction between Ni,Na-phenylsilsesquioxane and 4',4''''-(1,4-phenylene)bis(2,2':6',2''-terpyridine) (Fig. 120) which can act as a linker in the formation of supramolecular compositions [198, a-b] was performed.

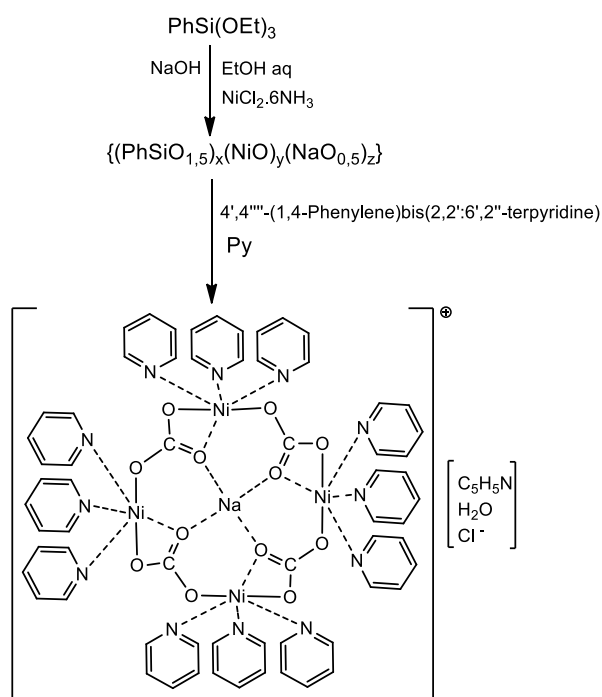


Figure 119. Synthesis of complex $[\text{Ni}_4(\text{CO}_3)_4(\text{Py})_8\text{Na}] \cdot \text{Cl} \cdot \text{Py} \cdot \text{H}_2\text{O}$ 53.

After crystallization of reaction mixture from pyridine solution, an unexpected complex $[\text{Ni}_4(\text{CO}_3)_4(\text{Py})_8\text{Na}] \cdot \text{Cl} \cdot \text{Py} \cdot \text{H}_2\text{O}$ **53** was isolated in 26% yield (Fig. 121). Certainly, appearance of carbonate fragments cannot be explained by the formal logic of synthesis. It is assumed that carbonate formation occurred upon contact of sodium ions with atmospheric CO_2 (synthesis and crystallization were carried out in air). A similar case was noted in [175] linked with the appearance of a sodium carbonate molecule encapsulated in the structure of Ni(II)-phenylsilsesquioxane cage. Most probably, the formation of complex **53** proceeds through the stage of the exchange reaction of sodium carbonate with nickel ions.

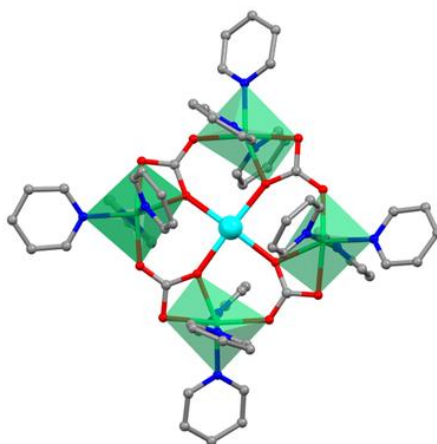


Figure 120. The structure of complex $[\text{Ni}_4(\text{CO}_3)_4(\text{Py})_8\text{Na}] \cdot \text{Cl} \cdot \text{Py} \cdot \text{H}_2\text{O}$ **53**.

Another unexpected feature of product **53** is the complete elimination of the silsesquioxane component. However, it was noted that there are numerous publications describing structural rearrangements during the synthesis of metallasilsesquioxanes, including oxidative processes [199, a-b], an appearance of metal oxide structural fragments [182], complete elimination of metal ions from the silsesquioxane matrix [200]. The formation of compound **53** can be regarded as a variation of the last of the above-mentioned processes, accompanied by spontaneous fixation of atmospheric CO_2 .

Structurally, the complex **53** is an example of architecture with a square-planar $[\text{Ni}_4(\text{CO}_3)_4\text{Na}]^+$ core, where four Ni(II) ions are coordinated by terminal pyridine molecules and bonded by carbonate linkers. The sodium ion is located in the center of this fragment (Fig. 122). Distorted octahedral coordination environment of each nickel ion is the same and is realized *via* the participation of three oxygen atoms of the carbonate bridges and three nitrogen atoms of the terminal pyridine ligands. The positive charge of the $[\text{Ni}_4(\text{CO}_3)_4\text{Na}]^+$ core is balanced by the presence of external Cl^- anion. Ni-Ni intramolecular distances in a square fragment are in the range of 5.200 – 5.266 Å. The central Na^+ ion adopts a flat-square geometry with distances Na-O in the range 2.195 – 2.227 Å and O-Na-O angles in the range 88.17 – 91.60°. Lengths of the Ni-O bonds are in the range 2.031 – 2.102 Å, while Ni-N = 2.099 – 2.142 Å. Two angles N-Ni-N are different and are in the range 88.25 – 89.80°. The

same situation is noted for the O-Ni-O angles, the values of which vary between 62.84 – 63.42°, 107.31 – 110.69°, and 170.32 – 173.56°.

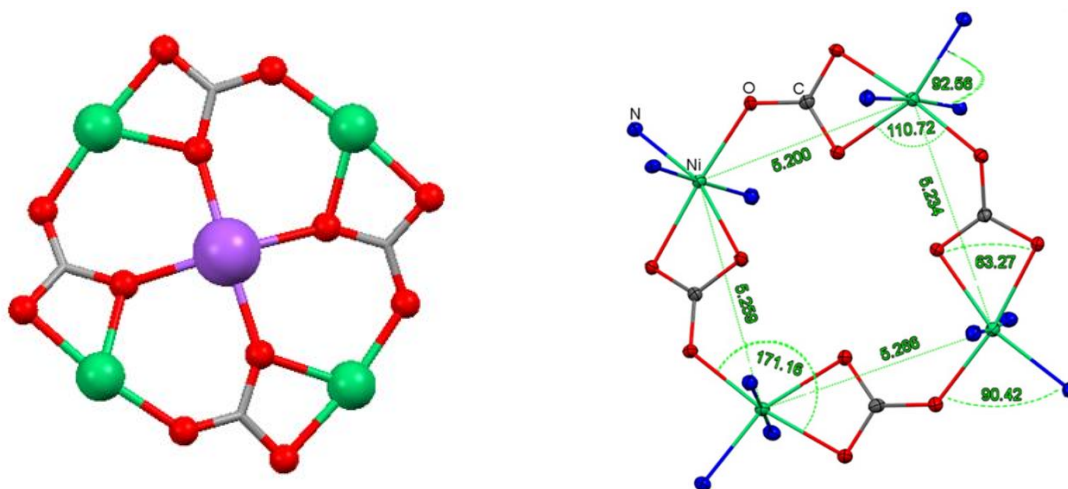


Figure 121. The geometry of Ni (II) site **53** (left); Ni₄ fragment with selected angles and distances (the central Na atom has been omitted for clarity) (right).

The crystal packing of compound **53** (Fig. 123) is characterized by the shortest intermolecular Ni-Ni distance of 7.893 Å, as well as the presence of hydrogen bonds between one oxygen atom of the carbonate ligand, molecule of crystallized water, and chloride ion.

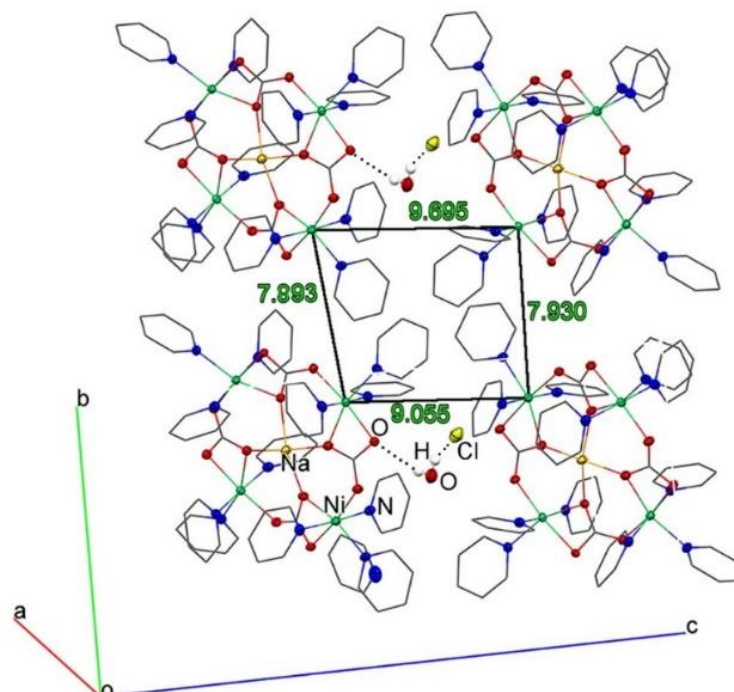


Figure 122. The structure of the crystal packing of the complex **53**.

Magnetic properties of **53** were studied. At room temperature, **53** exhibits a χT value of 3.86 cm³·K·mol⁻¹ which is in relatively good agreement with the value of 4.00 cm³·K·mol⁻¹ expected for

four non-interacting octahedral Ni²⁺ ions ($S = 1$, $g = 2.00$). The thermal dependence of χT shows an increase upon lowering the temperature to reach a maximum at 8 K with a χT value equal to 12.56 cm³·K·mol⁻¹ (Fig. 124, left) suggesting the presence of dominant ferromagnetic interactions between the spin carriers. This maximum value remains however greater than that of 10.00 cm³·K·mol⁻¹ expected for a $S = 4$ specie that would result from a ferromagnetic coupling between four Ni²⁺ ions.

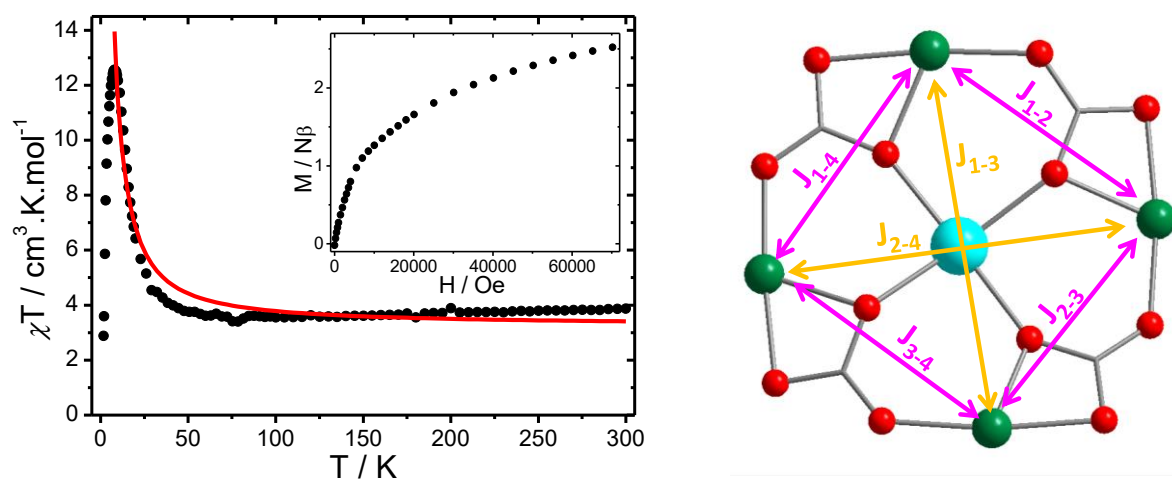


Figure 123. Temperature dependence of χT under an applied magnetic field of 1000 Oe for **53**; Inset: Field dependence of the magnetization at 1.8 K for **53** (left); The tetranuclear core and the considered exchange interactions (right).

Below 8 K, a sharp decrease of χT is observed which could be ascribed to the presence of intermolecular interactions and/or zero-field splitting. The field dependence of the magnetization at 1.8 K shows a value of 2.52 $N\beta$ under a 70 kOe field without any saturation indicating the presence of a magnetic anisotropy (Fig. 124, inset). With the aim to evaluate the strength of the exchange interactions, the PHI software was employed to model the thermal dependence of χT , with the discarded low temperature region. Two different exchange interactions were considered: between either neighboring (J_{adj}) and opposite (J_{opp}) Ni²⁺ ions (Fig. 124, right). In addition, an intermolecular zJ' term was also included. However, this leads to a relatively poor fitting with the following parameters are $J_{\text{adj}} = 2.4 \pm 0.3$ cm⁻¹; $J_{\text{opp}} = 2.4 \pm 0.6$ cm⁻¹, $g = 1.8000 \pm 0.0008$ (the g factor is too weak for Ni²⁺) and $zJ' = 0.117 \pm 0.003$ cm⁻¹. Note that due to the presence of four crystallographically different Ni²⁺ ions in association with various distances and bridging angles, these parameters are represented as average values.

In order to investigate the occurrence a magnetic ordering, the zero-field cooled/field-cooled (ZFC/FC) procedure was carried out. The ZFC curve of **53** exhibits a peak with a maximum located at $T_{\text{max}} = 3.8$ K whereas the FC curve continuously increases (Fig. 125, left). The divergence of the ZFC/FC curves, defined as the irreversible temperature T_{irr} is observed at about 5 K. This magnetic irreversibility is further confirmed by the opening of the hysteresis loop at 1.8 K with a coercive field of 900 Oe (Fig. 125, right) indicating the presence of most likely a short-range magnetic ordering.

This latter may arise from the slow relaxation of the magnetisation of two different origins: (i) the blocking process of isolated or weakly interacted magnetic molecules usually called a superparamagnetic-like or SMM behaviour, or (ii) a collective transition of magnetic molecules induced by a relatively strong dipolar interactions with random distribution associated with a spin frustration, usually known as a spin glass comportment.

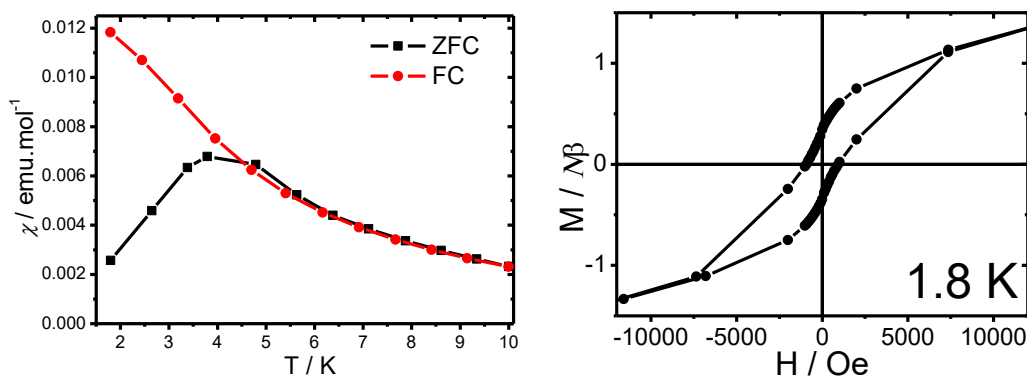


Figure 124. FC/ZFC curves performed under an applied magnetic field of 100 Oe for **53** (left); Hysteresis loops obtained at 1.8 K for **53** (right).

In order to investigate the relaxation dynamic, which is usually helpful to determine the origin of the slow relaxation, alternating current (AC) measurements were conducted. The temperature dependence of the in-phase (χ') and the out-of-phase (χ'') components of the ac susceptibility was measured in zero-dc field and reveals a frequency dependence for both components pointing out the occurrence of a slow relaxation of the magnetization (Fig. 126). Hence, both maxima of χ' and χ'' components are shifted towards higher temperature as the frequency increases from 1 to 1500 Hz. The first analysis in order to discriminate between the SMM and spin-glass behaviours could be done by calculating the Mydosh parameter ϕ ($\phi = (T_{max} - T_{min}) / (T_{max} \times \log v_{max} - \log v_{min})$), which monitors the amplitude of the out-of-phase peaks' shift with frequency. For **53**, this parameter is equal to 0.08, which is lower than the values observed for classical superparamagnets (ϕ is usually higher than 0.1) and thus rather indicates the occurrence of a spin-glass behavior. Secondly, the extraction on the relaxation time, τ , allows to nicely fit its temperature dependence with an Arrhenius law, $\tau = \tau_0 \exp(U_{eff}/k_B T)$, where U_{eff} is the average energy barrier for the reversal of the magnetization, τ_0 is the attempt time and k_B is the Boltzmann constant. This gave the U_{eff} and τ_0 values equal to 63 cm⁻¹ and 1.36.10⁻¹³ s, respectively. The obtained τ_0 value is however slightly lower than those expected for pure superparamagnetic systems (10⁻⁸ – 10⁻¹² s). Thirdly, fitting with a critical scaling law, $\tau = \tau_0 [T_g / (T_{max} - T_g)]^{z\nu}$ (where T_g is the glass temperature and $z\nu$ a critical exponent), usually used to describe the relaxation of spin glasses gave the following parameters: $\tau_0 = 9.74 \times 10^{-3}$ s, $T_g = 1.83$ K and $z\nu = 12.3$. The critical exponent is found slightly out-of-the range ($4 < z\nu < 12$) observed for spin-

glasses, whereas the glass temperature is somewhat lower in comparison with the maximum temperature on the ZFC curve ($T_{\max} = 3.8$ K). This therefore indicates a complex relaxation dynamic in **53**, which most likely fits with the presence of the spin-glass behaviour.

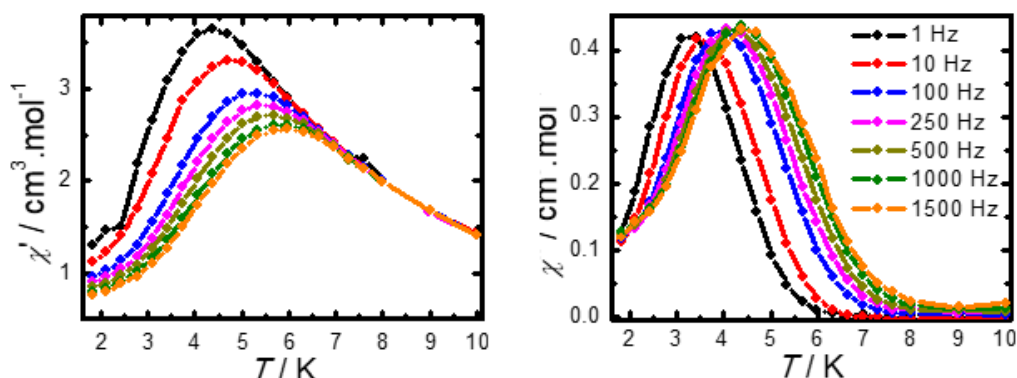


Figure 125. Temperature dependence of the in-phase (χ') and out-of-phase (χ'') susceptibilities for **53** under a zero dc-field.

To ultimately confirm the spin-glass dynamics, the ZFC relaxation curves with temporary cooling (memory effect) have been measured. The magnetization as a function of the time reveals the typical jump when the temperature switches from 4.0 to 1.8 K. The initial relaxation dynamics continues after warming to 4.0 K confirming the distribution of relaxation times expected for a spin-glass system.

3.2 Ni(II) - containing germsquioxanes

Before the start of this dissertation work, such compounds were never described in the literature. Using the self-assembly reaction between $\text{PhGe}(\text{OMe})_3$, NaOH , and $[\text{Ni}(\text{NH}_3)_6]\text{Cl}_2$ in ethanol, the first example of such complex with the composition $[(\text{PhGeO}_{1.5})_{10}(\text{NiO})_4(\text{NaO}_{0.5})_2] \cdot 9\text{EtOH} \cdot 4\text{H}_2\text{O}$ **54** was obtained in 30% yield (Fig. 127) [201].

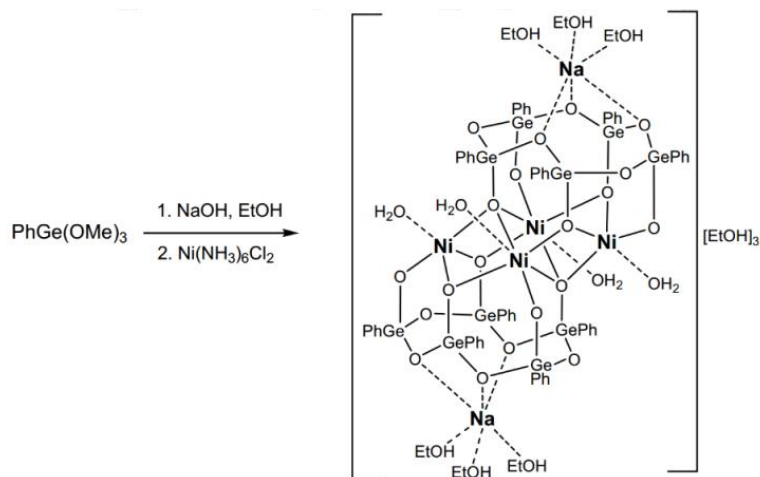


Figure 126. Synthesis of complex $[(\text{PhGeO}_{1.5})_{10}(\text{NiO})_4(\text{NaO}_{0.5})_2] \cdot 9\text{EtOH} \cdot 4\text{H}_2\text{O}$ **54**.

X-ray study of **54** showed that the product is a hexanuclear (Ni_4Na_2) framework, which exhibits a new type of molecular architecture among all known examples of metal complexes with germesquioxane ligands (Fig. 128). It is also noteworthy that this type of nuclearity has never been found among nickel-containing silsesquioxanes, which emphasizes the individuality of the metallagermesquioxanes chemistry.

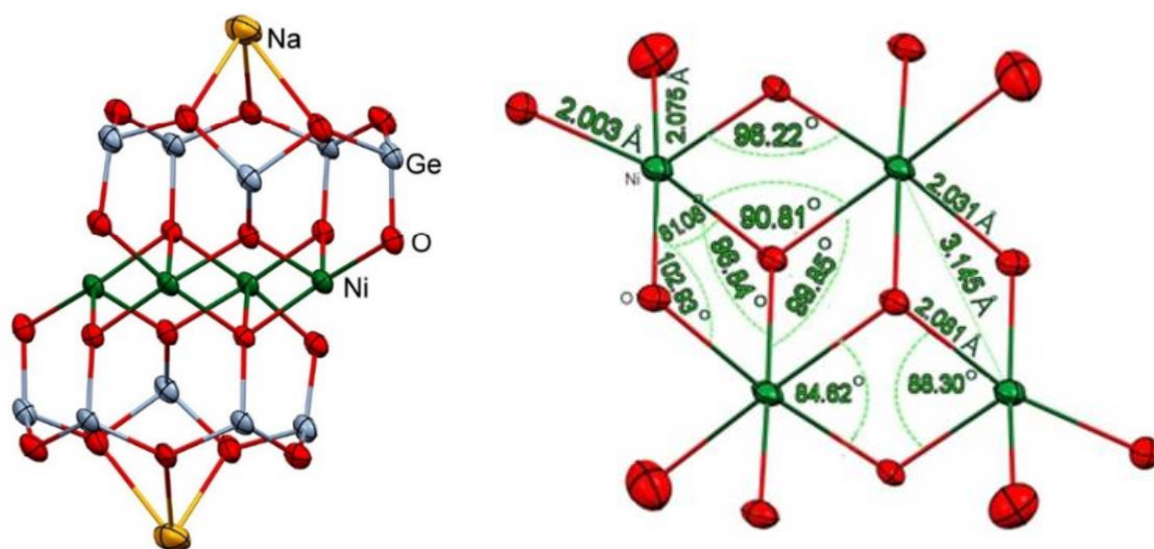


Figure 127. The structure of complex $[(\text{PhGeO}_{1.5})_{10}(\text{NiO})_4(\text{NaO}_{0.5})_2] \cdot 9\text{EtOH} \cdot 4\text{H}_2\text{O}$ **54**.

Structure of complex **54** is a skewed sandwich with two cisoid germesquioxane ($\text{PhGeO}_{1.5}$)₅ ligands coordinating the metal-containing $\{\text{NiO}\}_4$ belt (Fig. 128, right). Noteworthy that similar pentameric ligands were described in the structure of Fe,Na-phenylgermesquioxane [47], however, the type of molecular topology of this compound is not similar to compound **54**. Two apical sodium ions are coordinated in a pseudo-crown ether manner to germesquioxane cycles. Interestingly, four Ni(II) ions have different types of coordination environment: two of them adopt distorted octahedral geometry, while the other two have pentagonal coordination and assume a square-pyramidal geometry. Intramolecular Ni-O distances are in the range 1.990 – 2.161 Å. All Ni-O-Ni angles differ from each other (their range is from 90.8 to 102.9°). Note that “key geometric parameters” of compound **54** and two reference nickelsilsesquioxane complexes differ significantly (Table 19).

Table 19. Comparison of the structural parameters of multinuclear Ni (II) complexes.

	Ni-Ni, Å	Ni-O-(Ni), Å	∠Ni-O-Ni
$\text{Ge}_{10}\text{Ni}_4\text{Na}_2$	3.021 – 3.145; 3.279; 5.223	1.990 – 2.160	90.8 – 102.9
$\text{Si}_{12}\text{Ni}_4\text{Na}_8$ [47]	3.143 – 3.147; 3.161; 5.439	2.049 – 2.130	96.2 – 99.1
$\text{Si}_{12}\text{Ni}_4\text{Na}_4\text{K}_2$ [47]	3.156 – 3.183; 3.162; 5.454	2.059 – 2.135	95.9 – 100.2

The cage molecules of **54** are well isolated in crystal packing, without organization of hydrogen bonding to each other (Fig. 129). The smallest intermolecular Ni-Ni distance is 12.35 Å.

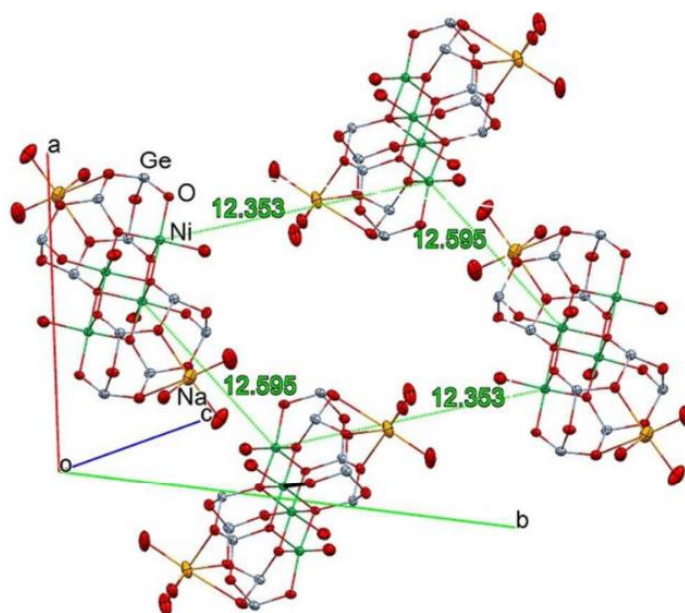


Figure 128. The structure of the crystal packing of the complex **54**.

Magnetic properties of nickel-containing germesquioxane $[(\text{PhGeO}_{1.5})_{10}(\text{NiO})_4(\text{NaO}_{0.5})_2] \cdot 9\text{EtOH} \cdot 4\text{H}_2\text{O}$ **54** were studied. At room temperature, **54** had a χT value of $4.49 \text{ cm}^3 \cdot \text{K} \cdot \text{mol}^{-1}$, which is in good agreement with the $4.41 \text{ cm}^3 \cdot \text{K} \cdot \text{mol}^{-1}$, which corresponds to four non-interacting octahedral Ni^{2+} ions ($S = 1$; $g = 2.1$). Upon cooling temperature, the χT value decreases, reaching a minimum at 35 K, and then sharply increases to $6.33 \text{ cm}^3 \cdot \text{K} \cdot \text{mol}^{-1}$ at 11 K (Fig. 130, left). The value obtained is noticeably lower than the value of $11.02 \text{ cm}^3 \cdot \text{K} \cdot \text{mol}^{-1}$ expected in the case of ferromagnetic interactions between four ions Ni^{2+} $S = 4$ ($g = 2.1$). Consequently, the observed minimum indicates the presence of both antiferromagnetic and ferromagnetic interactions, which compete with each other. This is confirmed by the value of magnetization at 1.8 K in a field of 7 T (Fig. 130, right).

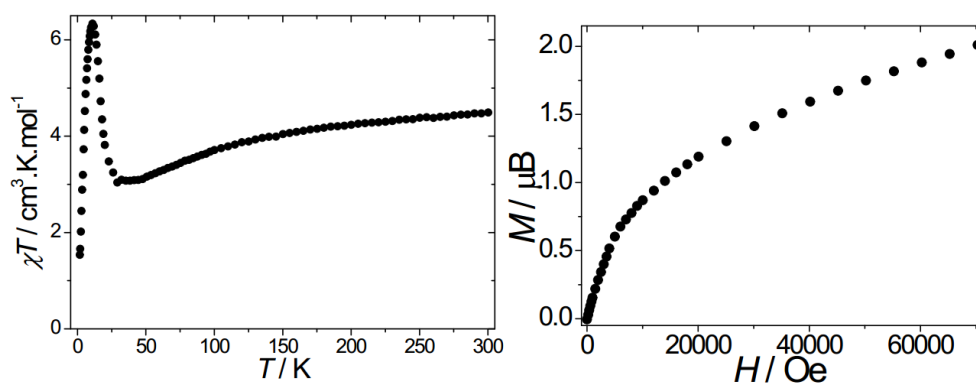


Figure 129. Temperature dependence of χT under a 1000 Oe DC field (left); Field dependence of the magnetization at 1.8 K (right).

At 1.8 K for complex **54** (at a coercive field of 580 Oe), a hysteresis loop appears (Fig. 131, left), which indicates a slow relaxation of the magnetization. This is additionally confirmed by the curves of magnetization during cooling (ZeroField Cooled, ZFC) and heating (Field-Cooled, FC) obtained in a magnetic field of 100 Oe (Fig. 131, right)

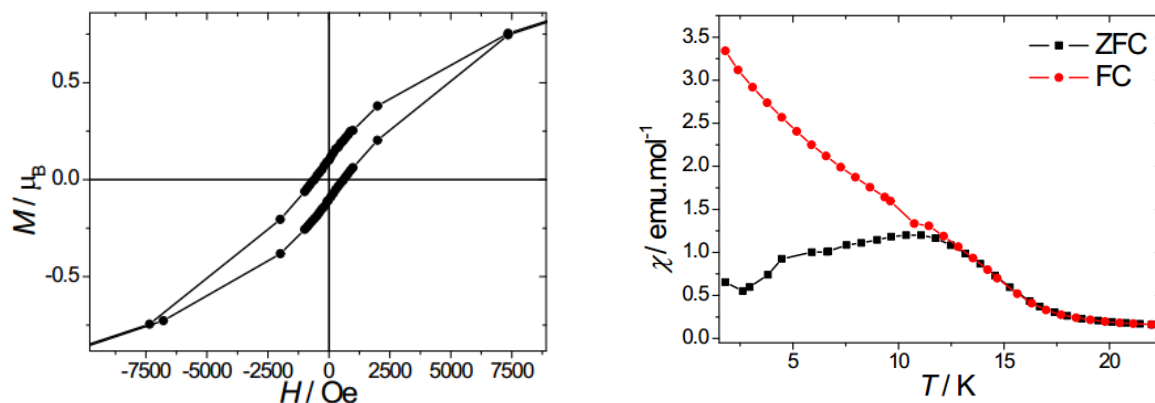


Figure 130. Hysteresis loop at 1.8 K (left); ZFC/FC curves obtained with an applied magnetic field a dc field of 100 Oe (right).

The dynamics of delayed relaxation of **54** was investigated using alternating current (AC) measurements. In a field with zero direct currents, the clear frequency dependence of both in-phase (χ') and antiphase (χ'') susceptibilities were observed (Fig. 132, left). It is noteworthy that both maxima shift to higher temperatures with increasing frequency, which indicates the presence of two different relaxation processes: low- temperature (LT) and high-temperature (HT).

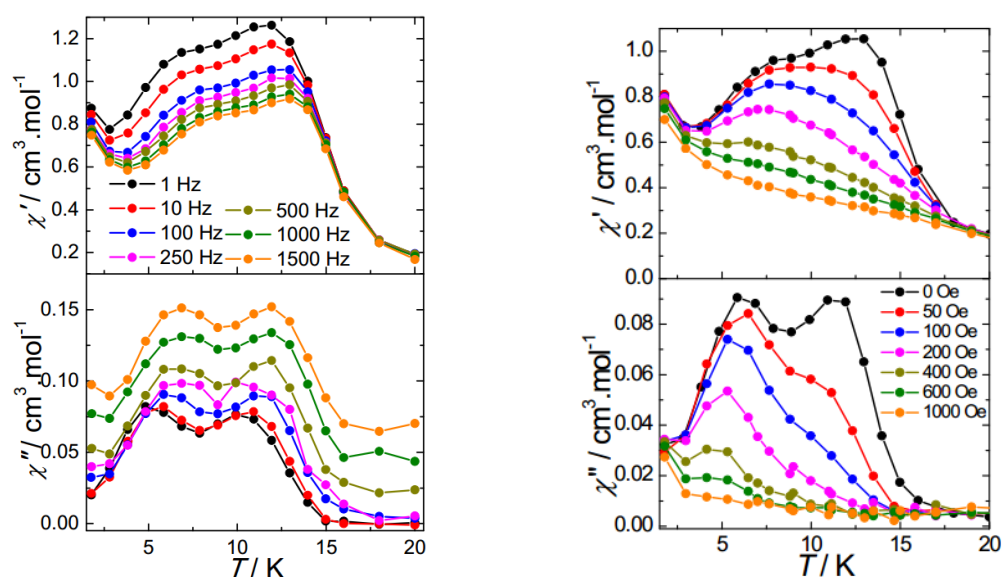


Figure 131. Temperature dependence of the in-phase (χ') and out-of phase (χ'') susceptibilities performed under a zero-DC field for **54** (left). Temperature dependence of the in-phase and out-of-phase susceptibilities measured with various dc magnetic fields for **54** (right).

For each relaxation, the temperature dependence of the relaxation time was simulated using the Arrhenius law, $\tau = \tau_0 \exp(U_{eff} / k_B T)$, where U_{eff} is the average energy barrier for magnetization reversal, k_B is the Boltzmann constant. After approximation, the following data: $U_{eff} = 97 \text{ cm}^{-1}$, $\tau_0 = 5.8 \times 10^{-13} \text{ s}$ and $U_{eff} = 328 \text{ cm}^{-1}$, $\tau_0 = 5.8 \times 10^{-13} \text{ s}$, for LT and HT relaxations, respectively, were obtained. The observed slow relaxation indicates that **54** exhibits spin glass properties.

The measurements of the relaxation of magnetization upon temporary cooling **54** have demonstrated a "memory effect" (ZeroField Cooled, ZFC). When the temperature decreases from 11 to 7 K, the value of magnetization changes abruptly to a constant value; when returning to 11 K, the relaxation dynamics returns to the initial level. This fact proves the distribution of relaxation times, reflecting the presence of spin glass behavior (Fig. 133).

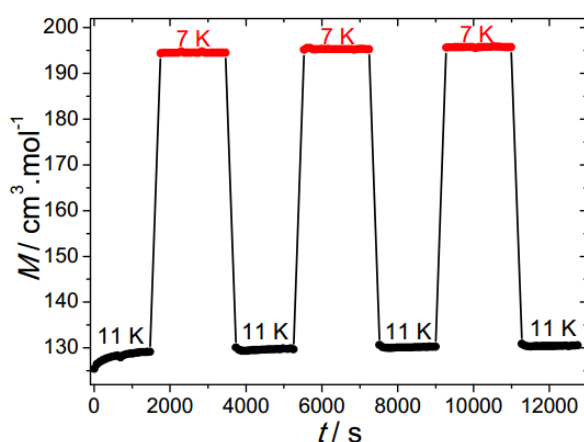


Figure 132. ZFC relaxation curve with temporary cooling measured at 11 and 7 K with an applied magnetic field of 100 Oe for **54**.

The origin of this slow dynamic is rather complex, and several parameters affect the magnetic behavior of this compound: (i) numerous magnetic exchange pathways are present in the oxo-cubane core $\{\text{NiO}\}_4$, (ii) all Ni-O-Ni angles are different and are in the range between 90.8 and 102.9° . It is well known that the transition from ferro-antiferromagnetic interactions in systems with bridging oxygen atoms occurs at angles exceeding 99° [202]. This can explain the presence and competition between ferro- and antiferromagnetic exchange interactions inside the tetranuclear center, leading to the observed spin frustration; (iii) the different geometries of nickel centers in the oxo-cubane core and especially the presence of highly anisotropic penta-coordinated nickel ions; (iv) two orientation types of molecules in crystal packing, which should cause different orientations of the total spin of each molecule. We also note that even if the intermolecular distances are large enough (more than 12 \AA) and the **54** molecules are well isolated from each other in the crystal packing, the influence of weak dipole interactions on the magnetic regime cannot be ruled out either.

Chapter 4. Tetranuclear Tb(III) and Eu(III) - containing silsesquioxanes: synthesis, structure and investigation of magnetic and luminescent properties

In the previous works it was confirmed that the investigation of mono or polynuclear complexes containing lanthanide ions presents a great deal of interest due to their high magnetic anisotropy conducting sometimes to SMM behavior [203, a-b] or thanks to their interesting luminescent properties [204]. However, the examples of lanthanide-based silsesquioxanes remain very rare, as it was noted in Chapter I. In this work, we have proposed a new synthetic approach to the synthesis of cage silsesquioxanes containing Eu^{3+} and Tb^{3+} ions. The synthesis scheme includes two stages: *in situ* formation of phenylsiloxanolate $[\text{PhSi}(\text{O})\text{ONa}]_x$ and subsequent exchange interaction with lanthanide nitrates and ammonium Et_4NCl or phosphonium Ph_4P^+ salts (Fig. 134). The following compounds were isolated: $(\text{Et}_4\text{N})_2[(\text{PhSiO}_{1.5})_8(\text{EuO}_{1.5})_4(\text{O})(\text{NO}_{2.5})_6(\text{EtOH})_2(\text{MeCN})_2] \cdot 4\text{MeCN}$ **55** (42% yield), $(\text{Ph}_4\text{P})_2[(\text{PhSiO}_{1.5})_8(\text{EuO}_{1.5})_4(\text{O})(\text{NO}_{2.5})_6(\text{EtOH})_2(\text{MeCN})_2]$ **56** (16% yield), $(\text{Et}_4\text{N})_2[(\text{PhSiO}_{1.5})_8(\text{TbO}_{1.5})_4(\text{O})(\text{NO}_{2.5})_6(\text{EtOH})_2(\text{MeCN})_2] \cdot \text{MeCN}$ **57** (43% yield) and $(\text{Ph}_4\text{P})_4[(\text{PhSiO}_{1.5})_8(\text{TbO}_{1.5})_4(\text{O})_2(\text{NO}_{2.5})_8] \cdot 10\text{MeCN}$ **58** (20% yield). The details of the synthesis are described in the Experimental Section on this manuscript and the details of the crystal structures are given in Annex 2 (Table 31).

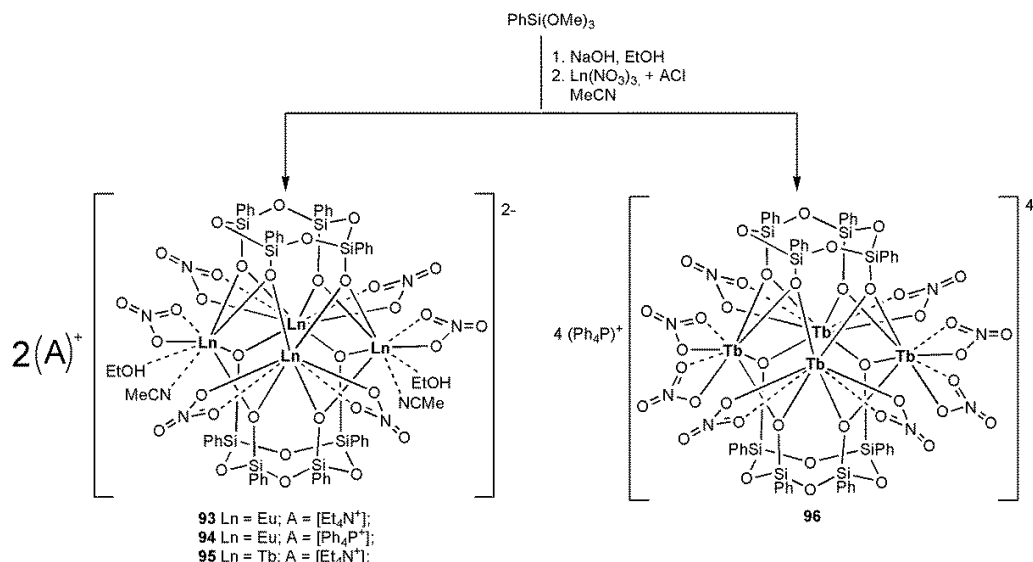


Figure 133. Synthesis of complex **55** - **58**.

Four compounds have a similar structural topology (new type of molecular architecture in comparison to previously published lanthanide-containing silsesquioxanes). X-Ray diffraction analysis indicates that compounds **55** – **57** crystallize in the triclinic P-1 space group and present closed crystal structures. On the other hand, compound **58** crystallizes in P21/c space group, but its molecular architecture is also similar to the others. For clarity, the crystal structure of only **55** will be

described in details. Thus, compound **55** forms a prismatic framework formed by a four-nuclear belt (EuO_2)₄, which is located between two cyclic tetrameric phenylsiloxanolate fragments (Fig. 135, left). The ligands of this type are very rare components of metallasilsesquioxane structures, previously reported only for Ti₄- [205] and Co₈-structures [107]. Eu³⁺ ions are combined into a distorted square fragment by two bridging oxygen atoms in **55**. Europium ions have two types of eight-coordinated coordination environment. Two europium atoms are additionally coordinated by four oxygen atoms of two nitrate ligands, and others are coordinated by two oxygen atoms of one nitrate, one ethanol and one acetonitrile (Fig. 135, right). The Eu-O distances are in the range 2.341 – 2.357 Å, and Eu-N = 2.572 Å. The O-Eu-O angles in the square fragment are 81.02 and 119.77 °. The geometry of both types of europium ions is a distorted square antiprism. The intramolecular Eu³⁺-Eu³⁺ distances are 3.744 and 3.791 Å.

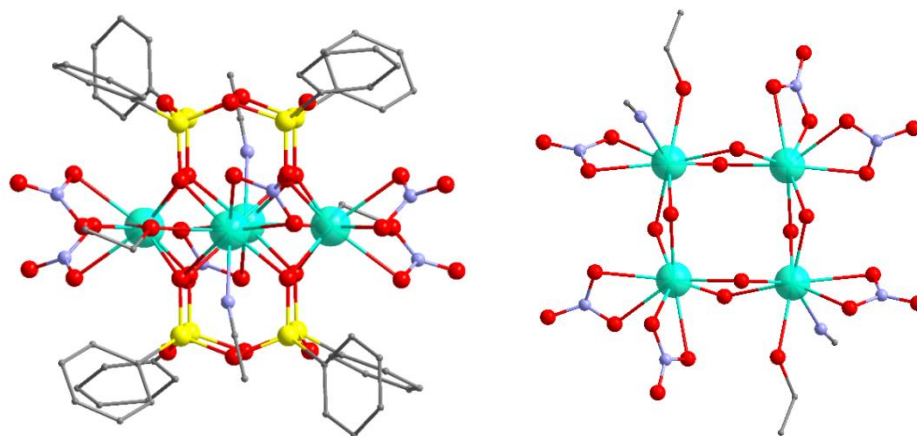


Figure 134. The structure of complex **55** (left), the structure of (EuO_2)₄ core (right).

The structure geometries and the packing principle in the crystalline phase for the compounds **56** and **57** are similar to **55**; the corresponding distances and angles are summarized in Table 20.

Table 20. Average values of angles and distances **55** – **57**.

№	Distance Ln-O, Å	Distance Ln-N, Å	Angle O-Ln-O, °	Intermolecular distance Ln – Ln, Å
56	2.341 – 2.379	2.577	70.91, 107.40	7.918
57	2.312 – 2.348	2.542	71.04, 107.53	7.997
58	2.295 – 2.347	2.535	71.49, 106.47°	12.211

The crystal packing **55** is characterized by the same arrangement of the cage fragments, while the arrangement of cations is different (Fig. 136). The shortest intermolecular distance Eu^{3+} - $\text{Eu}^{3+} = 7.954$ Å.

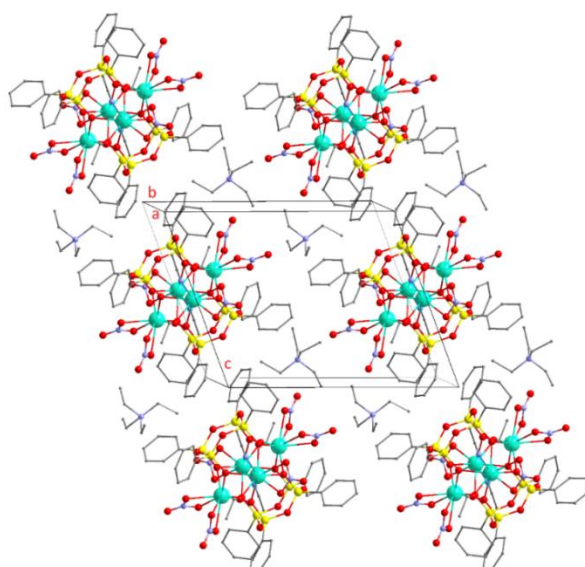


Figure 135. The structure of the crystal packing of the complex **55**.

It is noteworthy that the shortest intermolecular Tb-Tb distance in compound **58** is 12.211 Å, which is much larger than **56** and **57**. It is supposed, the presence of four cationic Ph₄P⁺ fragments in structure **58** led to the isolation of the frameworks during crystal packing (Fig. 137, left). Also, all four terbium ions **58** are coordinated by four bridging oxygen atoms and four oxygen atoms of two nitrates in contrast to **56** – **57** (Fig. 137, right).

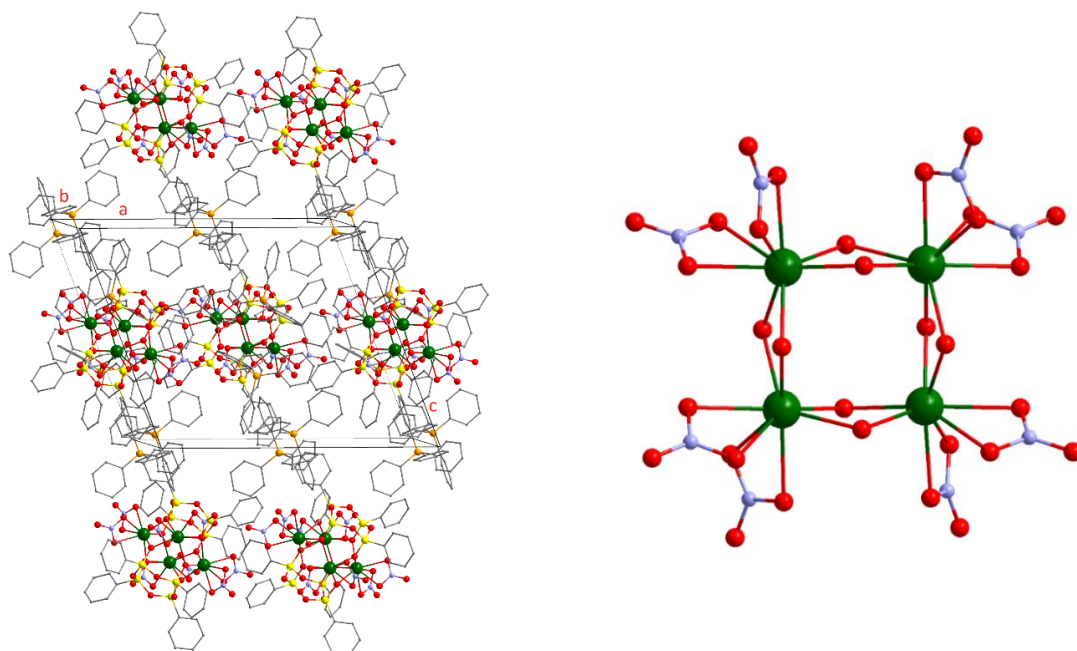


Figure 136. The structure of the crystal packing of the complex **58** (left), the structure (TbO₂)₄ core (right).

The magnetic properties of Tb³⁺-containing (Et₄N)₂[(PhSiO_{1.5})₈(TbO_{1.5})₄(O)(NO_{2.5})₆(EtOH)₂(MeCN)₂] • MeCN **57** and (Ph₄P)₄[(PhSiO_{1.5})₈(TbO_{1.5})₄(O)₂(NO_{2.5})₈] • 10MeCN **58** were investigated by using SQUID-MPMS

magnetometer by Dr. Gauter Félix (ICGM, University of Montpellier). The temperature dependence of the magnetic susceptibility, performed in the constant current mode, was obtained for an applied magnetic field of 1000 Oe. At room temperature the χT values are $46.10 \text{ cm}^3 \cdot \text{K} \cdot \text{mol}^{-1}$ and $44.10 \text{ cm}^3 \cdot \text{K} \cdot \text{mol}^{-1}$ for **57** and **58**, which is slightly lower than the theoretical value of $47.28 \text{ cm}^3 \cdot \text{K} \cdot \text{mol}^{-1}$ expected for four Tb^{3+} ions using the free-ion approximation. (${}^7\text{F}_6$, $S = 3$, $L = 3$, $g = 3/2$, $\chi T = 11.82 \text{ cm}^3 \cdot \text{K} \cdot \text{mol}^{-1}$) [86]. Upon cooling temperature, the compounds exhibit a typical decrease in χT caused by thermal depopulation of Stark sublevels and / or by the presence of antiferromagnetic interactions between Tb^{3+} centers (Fig. 138). The field dependences of the magnetization, performed at 1.8 K, show an S-shaped curve for **57**, which indicates the presence of a spin-flip of the magnetic moment associated with various Tb^{3+} ions in an applied magnetic field [206]. At the same time, for **58** in the region of weak fields, a linear increase in magnetization from the field is observed.

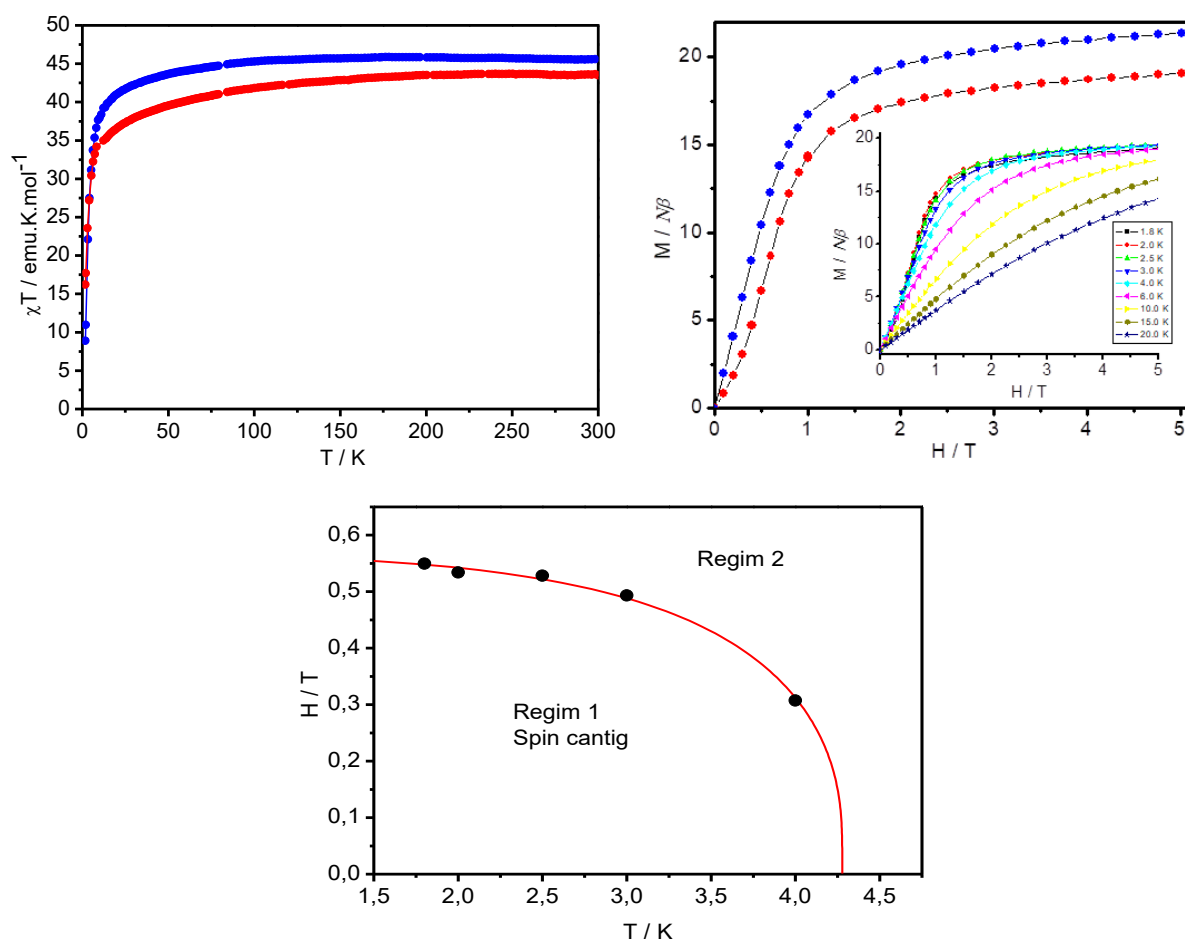


Figure 137. Temperature dependence of χT under a 1000 Oe DC field for **57** (blue) and **58** (red) (left); Field dependence of the magnetization at 1.8 K for **57** (red) and **58** (blue). Insert: Field dependence of the magnetization performed at different temperature for **57** (right); H/T phase diagram drawn from inflexion points of field dependence of the magnetization performed with different temperatures indicating the limit of the spin canting regime 1 and transition to oriented paramagnetic regime 2. The solid lines are guides for eyes.

The dynamic magnetic measurements performed in the alternating current mode (ac) were performed to determine the behavior of the spin-flip. In a zero DC field, the in-phase component of the magnetic susceptibility (χ') shows a frequency-independent peak at 3.32 K, while the in-phase susceptibility (χ'') is almost zero and shows a slight increase at 1.8 K (Fig. 139). The difference in magnetic behavior between **57** and **58** can be related to: (i) the presence of two Tb ions with different coordination environments in **58**, which can generate different orientations of the anisotropy axes and explain the spin rotation mode in a weak field, and (ii) a stronger intermolecular interaction in **57** due to the closer intermolecular distances Tb-Tb = 7.954 Å compared to 12.211 Å in **58**, where the frameworks are more isolated in the crystal packing.

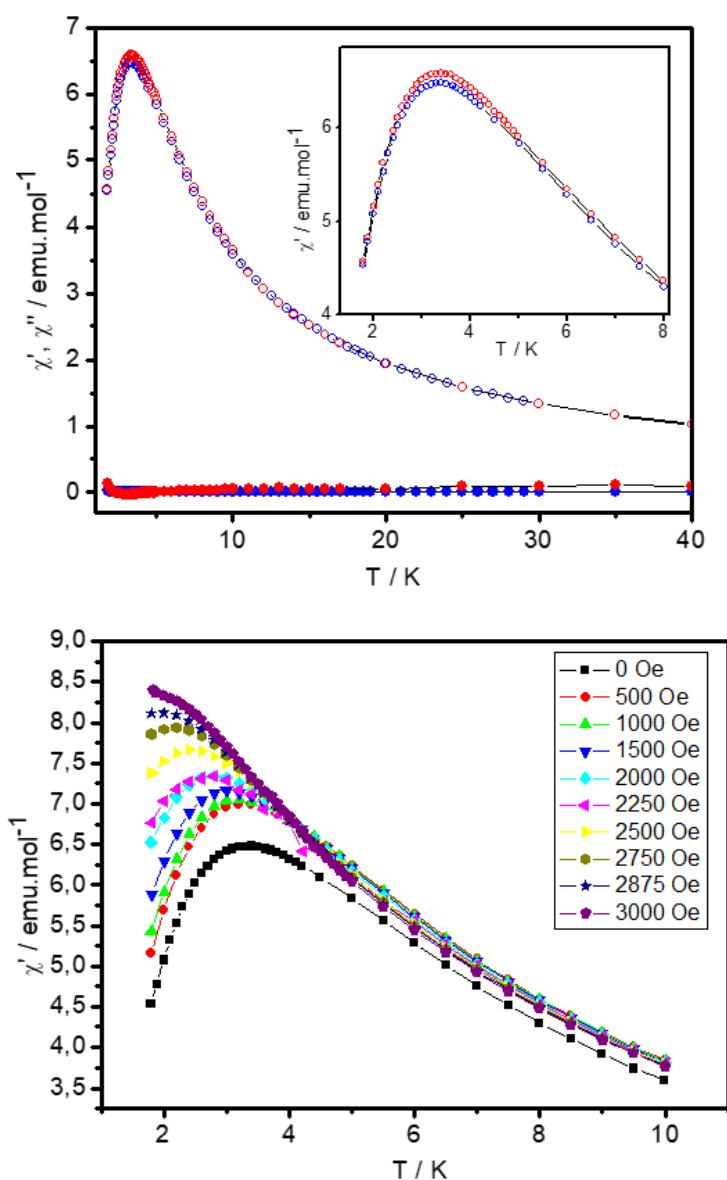


Figure 138. Temperature dependence of χ' and χ'' components of the ac susceptibility performed at 500 (red) and 1500 Hz (blue) for **57** in zero dc field (top); Temperature dependence of χ' components performed with different applied magnetic field at 500 Hz for **57** (bottom).

The photoluminescence of **55** – **58** was investigated in the solid state at 77 K and room temperature (annexes) (cooperation with Dr. Ekaterina Mamontova, ICGM, University of Montpellier). For all samples, the excitation in the UV or blue regions results in typical emission from lanthanide, Eu^{3+} or Tb^{3+} . The emission spectra **55** and **56**, taken at 77 K, exhibit Eu^{3+} intra $^4\text{F}_6$ lines attributed to the $^5\text{D}_0 \rightarrow ^7\text{F}_{0-4}$ transitions (Fig. 140). The weak $^5\text{D}_0 \rightarrow ^7\text{F}_0$ transition observed at 579 nm confirms the low symmetry of the coordination environment of Eu^{3+} ions, while the symmetric shape of this band indicates relatively small differences in the Eu-O bond lengths and angles at two europium ions in accordance with the crystal structure.

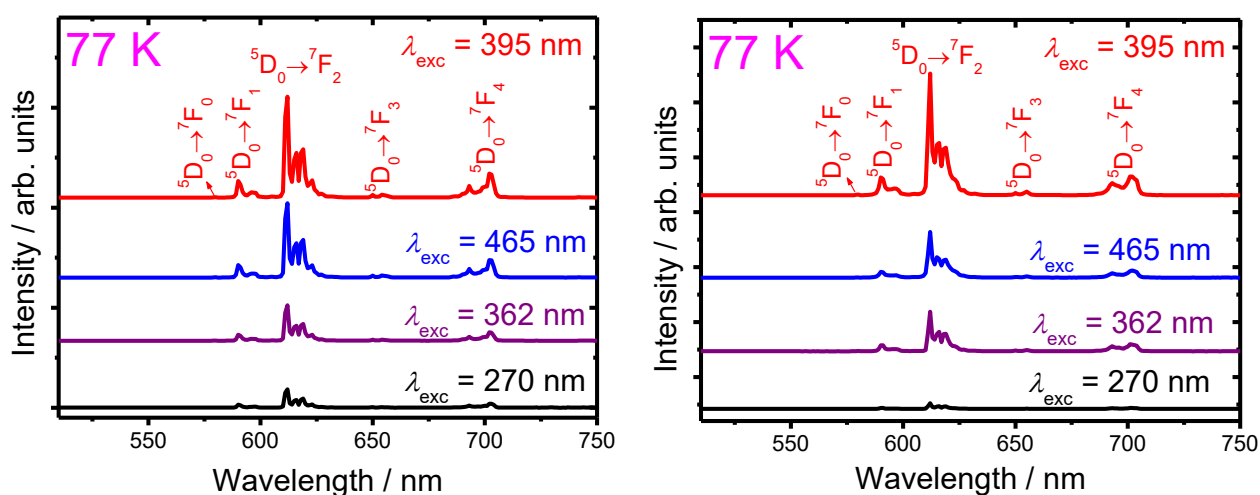


Figure 139. Low temperature emission spectra of **55** (left) and **56** (right) excited at 270, 362, 395, 465 nm.

The existence of more than three lines for the $^5\text{D}_0 \rightarrow ^7\text{F}_1$ transition is also consistent with the distorted square antiprismatic geometry of the two europium centers. As expected for compounds with low symmetry of europium atoms, the $^5\text{D}_0 \rightarrow ^7\text{F}_2$ transition dominates the emission spectra and is responsible for the red emission of compounds. The slightly different coordination environment of two Eu^{3+} ions is also reflected in the splitting of the electronic transitions $^5\text{D}_0 \rightarrow ^7\text{F}_2$ and $^5\text{D}_0 \rightarrow ^7\text{F}_4$ [207, a-b]. The characteristic luminescence of Tb^{3+} was observed in the emission spectra **57** and **58**, recorded at 77 K, with the emission peaks assigned to intra $^4\text{f}_8$: $^5\text{D}_4 \rightarrow ^7\text{F}_{6-0}$ transitions (Fig. 141). The most intense emission for the two complexes was observed at 543 nm, which corresponds to the $^5\text{D}_4 \rightarrow ^7\text{F}_5$ transition.

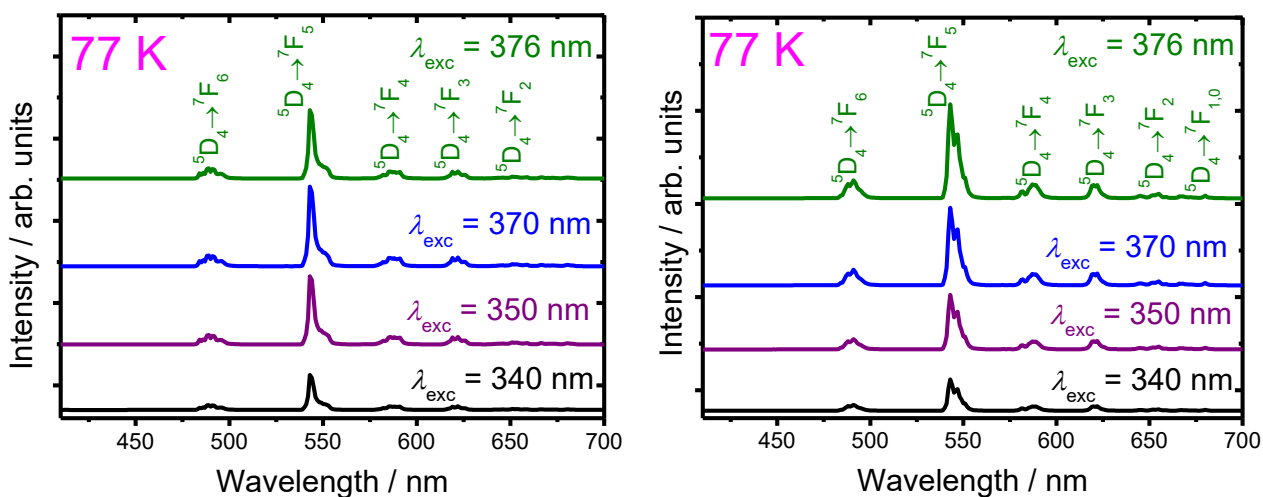


Figure 140. Low temperature emission spectra of **57** (left) and **58** (right) excited at 340, 350, 370, 376 nm.

Figure 142 shows the excitation spectra of **55** and **56** for the $^5D_0 \rightarrow ^7F_2$ transition (77 K). They demonstrate a series of straight lines that can be attributed to intra- $4f_6$: $^7F_0 \rightarrow ^5D_{4-0}$, $^5L_{8-6}$, $^5G_{6-2}$, 5F_3 , 6F_1 , 6H_5 , 6K_6 transitions.

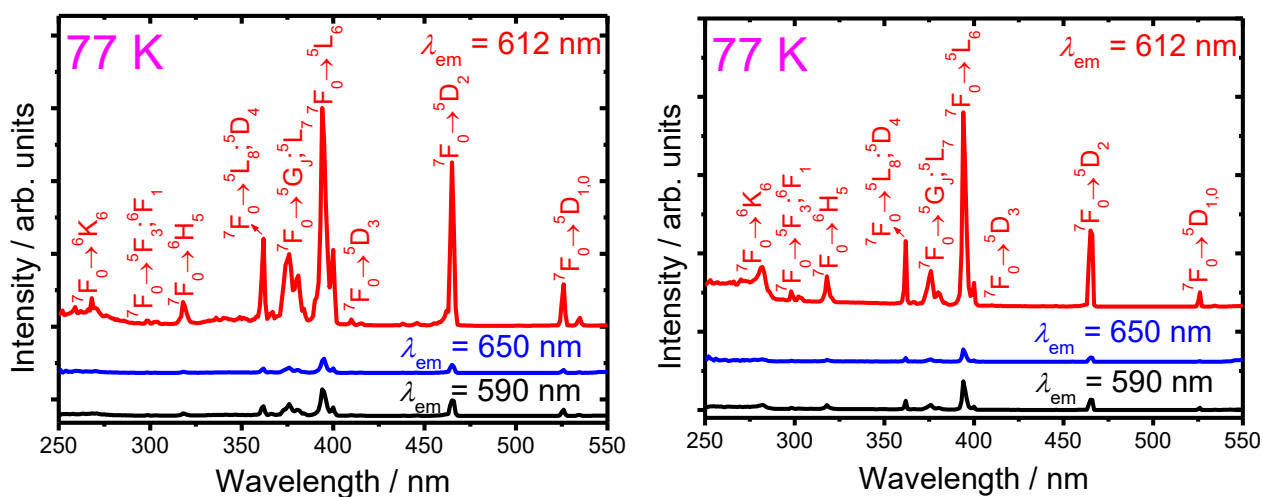


Figure 141. Low temperature excitation spectra of **55** (left) and **56** (right) excited at 590, 650, 612 nm.

The excitation spectra of compounds **57** and **58** for the $^5D_4 \rightarrow ^7F_5$ transition demonstrate a series of sharp Tb^{3+} lines corresponding to intra- $4f_6$: 7F_6 and $^5G_{4-6}$, $^5L_{9-10}$, $^5D_{1-3}$, 5H_7 transitions (Fig. 143) [208]. Consequently, the absence of broad bands associated with the ligand in the excitation spectra of all compounds clearly indicates a direct sensitization of lanthanide ions through f-f transitions rather than energy transfer with the participation of ligands. Thus, although silsesquioxane ligands and coordinated nitrate and solvate molecules do not act as a sensitizer, they also do not quench the emission of Eu^{3+} and Tb^{3+} .

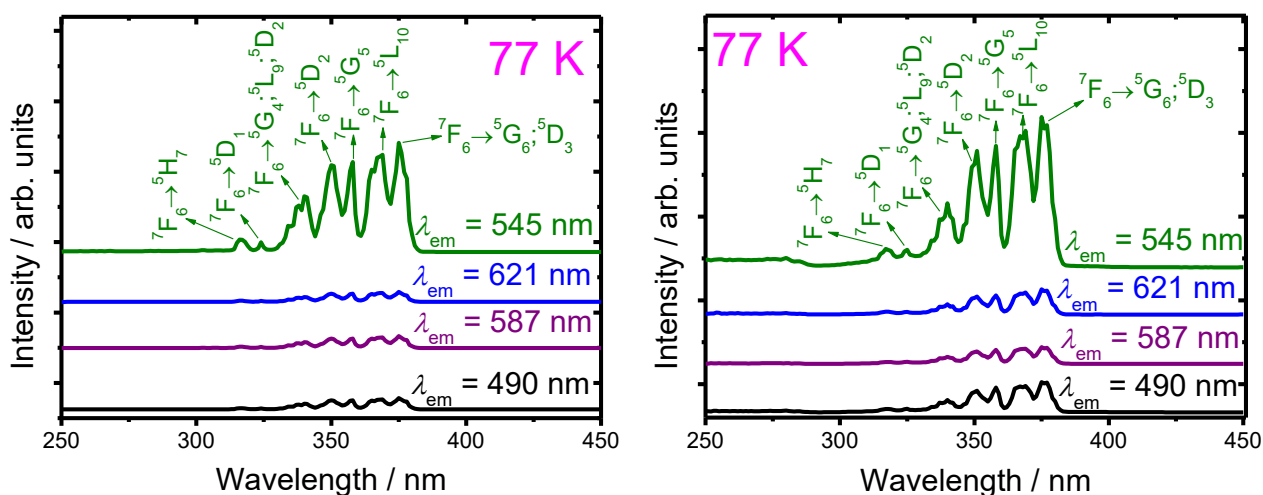


Figure 142. Low temperature excitation spectra of **57** (left) and **58** (right) excited at 490, 587, 621, 545 nm.

The dependences of the emission decay in the solid state **55** - **58** were studied at 295 K for the $^5D_0 \rightarrow ^7F_2$ transition (**55** and **56**) and for the $^5D_4 \rightarrow ^7F_5$ transition (**57** and **58**). The dependences allowed to get determine the luminescence lifetimes. They are 0.777 ± 0.003 and 0.692 ± 0.010 ms for **55**, **56**, and 1.742 ± 0.012 and 1.81 ± 0.010 ms for **57** and **58**, respectively, which corresponds to the characteristic values for europium and terbium complexes [209].

In summary, four new Eu^{3+} and Tb^{3+} -based silsesquioxane architectures have been synthesized, and their magnetic and luminescent properties have been investigated. They present unusual prism-like topology of cages with four lanthanide ions linked through oxygen atoms and situated between two cyclic tetraphenylcyclotetrasiloxanolate moieties. The investigation of the magnetic properties reveals that one of the Tb^{3+} -based cages presents a field induced spin-flip transition from the spin-canted state to the oriented paramagnetic regime. Remarkably, these compounds present Eu^{3+} or Tb^{3+} -characteristic luminescence at low and room temperatures and may be considered as first luminescent lanthanide-based silsesquioxanes.

CONCLUSION

The aim of this work was **the synthesis of several families of sil- and germsesquioxanes containing transition metal and lanthanide ions and investigation of their catalytic, magnetic and luminescent properties**. In line with this consideration, several objectives have been addressed:

1. An approach based on self-assembling reaction have been improved to the controlled synthesis of Cu(II)-containing silsesquioxanes. In this way, 51 polynuclear metalsilsesquioxanes were obtained containing from 2 to 11 copper(II) ions as part of framework fragments. All crystal structures were investigated and established by single crystals X-ray diffraction analysis. An impact of the steric factor governed by an organic substituent at the silicon atoms on the complex topology was investigated: 6 complexes with Me- substituents at the silicon atom and 44 complexes with Ph- substituents were investigated. It was also shown that the solvent nature influences the framework nuclearity: the use of DMSO promotes to increase the number of Cu(II) in the cage $[(\text{MeSiO}_{1.5})_{18}(\text{CuO})_9] \cdot \text{DMSO}$ **1**), while the employment of pyridine helps to decrease it $[(\text{PhSiO}_{1.5})_{10}(\text{CuO})_5(\text{Py})_5]$ **13**).

An unusual structural feature of hexanuclear coppersesquioxanes complexes (2,2'-bipyridine, 1,10- phenanthroline, bathophenanthroline ligands) was observed. Namely, the presence of two pentameric sesquioxane ligands was not enough to maintain a charge balance for Cu_6^{2+} complexes. For this reason, several anions (HO^- , MeO^- , Fm^- , AcO^-) were found in the composition of corresponding complexes. An appearance of formate and acetate groups is a consequence of mild oxidation of alcohol (methanol or ethanol) used as a reaction media. Moreover, the study of the effect of bidentate N-containing ligands on the structural topology demonstrated the formation of a supramolecular packing due to the π - π stacking interactions between the aromatic systems of nitrogen ligands (phenanthroline, $[(\text{PhSiO}_{1.5})_{10}(\text{CuO})_6(\text{HO}_{0.5})_2(1,10\text{-phen})_2] \cdot 4.75\text{DMSO}$ **27**) of neighboring molecules (not observed for bipyridine, bathophenanthroline, and 3,5-dimethylpyrazole).

The effect of bidentate P,P-ligands on the architecture of the resulting complexes was studied. It was shown that the 1,2-bis(diphenylphosphino)ethane part of the cationic fragments $\text{Cu}^{\text{I}}(\text{dppe})_2$ promotes the formation of the unusual Cu_9Na_4 and Cu_4Na_2 cages. The versatility of the self-assembly reaction to obtaining Ge-containing Cu(II) complexes was also demonstrated. The occurrence of oxidative processes $\text{dppm} \rightarrow \text{dppmO}_2$, under mild conditions in the presence of copper ions (without the additional introduction of oxidizing reagents) during $[(\text{PhSiO}_{1.5})_{12}(\text{CuO})_4(\text{NaO}_{0.5})_4(\text{dppmO}_2)_2]$ **36** formation was described.

Finally, the regularity of a formation of 1D and 2D coordination polymers based on Cu₂- and Cu₄-phenylsilsesquioxanes through the use of bridging ligands and alkali metal ions with a large size (K⁺, Cs⁺) was demonstrated.

2. A new approach to the directed synthesis of Cu(II)-containing germsesquioxanes was explored. Five new polyhedral Cu(II)- or Cu(III)/Fe(III)-phenylgermsesquioxanes complexes (**38** - **42**) with different compositions and structures, depending on the stoichiometric ratio of reagents, solvent systems, and type of ligands were synthesized and characterized. For the first time, the highly polynuclear complex containing 42 Cu(II) ions, [Na₄Cu₄₂(Ph₂Ge₂O₅)₁₂(OH)₄₀] **39**, was prepared, characterized and its structure was investigated.

3. The catalytic and magnetic properties of synthesized Cu(II)-based sil- and germsesquioxane complexes have been investigated. The high catalytic activity of numerous copper(II)-containing (Cu₂Fe₅, Cu₅, Cu₆, Cu₁₁, Cu₄₂) sil- and germsesquioxane complexes in the oxidative amidation of benzyl alcohol has been demonstrated. It has been shown that catalytic activity of MS for primary amines is higher than for secondary ones. It was found that the amidation is effective at low catalyst loads (up to 100 ppm Cu(II)), which made it possible to reach TON 8600 and TOF 478 h⁻¹. The high catalytic activity of copper(II)-containing (Cu₂Fe₅, Cu₄, Cu₅, Cu₆, Cu₉, Cu₁₁, Cu₄₂) sil- and germsesquioxane complexes in the oxidative functionalization of hydrocarbons has also been investigated. It has been found that the oxidation is effective for various substrates (alkanes, arenes and alcohols). The effect of a co-catalyst and a peroxide on the yields of oxidation products has been demonstrated and the mechanism of the oxidation reaction has been proposed.

Magnetic studies have demonstrated the presence of antiferromagnetic interactions in [(PhSiO_{1.5})₁₂(CuO)₄(NaO_{0.5})₄(1,4-diox)₄(H₂O)₃] • 2PhCN • 2(1,4-diox) • H₂O **47**, [(PhSiO_{1.5})₁₂(CuO)₄(NaO_{0.5})(CsO_{0.5})₃(DMF)₄(DMSO)(H₂O)] • 1.5DMF **50**, [(PhSiO_{1.5})₁₀(CuO)₂(NaO_{0.5})₂(H₂O)₆] **51** and (PhSiO_{1.5})₁₂(CuO)₄(NaO_{0.5})₂(CsO_{0.5})₂(DMF)₈ • 0.5H₂O **52** compounds.

4. The synthesis of Ni(II)-containing sil- and germsesquioxanes has been investigated. Ni₄Na₂-phenylgermsesquioxane and Ni₄-pyridine-carbonate complex were obtained (the latter is a product of structural rearrangement in the preparation of Ni(II) -phenylsilsesquioxane) and characterized by single crystal X-ray diffraction analysis. Both of them exhibit slow relaxation of the magnetization due to the spin glass behavior.

5. Four new tetranuclear Eu³⁺ and Tb³⁺-based metallasilsesquioxanes architectures have been synthesized, characterized and their magnetic and luminescent properties have been investigated. They present unusual prism-like topology of cages with four lanthanide ions linked through oxygen atoms and situated between two cyclic tetraphenylcyclotetrasiloxanolate moieties. The investigation of the magnetic properties reveals that one of the Tb³⁺-based cages presents a field induced spin-flip

transition from the spin-canted state to the oriented paramagnetic regime. Remarkably, these compounds present Eu^{3+} or Tb^{3+} -characteristic luminescence at low and room temperatures and may be considered as first luminescent lanthanide-based metallasilsesquioxanes.

EXPERIMENTAL SECTION

Materials

All reactions were carried out in air (unless otherwise stated). All solvents were purified by distillation according to standard procedures. Phenyltriethoxysilane, phenyltrimethoxysilane, phenyltrimethoxygermane, and phenyltrichlorogermane (Acros Organics) were used without further purification. Synthesis of $[\text{PhGeO}_{1.5}]_n$. A solution of 2 g (7.89 mmol) of PhGeCl_3 in 40 ml of toluene was added dropwise (at room temperature, during 1 hour) into the beaker equipped with a magnetic stirrer and filled with 60 ml of mixture of *n*-butanol/water ($V/V = 2/1$). Resulted mixture was left under stirring for 12 hours, then the hydrolysate of PhGeCl_3 , as the organic phase, was separated. Thereafter, the hydrolysate was washed with deionized water till neutral pH and dried in vacuo. Anal. Calcd for $[\text{C}_6\text{H}_5\text{GeO}_{1.5}]$, %: C, 41.48; H, 2.90; Ge, 41.81. Found (for vacuum-dried sample), %: C, 41.39; H, 3.01; Ge, 41.78. Yield 1.23 g (91%).

Research methods and equipment

Elemental analysis was performed at the Microanalysis Laboratory of the INEOS RAS.

Energy dispersive X-ray spectroscopy (EDX) was performed at the analytical laboratory of the University of Montpellier using a Quanta 200 scanning electron microscope connected to an Oxford INCA analyzer.

IR spectra were recorded on a Nicolet 6700 FTIR, FTIR Shimadzu IR Prestige-21 or PerkinElmer Spectrum Two FT-IR Spectrometer for pellet samples in KBr in the range 4000 - 600 cm^{-1} . For all metallamethylsilsesquioxanes **1 - 6**, a set of signals was established: 1378 cm^{-1} ($\delta\text{Me-Si}$), 950 - 1050 cm^{-1} ($\nu\text{Si-O}$, $\nu\text{Si-O-Si}$), 900 cm^{-1} ($\nu\text{Si-O}$ in the Si fragment $-\text{O-M}$). For all metallaphenylsilsesquioxanes **7 - 36**, **43 - 52**, **54 - 117**, a set of signals was established: 1120 cm^{-1} ($\nu\text{Ph-Si}$), 940 - 1100 cm^{-1} ($\nu\text{Si-O}$, $\nu\text{Si-O-Si}$), 900 cm^{-1} ($\nu\text{Si-O}$ in the Si-O-M fragment), 730 - 670 cm^{-1} ($\sigma\text{C-H}$ of the monosubstituted aromatic fragment). For metallaphenylgermanosequioxanes **38 - 42**, **53** the following set of similar signals in the spectrum was obtained: 3465 cm^{-1} ($\nu\text{O-H}$), 846 - 827 cm^{-1} ($\nu\text{Ge-O-Ge}$), 794 - 756 cm^{-1} ($\nu\text{Ge-O-Fe}$), 732 - 722 cm^{-1} ($\nu\text{Fe-O-Fe}$), 694 cm^{-1} ($\nu\text{Fe-O-Fe}$), 668 cm^{-1} ($\nu\text{Ge-C-Ph}$), 563-509 cm^{-1} ($\delta\text{Fe-O-Fe}$), 456 cm^{-1} ($\delta\text{Ge-O-Ge}$).

X-ray. Single crystals of compounds **3**, **7 - 43**, **45 - 46**, **48 - 49**, **53** were studied on a Bruker APEX DUO diffractometer at various temperatures in the range 100 - 120 K, single crystals of compounds **5**, **44**, **47**, **52**, **54** were studied on a diffractometer on a Bruker Smart APEX II diffractometer at 100 K, and compounds **55 - 58** were studied using a Bruker D8 VENTURE- μS 3.0 two-wave diffractometer equipped with two micro X-ray sources at a copper wavelength (Cu k-alpha, 1.54 Å) and a two-dimensional zero-wavelength PHOTON II sensor. Single crystals of compounds **1**, **2**, **4**, **6**,

50, 51 were studied on synchrotron. The structures were solved by direct methods and refined by the full-matrix least-squares method in F2 with anisotropic displacement parameters for non-hydrogen atoms. Hydrogen atoms were placed in the calculated positions and refined within the framework of the riding model with fixed isotropic displacement parameters [$U_{iso}(\text{H}) = 1.5U_{eq}(\text{C})$ for CH_3 -groups and $1.2U_{eq}(\text{C})$ for other groups]. All calculations were performed using the SHELXTL software package. Crystallographic data for all new compounds studied were deposited at the Cambridge Crystallographic Data Center, CCDC. The main crystallographic data and experimental parameters for compounds **1 - 57** are given below.

^1H NMR spectra were obtained on a Bruker Avance 400 MHz spectrometer. Chemical shifts are reported in ppm and refer to the peak of the solvent (CDCl_3 at 7.26 ppm). Data are presented as *s* = singlet, *d* = doublet, *t* = triplet, *q* = quadruplet, *qt* = quartet, *sept* = septuplet, *m* = multiplet; coupling constants in Hz; integration. **^{13}C NMR spectra** were recorded on a Bruker Avance III HD 100 MHz spectrometer. Chemical shifts are reported in ppm and refer to the peak of the solvent (CDCl_3 at 77.16 ppm).

Gas chromatography. The products obtained by the oxidation of unsaturated hydrocarbons or alcohols were analyzed using an LHM-80-6 instrument, a 2 m column with 5% Carbowax 1500 at 0.25 – 0.315 mm Inerton AW-HMDS; argon carrier gas.

Catalytic experiments. Oxidative amidation. Amine hydrochloride (0.5 mmol), CaCO_3 (25.0 mg, 0.25 mmol), CH_3CN (1 ml), weighed portions of catalysts **17, 26, 33 - 35, 38 – 39, 41** (Table 10), benzyl alcohol (105 μL , 1.0 mmol) and TBHP (5.5 M in nonane, 225 μL , 1.25 mmol) were sequentially added to a sealed tube. The mixture was stirred at 80 ° C for 2 h, and TBHP (5.5 M in nonane, 225 μL , 1.25 mmol) was added to the mixture again. After 22 h at 80 ° C, the mixture was cooled to room temperature and 1M HCl was added. The mixture was extracted twice with AcOEt, the combined organic phases were washed with saturated NaHCO_3 solution and brine and concentrated under reduced pressure. To remove excess benzyl alcohol, 80 ml of H_2O was added and evaporated under reduced pressure. The crude product was then purified by silica gel chromatography using cyclohexane / AcOEt gradients to give the pure compounds.

(±)-*N*-(α -methylbenzyl) benzamide

^1H NMR (300 MHz, CDCl_3) δ 7.66 (d, $J = 7.4$ Hz, 2H), 7.37 - 7.09 (m, 8H), 6.74 (d, $J = 7.4$ Hz, 1H), 5.19 (p, $J = 7.0$ Hz, 1H), 1.44 (d, $J = 6.9$ Hz, 3H).

^{13}C NMR (126 MHz, CDCl_3) δ 166.7, 143.3, 134.6, 131.4, 128.7, 128.5, 127.3, 127.1, 126.3, 49.2, 21.8.

***N*-cyclohexylbenzamide**

^1H NMR (300 MHz, CDCl_3) δ 7.79 - 7.70 (m, 2H), 7.47 - 7.31 (m, 3H), 6.30 (d, $J = 6.0$ Hz, 1H), 4.01 - 3.85 (m, 1H), 2.03 - 1.93 (m, 2H), 1.77 - 1.66 (m, 2H), 1.66 - 1.54 (m, 1H), 1.44 - 1.06 (m, 5H).

^{13}C NMR (126 MHz, CDCl_3) δ 166.7, 135.1, 131.2, 128.4, 127.0, 48.8, 33.2, 25.6, 25.0.

N-nbutylbenzamide

^1H NMR (300 MHz, CDCl_3) δ 7.80 – 7.71 (m, 2H), 7.49 – 7.32 (m, 3H), 6.56 (s, 1H), 3.46 – 3.34 (m, 2H), 1.62 – 1.50 (m, 2H), 1.44 – 1.29 (m, 2H), 0.91 (t, $J = 7.2$ Hz, 3H).

^{13}C NMR (75 MHz, CDCl_3) δ 167.7, 134.9, 131.3, 128.5, 127.0, 39.9, 31.8, 20.2, 13.8.

N, N-dibenzylbenzamide

^1H NMR (300 MHz, CDCl_3) δ 7.57 – 7.50 (m, 2H), 7.44 – 7.28 (m, 11H), 7.21 – 7.14 (m, 2H), 4.60 (s, 2H), 4.44 (s, 2H).

^{13}C NMR (75 MHz, CDCl_3) δ 172.3, 137.0, 136.5, 136.2, 129.7, 128.8, 128.6, 128.4, 127.6, 127.0, 126.8, 51.6, 46.9.

N-benzoylmorpholine

^1H NMR (300 MHz, CDCl_3) δ 7.37 – 7.29 (m, 5H), 3.97 (s, 4H), 3.55 (s, 2H), 3.37 (s, 2H).

^{13}C NMR (126 MHz, CDCl_3) δ 170.5, 135.3, 130.0, 128.6, 127.1, 66.9, 48.2, 42.6.

Catalytic experiments. C-H functionalization. Weighed portions of catalysts **1**, **13**, **16** – **17**, **22**, **33** – **36**, **38** – **39** **41** (Table 11 - 17) were introduced into the reaction mixture in the form of a solid powder. The alkane or alcohol was dissolved in acetonitrile, a cocatalyst (HNO_3 or CF_3COOH) was added (unless otherwise stated) and the reaction started when hydrogen peroxide was introduced in one portion. The reactions were carried out not in an inert atmosphere, in thermostated containers (made of borosilicate glass) with vigorous stirring. After the end of the process, nitromethane as a standard compound was added to the reaction and the mixture was analyzed by GC. Samples obtained from the oxidation of alkanes were usually analyzed twice (before and after PPh_3 treatment) by GC. This method (comparison of chromatograms of the same sample obtained before and after the addition of PPh_3) makes it possible to estimate the real concentration of alkyl hydroperoxide, ketone (aldehyde), and alcohol present in the reaction solution.

Magnetic measurements. Samples **46**, **48**, **49**, **50**, **52**, **53**, **56**, **57** were studied using Quantum Design MPMS-XL and Quantum Design PPMS-9 SQUID magnetometers operating in the temperature range 1.8 - 350 K with a magnetic field of 7 Tesla. The diamagnetic contribution was taken into account using Pascal's constants.

Photoluminescence measurements. The emission and excitation spectra **54** - **57** were recorded at 77 K and 295 K on an Edinburgh FLS-920 spectrofluorimeter. A 450 W Xe arc lamp was used as an excitation source. The emission spectra were corrected taking into account the detection and optical spectral response of the spectrofluorimeter. Low-temperature measurements (77 K) were carried out using a liquid nitrogen dewar (quartz).

Synthesis

Synthesis of complex $[(\text{MeSiO}_{1.5})_{18}(\text{CuO})_9] \cdot \text{DMSO}$ **1**. Three grams (0.022 mol) of $\text{MeSi}(\text{OMe})_3$ in 50 mL of ethanol and 0.79 g (0.044 mol) of water were stirred for 30 min. Then 0.90 g (0.025 mol) of NaOH was added, and the resulting white-colored mixture was heated to reflux for 2 h. Afterwards the solution was cooled down to room temperature, and 1.35 g (0.01 mol) of CuCl_2 in 50 mL of dimethyl sulfoxide (DMSO) was added at once. The solution was heated at reflux for 3 h, then cooled to room temperature and left under intensive stirring for additional 12 h. The resulting mixture was filtered from insoluble precipitate. Crystallization of filtrate gave in 3–4 weeks crystal product. Several crystals were used for single-crystal X-ray diffraction analysis (Table 21). Elem. analysis, calcd for $[(\text{MeSiO}_{1.5})_{18}(\text{CuO})_9]$, %: Cu, 29.72; Si, 26.27. Found (for vacuum-dried sample), %: Cu, 29.59; Si, 26.04. Yield 0.94 g (44%).

Synthesis of complex $[(\text{MeSiO}_{1.5})_{12}(\text{CuO})_6] \cdot 6\text{DMF}$ **2**. 3 g (0.022 mol) of $\text{MeSi}(\text{OMe})_3$ in 50 ml of ethanol and 0.79 g (0.044 mol) of water were stirred for 30 minutes. Then 0.90 g (0.025 mol) of NaOH was added and resulted white-colored mixture was heated to reflux for 2 hours. Afterwards solution was cooled down to room temperature and 1.35 g (0.01 mol) of CuCl_2 in 50 ml DMF was added at once. Solution was heated under reflux for 3 hours, then cooled down to room temperature and left under intensive stirring for additional 12 hours. Result mixture was filtered from insoluble part. Crystallization of filtrate gave in one-week crystal product. Several crystals were used for single crystal X-Ray investigation (Table 21). Elem. analysis, calctd. for $[(\text{MeSiO}_{1.5})_{12}(\text{CuO})_6]$, %: Cu, 29.72; Si, 26.27. Found (for vacuum dried sample), %: Cu, 29.62; Si, 26.04. Yield 1.07 g (50 %).

Synthesis of complex $[(\text{MeSiO}_{1.5})_{20}(\text{HO}_{0.5})_{3.33}(\text{CuO})_{12}(\text{C}_{12}\text{H}_8\text{N}_2)_4(\text{AcO}_{0.5})_{0.67}] \cdot 4\text{DMSO} \cdot 4\text{H}_2\text{O}$ **3**. 19 grams (0.005 mol) of 1,10-phenanthroline was added at once to solution, produced as described in the section dedicated to the synthesis of **1** (prior to crystallization stage). Mixture was stirred for 4 h at room temperature. Then it was left in a cool place (15 °C) for crystallization. After one week the formation of crystalline material was observed. Several crystals were used for single-crystal X-ray diffraction analysis (Table 21). Elem. analysis, calcd for $[(\text{MeSiO}_{1.5})_{20}(\text{HO}_{0.5})_{3.33}(\text{CuO})_{12}(\text{C}_{12}\text{H}_8\text{N}_2)_4(\text{CH}_3\text{COO}_{0.5})_{0.67}]$, %: Cu, 24.74; N, 3.64; Si, 18.23. Found (for vacuum-dried sample), %: Cu, 24.31; N, 3.52; Si, 18.01. Yield 0.69 g (27%).

Synthesis of complex $[(\text{MeSiO}_{1.5})_{10}(\text{CuO})_6(\text{MeO}_{0.5})_2(1,10\text{-phen})_2] \cdot 0.5(1,4\text{-diox}) \cdot 2.5\text{MeOH}$ **4**. The synthesis and crystallization were performed under nitrogen atmosphere. 3 g (0.022 mol) of $\text{MeSi}(\text{OMe})_3$ in 50 ml of ethanol and 0.79 g (0.044 mol) of water were stirred for 30 minutes. Then 1.14 g (0.029 mol) of NaOH was added and resulted white-colored mixture was heated to reflux for 2 hours. Afterwards solution was cooled down to room temperature and 1.77 g (0.013 mol) of CuCl_2 in 50 ml DMSO was added at once. Solution was heated under reflux for 3 hours, then cooled down

to room temperature and left under intensive stirring for additional 12 hours. 0.79 g (0.0044 mol) of 1,10-phenanthroline was added at once to resulted mixture. Solution was left under stirring for 30 min and then was filtered from insoluble part. All volatiles were removed in vacuum. Solid part was recrystallized from dioxane/methanol mixture (25 ml/10 ml). Several crystals were used for single crystal X-Ray investigation (Table 21). Elem. analysis, calcd for $[(\text{MeSiO}_{1.5})_{10}(\text{CuO})_6(\text{MeO}_{0.5})_2(\text{C}_{12}\text{H}_8\text{N}_2)_2]$, %: Cu, 24.52; N, 3.60; Si, 18.06. Found (for vacuum dried sample), %: Cu, 24.41; N, 3.53; Si, 18.00. Yield 2.80 g (82 %).

Synthesis of complex $[(\text{MeSiO}_{1.5})_{10}(\text{CuO})_6(\text{MeO}_{0.5})_2(2,2'\text{-bipy})_2] \cdot 2\text{MeOH}$ **5**. 0,78 grams (0.005 mol) of 2,2'-bipyridine was added at once to solution, produced as described in the section dedicated to the synthesis of **1** (prior to crystallization stage, 45 mL of methanol/ethanol (1:1) mixture was used instead of DMSO). Mixture was stirred for 4 h at room temperature, and then it was left in a cool place (15 °C) for crystallization. After one week the formation of crystalline material was observed. Several crystals were used for single-crystal X-ray diffraction analysis (Table 21). Elem. analysis, calcd for $[(\text{MeSiO}_{1.5})_{10}(\text{CuO})_6(\text{MeO}_{0.5})_2(\text{C}_{10}\text{H}_8\text{N}_2)_2]$, %: Cu, 25.30; N, 3.72; Si, 18.64. Found (for vacuum-dried sample), %: Cu, 24.74; N, 3.64; Si, 18.23%. Yield 0.50 g (20%).

Synthesis of complex $[(\text{MeSiO}_{1.5})_8(\text{CuO})_3(2,2'\text{-bipy})_2] \cdot 3\text{EtOH}$ **6**. 2,2'-bipyridine (1.57 g, 0.010 mol) was added at once to solution, produced as described in the section concerning the synthesis of **1** (prior to crystallization stage, 45 mL of methanol/ethanol (1:1) mixture was used instead of DMSO). Mixture was stirred for 4 h at room temperature, and then it was left in a cool place (15 °C) for crystallization. After one week the formation of crystalline material was observed. Several crystals were used for single-crystal Xray diffraction analysis (Table 21). Elem. analysis, calcd for $[(\text{MeSiO}_{1.5})_8(\text{CuO})_3(\text{C}_{10}\text{H}_8\text{N}_2)_2]$, %: Cu, 17.52; N, 5.15; Si, 20.65. Found (for vacuum-dried sample), %: Cu, 17.40; N, 5.02; Si, 20.23%. Yield 0.58 g (16%).

Syntheses of complexes **7-14**, 2 g (0.01 mol) of $\text{PhSi}(\text{OMe})_3$ and 0.405 g (0.01 mol) of NaOH were dissolved in 25 mL of ethanol and the resulting mixture was heated to reflux for 2 h. Afterwards the solution was cooled to room temperature and 0.672 g (0.005 mol) of CuCl_2 was added at once. The solution was left under stirring for 3 h and filtered off from the insoluble precipitate. The filtrate was left for crystallization (being mixed with 15 ml of DMF, complex **13** to **14**) or dried in vacuum and recrystallized from corresponding solvate systems (complexes **7-13**), see below for details. Several crystals of each product were studied by single crystals X-ray diffraction (Table 22-23).

Compound $[(\text{PhSiO}_{1.5})_{12}(\text{CuO})_6] \cdot \text{EtOH} \cdot \text{DMF}$ **7**. Anal. Calcd for $[(\text{PhSiO}_{1.5})_{12}(\text{CuO})_6]$, %: Cu, 18.80; Si, 16.62. Found (for vacuum-dried sample), %: Cu, 18.71; Si, 16.50%. Yield 0.75 g (44%).

Compound $[(\text{PhSiO}_{1.5})_{12}(\text{CuO})_6] \cdot \text{DMF} \cdot \text{THF}$ **8**. Recrystallization from mixture (20 ml/20 ml) of DMF/THF. Anal. calcd for $[(\text{PhSiO}_{1.5})_{12}(\text{CuO})_6]$, %: Cu, 18.80; Si, 16.62. Found (for vacuum-dried sample), %: Cu, 18.71; Si, 16.50. Yield 1.09 g (64%).

Compound $[(\text{PhSiO}_{1.5})_{12}(\text{CuO})_6] \cdot \text{DMSO}$ **9**. Recrystallization from 40 ml of DMSO. Anal. calcd for $[(\text{PhSiO}_{1.5})_{12}(\text{CuO})_6]$, %: Cu, 18.80; Si, 16.62. Found (for vacuum-dried sample), %: Cu, 18.69; Si, 16.49. Yield 0.89 g (53%).

Compound $[(\text{PhSiO}_{1.5})_{12}(\text{CuO})_6] \cdot \text{MeCN}$ **10**. Recrystallization from 50 ml of hot MeCN. Anal. calcd for $[(\text{PhSiO}_{1.5})_{12}(\text{CuO})_6]$, %: Cu, 18.80; Si, 16.62. Found (for vacuum-dried sample), %: Cu, 18.72; Si, 16.52. Yield 0.68 g (40%).

Compound $[(\text{PhSiO}_{1.5})_{12}(\text{CuO})_6] \cdot \text{PhCN} \cdot \text{THF}$ **11**. Recrystallization from 40 ml of PhCN. Anal. calcd for $[(\text{PhSiO}_{1.5})_{12}(\text{CuO})_6]$, %: Cu, 18.80; Si, 16.62. Found (for vacuum-dried sample), %: Cu, 18.68; Si, 16.48. Yield 0.25 g (15%).

Compound $[(\text{PhSiO}_{1.5})_{12}(\text{CuO})_6] \cdot \text{THF}$ **12**. Recrystallization from 40 ml of THF. Anal. calcd for $[(\text{PhSiO}_{1.5})_{12}(\text{CuO})_6]$, %: Cu, 18.80; Si, 16.62. Found (for vacuum-dried sample), %: Cu, 18.67; Si, 16.50. Yield 0.87 g (50%).

Compound $[(\text{PhSiO}_{1.5})_{10}(\text{CuO})_5(\text{Py})_5]$ **13**. Recrystallization from 40 ml of pyridine. Anal. calcd for $[(\text{PhSiO}_{1.5})_{10}(\text{CuO})_5]$, %: Cu, 18.80; Si, 16.62. Found (for vacuum-dried sample), %: Cu, 18.71; Si, 16.52. Yield 1.12 g (66%).

Compound $[(\text{PhSiO}_{1.5})_{10}(\text{CuO})_5(\text{DMF})_4] \cdot \text{H}_2\text{O}$ **14**. Recrystallization of dried complex **13** (0.5 g) from 40 ml of DMF. Anal. calcd for $[(\text{PhSiO}_{1.5})_{10}(\text{CuO})_5]$, %: Cu, 18.80; Si, 16.62. Found (for vacuum-dried sample), %: Cu, 18.72; Si, 16.50. Yield 0.39 g (78%).

Compound $[(\text{PhSiO}_{1.5})_{12}(\text{CuO})_6] \cdot \text{DMF}$ **15**. Recrystallization from 40 ml of DMF. Anal. calcd for $[(\text{PhSiO}_{1.5})_{12}(\text{CuO})_6]$, %: Cu, 18.80; Si, 16.62. Found (for vacuum-dried sample), %: Cu, 18.71; Si, 16.51. Yield 1.36 g (80%).

Synthesis of complex $\{[(\text{PhSiO}_{1.5})_{10}(\text{CoO})_5(\text{H}_2\text{O})_2]_2[(\text{PhSiO}_{1.5})_{10}(\text{CuO})_5]\}$ **16**. 2 g (0.01 mol) of $\text{PhSi}(\text{OMe})_3$ and 0.405 g (0.01 mol) of NaOH were dissolved in 25 mL of ethanol, and the resulting mixture was heated to reflux for 2 h. Afterwards the solution was cooled to room temperature, and mixture of 0.335 g (2.49 mmol) of CuCl_2 and 0.324 g (2.49 mmol) of CoCl_2 was added at once. The solution was left under stirring for 3 h and filtered off from the insoluble precipitate. Filtrate was dried in vacuum and recrystallized from 40 ml of pyridine. Several crystals of resulted crystalline product were studied by single crystals X-ray diffraction (Table 23). Anal. calcd for $\{[(\text{PhSiO}_{1.5})_{10}(\text{CoO})_5(\text{H}_2\text{O})_2]_2[(\text{PhSiO}_{1.5})_{10}(\text{CuO})_5]\}$, %: Co, 11.57; Cu, 6.24; Si, 16.54. Found (for vacuum-dried sample), %: Co, 11.49; Cu, 6.18; Si, 16.47. Yield 0.37 g (29%).

Syntheses of complexes **17 - 25**. A 1 g portion (5.04 mmol) of $\text{PhSi}(\text{OMe})_3$, 0.20 g (5 mmol) of NaOH, and 20 mL of an ethanol/methanol (1/1) mixture were placed in a three-neck round-bottom

flask (equipped with magnetic stirrer and condenser). The resulting solution was heated under reflux for 1.5 h and then was cooled to room temperature, and 0.226 g (1.68 mmol) of CuCl₂ was added at once. The mixture was stirred for 3 h and filtered from NaCl. The filtrate was dried under vacuum, and then 0.131 g (0.839 mmol) of 2,2'-bipyridine in solution: 35 mL of DMSO **17**, MeCN **18**, mixture MeCN/PhCN = 2/1 **19**, MeCN/PhCN = ½ **20**, PhCN **21**, THF **22**, mixture toluene / DMSO = 3/1 **23**, THF **24**, MeCN **25**. was placed in the same evaporation flask. The resulting solution was intensely stirred for 2.5 h with a magnetic stirrer and then filtered from the insoluble precipitate. The filtrate was stored in a vial equipped with a septum with a needle to allow the slow evaporation of solvents for crystallization. After 1 week the formation of crystalline material was observed; several single crystals were used for X-ray diffraction analysis (Table 24 - 25). The rest of the crystalline fraction was separated from the solution, washed with *n*-heptane, and dried under vacuum.

Compound [(PhSiO_{1.5})₁₀(CuO)₆(HO_{0.5})₂(2,2'-bipy)₂] • 2.5 DMSO **17**. Anal. Calcd for [(PhSiO_{1.5})₁₀(CuO)₆(HO_{0.5})₂(C₁₀H₈N₂)₂], %: Cu, 18.16; N, 2.67; Si, 13.38. Found (for vacuum-dried sample), %: Cu, 18.07; N, 2.59; Si, 13.29. Yield: 0.36 g (61%).

Compound [(PhSiO_{1.5})₁₀(CuO)₆(HO_{0.5})₂(2,2'-bipy)₂] • 2.5 MeCN • 2 H₂O **18**. Anal. Calcd for [(PhSiO_{1.5})₁₀(CuO)₆(HO_{0.5})₂(C₁₀H₈N₂)₂], %: Cu, 18.16; N, 2.67; Si, 13.38. Found (for vacuum -dried sample), %: Cu, 18.05; N, 2.60; Si, 13.27. Yield: 0.24 g (40%).

Compound [(PhSiO_{1.5})₁₀(CuO)₆(HO_{0.5})₂(2,2'-bipy)₂] • 4 MeCN **19**. Anal. Calcd for [(PhSiO_{1.5})₁₀(CuO)₆(HO_{0.5})₂(C₁₀H₈N₂)₂], %: Cu, 18.16; N, 2.67; Si, 13.38. Found (for vacuum-dried sample), %: Cu, 18.07; N, 2.61; Si, 13.30. Yield: 0.12 g (20%).

Compound [(PhSiO_{1.5})₁₀(CuO)₆(HO_{0.5})₂(2,2'-bipy)₂] • 3.5 PhCN • 0.5 H₂O **20**. Anal. Calcd for [(PhSiO_{1.5})₁₀(CuO)₆(HO_{0.5})₂(C₁₀H₈N₂)₂], %: Cu, 18.16; N, 2.67; Si, 13.38. Found (for vacuum-dried sample), %: Cu, 18.09; N, 2.60; Si, 13.29. Yield: 0.06 g (10%).

Compound [(PhSiO_{1.5})₁₀(CuO)₆(HO_{0.5})₂(2,2'-bipy)₂] • 3 PhCN **21**. Anal. Calcd for [(PhSiO_{1.5})₁₀(CuO)₆(HO_{0.5})₂(C₁₀H₈N₂)₂]: Cu, 18.16; N, 2.67; Si, 13.38. Found (for vacuum-dried sample): Cu, 18.07; N, 2.58; Si, 13.26. Yield: 0.08 g (14%).

Compound [(PhSiO_{1.5})₁₀(CuO)₆(HO_{0.5})₂(2,2'-bipy)₂] • 1.5 THF **22**. Anal. Calcd for [(PhSiO_{1.5})₁₀(CuO)₆(HO_{0.5})₂(C₁₀H₈N₂)₂], %: Cu, 18.16; N, 2.67; Si, 13.38. Found (for vacuum-dried sample), %: Cu, 18.10; N, 2.59; Si, 13.29. Yield: 0.28 g (48%).

Compound [(PhSiO_{1.5})₁₀(CuO)₆(MeO_{0.5})₂(2,2'-bipy)₂] **23**. Anal. Calcd for [(PhSiO_{1.5})₁₀(CuO)₆(HO_{0.5})₂(C₁₀H₈N₂)₃], %: Cu, 16.90; N, 3.73; Si, 12.45. Found (for vacuum-dried sample), %: Cu, 16.81; N, 3.68; Si, 12.37. Yield: 0.08 g (12%).

Compound [(PhSiO_{1.5})₁₀(CuO)₆(MeO_{0.5})₂(2,2'-bipy)₂] **24**. Anal. Calcd for [(PhSiO_{1.5})₁₀(CuO)₆(CH₃O_{0.5})₂(C₁₀H₈N₂)₂], %: Cu, 17.92; N, 2.63; Si, 13.20. Found (for vacuum-dried sample), %: Cu, 18.10; N, 2.59; Si, 13.29. Yield: 0.16 g (27%).

Compound $[(\text{PhSiO}_{1.5})_{10}(\text{CuO})_6(\text{AcO}_{0.5})_2(2,2'\text{-bipy})_2] \cdot \text{MeCN}$ **25**. Anal. Calcd for $[(\text{PhSiO}_{1.5})_{10}(\text{CuO})_6(\text{CH}_3\text{COO}_{0.5})_2(\text{C}_{10}\text{H}_8\text{N}_2)_2]$, %: Cu, 17.46; N, 2.57; Si, 12.86. Found (for vacuum-dried sample), %: Cu, 17.37; N, 2.49; Si, 12.77. Yield: 0.15 g (25%).

Syntheses of complexes **26 - 29**. A 1 g portion (5.04 mmol) of $\text{PhSi}(\text{OMe})_3$, 0.20 g (5 mmol) of NaOH, and 20 mL of an ethanol/methanol (1/1) mixture were placed in a three-neck round-bottom flask (equipped with a magnetic stirrer and condenser). The resulting solution was heated under reflux for 1.5 h and then was cooled to room temperature, and 0.226 g (1.68 mmol) of CuCl_2 was added at once. The mixture was stirred for 3 h and filtered from NaCl. The filtrate was dried under vacuum, and then 0.151 g (0.840 mmol) of 1,10-phenanthroline in 35 mL of solution: DMSO **26**, toluene **27**, DMF **28**, pyridine **29** was placed in the same evaporation flask. The resulting solution was intensely stirred for 2.5 h with a magnetic stirrer and then filtered from the insoluble precipitate. The filtrate was stored in a vial equipped with a septum with a needle to allow the slow evaporation of solvents for crystallization. After 1 week the formation of crystalline material was observed; several single crystals were used for X-ray diffraction analysis (for details of the X-ray diffraction study see Table 25-26). The rest of the crystalline fraction was separated from the solution, washed with n-heptane, and dried under vacuum.

Compound $[(\text{PhSiO}_{1.5})_{10}(\text{CuO})_6(\text{HO}_{0.5})_2(1,10\text{-phen})_2] \cdot 4$ DMSO **26**. Anal. Calcd for $[(\text{PhSiO}_{1.5})_{10}(\text{CuO})_6(\text{HO}_{0.5})_2(\text{C}_{12}\text{H}_8\text{N}_2)_2]$, %: Cu, 17.75; N, 2.61; Si, 13.08. Found (for vacuum-dried sample), %: Cu, 17.64; N, 2.53; Si, 12.99. Yield: 0.39 g (65%).

Compound $[(\text{PhSiO}_{1.5})_{10}(\text{CuO})_6(\text{HO}_{0.5})_2(1,10\text{-phen})_2] \cdot 4.75$ DMSO **27**. Anal. Calcd for $[(\text{PhSiO}_{1.5})_{10}(\text{CuO})_6(\text{HO}_{0.5})_2(\text{C}_{12}\text{H}_8\text{N}_2)_2]$, %: Cu, 17.75; N, 2.61; Si, 13.08. Found (for vacuum-dried sample), %: Cu, 17.66; N, 2.54; Si, 12.99. Yield: 0.22 g (37%).

Compound $[(\text{PhSiO}_{1.5})_{10}(\text{CuO})_6(\text{HO}_{0.5})_2(1,10\text{-phen})_2] \cdot 4$ DMF **28**. Anal. Calcd for $[(\text{PhSiO}_{1.5})_{10}(\text{CuO})_6(\text{HO}_{0.5})_2(\text{C}_{12}\text{H}_8\text{N}_2)_2]$, %: Cu, 17.75; N, 2.61; Si, 13.08. Found (for vacuum-dried sample), %: Cu, 17.68; N, 2.54; Si, 13.00. Yield: 0.28 g (47%).

Compound $[(\text{PhSiO}_{1.5})_{10}(\text{CuO})_6(\text{HO}_{0.5})_2(1,10\text{-phen})_2] \cdot 4$ Py **29**. Anal. Calcd for $[(\text{PhSiO}_{1.5})_{10}(\text{CuO})_6(\text{HO}_{0.5})_2(\text{C}_{12}\text{H}_8\text{N}_2)_2]$, %: Cu, 17.75; N, 2.61; Si, 13.08. Found (for vacuum-dried sample), %: Cu, 17.66; N, 2.52; Si, 12.99. Yield: 0.18 g (31%).

Syntheses of complexes **30-32**. A 1 g portion (5.04 mmol) of $\text{PhSi}(\text{OMe})_3$, 0.20 g (5 mmol) of NaOH, and 20 mL of an ethanol/methanol (1/1) mixture were placed in a three-neck round-bottom flask (equipped with a magnetic stirrer and condenser). The resulting solution was heated under reflux for 1.5 h and then was cooled to room temperature, and 0.226 g (1.68 mmol) of CuCl_2 was added at once. The mixture was stirred for 3 h and filtered from NaCl. The filtrate was dried under vacuum, and then 0.280 g (0.840 mmol) of bathophenanthroline in 35 mL solution of MeCN **30**, toluene **31**, benzene **32** was placed in the same evaporation flask. The resulting solution was intensely stirred for

2.5 h with a magnetic stirrer and then filtered from the insoluble precipitate. The filtrate was stored in a vial equipped with a septum with a needle to allow the slow evaporation of solvents for crystallization. After 1 week the formation of crystalline material was observed; several single crystals were used for X-ray diffraction analysis (Table 26-27). The rest of the crystalline fraction was separated from the solution, washed with n-heptane, and dried under vacuum.

Compound $[(\text{PhSiO}_{1.5})_{10}(\text{CuO})_6(\text{HO}_{0.5})_2(\text{Bphen})_2] \cdot \text{MeCN}$ **30**. Anal. Calcd for $[(\text{PhSiO}_{1.5})_{10}(\text{CuO})_6(\text{HO}_{0.5})_2(\text{C}_{24}\text{H}_{16}\text{N}_2)_2]$, %: Cu, 15.55; N, 2.28; Si, 11.45. Found (for vacuum-dried sample), %: Cu, 15.48; N, 2.20; Si, 11.36. Yield: 0.28 g (41%).

Compound $[(\text{PhSiO}_{1.5})_{10}(\text{CuO})_6(\text{HO}_{0.5})_2(\text{Bphen})_2] \cdot \text{DMSO}$ **31**. Anal. Calcd for $[(\text{PhSiO}_{1.5})_{10}(\text{CuO})_6(\text{HO}_{0.5})_2(\text{C}_{24}\text{H}_{16}\text{N}_2)_2]$, %: Cu, 15.55; N, 2.28; Si, 11.45. Found (for vacuum-dried sample), %: Cu, 15.47; N, 2.19; Si, 11.36. Yield: 0.21 g (30%).

Compound $[(\text{PhSiO}_{1.5})_{10}(\text{CuO})_6(\text{HO}_{0.5})_2(\text{Bphen})_2] \cdot \text{C}_7\text{H}_8$ **32**. Anal. Calcd for $[(\text{PhSiO}_{1.5})_{10}(\text{CuO})_6(\text{HO}_{0.5})_2(\text{C}_{24}\text{H}_{16}\text{N}_2)_2]$, %: Cu, 15.55; N, 2.28; Si, 11.45. Found (for vacuum-dried sample), %: Cu, 15.48; N, 2.18; Si, 11.34. Yield: 0.15 g (22%).

Synthesis of complex $\text{Ph}_{12}\text{Si}_{12}\text{O}_{12}(\text{OH})(\text{O}^-)_{11}\text{Cu}_5\text{Na}(2,2'\text{-bipy})_3 \cdot \text{H}_2\text{O} \cdot 7\text{THF}$ **33**. $\text{PhSi}(\text{OMe})_3$ (1.5 g, 7.56 mmol), NaOH (0.30 g, 7.56 mmol), and 20 mL of an ethanol were placed in a three-neck round-bottom flask (equipped with magnetic stirrer and condenser). The resulting solution was heated under reflux for 1 h and then was cooled to room temperature, and 0.34 g (2.52 mmol) of CuCl_2 was added at once. The mixture was stirred for 4 h and filtered from NaCl. The filtrate was mixed with 0.24 g (1.51 mmol) of 2,2'-bipyridine in 60 mL of THF. The resulting solution was intensely stirred for 3 h with a magnetic stirrer and then filtered from the insoluble precipitate. After approximately 7 days the formation of crystalline material was observed; several single crystals were used for X-ray diffraction analysis (Table 27). Anal. Calcd for $[(\text{PhSiO}_{1.5})_{12}(\text{CuO})_5(\text{NaO}_{0.5})(\text{HO}_{0.5})(\text{C}_{10}\text{H}_8\text{N}_2)_3]$, %: Cu, 12.93; Na, 0.94; N, 3.42; Si, 13.72. Found (for vacuum-dried sample), %: Cu, 12.93; Na, 0.94; N, 3.42; Si, 13.72. Yield: 0.38 g (24%).

Synthesis of complex $[(\text{PhSiO}_{1.5})_{12}(\text{PhSiO}_{1.5})_8(\text{CuO})_8(\text{NaO}_{0.5})_4\{\text{Cu}(\text{O}_{0.5})_4\}] \cdot 2[\text{Cu}(\text{dppe})_2]$ **34**. The $\text{PhSi}(\text{OEt})_3$ (1 g, 4.16 mmol) and NaOH (0.194 g, 4.85 mmol) were heated to reflux in ethanol (60 mL) for 1.5 h. CuCl_2 (0.28 g, 2.08 mmol) was added, and the resulting blue mixture was stirred without heating for 1 h. Afterwards, dppe (0.414 g, 1.04 mmol) was added at once, and the resulting mixture was heated under reflux for 3 h. The hot solution was filtered to remove the precipitate. The crystallization of the filtrate over 1 week gave a crystalline material, and several single crystals of which were used for X-ray analysis (Table 27). Elemental analysis calcd for $[(\text{PhSiO}_{1.5})_{12}(\text{CuO})_4(\text{NaO}_{0.5})_2] \cdot 2[\text{Cu}(\text{dppe})_4]$ (3651.23), %: Si 9.23, Cu 10.44, Na 1.26, P 6.79; found (for vacuum-dried sample), %: Si 9.17, Cu 10.38, Na 1.20, P 6.72. Yield 0.40 g (42%).

Synthesis of complex $[(\text{PhSiO}_{1.5})_{12}(\text{CuO})_4(\text{NaO}_{0.5})_2] \cdot 2[\text{Cu}(\text{dppe})_2]$ **35**. $\text{PhSi}(\text{OEt})_3$ (1 g, 4.16 mmol) and NaOH (0.216 g, 5.40 mmol) were heated to reflux in ethanol (60 mL) for 1.5 h. CuCl_2 (0.28 g, 2.08 mmol) was added, and the resulting blue mixture was stirred without heating for 1 h. Afterwards, dppe (0.414 g, 1.04 mmol) dissolved in toluene (45 mL) was added at once, and the resulting mixture was stirred for 2 h. The solution was filtered to remove the precipitate. The crystallization of the filtrate over 2 weeks gave a crystalline material, and several single crystals were used for XRD analysis (Table 27). Elemental analysis calcd for $[(\text{PhSiO}_{1.5})_{12}(\text{PhSiO}_{1.5})_8(\text{CuO})_8(\text{NaO}_{0.5})_4\{\text{Cu}(\text{O}_{0.5})_4\}] \cdot 2[\text{Cu}(\text{dppe})_2]$ (5160.39), %: Si 10.89, Cu 13.55, Na 1.78, P 4.80; found (for vacuumdried sample), %: Si 10.81, Cu 13.46, Na 1.60, P 4.71. Yield 0.49 g (46%).

Synthesis of complex $[(\text{PhSiO}_{1.5})_{12}(\text{CuO})_4(\text{NaO}_{0.5})_4(\text{dppmO}_2)_2]$ **36**. 1 g (4.16 mmol) of $\text{PhSi}(\text{OEt})_3$ and 0.17 g (4.16 mmol) of NaOH were heated at reflux in 55 ml of ethanol for 2 h. Then 0.19 g (2.08 mmol) of CuCl_2 was added and resulted blue-colored mixture was stirred without heating for 1.5 h. Afterwards 0.27 g (0.70 mmol) of dppm dissolved in 30 ml of toluene was added at once and resulted mixture was stirred for 2 h. Solution was filtered from precipitate. Crystallization of filtrate (in the presence of a trace of air) gave in 3 weeks a crystalline material, several single crystals were used for X-ray diffraction analysis (Table 27). Elemental analysis calcd for $[(\text{PhSiO}_{1.5})_{12}(\text{CuO})_4(\text{NaO}_{0.5})_4(\text{dppmO}_2)_2]$, %: Si, 11.93; Cu, 9.00; Na, 3.25; P, 4.39. Found (for vacuum dried sample), %: Si, 11.87; Cu, 8.95; Na, 3.21; P, 4.34. Yield 0.21 g (22 %).

Synthesis of complex $(\text{PhGeO})_{12}(\text{PhGe}_2)\text{O}[\text{Fe}_5\text{O}_{17}(\text{OH})]\text{Cu}_2(2,2\text{-bipy})_2$ **38**. Method A. To a methanol/toluene (50 mL/15 mL, placed in a round-bottom flask) solution were added compound **37** (0.300 g, 0.09 mmol) and, after total dissolution of 1, copper(II) chloride (0.012 g, 0.09 mmol). The mixture was rigorously stirred for 3 h. Then 2,2'-bipyridine (0.014 g, 0.09 mmol) was added at once to the solution and the resulting mixture was stirred overnight. Filtration of the mixture from the insoluble part gave a clear solution, suitable for crystallization. Slow evaporation of the solvents over two weeks gave a crystalline material. Several crystals were used for the single-crystal X-ray diffraction analysis (Table 28). Anal. Calcd for $\{[\text{Fe}_5\text{O}_{17}(\text{OH})]\text{Cu}_2(\text{bipy})_2(\text{PhGeO})_{12}(\text{PhGe})_2\text{O}\}$, %: Ge, 30.70; Fe, 8.43; Cu, 3.84; N, 1.69. Found (for vacuum-dried sample), %: Ge, 30.53; Fe, 8.32; Cu, 3.76; N, 1.60. Yield: 0.013 g (9%).

Method B. $\text{PhGe}(\text{OMe})_3$ (2.00 g, 8.2 mmol) was dissolved in 50 mL of methanol. Then 0.44 g (11.1 mmol) of NaOH was added, and the resulting mixture was heated to reflux for 2 h. Afterward the solution was cooled to room temperature, and 0.48 g (3.00 mmol) of FeCl_3 and 0.16 g (1.17 mmol) of CuCl_2 were added at once. The solution was stirred for 3 h, and then 0.18 g (1.17 mol) of bipy was added at once to the solution and the resulting mixture was stirred overnight. Filtration of the mixture from the insoluble part gave a clear solution, suitable for crystallization. Slow evaporation of solvents

over two weeks gave a crystalline material. Several crystals were used for the single-crystal X-ray diffraction analysis (cell parameters were found to be equal to those of the product of method A). Anal. Calcd for $\{[\text{Fe}_5\text{O}_{17}(\text{OH})]\text{Cu}_2(\text{bipy})_2(\text{PhGeO})_{12}(\text{PhGe})_2\text{O}\}$, %: Ge, 30.70; Fe, 8.43; Cu, 3.84; N, 1.69. Found (for vacuum-dried sample), %: Ge, 30.59; Fe, 8.34; Cu, 3.79; N, 1.61. Yield: 0.40 g (21%).

Synthesis of complex $[\text{Na}_4\text{Cu}_{42}(\text{Ph}_2\text{Ge}_2\text{O}_5)_{12}(\text{OH})_{40}]$ **39**. 1 g of $[\text{PhGeO}_{1.5}]_n$ (6.78 mmol referenced to a $[\text{PhGeO}_{1.5}]$ unit) were placed in a 100 mL round-bottomed flask, equipped with a magnetic stirrer and condenser, and mixed with 75 ml of ethanol. 0.62 g (9.23 mmol) of NaOH were added to the same flask. After 1.5 hour of intense stirring under reflux, the mixture became homogeneous and 0.26 g (4.11 mmol) of CuCl_2 were added to the mixture. Resulted solution was left under reflux for 1 hour and, after cooling to room temperature, was filtered from insoluble fraction. The resulted solution was dried in vacuo and dissolved in 50 ml the mixture of DMF/ CHCl_3 (V/V = 2/1). A slow spontaneous evaporation of solvates gave crystalline material within 3 weeks. Several single crystals were manually selected to be studied by X-ray diffraction (Table 28). The rest of crystalline phase was dried in vacuo. Anal. Calcd for $[\text{Na}_4\text{Cu}_{42}(\text{Ph}_2\text{Ge}_2\text{O}_5)_{12}(\text{OH})_{40}]$, %: Cu, 33.38; Na, 1.15; Ge, 21.80. Found (for vacuum-dried sample), %: Cu, 33.01; Na, 1.08; Ge, 21.66%. Yield 0.27 g (43%).

Synthesis of complex $[(\text{PhGeO}_{1.5})_{10}(\text{CuO})_6(\text{HO}_{0.5})_2(\text{C}_{12}\text{H}_8\text{N}_2)_2] \cdot 2\text{H}_2\text{O}$ **40**. $\text{PhGe}(\text{OMe})_3$ (1.20 g; 4.9 mmol) in 60 ml of an ethanol/methanol (1:1) solution was mixed with solid NaOH (0.24 g; 5.9 mmol). Mixture was heated under reflux for 2 h. Afterwards, the solution was cooled to room temperature and 0.40 g (3.0 mmol) of anhydrous CuCl_2 was added at once. The solution was left under stirring overnight and 0.18 g (0.9 mmol) of 1,10-phenanthroline were added. Resulted mixture was left under stirring for 4 h and then filtered from the insoluble part. The filtrate was stored in a warm place in a flask equipped by septum with two needles to admit a slow current of nitrogen and evaporation of the solvents. After approximately 7 days the formation of crystalline material 1 was occurred; a few selected single crystals were used for the X-ray diffraction analysis (Table 28). Anal. Calcd for $[(\text{PhGeO}_{1.5})_{10}(\text{CuO})_6(\text{HO}_{0.5})_2(\text{C}_{12}\text{H}_8\text{N}_2)_2]$, %: Cu, 14.70; N, 2.16; Ge, 28.01. Found (for vacuumdried sample), %: Cu, 14.61; N, 2.13; Ge, 27.95%. Yield 0.42 g (21%).

Synthesis of complex $[(\text{PhGeO}_{1.5})_{10}(\text{CuO})_6(\text{HO}_{0.5})_2(2,2'\text{-bipy})_2] \cdot 5\text{EtOH}$ **41**. $\text{PhGe}(\text{OMe})_3$ (1.20 g; 4.9 mmol) in 60 ml of an ethanol/methanol (1:1) solution was mixed with solid Na (0.14 g; 5.9 mmol). Mixture was heated under reflux for 2 h. Afterwards, the solution was cooled to room temperature and 0.40 g (3.0 mmol) of anhydrous CuCl_2 was added at once. The solution was left under stirring overnight and 0.15 g (0.9 mmol) of 2,2'-bipyridine were added. Resulted mixture was left under stirring for 4 h and then filtered from the insoluble part. The filtrate was stored in a warm place in a flask equipped by septum with two needles to admit a slow current of nitrogen and

evaporation of the solvents. After approximately 7 days the formation of crystalline material 2 was occurred; a few selected single crystals were used for the X-ray diffraction analysis (Table 28). Anal. Calcd for $[(\text{PhGeO}_{1.5})_{10}(\text{CuO})_6(\text{HO}_{0.5})_2(\text{C}_{10}\text{H}_8\text{N}_2)_2]$, %: Cu, 14.98; N, 2.20; Ge, 28.54. Found (for vacuumdried sample), %: Cu, 14.89; N, 2.14; Ge, 28.35%. Yield 0.78 g (39%).

Synthesis of complex $(\text{PhGeO}_2)_{10}\text{Cu}_6(2,2'\text{-bipy})_2(3,5\text{-Me}_2\text{Pz})_2$ **42**. Compound $\text{PhGe}(\text{OMe})_3$ (1.50 g; 6.17 mmol) in 65 ml of a methanol solution was mixed with solid NaOH (0.3 g; 7.4 mmol). Mixture was heated under reflux for 2 h. Afterwards, the solution was cooled to room temperature and 0.50 g (3.7 mmol) of anhydrous CuCl_2 was added at once. The solution was left under stirring overnight and the mixture 2,20-bipyridine (0.19 g, 1.2 mmol)/3,5- dimethylpyrazole (0.12 g, 1.2 mmol) dissolved in 50 ml of acetonitrile were added. Resulted mixture was left under stirring for 3 h and then filtered from the insoluble part. The filtrate was stored in a warm place in a flask to admit a slow evaporation of the solvents. After approximately 10 days the formation of crystalline material 1 was occurred; a few selected single crystals were used for the X-ray diffraction analysis (Table 28). Analysis calculated for $[(\text{PhGeO}_2)_{10}\text{Cu}_6(\text{C}_{10}\text{H}_8\text{N}_2)_2(\text{C}_5\text{H}_7\text{N}_2)_2]$, %: Cu, 14.11; N, 4.15; Ge, 26.89. Found (for vacuum dried sample), %: Cu, 14.06; N, 4.10; Ge, 26.81%. Yield 0.28 g (17%).

Synthesis of complexes **44** – **47**, **51**. Flasks were loaded with dried compound $[(\text{PhSiO}_{1.5})_{12}(\text{CuO})_4(\text{NaO}_{0.5})_4(\text{BuOH})_6]$ **43** (0.80 g, 0.33 mmol) and 55 ml of corresponding solvents: dimethyl sulfoxide (compound **44**), acetonitrile (compound **45**), 1,4-dioxane/ethanol (compound **46**), 1,4-dioxane/benzonitrile (compound **47**) or ethanol/toluene (compound **51**). Mixtures were stirred overnight and then filtrated from insoluble part. Slow evaporation of solvates gave the single crystals. After 7 days, crystals were separated, washed and dried in vacuo (see below details of elemental analyses and yields of dried products). Single crystals were analyzed by X-ray diffraction analysis (Table 29-30).

Compound $[(\text{PhSiO}_{1.5})_{12}(\text{CuO})_4(\text{NaO}_{0.5})_4(\text{DMSO})_8]$ **44**. Anal. calcd. for $[(\text{C}_6\text{H}_5\text{SiO}_{1.5})_{12}(\text{CuO})_4(\text{NaO}_{0.5})_4]$, %: Cu, 12.76; Na, 4.62; Si, 16.92. Found (for vacuum dried sample), %: Cu, 12.68; Na, 4.58; Si, 16.84. Yield 0.45 g (57%).

Compound $[(\text{PhSiO}_{1.5})_{12}(\text{CuO})_4(\text{NaO}_{0.5})_4(\text{MeCN})_6(\text{H}_2\text{O})_2] \cdot 2\text{MeCN}$ **45**. Anal. calcd. For $[(\text{C}_6\text{H}_5\text{SiO}_{1.5})_{12}(\text{CuO})_4(\text{NaO}_{0.5})_4]$, %: Cu, 12.76; Na, 4.62; Si, 16.92. Found (for vacuum dried sample), %: Cu, 12.70; Na, 4.57; Si, 16.86. Yield 0.36 g (45%).

Compound $[(\text{PhSiO}_{1.5})_{12}(\text{CuO})_4(\text{NaO}_{0.5})_4(1,4\text{-diox})(\text{EtOH})_4] \cdot 0.5\text{EtOH}$ **46**. Anal. calcd. For $[(\text{C}_6\text{H}_5\text{SiO}_{1.5})_{12}(\text{CuO})_4(\text{NaO}_{0.5})_4]$, %: Cu, 12.76; Na, 4.62; Si, 16.92. Found (for vacuum dried sample), %: Cu, 12.71; Na, 4.56; Si, 16.87. Yield 0.31 g (39%).

Compound $[(\text{PhSiO}_{1.5})_{12}(\text{CuO})_4(\text{NaO}_{0.5})_4(1,4\text{-diox})_4(\text{H}_2\text{O})_3] \cdot 2\text{PhCN} \cdot 2(1,4\text{-diox}) \cdot \text{H}_2\text{O}$ **47**. Anal. calcd. For $[(\text{PhSiO}_{1.5})_{12}(\text{CuO})_4(\text{NaO}_{0.5})_4]$, %: Cu, 12.76; Na, 4.62; Si, 16.92. Found: Cu, 12.71; Na, 4.56; Si, 16.87. Yield 0.44 g (55%).

Compound $[(\text{PhSiO}_{1.5})_{10}(\text{CuO})_2(\text{NaO}_{0.5})_2(\text{H}_2\text{O})_6]$ **51**. Anal. calcd. For $[(\text{PhSiO}_{1.5})_{10}(\text{CuO})_2(\text{NaO}_{0.5})_2]$, %: Cu, 8.40; Na, 3.04; Si, 18.56. Found (for vacuum dried sample), %: Cu, 8.31; Na, 2.96; Si, 18.27. Yield 0.11 g (18%).

Compound $[(\text{PhSiO}_{1.5})_{12}(\text{CuO})_4(\text{NaO}_{0.5})_2(\text{KO}_{0.5})_2(\text{DMF})_6]$ **48**. A flask was loaded with dried compound **43** (0.80 g, 0.4 mmol), 60 ml of dimethyl formamide and 0.06 g (0.8 mmol) of KCl. The mixture was heated under reflux for 4 hours and filtered. The filtrate was stored in cool place and formation of crystals were observed within a few days. Single crystals were analysed by the single crystal X-ray diffraction (Table 29). The crystals were separated, washed and dried in vacuo. Anal. calcd. For $[(\text{C}_6\text{H}_5\text{SiO}_{1.5})_{12}(\text{CuO})_4(\text{NaO}_{0.5})_2(\text{KO}_{0.5})_2]$, %: Cu, 12.55; K, 3.86; Na, 2.27; Si, 16.65. Found (for vacuum dried sample), %: Cu, 12.44; K, 3.80; Na, 2.19; Si, 16.59. Yield 39% (0.31 g).

Compound $[(\text{PhSiO}_{1.5})_{12}(\text{CuO})_4(\text{NaO}_{0.5})_3(\text{CsO}_{0.5})(\text{DMF})_4]$ **49**. A flask was loaded with dried compound **43** (0.8 g, 0.4 mmol) and 60 ml of dimethyl formamide. Solution was heated under reflux and 0.09 g (0.59 mmol) of CsF in 5 ml of water were added at once by syringe. Mixture was heated under reflux for 12 hours and filtered. Solution was stored in cool place and in a few days formation of crystal phase was observed. Single crystals were studied by the X-ray analysis (Table 30). After the moment of crystal' growth ceasing crystal phase was separated and dried in vacuo. Anal. calcd. for $[(\text{C}_6\text{H}_5\text{SiO}_{1.5})_{12}(\text{CuO})_4(\text{NaO}_{0.5})_3(\text{CsO}_{0.5})]$, %: Cu, 12.09; Cs, 6.32; Na, 3.28; Si, 16.03. Found (for vacuum dried sample), %: Cu, 11.99; Cs, 6.21; Na, 3.14; Si, 15.91. Yield 20% (0.168 g).

Compound $[(\text{PhSiO}_{1.5})_{12}(\text{CuO})_4(\text{NaO}_{0.5})(\text{CsO}_{0.5})_3(\text{DMF})_4(\text{DMSO} \cdot \text{H}_2\text{O})] \cdot 1.5\text{DMF}$ **50**. A flask was loaded with dried compound **43** (0.80 g, 0.4 mmol), 45 ml of dimethyl formamide and 35 ml of dimethyl sulfoxide. Solution was heated under reflux and 0.185 g (1.21 mmol) of CsF in 5 ml of water were added at once by syringe. Mixture was heated under reflux for 12 hours and filtered. Solution was stored in cool place and in a few days formation of crystal phase was observed. Single crystals were treated by the X-ray (Table 30). After 7 days the crystals were separated, washed and dried in vacuo. Anal. calcd. For $[(\text{C}_6\text{H}_5\text{SiO}_{1.5})_{12}(\text{CuO})_4(\text{NaO}_{0.5})(\text{CsO}_{0.5})_3]$, %: Cu, 10.95; Cs, 17.17; Na, 0.99; Si, 14.51. Found (for vacuum dried sample), %: Cu, 10.89; Cs, 17.06; Na, 0.96; Si, 14.42. Yield 40% (0.37 g).

Compound **52**. A flask was loaded with dried compound **43** (0.80 g, 0.4 mmol) and 60 ml of dimethyl formamide. Solution was heated under reflux and 0.122 g (0.80 mmol) of CsF in 5 ml of water were added at once by syringe. Mixture was heated under reflux for 12 hours and filtered. Solution was stored in cool place and in a few days formation of crystal phase was observed. Single crystals were treated by the X-ray (Table 30). After the moment of crystal' growth ceasing crystal phase was separated and dried in vacuo. Anal. calcd. for $[(\text{C}_6\text{H}_5\text{SiO}_{1.5})_{12}(\text{CuO})_4(\text{NaO}_{0.5})_2(\text{CsO}_{0.5})_2]$ Cu, 11.49; Cs, 12.02; Na, 2.08; Si, 15.23. Found (for vacuum dried sample), %: Cu, 11.40; Cs, 11.96; Na, 0.96; Si, 15.11. Yield 34% (0.30 g).

Synthesis of complex $[\text{Ni}_4(\text{CO}_3)_4(\text{Py})_8\text{Na}] \cdot \text{Cl} \cdot \text{Py} \cdot \text{H}_2\text{O}$ **53**. 3.0 g (12.48 mmol) of $\text{PhSi}(\text{OEt})_3$ and 0.49 g (12.48 mmol) of NaOH were placed in a flask (equipped with condenser and magnetic stirrer) and dissolved in 65 ml EtOH. The resulted mixture was heated at reflux for 2 hours. Afterwards $[\text{Ni}(\text{NH}_3)]\text{Cl}_2$ (1.45 g, 6.24 mmol) was added at once, and the suspension was heated at reflux for 12 hours (till total dissolution of hexaamminenickel(II) chloride), brought to room temperature and filtered from the insoluble precipitate of NaCl. To the yellow-colored filtrate, 4',4''-(1,4-Phenylene)bis(2,2':6',2''-terpyridine) (0.84 g, 1.56 mmol) was added at the mixture was left stirring overnight. Then, to the reaction, pyridine (40 ml) was added and the solution was filtered. Complex **53** was isolated as yellow crystals after approximately 15 days of slow evaporation of solvents. Several crystals were used for single crystal X-ray diffraction study (Table 30). Elemental analysis calcd. for $[\text{Ni}_4(\text{CO}_3)_4(\text{pyridine})_8\text{Na}]\text{Cl}$, %: Ni, 15.84; Na, 1.55; N, 11.34; Cl, 2.39. Found (for vacuum dried sample), %: Ni, 15.77; Na, 1.49; N, 11.26; Cl, 2.32. Yield 0.6 g (26%).

Synthesis of complex $[(\text{PhGeO}_{1.5})_{10}(\text{NiO})_4(\text{NaO}_{0.5})_2] \cdot 9\text{EtOH} \cdot 4\text{H}_2\text{O}$ **54**. $\text{PhGe}(\text{OMe})_3$ (2.00 g, 8.2 mmol) was dissolved in 45 mL of ethanol. Then 0.33 g (8.2 mmol) of NaOH was added, and the resulting mixture was heated to reflux for 2.5 h. Afterward 0.76 g (3.30 mmol) of $\text{Ni}(\text{NH}_3)_6\text{Cl}_2$ was added at once. The resulted mixture was heated to reflux for 12 h. Filtration of the mixture from insoluble part gave yellow-colored solution. Slow evaporation of solvents (ethanol/methanol) gave in 10 days crystalline material. Several crystals were used for the single crystal X-ray diffraction analysis (Table 31). Anal. calcd for $\text{C}_{60}\text{H}_{50}\text{Ge}_{10}\text{Na}_2\text{Ni}_4\text{O}_{20}$, %: Ge, 34.62; Ni, 11.19; Na, 2.19. Found (for vacuum dried sample), %: Ge, 34.50; Ni, 11.06; Na, 2.12. Yield 0.64 g (30%).

Synthesis of compounds **55** – **58** has been performed in a similar way. The mixture of $\text{PhSi}(\text{OMe})_3$ (8.0 mmol) and NaOH (8.0 mmol) were dissolved in 30 mL of ethanol. The resulting solution was heated to reflux for 1.0 h. Afterwards, (4.0 mmol) of $\text{Ln}(\text{NO}_3)_3 \cdot 6\text{H}_2\text{O}$ (Ln = Eu, Tb) (4.0 mmol) of Et_4NCl (for **55** and **57**) or Ph_4PCl (for **56** and **58**) dissolved in 30 mL of CH_3CN , were added at once. The resulted mixture was heated to reflux for 3 h. Filtration of the mixture from the insoluble part gave a non-colored solution. Slow evaporation of solvents (ethanol/ CH_3CN) gave in a period of 5-10 days a bunch of crystalline material. The single crystals suitable for single crystals X-Ray diffraction were collected (Table 31). The crystal products were dried in vacuum to perform elemental analysis and to calculate the yield.

Compound $(\text{Et}_4\text{N})_2[(\text{PhSiO}_{1.5})_8(\text{EuO}_{1.5})_4(\text{O})(\text{NO}_{2.5})_6(\text{EtOH})_2(\text{MeCN})_2] \cdot (\text{MeCN})_4$ **55**. Reactants loading: $\text{PhSi}(\text{OMe})_3$ (0.489 g, 2.5 mmol), NaOH (0.0988 g, 2.5 mmol), $\text{Eu}(\text{NO}_3)_3 \cdot 6\text{H}_2\text{O}$ (0.550 g, 1.23 mmol), Et_4NCl (0.203 g, 1.23 mmol). Anal. calcd for $\text{C}_{72}\text{H}_{98}\text{Eu}_4\text{N}_{10}\text{O}_{36}\text{Si}_8$: %C 34.42, %H 3.93, %N 5.58; Found (for vacuum dried sample), %: %C 33.83, %H 3.93, %N 5.095. EDX analysis Eu : Si = 1 : 2.03. Yield = 42.21%. (0.253 g).

Compound $(\text{Ph}_4\text{P})_2[(\text{PhSiO}_{1.5})_8(\text{EuO}_{1.5})_4(\text{O})(\text{NO}_{2.5})_6(\text{EtOH})_2(\text{MeCN})_2]$ **56**. Reactants loadings: $\text{PhSi}(\text{OMe})_3$ (0.465 g, 2.34 mmol), NaOH (0.094 g, 2.34 mmol), $\text{Eu}(\text{NO}_3)_3 \cdot 6\text{H}_2\text{O}$ (0.523 g, 1.2 mmol), Ph_4PCl (0.448 g, 1.2 mmol). Anal. calcd for $\text{C}_{104}\text{H}_{98}\text{Eu}_4\text{N}_8\text{O}_{36}\text{P}_2\text{Si}_8$: %C 42.63; %H 3.37; %N 3.82, %. Found (for vacuum dried sample), %: %C 42.14, %H 3.62, %N 3.79. EDX analysis $\text{Eu} : \text{Si} = 1 : 2.05$. Yield = 15.79 % (0.1357 g).

Compound $(\text{Et}_4\text{N})_2[(\text{PhSiO}_{1.5})_8(\text{TbO}_{1.5})_4(\text{O})(\text{NO}_{2.5})_6(\text{EtOH})_2(\text{MeCN})_2] \cdot \text{MeCN}$ **57**. Reactants loadings: $\text{PhSi}(\text{OMe})_3$ (0.484 g, 2.44 mmol), NaOH (0.0977 g, 2.44 mmol), $\text{Tb}(\text{NO}_3)_3 \cdot 6\text{H}_2\text{O}$ (0.553 g, 1.22 mmol), Et_4NCl (0.202 g, 1.22 mmol). Anal. calcd for $\text{C}_{72}\text{H}_{98}\text{Tb}_4\text{N}_{10}\text{O}_{36}\text{Si}_8$: %C 34.05, %H 3.89, %N 5.51. Found (for vacuum dried sample), %: %C 33.72, %H 3.62, %N 5.46. EDX analysis $\text{Tb} : \text{Si} = 1 : 1.97$. Yield = 43.21 % (0.3509 g).

Compound $(\text{Ph}_4\text{P})_4[(\text{PhSiO}_{1.5})_8(\text{TbO}_{1.5})_4(\text{O})_2(\text{NO}_{2.5})_8] \cdot (\text{MeCN})_{10}$ **58**. Reactants loadings: $\text{PhSi}(\text{OMe})_3$ (1.03 g, 5.2 mmol), NaOH (0.207 g, 5.2 mmol), $\text{Tb}(\text{NO}_3)_3 \cdot 6\text{H}_2\text{O}$ (1.172 g, 2.6 mmol), Ph_4PCl (0.975 g, 2.6 mmol). Anal. calcd for $\text{C}_{144}\text{H}_{120}\text{Tb}_4\text{N}_8\text{O}_{40}\text{P}_4\text{Si}_8$: %C 48.22; %H 3.37, %N 3.12, %O 17.84, %P 3.45, %Si 6.26, %Tb 17.72. Found (for vacuum dried sample), %: %C 48.14, %H 3.35, %N 3.19. EDX analysis $\text{Tb} : \text{Si} = 1 : 1.99$. Yield = 20.00 % (0.538 g).

ANNEXES

Annex 1. - The photoluminescence spectra of **55** - **58** at room temperature.

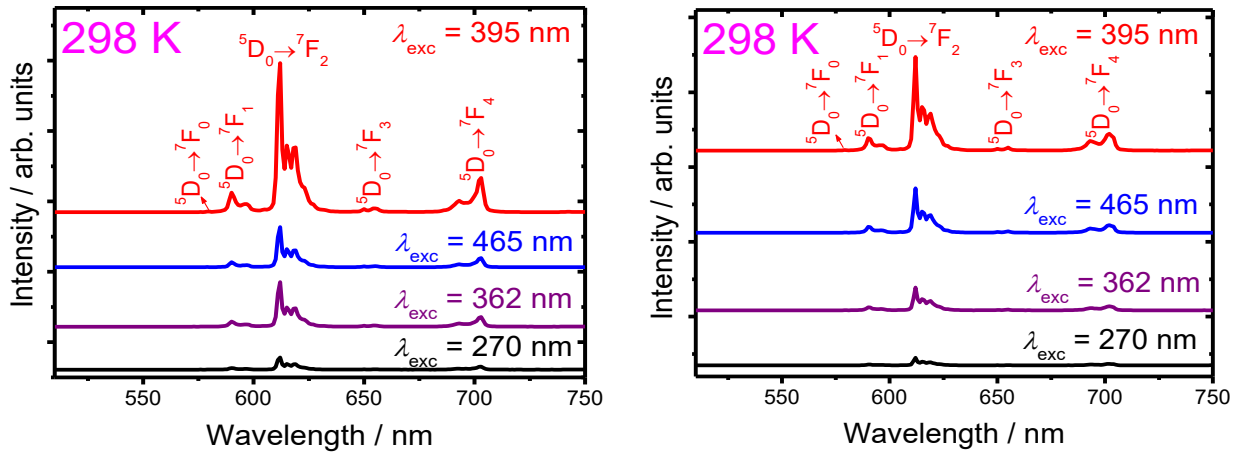


Figure 143. Room temperature emission spectra of **55** (left) and **56** (right) excited at 270, 362, 395, 465 nm.

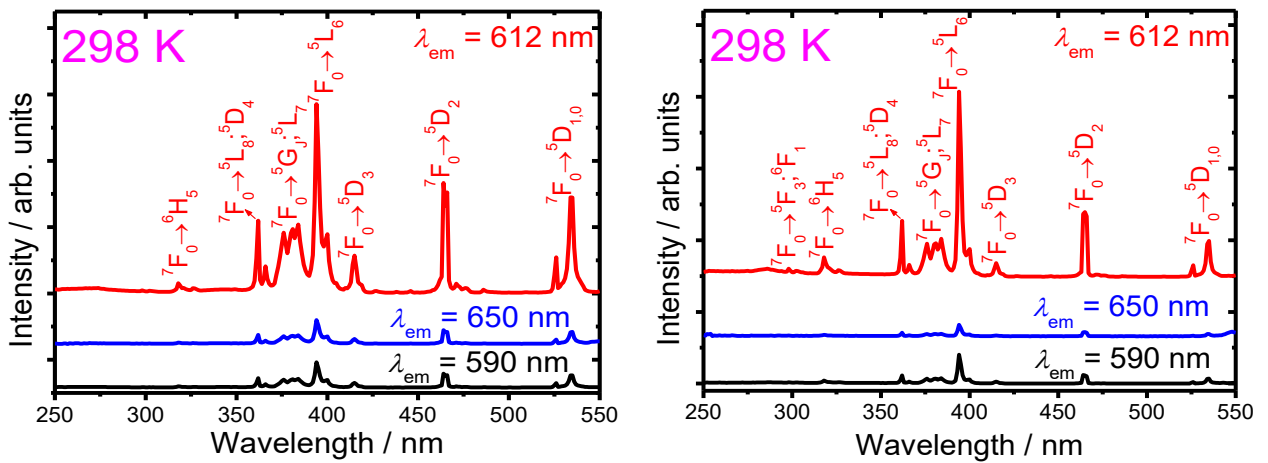


Figure 144. Room temperature excitation spectra of **55** (left) and **56** (right) excited at 612, 650, 690 nm.

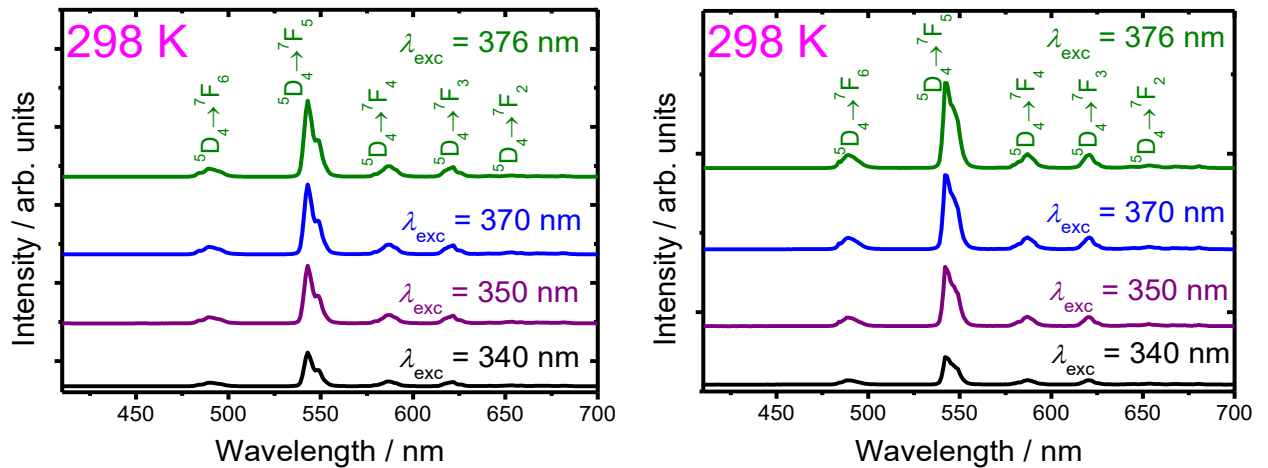


Figure 145. Room temperature emission spectra of **57** (left) and **58** (right) excited at 340, 350, 370, 376 nm.

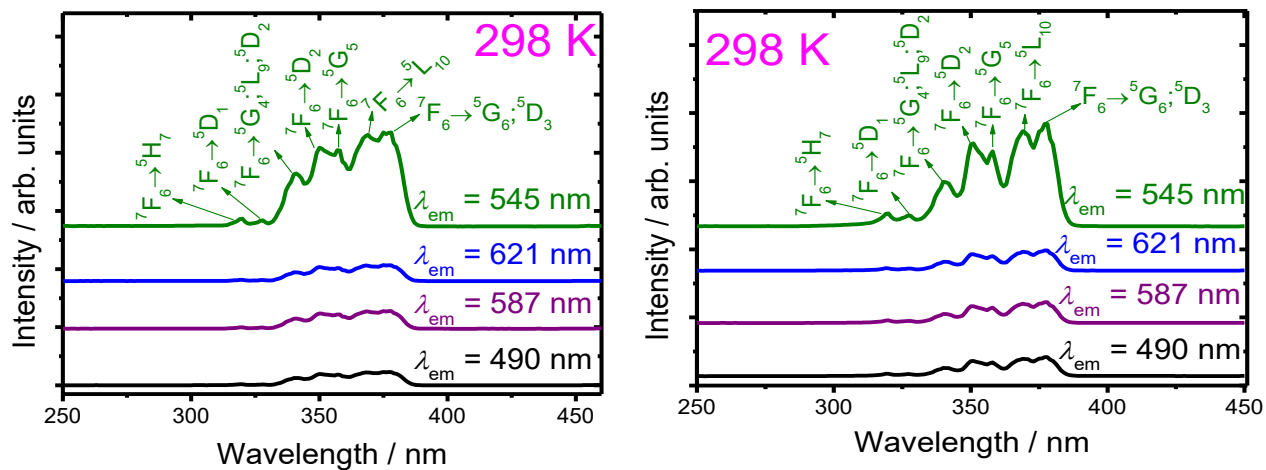


Figure 146. Room temperature excitation spectra of **57** (left) and **58** (right) excited at 490, 547, 587, 621 nm.

Annex 2. - The crystallographic data for structures **1 - 58**.

Table 21. The crystallographic data for structures **1 – 6**.

	1	2	3	4	5	6
CCDC	1509419	1577242	1509421	1525488	1509420	1509422
Empirical formula	C ₃₄ H ₁₀₃ Cu ₉ O ₄₅ S ₈ Si ₁₈	C ₃₀ H ₇₈ Cu ₆ N ₆ O ₃₀ Si ₁₂	C _{77.32} H _{129.32} Cu ₁₂ N ₈ O _{52.66} S ₄ Si ₂₀	C ₄₁ H ₆₆ Cu ₆ N ₄ O _{25.50} Si ₁₀	C ₃₄ H ₆₀ Cu ₆ N ₄ O ₂₄ Si ₁₀	C ₃₆ H ₆₄ Cu ₃ N ₄ O ₁₉ Si ₈
Formula weight	2566.12	1721.36	3466.12	1685.11	1571.00	1272.25
Temperature, K	120	100	120	100	120	100
Color / shape	Blue / prismatic	Blue / prismatic	Green / placoid	Blue / prismatic	Blue / prismatic	Blue / prismatic
Crystal size, mm	0.2 × 0.15 × 0.1	0.30 × 0.25 × 0.20	0.22 × 0.25 × 0.36	0.10 × 0.05 × 0.03	0.21 × 0.17 × 0.1	0.04 × 0.09 × 0.15
λ / Å	0.98700	0.96990	1.54178	0.96990	0.71073	0.96600
Crystal system	Rhombic	Monoclinic	Triclinic	Triclinic	Monoclinic	Monoclinic
Space group	<i>Pnma</i>	<i>P2₁/n</i>	<i>P-1</i>	<i>P-1</i>	<i>P2₁/n</i>	<i>C2/c</i>
<i>a</i> /Å	30.750 (6)	13.394 (3)	14.3152 (4)	14.497 (3)	11.4722 (4)	12.210 (2)
<i>b</i> /Å	20.975 (4)	15.433 (3)	14.7500 (4)	14.823 (3)	19.6547 (6)	17.480 (4)
<i>c</i> /Å	15.835 (3)	17.547 (4)	16.6756 (4)	16.597 (3)	12.9181 (4)	25.210 (5)
α /°	90	90	94.7850 (10)	95.38 (3)	90	90
β /°	90	98.65 (3)	105.7280 (10)	103.83 (3)	94.4790 (10)	98.74 (3)
γ /°	90	90	102.666 (2)	104.40 (3)	90	90
<i>V</i> /Å ³	10213 (28)	3585.9 (14)	3268.25 (15)	3309.5 (14)	2903.91 (16)	5318.1 (19)
<i>Z</i>	4	2	1	2	2	4
<i>d</i> _{calc} , g/cm ³	1.669	1.594	1.761	1.691	1.797	1.531
μ , mm ⁻¹	2.286	4.705	5.182	4.996	2.443	3.303
<i>F</i> (000)	5232	1764	1763	1716	1596	2636
<i>R</i> ₁ / %	13.42	5.20	4.41	8.92	3.11	7.18
w <i>R</i> ₂ / %	37.03	13.50	13.06	24.51	9.20	19.54
Independent reflections	7624 (0.1081)	7174 (0.0882)	12361 (0.0394)	13293 (0.0919)	8675 (0.0450)	5522 (0.1463)
Parameters refined	628	392	808	781	363	325
GOF on <i>F</i> ²	1.03	1.067	1.034	1.022	1.027	1.081

Table 22. The crystallographic data for structures **7** – **11**.

	7	8	9	10	11
CCDC	1566412	1566402	1566413	1566414	1566403
Empirical formula	C ₃₅₈ H ₄₄₀ Cu ₂₄ N ₅ O _{128.50} Si ₄₈	C ₉₄ H ₁₀₆ Cu ₆ N ₂ O ₃₀ Si ₁₂	C _{87.20} H _{107.40} Cu ₆ O _{32.50} S _{7.60} Si ₁₂	C ₈₈ H ₈₄ Cu ₆ N ₈ O ₂₄ Si ₁₂	C ₁₂₂ H ₁₀₆ Cu ₆ N ₆ O ₂₆ Si ₁₂
Formula weight	9742.69	2462.12	2637.58	2355.95	2790.44
Temperature, K	100	120	100	100	100
Color / shape	Colorless / acicular	Blue / prismatic	Colorless / prismatic	Colorless / prismatic	Blue / prismatic
Crystal size, mm	0.23 × 0.30 × 0.33	0.30 × 0.26 × 0.42	0.26 × 0.24 × 0.24	0.16 × 0.19 × 0.29	0.21 × 0.27 × 0.30
$\lambda / \text{Å}$	0.96990	0.71073	0.98700	0.96990	0.71073
Crystal system	Triclinic	Monoclinic	Monoclinic	Monoclinic	Monoclinic
Space group	<i>P</i> -1	<i>P</i> 2 ₁ / <i>c</i>	<i>P</i> 2 ₁ / <i>c</i>	<i>P</i> 2 ₁ / <i>c</i>	<i>P</i> 2 ₁ / <i>c</i>
<i>a</i> /Å	18.521 (4)	21.0550 (9)	23.000 (5)	14.291 (3)	15.0864 (5)
<i>b</i> /Å	24.515 (5)	18.6770 (8)	21.470 (4)	15.785 (3)	19.0777 (7)
<i>c</i> /Å	26.442 (5)	29.7478 (12)	23.190 (5)	22.847 (5)	21.4856 (7)
α /°	101.45 (3)	90	90	90	90
β /°	106.13 (3)	107.161 (1)	90.26 (3)	92.27 (3)	94.079 (1)
γ /°	100.62 (3)	90	90	90	90
<i>V</i> /Å ³	10932 (5)	11177.3 (8)	11451 (4)	5149.8(18)	6168.2(4)
<i>Z</i>	1	4	4	2	2
<i>d</i> _{calc} , g/cm ³	1.480	1.463	1.530	1.519	1.502
μ , mm ⁻¹	3.137	1.323	3.496	3.315	1.207
<i>F</i> (000)	5019	5064	5416	2404	2860
<i>R</i> ₁ / %	8.49	4.59	6.69	5.61	3.52
<i>wR</i> ₂ / %	20.77	11.53	16.82	15.22	8.24
Independent reflections	29358 (0.0849)	21394 (0.0459)	13990 (0.0669)	7090 (0.0561)	30923 (0.0352)
Parameters refined	2333	1294	1222	627	1511
GOF on <i>F</i> ²	1.035	1.023	1.005	1.013	1.043

Table 23. The crystallographic data for structures **12** – **16**.

	12	13	14	15	16
CCDC	1566404	1566405	1566406	1566415	1566416
Empirical formula	C ₁₀₈ H ₁₃₀ Cu ₆ O ₃₃ Si ₁₂	C ₁₀₀ H ₉₀ Cu ₅ N ₈ O ₂₀ Si ₁₀	C ₇₈ H ₉₄ Cu ₅ N ₆ O ₂₇ Si ₁₀	C ₉₃ H ₁₀₉ Cu ₆ N ₇ O ₃₁ Si ₁₂	C ₂₅₅ H ₂₂₅ Co ₁₀ Cu ₅ N ₁₅ O ₆₂ Si ₃₀
Formula weight	2674.43	2322.39	2146.19	2539.26	6241.27
Temperature, K	120	120	120	100	100
Color / shape	Green / prismatic	Blue / prismatic	Blue / prismatic	Blue / prismatic	Colorless / prismatic
Crystal size, mm	0.19 × 0.20 × 0.31	0.33 × 0.22 × 0.24	0.20 × 0.26 × 0.33	0.20 × 0.24 × 0.28	0.16 × 0.30 × 0.56
$\lambda / \text{Å}$	0.71073	0.71073	0.71073	0.96990	0.96990
Crystal system	Triclinic	Monoclinic	Monoclinic	Monoclinic	Monoclinic
Space group	<i>P</i> -1	<i>C</i> 2	<i>P</i> 2 ₁ / <i>n</i>	<i>P</i> 2 ₁ / <i>n</i>	<i>P</i> <i>c</i>
<i>a</i> /Å	15.813 (6)	23.596 (3)	16.6330 (17)	16.140 (3)	14.404 (3)
<i>b</i> /Å	16.784 (6)	15.934 (2)	21.510 (3)	24.390 (5)	25.369 (5)
<i>c</i> /Å	25.746 (9)	17.047 (2)	26.998 (3)	27.800 (6)	46.860 (9)
$\alpha / ^\circ$	83.207 (6)	90	90	90	90
$\beta / ^\circ$	78.264 (6)	127.986 (2)	104.324 (2)	92.20 (3)	91.03 (3)
$\gamma / ^\circ$	72.224 (6)	90	90	90	90
<i>V</i> /Å ³	6360 (4)	5051.4 (11)	9358.9 (19)	10936 (4)	17121(6)
<i>Z</i>	2	2	4	4	2
<i>d</i> _{calc} , g/cm ³	1.397	1.527	1.523	1.542	1.211
μ , mm ⁻¹	1.170	1.228	1.323	3.144	2.190
<i>F</i> (000)	2768	2382	4420	5224	6382
<i>R</i> ₁ / %	9.18	3.57	3.50	9.20	11.65
<i>wR</i> ₂ / %	26.05	7.67	9.18	28.83	23.64
Independent reflections	12636 (0.0918)	12998 (0.0357)	15001 (0.0350)	7782 (0.0920)	22797 (0.1165)
Parameters refined	1428	648	1166	1357	1726
GOF on <i>F</i> ²	0.918	0.976	1.034	0.948	1.081

Table 24. The crystallographic data for structures **17** – **21**.

	17	18	19	20	21
CCDC	1565113	1565028	1565029	1565114	1565030
Empirical formula	C ₈₅ H ₈₃ Cu ₆ N ₄ O _{24.5} S _{2.5} Si ₁₀	C ₈₈ H ₈₄ Cu ₆ N ₈ O ₂₄ Si ₁₀	C ₈₈ H ₈₀ Cu ₆ N ₈ O ₂₂ Si ₁₀	C _{104.5} H ₈₆ Cu ₆ N _{7.5} O _{22.25} Si ₁₀	C ₁₀₁ H ₈₃ Cu ₆ N ₇ O ₂₂ Si ₁₀
Formula weight	2294.84	2299.77	2263.74	2464.94	2408.88
Temperature, K	100	120	120	100	120
Color / shape	Colorless / prismatic	Blue / prismatic	Blue / prismatic	Colorless / prismatic	Blue / prismatic
Crystal size, mm	0.10 × 0.12 × 0.12	0.21 × 0.29 × 0.38	0.15 × 0.25 × 0.80	0.05 × 0.10 × 0.12	0.21 × 0.24 × 0.24
$\lambda / \text{Å}$	0.96990	1.54178	1.54178	0.96990	0.71073
Crystal system	Monoclinic	Monoclinic	Monoclinic	Monoclinic	Monoclinic
Space group	<i>P</i> 2 ₁ / <i>n</i>	<i>P</i> 2 ₁ / <i>n</i>	<i>P</i> 2 ₁ / <i>n</i>	<i>P</i> -1	<i>P</i> 2 ₁ / <i>n</i>
<i>a</i> /Å	13.770 (3)	13.5219 (2)	13.7298 (2)	16.300 (3)	14.2574 (8)
<i>b</i> /Å	15.960 (3)	16.0385 (2)	15.8642 (2)	18.975 (4)	28.1840 (15)
<i>c</i> /Å	23.260 (5)	22.0466 (3)	23.2285 (3)	21.831 (4)	26.3345 (14)
$\alpha / ^\circ$	90	90	90	80.50 (3)	90
$\beta / ^\circ$	105.26 (3)	98.283 (1)	105.3692 (5)	74.91 (3)	103.726 (1)
$\gamma / ^\circ$	90	90	90	68.85 (3)	90
<i>V</i> /Å ³	4931.6 (19)	4731.39 (11)	4878.52 (11)	6061 (3)	10279.8 (10)
<i>Z</i>	2	2	2	2	4
<i>d</i> _{calc} , g/cm ³	1.545	1.614	1.541	1.351	1.556
μ , mm ⁻¹	3.523	3.346	3.220	2.774	1.410
<i>F</i> (000)	2342	2348	2304	2515	4904
<i>R</i> ₁ / %	10.26	2.79	3.80	10.69	5.79
<i>wR</i> ₂ / %	28.17	7.95	10.14	24.48	13.40
Independent reflections	8836 (0.0919)	8360 (0.0219)	9522 (0.0326)	25171 (0.0822)	24520 (0.1374)
Parameters refined	477	619	541	905	1317
GOF on <i>F</i> ²	1.030	1.052	1.019	1.024	1.009

Table 25. The crystallographic data for structures **23** – **27**.

	22	23	24	25	26
CCDC	1565115	1565116	1565117	1565118	1565031
Empirical formula	C ₈₆ H ₈₀ Cu ₆ N ₄ O _{23.5} Si ₁₀	C ₉₀ H ₇₈ Cu ₆ N ₆ O ₂₃ Si ₁₀	C ₈₂ H ₇₂ Cu ₆ N ₄ O ₂₂ Si ₁₀	C ₈₈ H ₇₈ Cu ₆ N ₆ O ₂₄ Si ₁₀	C ₈₈ H ₈₀ Cu ₆ N ₄ O ₂₄ S ₂ Si ₁₀
Formula weight	2207.68	2273.72	2127.57	2265.77	2303.82
Temperature, K	100	100	100	100	120
Color / shape	Colorless / prismatic	Colorless / prismatic	Colorless / prismatic	Blue / needle	Blue / placoid
Crystal size, mm	0.13 × 0.15 × 0.21	0.15 × 0.18 × 0.24	0.10 × 0.12 × 0.15	0.05 × 0.05 × 0.12	0.13 × 0.24 × 0.36
λ / Å	0.96990	0.96990	0.98700	0.96990	1.54178
Crystal system	Monoclinic	Trigonal	Monoclinic	Monoclinic	Monoclinic
Space group	<i>P</i> 2 ₁ / <i>n</i>	<i>R</i> -3	<i>P</i> 2 ₁ / <i>n</i>	<i>P</i> 2 ₁ / <i>c</i>	<i>P</i> 2 ₁ / <i>n</i>
<i>a</i> /Å	13.770 (3)	32.200(5)	13.770(3)	13.459(3)	14.9355(4)
<i>b</i> /Å	16.405 (3)	32.200(5)	16.010(3)	15.908(3)	22.9024(6)
<i>c</i> /Å	22.785 (5)	29.840(6)	23.200(5)	23.614(5)	16.0023(4)
α /°	90	90	90	90	90
β /°	105.02 (3)	90	106.19(3)	105.84(3)	103.692(1)
γ /°	90	120	90	90	90
<i>V</i> /Å ³	4971.1 (19)	26794(11)	4911.8(18)	4863.9(19)	5318.2(2)
<i>Z</i>	2	9	2	2	2
<i>d</i> _{calc} , g/cm ³	1.475	1.268	1.439	1.547	1.439
μ , mm ⁻¹	3.334	2.812	3.557	3.444	3.325
<i>F</i> (000)	2252	10422	2164	2308	2344
<i>R</i> ₁ / %	9.71	9.45	7.51	9.50	5.02
<i>wR</i> ₂ / %	23.18	23.73	17.54	23.21	14.11
Independent reflections	9790 (0.0842)	12656 (0.0772)	5579 (0.0568)	10283 (0.0840)	9391 (0.0593)
Parameters refined	389	407	417	491	564
GOF on <i>F</i> ²	1.034	1.045	1.034	1.015	1.057

Table 26. The crystallographic data for structures **27** – **31**.

	27	28	29	30	31
CCDC	1565119	1565120	1565032	1565122	1565123
Empirical formula	C ₈₄ H ₆₈ Cu ₆ N ₄ O ₂₂ Si ₁₀	C ₉₆ H ₉₆ Cu ₆ N ₈ O ₂₆ Si ₁₀	C ₁₀₄ H ₈₈ Cu ₆ N ₈ O ₂₂ Si ₁₀	C _{116.5} H ₉₇ Cu ₆ N ₈ O ₂₂ Si ₁₀	C ₁₀₈ H ₈₄ Cu ₆ N ₄ O ₂₂ Si ₁₀
Formula weight	2147.56	2439.94	2463.96	2623.16	2451.93
Temperature, K	100	100	120	120	100
Color / shape	Colorless / prismatic	Blue / prismatic	Blue / prismatic	Blue / prismatic	Colorless / prismatic
Crystal size, mm	0.10 × 0.15 × 0.20	0.06 × 0.10 × 0.12	0.09 × 0.14 × 0.19	0.24 × 0.27 × 0.29	0.10 × 0.15 × 0.15
$\lambda / \text{\AA}$	0.98700	0.96990	0.71073	0.71073	0.96990
Crystal system	Monoclinic	Monoclinic	Monoclinic	Monoclinic	Monoclinic
Space group	<i>P</i> 2 ₁ / <i>n</i>	<i>P</i> 2 ₁ / <i>n</i>	<i>C</i> 2/ <i>c</i>	<i>P</i> 2 ₁ / <i>n</i>	<i>P</i> 2 ₁ / <i>n</i>
<i>a</i> / \AA	15.650(3)	13.890 (3)	31.315 (5)	18.6215 (11)	19.236 (4)
<i>b</i> / \AA	21.820(4)	21.385 (4)	19.829 (3)	15.6270 (9)	16.036 (3)
<i>c</i> / \AA	17.160(3)	17.430 (4)	22.034 (4)	21.4674 (12)	21.496 (4)
$\alpha / ^\circ$	90	90	90	90	90
$\beta / ^\circ$	97.78(3)	92.54 (3)	102.216 (3)	99.919 (1)	99.95 (3)
$\gamma / ^\circ$	90	90	90	90	90
<i>V</i> / \AA^3	5805.9(19)	5172.3 (18)	13371 (4)	6153.6 (6)	6531 (2)
<i>Z</i>	2	2	4	2	2
<i>d</i> _{calc} , g/cm ³	1.228	1.567	1.224	1.416	1.247
μ , mm ⁻¹	3.011	3.255	1.086	1.185	2.572
<i>F</i> (000)	2180	2500	5032	2677	2500
<i>R</i> ₁ / %	6.66	6.82	10.26	5.15	7.82
w <i>R</i> ₂ / %	17.57	19.86	27.71	16.02	17.72
Independent reflections	8338 (0.0564)	10482 (0.0824)	13172 (0.1271)	17999 (0.0580)	13922 (0.0850)
Parameters refined	419	663	615	725	485
GOF on <i>F</i> ²	1.062	1.042	1.039	1.048	1.040

Table 27. The crystallographic data for structures **32** – **36**.

	32	33	34	35	36
CCDC	1565124	1852742	1549070	1549108	1883934
Empirical formula	C ₁₀₈ H ₈₄ Cu ₆ Na ₄ O ₂₂ Si ₁₀	C ₁₂₄ H _{131.67} Cu ₅ N ₆ NaO _{30.83} Si ₁₂	C ₁₈₄ H ₁₈₀ Cu ₆ Na ₂ O ₂₈ P ₈ Si ₁₂	C ₂₅₀ H ₂₄₈ Cu ₁₁ Na ₄ O ₅₀ P ₈ Si ₂₀	C ₁₅₈ H ₁₆₀ Cu ₄ Na ₄ O ₃₂ P ₄ Si ₁₂
Formula weight	2452.00	2696.17	3851.33	5652.93	3377.99
Temperature, K	100	120	100	100	100
Color / shape	Colorless / prismatic	Blue / prismatic	Blue / prismatic	Blue / prismatic	Blue / prismatic
Crystal size, mm	0.05 × 0.08 × 0.10	0.15 × 0.25 × 0.5	0.23×0.21×0.11	0.90×0.25×0.18	0.20 ×0.12 ×0.10
λ / Å	0.96990	1.54178	1.54178	0.71073	0.96990
Crystal system	Triclinic	Monoclinic	Monoclinic	Triclinic	Monoclinic
Space group	<i>P</i> -1	<i>P</i> 2 ₁ / <i>c</i>	<i>P</i> 2 ₁ / <i>c</i>	<i>P</i> -1	<i>P</i> 2 ₁ / <i>n</i>
<i>a</i> /Å	16.698 (3)	28.8235 (9)	26.0271 (10)	18.7211 (12)	16.458 (3)
<i>b</i> /Å	26.676 (5)	24.5281 (8)	24.5742 (10)	19.4236 (13)	24.128 (5)
<i>c</i> /Å	28.385 (6)	20.8021 (7)	28.5606 (10)	20.9937 (14)	21.698 (4)
α /°	101.00 (3)	90	90	101.2440 (14)	90
β /°	103.28 (3)	105.820 (2)	98.459 (2)	100.7125 (14)	99.55 (3)
γ /°	100.35 (3)	90	90	116.0771 (13)	90
<i>V</i> /Å ³	11744 (5)	14149.7 (8)	18068.5 (12)	6397.7 (7)	8497 (3)
<i>Z</i>	3	4	8	1	2
<i>d</i> _{calc} , g/cm ³	1.040	1.266	1.416	1.467	1.320
μ , mm ⁻¹	2.145	2.377	2.810	1.119	1.610
<i>F</i> (000)	3750	5551	7968	2911	3504
<i>R</i> ₁ / %	9.36	9.10	6.96	4.78	8.44
<i>wR</i> ₂ / %	21.84	23.95	17.89	13.84	18.75
Independent reflections	19229 (0.0754)	27370 (0.2395)	25652 (0.0696)	27916 (0.0478)	17712 (0.0865)
Parameters refined	1397	1315	1981	1616	944
GOF on <i>F</i> ²	1.056	1.012	0.179	1.07	1.054

Table 28. The crystallographic data for structures **38** – **42**.

	38	39	40	41	42
CCDC	1572284	1857969	1888654	1888655	1902480
Empirical formula	C ₁₀₄ H ₈₇ N ₄ O ₃₁ Cu ₂ Fe ₅ Ge ₁₄	C ₁₆₃ H ₂₀₇ N ₆ O ₁₀₈ Na ₄ Cl ₃ Cu ₄₂ Ge ₂₄	C ₈₄ H ₇₂ Cu ₆ Ge ₁₀ N ₄ O ₂₄	C ₉₀ H ₉₈ Cu ₆ Ge ₁₀ N ₄ O ₂₇	C ₉₀ H ₈₀ N ₈ O ₂₀ Ge ₁₀ Cu ₆
Formula weight	3311.66	8587.48	2628.59	2775.13	2897.01
Temperature, K	100	100	120	100	100
Color / shape	Colorless / needle	Blue / prismatic	Blue / prismatic	Blue / prismatic	Blue / prismatic
Crystal size, mm	0.05×0.10×0.15	0.06 × 0.09 × 0.12	0.21 × 0.19 × 0.22	0.17 × 0.17 × 0.20	0.20 × 0.20 × 0.26
$\lambda / \text{Å}$	0.96990	0.96990	1.54178	0.98700	0.96990
Crystal system	Tetragonal	Monoclinic	Monoclinic	Monoclinic	Triclinic
Space group	<i>P4/ncc</i>	<i>C2/m</i>	<i>P2₁/n</i>	<i>P2₁/n</i>	<i>P-1</i>
<i>a</i> /Å	41.7968 (7)	40.682 (8)	17.1895 (6)	16.500 (3)	15.963(3)
<i>b</i> /Å	41.7968(7)	26.453 (5)	17.3844 (6)	16.530 (3)	15.973(3)
<i>c</i> /Å	33.2895 (10)	18.950 (4)	18.3975 (6)	19.310 (4)	22.743(5)
$\alpha / ^\circ$	90	90	90	90	82.06(3)
$\beta / ^\circ$	90	116.35 (3)	111.705 (2)	97.56 (3)	74.46 (3)
$\gamma / ^\circ$	90	90	90°	90°	75.86(3)
<i>V</i> /Å ³	58156 (3)	18274 (8)	5107.92	5220.93	5401(2)
<i>Z</i>	16	2	2	2	2
<i>d</i> _{calc} , g/cm ³	1.513	1.561	1.70877	1.76483	1.781
μ , mm ⁻¹	8.218	10.013	5.102	9.629	9.639
<i>F</i> (000)	25968	8344	2580	2752	2872
<i>R</i> ₁ / %	12.75	10.35	8.13	7.46	8.54
<i>wR</i> ₂ / %	22.30	24.03	24.90	17.71	21.78
Independent reflections	14359 (0.1364)	19585 (0.097)	6522 (0.0813)	4134 (0.0746)	22099 (0.091)
Parameters refined	986	693	461	383	1110
GOF on <i>F</i> ²	0.973	1.034	1.035	1.070	1.073

Table 29. The crystallographic data for structures **44** – **48**.

	44	45	46	47	48
CCDC	1517969	1517970	1517974	1517975	1517976
Empirical formula	C ₈₈ H ₁₀₈ Cu ₄ Na ₄ O ₃₂ S ₈ Si ₁₂	C ₈₈ H ₈₈ Cu ₄ N ₈ Na ₄ O ₂₆ Si ₁₂	C ₈₅ H ₉₅ Cu ₄ Na ₄ O _{30.5} Si ₁₂	C ₁₁₄ H ₁₃₃ Cu ₄ N ₂ Na ₄ O ₄₂ Si ₁₂	C ₉₀ H ₁₀₂ Cu ₄ K ₂ N ₆ Na ₂ O ₃₀ Si ₁₂
Formula weight	2704.65	2356.86	2287.80	2886.42	2463.19
Temperature, K	120	120	120	100	120
Color / shape	Blue / prismatic	Green / prismatic	Blue / prismatic	Blue / prismatic	Blue / prismatic
Crystal size, mm	0.26 × 0.22 × 0.17	0.31 × 0.27 × 0.21	0.34 × 0.21 × 0.15	0.38 × 0.31 × 0.21	0.36 × 0.28 × 0.15
$\lambda / \text{\AA}$	0.71073	1.54178	1.54178	0.71073	1.54178
Crystal system	Orthorhombic	Triclinic	Monoclinic	Monoclinic	Monoclinic
Space group	<i>Fdd2</i>	<i>P</i> -1	<i>Cc</i>	<i>P2</i> ₁ / <i>n</i>	<i>C2</i> / <i>c</i>
<i>a</i> /\AA	39.603 (3)	12.4652 (3)	39.0472 (11)	19.936 (4)	15.3886 (3)
<i>b</i> /\AA	44.958 (3)	14.2001 (4)	12.7721 (3)	24.531 (5)	27.7686 (5)
<i>c</i> /\AA	12.7721 (9)	15.2042 (4)	28.8454 (14)	26.959 (6)	26.0338 (5)
$\alpha / ^\circ$	90	97.541 (2)	90	90	90
$\beta / ^\circ$	90	94.028 (1)	131.761 (1)	104.474 (4)	101.962 (1)
$\gamma / ^\circ$	90	101.067 (1)	90	90	90
<i>V</i> /\AA ³	22740 (3)	2605.73 (12)	10730.7 (7)	12766 (5)	10883.2 (4)
<i>Z</i>	8	1	4	4	4
<i>d</i> _{calc} , g/cm ³	1.580	1.502	1.416	1.502	1.500
μ , mm ⁻¹	1.414	3.045	2.947	0.868	3.562
<i>F</i> (000)	11306	1208	4708	5980	5072
<i>R</i> ₁ / %	4.53	2.75	8.09	9.79	6.71
w <i>R</i> ₂ / %	11.31	7.31	20.20	26.18	20.50
Independent reflections	17419 (0.068)	12735 (0.024)	13525 (0.032)	24993 (0.025)	9401 (0.035)
Parameters refined	676	1290	953	1528	679
GOF on <i>F</i> ²	1.06	1.05	1.09	1.04	1.041

Таблица 30. Кристаллографические данные для структур 49 – 53.

	49	50	51	52	53
CCDC	1517973	1517978	1517971	1517968	1980662
Empirical formula	C _{90.5} H _{106.5} CS ₃ Cu ₄ N _{5.5} NaO _{31.5} SSi ₁₂	C ₈₄ H ₈₈ CsCu ₄ N ₄ Na ₃ O ₂₈ Si ₁₂	C ₆₀ H ₆₂ Cu ₂ Na ₂ O ₂₄ Si ₁₀	C ₉₀ H ₁₀₃ Cs ₂ Cu ₄ N ₆ Na ₂ O _{30.5} Si ₁₂	C ₆₉ H ₆₇ ClN ₁₃ NaNi ₄ O ₁₃
Formula weight	2820.33	2394.70	1621.05	2659.82	1579.63
Temperature, K	120	100	100	120	120
Color / shape	Blue / prismatic	Blue / prismatic	Blue / prismatic	Blue / prismatic	Green / prismatic
Crystal size, mm	0.35 × 0.26 × 0.18	0.15 × 0.10 × 0.10	0.12 × 0.10 × 0.08	0.30 × 0.20 × 0.13	0.23 × 0.27 × 0.38
$\lambda / \text{Å}$	1.54178	0.96990	0.96690	1.54178	0.71073
Crystal system	Triclinic	Monoclinic	Monoclinic	Triclinic	Monoclinic
Space group	<i>P</i> -1	<i>C</i> 2/ <i>c</i>	<i>C</i> 2/ <i>c</i>	<i>P</i> -1	<i>P</i> <i>c</i>
<i>a</i> /Å	14.0768 (3)	15.330 (3)	25.420 (5)	13.5529 (4)	12.1370 (6)
<i>b</i> /Å	15.1880 (3)	27.390 (6)	16.080 (3)	15.0155 (5)	13.0455 (7)
<i>c</i> /Å	28.3921 (6)	26.060 (5)	20.020 (4)	15.3739 (5)	25.0175 (13)
$\alpha / ^\circ$	78.743 (1)	90	90	86.574 (1)	90
$\beta / ^\circ$	82.067 (1)	101.36 (3)	116.21(3)	68.255 (1)	101.3760 (10)
$\gamma / ^\circ$	87.767 (1)	90	90	70.240 (1)	90
<i>V</i> /Å ³	5896.0 (2)	10728 (4)	7342(3)	2727.22 (15)	3883.3 (3)
<i>Z</i>	1	4	4	1	2
<i>d</i> _{calc} , g/cm ³	1.589	1.483	1.467	1.620	1.351
μ , mm ⁻¹	9.917	3.084	1.911	8.003	1.060
<i>F</i> (000)	2832	4864	3336	1345	1632
<i>R</i> ₁ / %	6.77	12.83	12.21	2.62	4.05
<i>wR</i> ₂ / %	15.40	34.54	28.57	7.26	9.25
Independent reflections	19955 (0.026)	8621 (0.096)	4187 (0.092)	9000 (0.035)	23581 (0.0575)
Parameters refined	1243	362	460	673	914
GOF on <i>F</i> ²	1.06	0.969	0.94	1.07	0.974

Table 31. Crystal data and structure refinement for **54** – **58**.

	54	55	56	57	58
CCDC	1827287	2002347	2002348	2002352	2002353
Empirical formula	C ₄₂ H ₆₅ Ge ₅ NaNi ₂ O ₁₈	C ₈₀ H ₁₁₀ Eu ₄ N ₁₄ O ₃₆ Si ₈	C ₁₀₄ H ₉₈ Eu ₄ N ₈ O ₃₆ P ₂ Si ₈	C ₇₈ H ₁₀₇ N ₁₃ O ₃₆ Si ₈ Tb ₄	C ₁₆₄ H ₁₅₀ N ₁₈ O ₄₀ P ₄ Si ₈ Tb ₄
Formula weight	1361.30	2676.42	2930.45	2663.21	3997.34
Temperature, K	120	173	173	173	173
Color / shape	Green / prismatic	Colorless / prismatic	Colorless / prismatic	Colorless / prismatic	Colorless / prismatic
Crystal size, mm	0.21 × 0.31 × 0.23	0.08 × 0.10 × 0.12	0.10 × 0.15 × 0.20	0.10 × 0.10 × 0.15	0.12 × 0.15 × 0.15
$\lambda / \text{Å}$	0.71073	0.71073	0.71073	0.71073	0.71073
Crystal system	Monoclinic	Triclinic	Triclinic	Triclinic	Monoclinic
Space group	<i>P</i> 2 ₁ / <i>n</i>	<i>P</i> -1	<i>P</i> -1	<i>P</i> -1	<i>P</i> 2 ₁ / <i>c</i>
<i>a</i> /Å	15.328 (3)	13.3158 (6)	13.2998 (13)	13.3011 (5)	18.3256 (9)
<i>b</i> /Å	22.205 (4)	13.4343 (6)	14.2851 (16)	13.4050 (5)	22.4383 (11)
<i>c</i> /Å	16.163 (3)	16.2324 (7)	16.6759 (17)	16.1776 (6)	21.7242 (10)
$\alpha / ^\circ$	90	67.939 (1)	100.915 (5)	68.019 (1)	90
$\beta / ^\circ$	102.383 (3)	85.264 (1)	108.822 (3)	85.420 (1)	110.481 (2)
$\gamma / ^\circ$	90	80.075 (1)	102.564 (5)	80.116 (1)	90
<i>V</i> /Å ³	5373.0 (15)	2650.4 (2)	2809.1 (5)	2634.72 (17)	8368.2 (7)
<i>Z</i>	4	1	1	1	2
<i>d</i> _{calc} , g/cm ³	1.683	1.677	1.732	1.679	1.586
μ , mm ⁻¹	3.519	2.510	2.402	2.826	1.849
<i>F</i> (000)	2752.0	1340	1460	1326	4024
<i>R</i> ₁ / %	7.94	2.08	2.35	1.99	3.86
w <i>R</i> ₂ / %	20.12	5.26	5.52	5.13	10.07
Independent reflections	10589 (0.0794)	20197 (0.0280)	24688 (0.0382)	20170 (0.0308)	34808 (0.0541)
Parameters refined	639	655	736	667	983
GOF on <i>F</i> ²	1.068	1.043	1.049	1.048	1.036

REFERENCE

1. A.N. Bilyachenko, M.M. Levitsky, V.N. Khrustalev, Metal oxide clusters in organoelement matrices, Peoples' Friendship University of Russia (RUDN University), **2019**, pp. 176; ISBN 9785209099055.
2. M.M. Levitsky, A.N. Bilyachenko, E.S. Shubina, J. Long, Y. Guari, J. Larionova, Magnetic cage-like metallasilsesquioxanes, *Coordination Chemistry Reviews*, **2019**, 398, 213015 – 213062.
3. a) M.M. Levitsky, A.I. Yalymov, A.N. Kulakova, A.A. Petrov, A.N. Bilyachenko, Cage-like metallasilsesquioxanes in catalysis: A review, *Journal of Molecular Catalysis A: Chemistry*, **2017**, 426, 297 – 304; b) M.M. Levitskii, V. Smirnov, B. Zavin, A.N. Bilyachenko, A.Y. Rabkina, Metalasiloxanes: New structure formation methods and catalytic properties, *Kinetics and Catalysis*, **2009**, 50, 490 – 507; c) M.M. Levitsky, A.N. Bilyachenko, G.B. Shul'pin, Oxidation of C–H compounds with peroxides catalyzed by polynuclear transition metal complexes in Si- or Ge-sesquioxane frameworks, *Journal Organometallic Chemistry*, **2017**, 849, 201 – 218.
4. Organic Chemistry IUPAC Nomenclature. Rules C-821. Amides.
5. J.H. Fletcher, O.C. Dermer, R.B. Fox, Nomenclature of Organic Compounds. Advances in Chemistry, Chapter 21: Amides and Imides, American Chemical Society Committee on Nomenclature, **1974**, 126, 166 – 173; ISBN 9780841201910.
6. a) J.M. Humphrey, A.R. Chamberlin, Chemical Synthesis of Natural Product Peptides: Coupling Methods for the Incorporation of Noncoded Amino Acids into Peptides, *Chemistry Review*, **1997**, 97, 2243 – 2266; b) J.S. Carey, D. Laffan, C. Thomson, M.T. Williams, Analysis of the reactions used for the preparation of drug candidate molecules, *Organic & Biomolecular Chemistry*, **2006**, 4, 2337 – 2347.
7. a) M.G. Peter, G. Snatzke, F. Snatzke, K.N. Nagarajan, H. Schmid, Über die absolute Konfiguration der Cantharsäure und des Palasonins, *Helvetica Chimica Acta*, **1974**, 57, 32 – 64; b) R.J. Bochis, M.H. Fisher, The structure of palasonin, *Tetrahedron Letters*, **1968**, 9, 1971 – 1974.
8. K. Matsumoto, K. Nagashima, T. Kamigauchi, Y. Kawamura, Y. Yasuda, K. Ishii, N. Uotani, T. Sato, H. Nakai, Y. Terui, J. Kikuchi, Y. Ikenisi, T. Yoshida, T. Kato, H. Itazaki, Salfredins, New Aldose Reductase Inhibitors Produced by *Crucibulum* sp. RF-3817, *The Journal of Antibiotics*, **1995**, 48, 439 – 446.
9. a) A. Shoji, M. Kuwahara, H. Ozaki, H. Sawai, Modified DNA Aptamer That Binds the (R)-Isomer of a Thalidomide Derivative with High Enantioselectivity, *Journal of the American Chemical Society*, **2007**, 129, 1456 – 1464; b) F.A. Luzzio, D.Y. Dubeau, E.R. Lepper, W.D. Figg, Synthesis of Racemic *cis*-5-Hydroxy-3-phthalimidoglutaramide. A Metabolite of Thalidomide Isolated from Human Plasma, *Journal of Organic Chemistry*, **2005**, 70, 10117 – 10120; c) M.E. Franks, G.R. Macpherson, W.D. Figg, Thalidomide, *Lancet*, **2004**, 363, 1802 – 1813.
10. T. Nakano, C. Djerassi, R.A. Corral, O. O. Orazi, Structure of Julocrotine, *Journal of Organic Chemistry*, **1961**, 26, 1184 – 1191.
11. N.K. Hart, S.R. Johns, J.A. Lambertson, Alkaloids of *Lamprolobium fruticosum* Benth, *Journal of Chemistry Society Chemistry Communication*, **1968**, 6, 302.
12. C. Gaul, J.T. Njardarson, D. Shan, D.C. Dorn, K.D. Wu, W.P. Tong, X.Y. Huang, M.A.S. Moore, S.J. Danishefsky, The Migrastatin Family: Discovery of Potent Cell Migration Inhibitors by Chemical Synthesis, *Journal of the American Chemical Society*, **2004**, 126, 11326 – 11337.
13. a) M.K. Hargreaves, J.G. Pritchard, H.R. Dave, Cyclic carboxylic monoimides, *Chemistry Review*, **1970**, 70, 439 – 469; b) Y. Kamitori, M. Hojo, R. Masuda, T. Kimura, T. Yoshida, Selective protection of carbonyl compounds. Silica gel treated with thionyl chloride as an effective catalyst for thioacetalization, *Journal of Organic Chemistry*, **1986**, 51, 1427 – 1431.
14. M.I. Kohan, *Nylon Plastics Handbook*, Hanser Pub Inc, **1995**, pp. 45; ISBN 1569901899.
15. N.S. Zefirov, I.L. Knunyants, N.N. Kulov, *Chemical Encyclopedia, Soviet Encyclopedia*, **1988**, pp. 127; ISBN 5852700355.
16. O. A. Reutov, A. L. Kurtz, K. P. Butin, *Organic chemistry in 4 volumes, BINOM. Laboratoriya Snaniy*, **2004**, 3, 237 – 239; ISBN 9785996313358.

-
17. N.S. Zefirov, I.L. Knunyants, N.N. Kulov, *Chemical Encyclopedia, Soviet Encyclopedia*, **1995**, 4, 451 – 452; ISBN 5852700924.
 18. O.A. Reutov, A.L. Kurtz, K.P. Butin, *Organic chemistry in 4 volumes, BINOM. Laboratorya Snaniy*, **2004**, 3, 240 – 252; ISBN 9785996313358.
 19. C. Schotten, Ueber die Oxydation des Piperidins, *Berichte der deutschen chemischen Gesellschaft*, **1884**, 17, 2544 – 2547.
 - 20 R.F. Schmidt, Über den Imin-Rest, *Berichte der deutschen chemischen Gesellschaft*, **1924**, 57, 704 – 706.
 21. A. Haller, E. Bauer, Sur les produits de la réaction de l'amidure de sodium sur les cétones, *Comptes Rendus Chimie*, **1908**, 147, 824 – 826.
 22. J. Zabitsky, *The Chemistry of Amides*, Interscience Publishers, **1970**, pp. 119; ISBN 0471980498.
 23. J. Zabitsky, *The Chemistry of Amides*, Interscience Publishers, **1970**, pp. 122; ISBN 0471980498.
 24. J.J. Ritter, P.P. Minieri, A New Reaction of Nitriles. I. Amides from Alkenes and Mononitriles, *Journal of American Chemistry*, **1948**, 70, 4045 – 4048.
 25. E. Beckmann, Zur Kenntniss der Isonitrosoverbindungen, *Berichte der deutschen chemischen Gesellschaft*, **1886**, 19, 988 – 993.
 26. V.I. Ovchinnikova, V.R. Ruchinsky, Caprolactam production, "Chemistry", **1977**, pp. 264.
 27. A.W. Chapman, CCLXIX.-Imino-aryl ethers. Part III. The molecular rearrangement of N-phenylbenziminophenyl ether, *Journal of Chemistry Society*, **1925**, 127, 1992 – 1998.
 28. M. Polonovski, *Bulletin de la Société Chimique de France*, **1927**, 41, 1190.
 29. a) C.L. Allen, J.M. Williams, Metal-catalysed approaches to amide bond formation, *Journal of Chemistry Society Review*, **2011**, 40, 3405 – 3415; b) G.E. Dobereiner, R.H. Crabtree, Dehydrogenation as a Substrate-Activating Strategy in Homogeneous Transition-Metal Catalysis, *Chemistry Review*, **2010**, 110, 681 – 703; c) D. Milstein, Discovery of Environmentally Benign Catalytic Reactions of Alcohols Catalyzed by Pyridine-Based Pincer Ru Complexes, Based on Metal–Ligand Cooperation, *Topic in Catalysis*, **2010**, 53, 915 – 923; d) C. Chen, S.H. Hong, *Organic & Biomolecular Chemistry*, **2011**, 9, 20 – 26.
 30. T.N. Reddy, A. Beatriz, V.J. Rao, D.P. de Lima, Carbonyl Compounds' Journey to Amide Bond Formation, *Chemistry an Asian Journal*, **2019**, 14, 344 – 347.
 31. a) C. Gunanathan, Y. Ben-David, D. Milstein, Direct synthesis of amides from alcohols and amines with liberation of H₂, *Science*, **2007**, 317, 790 – 792; b) L.U. Nordstrøm, H. Vogt, R. Madsen, Amide Synthesis from Alcohols and Amines by the Extrusion of Dihydrogen, *Journal American Chemistry Society*, **2008**, 130, 17672 – 17673; c) T. Naota, S.-I. Murahashi, Ruthenium-Catalyzed Transformations of Amino Alcohols to Lactams, *Synlett*, **1991**, 693 – 694; d) S.C. Ghosh, S. Muthaiah, Y. Zhang, X. Xu, S.H. Hong, Direct Amide Synthesis from Alcohols and Amines by Phosphine-Free Ruthenium Catalyst Systems, *Advanced Synthesis & Catalysis*, **2009**, 351, 2643 – 2649; e) H. Zeng, Z. Guan, Direct Synthesis of Polyamides via Catalytic Dehydrogenation of Diols and Diamines, *Journal American Chemistry Society*, **2011**, 133, 1159 – 1161; f) C. Chen, Y. Miao, K. de Winter, H.-J. Wang, P. Demeyere, Y. Yuan, F. Verpoort, Ruthenium-Based Catalytic Systems Incorporating a Labile Cyclooctadiene Ligand with N-Heterocyclic Carbene Precursors for the Atom-Economic Alcohol Amidation Using Amines, *Molecules*, **2018**, 23, 2413 – 2423; g) B.M. Trost, N. Maulide, R.C. Livingston, A Ruthenium-Catalyzed, Atom-Economical Synthesis of Nitrogen Heterocycles, *Journal American Chemistry Society*, **2008**, 130, 16502 – 16503.
 32. a) K.-I. Fujita, Y. Takahashi, M. Owaki, K. Yamamoto, R. Yamaguchi, Synthesis of Five-, Six-, and Seven-Membered Ring Lactams by Cp*Rh Complex-Catalyzed Oxidative N-Heterocyclization of Amino Alcohols, *Organic Letters*, **2004**, 6, 2785 – 2788; b) T. Zweifel, J.V. Naubron, H. Grutzmacher, Catalyzed Dehydrogenative Coupling of Primary Alcohols with Water, Methanol, or Amines, *Angewandte Chemie International Edition*, **2009**, 48, 559 – 563.

33. K. Fujita, K. Yamamoto, R. Yamaguchi, Oxidative Cyclization of Amino Alcohols Catalyzed by a Cp*Ir Complex. Synthesis of Indoles, 1,2,3,4-Tetrahydroquinolines, and 2,3,4,5-Tetrahydro-1-benzazepine, *Organic Letters*, **2002**, 4, 2691 – 2694.
34. J. Zhang, M. Senthilkumar, S.C. Ghosh, S.H. Hong, Synthesis of Cyclic Imides from Simple Diols, *Angewandte Chemie International Edition*, **2010**, 49, 6391 – 6395.
35. a) R.M. de Figueiredo, J.-S. Suppo, J.-M. Campagne, Nonclassical Routes for Amide Bond Formation, *Chemical Reviews*, **2016**, 116, 12029 – 12122; b) J.-F. Soulé, H. Miyamura, S. Kobayashi, Powerful Amide Synthesis from Alcohols and Amines under Aerobic Conditions Catalyzed by Gold or Gold/Iron, -Nickel or -Cobalt Nanoparticles, *Journal American Chemistry Society*, **2011**, 133, 18550 – 18553; c) A. Ojeda-Porras, D. Gamba-Sanchez, Recent Developments in Amide Synthesis Using Nonactivated Starting Materials, *The Journal of Organic Chemistry*, **2016**, 81, 11548 – 11555.
36. S.K. Klitgaard, K. Egeblad, U.V. Mentzel, A.G. Popov, T. Jensen, E. Taarning, I.S. Nielsen, C.H. Christensen, Oxidations of amines with molecular oxygen using bifunctional gold–titania catalysts, *Green Chemistry*, **2008**, 10, 419 – 423.
37. Y. Wang, D. Zhu, L. Tang, S. Wang, Z. Wang, Highly efficient amide synthesis from alcohols and amines by virtue of a water-soluble gold/DNA catalyst, *Angewandte Chemie International Edition*, **2011**, 50, 8917 – 8921.
38. K.-I. Shimizu, K. Ohshima, A. Satsuma, Direct Dehydrogenative Amide Synthesis from Alcohols and Amines Catalyzed by γ -Alumina Supported Silver Cluster, *Chemistry - A European Journal*, **2009**, 15, 9977 – 9980.
39. X. Bantreil, C Fleith, J. Martinez, F. Lamaty, Copper-Catalyzed Direct Synthesis of Benzamides from Alcohols and Amines, *ChemCatChem*, **2012**, 4, 1922 – 1925.
40. X. Bantreil, N. Kanfara, N. Gehina, E. Golliarda, P. Ohlmann, J. Martineza, F. Lamatya, Iron-catalyzed benzamide formation. Application to the synthesis of moclobemide, *Tetrahedron*, **2014**, 70, 5093 – 5099.
41. a) X.-F. Wu, M. Sharif, A. Pews-Davtyan, P. Langer, K. Ayub, M. Beller, The First ZnII-Catalyzed Oxidative Amidation of Benzyl Alcohols with Amines under Solvent-Free Conditions, *European Journal Organic Chemistry*, **2013**, 2783 – 2787; b) X.-F. Wu, Non-Redox-Metal-Catalyzed Redox Reactions: Zinc Catalysts. *Chemistry - An Asian Journal*, **2012**, 7, 2502 – 2509; c) S. Enthaler, Rise of the Zinc Age in Homogeneous Catalysis?, *ACS Catalysis*, **2013**, 3, 150 – 158.
42. a) S. Gaspa, A. Porcheddu, L. De Luca, Iron-catalyzed oxidative amidation of alcohols with amines, *Organic and Biomolecular Chemistry*, **2013**, 11, 3803 - 3807, b) S.C. Ghosh, J.S.Y. Ngiam, A. M. Seayad, D. T. Tuan, C. W. Johannes, A. Chen, Tandem oxidative amidation of benzyl alcohols with amine hydrochloride salts catalyzed by iron nitrate, *Tetrahedron Letters*, **2013**, 54, 4922 – 4925.
43. a) A. Kumar, N.A. Espinosa-Jalapa, G. Leitus, Y. Diskin-Posner, L. Avram, D. Milstein, Direct Synthesis of Amides by Dehydrogenative Coupling of Amines with either Alcohols or Esters: Manganese Pincer Complex as Catalyst, *Angewandte Chemie International Edition*, **2017**, 56, 14992; b) R. Vanjari, T. Guntreddi, K. N. Singh, MnO₂ Promoted Sequential C-O and C-N Bond Formation via C-H Activation of Methylarenes: A New Approach to Amides, *Organic Letters*, **2013**, 15, 4908 – 4911.
44. A.N. Bilyachenko, M.S. Dronova, A.I. Yalymov, F. Lamaty, X. Bantreil, J. Martinez, C. Bizet, L.S. Shul'pina, A.A. Korlyukov, D.E. Arkhipov, M.M. Levitsky, E.S. Shubina, A.M. Kirillov, G.B. Shul'pin, Cage-like Copper(II) Silsesquioxanes: Transmetalation Reactions and Structural, Quantum Chemical, and Catalytic Studies, *Chemistry European Journal*, **2015**, 21, 1 – 14.
45. a) A.N. Bilyachenko, M.S. Dronova, A.I. Yalymov, A.A. Korlyukov, L.S. Shul'pina, D.E. Arkhipov, E.S. Shubina, M.M. Levitsky, A.D. Kirilin, G.B. Shul'pin, New Binuclear Cage-like Copper(II) Silsesquioxane (“Cooling Tower”); Its High Catalytic Activity in Oxidation of Benzene and Alcohols, *European Journal Inorganic Chemistry*, **2013**, 30, 5240 – 5246; b) M.S. Dronova, A.N. Bilyachenko, A.I. Yalymov, Y.N. Kozlov, L.S. Shul'pina, A.A. Korlyukov, D.E. Arkhipov, M.M.

- Levitsky, E.S. Shubina, G.B. Shul'pin, Solvent-controlled synthesis of tetranuclear cage-like copper(II) silsesquioxanes. Remarkable features of the cage structures and their high catalytic activity in oxidation of benzene and alcohols with peroxides, *Dalton Transaction*, **2014**, 43, 872 – 882.
46. X. Bantreil, P. Navals, J. Martinez, F. Lamaty, *European Journal Organic Chemistry*, **2015**, 2, 417 – 422.
47. A.N. Bilyachenko, M.M. Levitsky, A.I. Yalymov, A.A. Korlyukov, V.N. Khrustalev, A.V. Vologzhanina, L.S. Shul'pina, N.S. Ikonnikov, A.E. Trigub, P.V. Dorovatovskii, X. Bantreil, F. Lamaty, J. Long, J. Larionova, I.E. Golub, E.S. Shubina, G.B. Shul'pin, Cage-like Fe,Na-Germesquioxanes: Structure, Magnetism, and Catalytic Activity, *Angewandte Chemie International Edition*, **2016**, 55, 15360 – 15363.
48. X. Bantreil, P. Navals, J. Martinez, F. Lamaty, Iron/Caffeine as a Catalytic System for Microwave-Promoted Benzamide Formation, *European Journal Organic Chemistry*, **2015**, 417 – 422.
49. R. M. de Figueiredo, J.-S. Suppo, J.-M. Campagne, Nonclassical Routes for Amide Bond Formation, *Chemistry Review*, **2016**, 116, 12029 – 12122.
50. a) G. Dyker, *Handbook of C–H Transformations: Applications in Organic Synthesis*, Wiley-VCH, 2005, pp. 688, ISBN 9783527619450; b) Yu J.-Q., Shi Z. C–H Activation, Springer-Verlag, Berlin, 2010, pp. 380, ISBN 9783642123566; c) U. Neuenschwander, N. Turrà, C. Aellig, P. Mania, I. Hermans, Understanding Selective Oxidations, *CHIMIA International Journal for Chemistry*, **2010**, 64, 225 – 230.
51. a) G.A. Olah, A. Molnar, G.K.S. Prakash, *Hydrocarbon Chemistry*, John Wiley & Sons, Hoboken, New Jersey, **2017**, pp. 1216, SBN 9781119390510; b) P. J. Pérez, Ed., *Alkane C-H Activation by Single-Site Metal Catalysis*, Springer, **2012**, pp. 270, ISBN 9789048136988.
52. T.B. Gunnoe, Metal-mediated Carbon–Hydrogen Bond Activation, in: A. Bakac (Ed.), *Physical Organic Chemistry: Reactions, Processes, Applications*, John Wiley & Sons, Hoboken, New Jersey, **2010**, pp. 403, ISBN 9783527697649.
53. R.W. Murray, H. Gu, Linear Free Energy Relationship Studies of the Dimethyldioxirane C–H Bond Insertion Reaction, *Journal of Organic Chemistry*, **1995**, 60, 5673 – 5677.
54. A.A. Fokin, B.A. Tkachenko, O.I. Korshunov, P.A. Gunchenko, P.R. Schreiner, Molecule-Induced Alkane Homolysis with Dioxiranes, *Journal of the American Chemical Society*, **2001**, 123, 11248 – 11252.
55. a) M.E. González-Núñez, J. Royo, R. Mello, M. Báguena, J. Martínez Ferrer, C.R. de Arellano, G. Asensio, G.K.S. Prakash, Oxygenation of Alkane C–H Bonds with Methyl(trifluoromethyl)-dioxirane: Effect of the Substituents and the Solvent on the Reaction Rate, *The Journal of Organic Chemistry*, **2005**, 70, 7919 – 7924; b) R. Mello, M. Fiorentino, C. Fusco, R. Curci, Oxidations by Methyl(trifluoromethyl)dioxirane. Oxyfunctionalization of Saturated Hydrocarbons, *Journal of the American Chemical Society*, **1989**, 111, 6749 – 6757.
56. a) B.H. Brodsky, J. Du Bois, Oxaziridine-Mediated Catalytic Hydroxylation of Unactivated 3° C–H Bonds Using Hydrogen Peroxide, *Journal of the American Chemical Society*, **2005**, 127, 15391 – 15393; b) D.D. des Marceau, A. Donadelli, V. Montanari, V.A. Petrov, G. Resnati, Mild and selective oxyfunctionalization of hydrocarbons by perfluorodialkyloxaziridines, *Journal of the American Chemical Society*, **1993**, 115, 4897 – 4898.
57. H.-J. Schneider, W. Muller, Mechanistic and Preparative Studies on the Regio- and Stereoselective Paraffin Hydroxylation with Peracids, *The Journal of Organic Chemistry*, **1985**, 50, 4609 – 4615.
58. Y. Ogawa, S. Iwasaki, S. Okuda, Photochemical aromatic hydroxylation by aromatic amine remarkable solvent effect on NIH-Shift, *Tetrahedron Letters*, **1981**, 22, 3637 – 3640.
59. L.-Q. Cui, K. Liu, C. Zhang, Effective oxidation of benzylic and alkane C–H bonds catalyzed by sodium o-iodobenzenesulfonate with Oxone as a terminal oxidant under phase-transfer conditions, *Organic Biomolecule Chemistry*, **2011**, 9, 2258 – 2265.

-
60. H. Mimoun, L. Saussine, E. Daire, M. Postel, J. Fischer, R. Weiss, Vanadium(V) Peroxo Complexes. New Versatile Biomimetic Reagents for Epoxidation of Olefins and Hydroxylation of Alkanes and Aromatic Hydrocarbons, *Journal of American Chemistry Society*, **1983**, 105, 3101 – 3110.
61. L.P. Ermolenko, C. Giannotti, Aerobic photocatalysed oxidation of alkanes in the presence of decatungstates: products and effects of solvent and counter-ion of the catalyst, *Journal of Chemistry Society*, **1996**, 1205 – 1210.
62. a) S. Lee, P.L. Fuchs, Chemospecific Chromium[VI] Catalyzed Oxidation of C–H Bonds at –40 °C. *Journal of the American Chemical Society*, **2002**, 124, 13978 – 13979; b) S. Lee, P.L. Fuchs, An Efficient C–H Oxidation Protocol for α -Hydroxylation of Cyclic Steroidal Ethers, *Organic Letters*, **2004**, 6, 1437 – 1440.
63. a) W. Adam, J. Lin, C. R. Saha-Moller, W.A. Herrmann, R.W. Fischer, J.D.G. Correia, Homogeneous Catalytic Oxidation of Arenes and a New Synthesis of Vitamin K₃, *Angewandte Chemie International Edition*, **1995**, 33, 2475 – 2477; b) M.L. Kuznetsov, A.J.L. Pombeiro, Radical Formation in the [MeReO₃]-Catalyzed Aqueous Peroxidative Oxidation of Alkanes: A Theoretical Mechanistic Study, *Inorganic Chemistry*, **2009**, 48, 307 – 318.
64. E. McNeill, J.D. Bois, Ruthenium-Catalyzed Hydroxylation of Unactivated Tertiary C–H Bonds, *Journal of the American Chemical Society*, **2010**, 132, 10202 – 10204.
65. S. Hikichi, H. Komatsuzaki, M. Akita, Y. Moro-oka, Aliphatic C-H Bond Oxygenation by the Co^{II}OOX Species with the Hindered Hydrotris(pyrazolyl)borate Ligand (X) Co(II), Alkyl, H), *Journal of American Chemistry Society*, **1998**, 120, 4699 – 4710.
66. a) R. Curci, S. Giannattasio, O. Sciacovelli, L. Troisi, Mechanisms of peroxidic oxygen transfer to organic substrates: Oxidation of organic sulphides by chromium(vi)oxide diperoxide, *Tetrahedron*, **1984**, 40, 2763 – 2771; b) G. W.J. Fleet, W. Little, Oxidation of alcohols by heterocyclic complexes of oxodiperoxychromium(VI), CrO₅, *Tetrahedron Letters*, **1977**, 18, 3749 – 3750.
67. H. Mimoun, Oxygen Transfer from Inorganic and Organic Peroxides to Organic Substrates: A Common Mechanism, *Angewandte Chemie International Edition*, **1982**, 21, 734 – 750.
68. H. Mimoun, Metal-Oxo and Metal-Peroxo Species in Catalytic Oxidations, Springer, **2000**, pp. 334, ISBN 978-3540669432.
69. J.H.B. Chenier, S.B. Tong, J.A. Howard, Absolute rate constants for hydrocarbon autoxidation. 25. Rate constants for hydrogen atom abstraction from alkanes by the *tert*-butylperoxy radical, *Canadian Journal of Chemistry*, **1978**, 56, 3047 – 3053.
70. N.D. Litvinas, B.H. Brodsky, J. DuBois, C–H Hydroxylation Using a Heterocyclic Catalyst and Aqueous H₂O₂, *Angewandte Chemie International Edition*, **2009**, 48, 4513 – 4516.
71. D. Mansuy, J.-F. Bartoll, M. Momenteau, Alkane hydroxylation catalyzed by metalloporphyrins: evidence for different active oxygen species with alkylhydroperoxides and iodosobenzene as oxidants, *Tetrahedron Letters*, **1982**, 23, 2781 – 2784.
72. a) H.M. Goff, M.A. Phillippi, Imidazole Complexes of Low-Spin Iron(III) Porphyrin α -Cation Radical Species. Models for the Compound I Cation Radical State of Peroxidases, *Journal of American Chemical Society*, **1983**, 105, 7567 – 7571; b) M. Kainosho, Hydroxylation and Epoxidation Catalyzed by Iron-Porphine Complexes. Oxygen Transfer from Iodosylbenzene, *Journal of American Chemical Society*, **1979**, 1032 – 1033.
73. a) J.A. Smegal, B.C. Schardt, C.L. Hill, Isolation, Purification, and Characterization of Intermediate (iodosylbenzene)metalloporphyrin Complexes from the (Tetraphenylporphinato) manganese(II)-Iodosylbenzene, *Journal of American Chemical Society*, **1983**, 105, 3510 – 3515.
74. P. Zachař, G. Petkova, D. Sýkora, V. Král, Selective oxygenation of α -olefins by means of metalloporphyrin catalysts mimicking cytochrome P-450, *Collection of Czechoslovak Chemical Communications*, **2011**, 76, 10, 1163 – 1175.
75. a) C. Kim, K. Chen, J. Kim, L. Que, Stereospecific Alkane Hydroxylation with H₂O₂ Catalyzed by an Iron(II)-Tris(2-pyridylmethyl)amine Complex, *Journal of American Chemical Society*, **1997**, 119, 1163 – 1165.

119, 5964 – 5965; 6) K. Chen, L. Que, Stereospecific Alkane Hydroxylation by Non-Heme Iron Catalysts: Mechanistic Evidence for an FeVdO Active Species, *Journal of American Chemical Society*, **2001**, 123, 6327 – 6337.

76. a) L. Gomez, I. Garcia-Bosch, A. Company, J. Benet-Buchholz, A. Polo, X. Sala, X. Ribas, M. Costas, Stereospecific C–H Oxidation with H₂O₂ Catalyzed by a Chemically Robust Site-Isolated Iron Catalyst, *Angewandte Chemie International Edition*, **2009**, 48, 5720 – 5723; 6) L. Gomez, M. Canta, D. Font, I. Prat, X. Ribas, M. Costas, Regioselective Oxidation of Nonactivated Alkyl C–H Groups Using Highly Structured Non-Heme Iron Catalysts, *Journal of Organic Chemistry*, **2013**, 78, 1421 – 1433.

77. a) M.S. Chen, M.C. White, A Predictably Selective Aliphatic C–H Oxidation Reaction for Complex Molecule Synthesis, *Science*, **2007**, 318, 783 – 787; b) T. Okuno, S. Ito, S. Ohba, Y. Nishida, [small micro]-Oxo bridged diiron(III) complexes and hydrogen peroxide: oxygenation and catalase-like activities. *Journal of the Chemical Society, Dalton Transactions* **1997**, 19, 3547–3551; c) A. Company, L. Gómez, X. Fontrodona, X. Ribas, M. Costas, A Novel Platform for Modeling Oxidative Catalysis in Non-Heme Iron Oxygenases with Unprecedented Efficiency, *Chemistry – A European Journal*, **2008**, 14, 5727 – 5731.

78. M.V. Kirillova, T.A. Fernandes, V. André, A.M. Kirillov, Mild C–H Functionalization of Alkanes Catalyzed by Bioinspired Copper(II) Cores, *Organic and Biomolecular Chemistry*, **2019**, 17, 7706 – 7714.

79. a) M.M. Levitsky, A.I. Yalymov, A.N. Kulakova, A.A. Petrov, A.N. Bilyachenko, Cage-like metallasilsesquioxanes in catalysis: A review, *Journal of Molecular Catalysis A: Chemical*, **2017**, 426, Part B, 297 – 304; 6) G.B. Shul'pin, Hydrocarbon Oxygenations with Peroxides Catalyzed by Metal Compounds, *Mini-Review Organic Chemistry*, **2009**, 6, 95 – 104.

80. A.N. Bilyachenko, M.S. Dronova, A.I. Yalymov, A.A. Korlyukov, L.S. Shul'pina, D.E. Arkhipov, E.S. Shubina, M.M. Levitsky, A.D. Kirilin, G.B. Shul'pin, Binuclear Cage-Like Copper(II) Silsesquioxane (“Cooling Tower”) – Its High Catalytic Activity in the Oxidation of Benzene and Alcohols, *European Journal Inorganic Chemistry*, **2013**, 5240 – 5246.

81. M.S. Dronova, A.N. Bilyachenko, A.I. Yalymov, Y.N. Kozlov, L.S. Shul'pina, A.A. Korlyukov, D.E. Arkhipov, M.M. Levitsky, E.S. Shubina, G.B. Shul'pin, Solvent-controlled synthesis of tetranuclear cage-like copper(II) silsesquioxanes. Remarkable features of the cage structures and their high catalytic activity in oxidation of benzene and alcohols with peroxides, *Dalton Transactions*, **2014**, 43, 872 – 882.

82. a) G.B. Shul'pin, D. Attanasio, L. Suber, Oxidations by a H₂O₂-VO₃ –pyrazine-2-carboxylic acid reagent. Oxidation of alkanes in CH₃CN to produce alkyl peroxides, *Russian Chemical Bulletin*, **1993**, 42, 55 – 59; b) G.B. Shul'pin, A.N. Druzhinina, G.V. Nizova, Oxidations by a H₂O₂-VO₃ –pyrazine-2-carboxylic acid reagent. 2. Oxidation of alcohols and aromatic hydrocarbons, *Russian Chemical Bulletin*, **1993**, 42, 1326 – 1329; c) G.B. Shul'pin, Y. Ishii, S. Sakaguchi, T. Iwahama, Oxidation with the “O₂ - H₂O₂ - vanadium complex - pyrazine-2-carboxylic acid” reagent *Russian Chemical Bulletin*, **1999**, 48, 887 – 890; d) M.H.C. de la Cruz, Y.N. Kozlov, E.R. Lachter, G.B. Shul'pin, Oxidations by the reagent “O₂-H₂O₂-vanadium derivative-pyrazine-2-carboxylic acid”. Part 13. Kinetics and mechanism of the benzene hydroxylation, *New Journal of Chemistry*, **2003**, 27, 634 – 638.

83 F.J. Feher, Polyhedral oligometallasilsesquioxanes (POMSS) as models for silica-supported transition-metal catalysts. Synthesis and characterization of (C₅Me₅)Zr[(Si₇O₁₂)(c-C₆H₁₁)₇], *Journal of American Chemistry Society*, **1986**, 108, 3850 – 3852.

84 D. Gatteschi, R. Sessoli, J. Villain, *Molecular Nanomagnets*, Oxford University Press on Demand, 2006; R. Sessoli, D. Gatteschi, A. Caneschi, M.A. Novak, *Nature*, 1993, 365, 141 – 143.

85. K.M. Mertes, Y. Suzuki, M.P. Sarachik, Y. Myasoedov, H. Shtrikman, E. Zeldov, E.M. Rumberger, D.N. Hendrickson, G. Christou, Mn₁₂-acetate: a prototypical single molecule magnet, *Solid State Communications*, **2003**, 127, 131 – 139.

86. F.-S. Guo, B. M. Day, Y.-C. Chen, M.-L. Tong, A. Mansikkamäki, R.A. Layfield, Magnetic hysteresis up to 80 kelvin in a dysprosium metallocene single-molecule magnet, *Science*, **2018**, 362, 1400 – 1403.
87. a) J.S. Miller, M. Drillon, *Magnetism: Molecules to Materials IV*, John Wiley & Sons, **2001**, pp. 485, ISBN:9783527304295; b) J.S. Miller, *Magnetically ordered molecule-based materials*, *Chemical Society Reviews*, **2011**, 40, 3266 – 3296.
88. a) A. Müller, J. Döring, A Novel Heterocluster with D₃-Symmetry Containing Twenty-One Core Atoms: [As₆V₁₅O₄₂(H₂O)]⁶⁻, *Angewandte Chemie International Edition*, **1988**, 27, 1721; b) A. Wutkowski, C. Näther, J. van Leusen, P. Kögerler, W. Bensch, Interconnection of [V₁₅As₆O₄₂(H₂O)]⁶⁻ Clusters by Cu²⁺-centered Complexes: Synthesis, Crystal Structure and Selected Properties, *Zeitschrift für Naturforschung*, **2014**, 69, 1306 – 1314.
89. V.H. Tran, B. Swiatek-Tran, Spin-glass behaviour in the coordination polymer [Co(C₃H₃N₂)₂]_n, *Dalton Transactions*, **2008**, 4860 – 4865.
90. X.-Y. Cao, J.W. Hubbard, J. Guerrero-Medina, A.J. Hernández-Maldonado, L. Mathivathanan, C. Rinaldi, Y. Sanakis, R.G. Raptis, Spin-glass behavior of a hierarchically-organized, hybrid microporous material, based on an extended framework of octanuclear iron-oxo units, *Dalton Transactions*, **2015**, 44, 3399 – 3409.
91. E. Rentschler, D. Gatteschi, A. Cornia, A. C. Fabretti, A.-L. Barra, O. I. Shchegolikhina, A.A. Zhdanov, *Molecule-Based Magnets: Ferro- and Antiferromagnetic Interactions in Copper (II)-Polyorganosiloxanolate Clusters*, *Inorganic Chemistry*, **1996**, 35, 4427 – 4431.
92. a) V.A. Igonin; O.I. Shchegolikhina; S.V. Lindeman, M.M. Levitsky, Yu. T. Struchkov, A.A. Zhdanov, Novel class of transition metal coordination compounds with macrocyclic organosiloxanolate ligands; their synthesis and crystal structure, *Journal Organometallic Chemistry*, **1992**, 423, 351 – 360; b) R. Shannon, Revised effective ionic radii and systematic studies of interatomic distances in halides and chalcogenides, *Acta Crystallographica Section A*, **1976**, 32, 75.
93. L.D. Landau, E.M. Lifshits, *Quantum mechanics (nonrelativistic theory) // Course of theoretical physics / ed. D. A. Mirtova. - 6th ed., - M. : FIZMATLIT, 2004, T. III., pp. 800, ISBN 5922105302.*
94. J. Stöhr, H.C. Siegmann, *Magnetism: From Fundamentals to Nanoscale Dynamics. - Springer-Verlag Berlin Heidelberg, 2006, 152, pp. 820, ISBN 9783540302827.*
95. V.A. Igonin, S.V. Lindeman, Yu. T. Struchkov, O.I. Shchegolikhina, A.A. Zhdanov. Yu.A. Molodtsova, I.V. Rasumovskaya, Structures of complexes of copper with macrocyclic organosiloxanolate ligands, *Metalloorganicheskaya Khimiya*, **1991**, 4, 1355 – 1362;
96. W. H. Crawford, H. W. Richardson, J. R. Wasson, D. J. Hodgson, W. E. Hatfield, Relationship between the Singlet-Triplet Splitting and the Cu-O-Cu Bridge Angle in Hydroxo-Bridged Copper Dimers, *Inorganic Chemistry*, **1976**, 15, 2107 - 2110.
97. L. Zherlitsyna, N. Auner, M. Bolte, Y.A. Pozdniakova, O.I. Shchegolikhina, K. Lyssenko, V. Pashchenko, B. Wolf, M. Lang, F. Schütz, M. Kollar, F. Sauli, P. Kopietz, Synthesis, Structure and Magnetic Properties of a Novel Hexanuclear Copper Methylsiloxane Complex, *European Journal Inorganic Chemistry*, **2007**, 4827 – 4838.
98. G.L. Abbati, A. Caneschi, A. Cornia, A.C. Fabretti, Y.A. Pozdniakova, O.I. Shchegolikhina, Towards Stepwise Cluster Assembly: A Decacopper (II) Complex Obtained by Controlled Expansion of a Metallasiloxane Cage, *Angewandte Chemie International Edition*, **2002**, 41, 4517 – 4519.
99. a) D.M. Corsi, N.N. Murthy, V.G. Young, Jr., K.D. Karlin, Synthesis, Structure, and Solution NMR Studies of Cyanide – Copper (II) and Cyanide-Bridged Iron (III) – Copper (II) Complexes, *Inorganic Chemistry*, **1999**, 38, 848 – 858; b) A.W. Addison, T.N. Rao, J. Reedijk, J. van Rijn, G.C. Vershoor, Synthesis, structure, and spectroscopic properties of Copper (II) compounds containing nitrogen – sulphur donor ligands; the crystal and molecular structure of aqua[1,7-bis(N-methylbenzimidazol-2'-yl)-2,6-dithiaheptane]copper(II) perchlorate, *Journal of the Chemical Society, Dalton Transaction*, **1984**, 1349 – 1356.

-
100. G.L. Abbati, A. Cornia, A. Caneschi, A.C. Fabretti, C. Mortalo, Self-Assembly of High-Nuclearity Metal Clusters: Programmed Expansion of a Metallasiloxane Cage to an Octacopper(II) Cluster, *Inorganic Chemistry*, **2004**, 43, 4540 – 4542.
101. V. Pashchenko, B. Brendel, B. Wolf, M. Lang, K. Lyssenko, O.I. Shchegolikhina, Yu.A. Molodtsova, L. Zherlitsyna, N. Auner, F. Schütz, M. Kollar, P. Kopietz, N Harrison, Synthesis, Structure and Magnetic Properties of a Novel Linear CuII-Trimer Complex, *European Journal Inorganic Chemistry*, **2005**, 4617 – 4625.
102. Yu.T. Struchkov, S.V. Lindeman, Structures of polymetallaorganosiloxanates - a novel class of organosilicon metal complexes, *Journal of Organometallic Chemistry*, **1995**, 488, 9 – 14.
103. E.A. Meyer, R.K. Castellano, F. Diederich, Interactions with aromatic rings in chemical and biological recognition, *Angewandte Chemie International Edition*, **2003**, 42, 1210 – 1250.
104. V. Pashchenko, M. Lang, B. Wolf, L. Zherlitsyna, N. Auner, O.I. Shchegolikhina, Y. Pozdniakova, F. Schutz, P. Kopietz, M. Kollar, Structural and magnetic investigations on new molecular quantum rings, *Comptes Rendus Chimie*, **2007**, 10, 89 – 95.
105. V.H. Crawford, H.W. Richardson, J.R. Wasson, D.J. Hodgson, W.E. Hatfield, Relationship between the Singlet-Triplet Splitting and the Cu-O-Cu Bridge Angle in Hydroxo-Bridged Copper Dimers, *Inorganic Chemistry*, **1976**, 15, 2107 – 2110.
106. C. Mortalò, A. Caneschi, A. Cornia, E. Diana, S. Faranda, V. Marvaud, M. Pizzotti, O.I. Shchegolikhina, C. Zucchi, G. Pályi, New Cyclosiloxanolate Cluster Complexes of Transition Metals, *Journal of Cluster Science*, **2007**, 18, 217 – 236.
107. G.L. Abbati, A.L. Barra, A. Caneschi, A. Cornia, A.C. Fabretti, D. Gatteschi, Yu.A. Pozdniakova, O.I. Shchegolikhina, Rational design of large-spin clusters based on the hexacopper(II) siloxanolate core, *Comptes Rendus Chimie*, **2003**, 6, 645 – 656.
108. A.N. Bilyachenko, M.M. Levitsky, V.N. Khrustalev, *Metallorganosiloxanes. Modern concepts and methods*, RUDN University, Moscow, **2018**, p. 265, ISBN 9785209087793.
109. V.H. Crawford, H.W. Richardson, J.R. Wasson, D.J. Hodgson, W.E. Hatfield, Relation between the singlet-triplet splitting and the copper-oxygen-copper bridge angle in hydroxo-bridged copper dimers, *Inorganic Chemistry*, **1976**, 15, 2107 – 2110.
110. U.N. Nehete, H.W. Roesky, H. Zhu, S. Nembenna, H.-G. Schmidt, M. Noltemeyer, D. Bogdanov, K. Samwer, Polyhedral Cobalt(II) and Iron(II) Siloxanes: Synthesis and X-ray Crystal Structure of $[(\text{RSi}(\text{OH})\text{O}_2)\text{Co}(\text{OPMe}_3)]_4$ and $[(\text{RSiO}_3)_2(\text{RSi}(\text{OH})\text{O}_2)_4(\mu^3\text{-OH})_2\text{Fe}_8(\text{THF})_4]$, (R = 2,6-*i*Pr₂C₆H₃)N(SiMe₃)), *Inorganic Chemistry*, **2005**, 44, 7243 – 7248.
111. A.N. Bilyachenko, A.I. Yalymov, A.A. Korlyukov, J. Long, J. Larionova, Y. Guari, Y.V. Zubavichus, A.L. Trigub, E.S. Shubina, I.L. Eremenko, N.N. Efimov, M.M. Levitsky, Heterometallic Na₆Co₃ Phenylsilsesquioxane Exhibiting Slow Dynamic Behavior in its Magnetization, *Chemistry European Journal*, **2015**, 21, 18563 – 18565.
112. J.M. Zadrozny, J. Telser, J.R. Long, Slow magnetic relaxation in the tetrahedral cobalt(II) complexes $[\text{Co}(\text{EPh})_4]^{2-}$ (E = O, S, Se), *Polyhedron*, **2013**, 64, 209 – 217.
113. A.N. Bilyachenko, A.I. Yalymov, M.M. Levitsky, A.A. Korlyukov, M.A. Es'kova, J. Long, J. Larionova, Y. Guari, L. S. Shul'pina, N.S. Ikonnikov, A.L. Trigub, Y.V. Zubavichus, I.E. Golub, E.S. Shubina, G.B. Shul'pin, First Cage-Like Pentanuclear Co(II)-Silsesquioxane, *Dalton Transactions*, **2016**, 45, 13663 – 13666.
114. Y.-N. Liu, H.-F. Su, Y.-W. Li, Q.-Y. Liu, Z. Jaglicic, W.-G. Wang, C.-H. Tung, D. Sun, Space Craft-like Octanuclear Co(II)-Silsesquioxane Nanocages: Synthesis, Structure, Magnetic Properties, Solution Behavior, and Catalytic Activity for Hydroboration of Ketones, *Inorganic Chemistry*, **2019**, 58, 4574 – 4582.
115. Y.-N. Liu, J.-L. Hou, Z. Wang, R. K. Gupta, Z. Jaglicic, M. Jagodic, W.-G. Wang, C.-H. Tung, D. Sun, An Octanuclear Cobalt Cluster Protected by Macrocyclic Ligand: In Situ Ligand-Transformation-Assisted Assembly and Single-Molecule Magnet Behavior, *Inorganic Chemistry*, **2020**, 59, 5683 – 5693.

116. J.M. Frost, K.L.M. Harriman, M. Murugesu, The rise of 3-d single-ion magnets in molecular magnetism: towards materials from molecules? *Chemistry Science*, **2016**, 7, 2470 – 2491.
117. S. Schmitz, J. van Leusen, A. Ellern, P. Kögerler, K.Y. Monakhov, Thioether-terminated nickel (II) coordination clusters with {Ni₆} horseshoe- and {Ni₈} rollercoaster-shaped cores, *Inorganic Chemistry Frontiers*, **2016**, 3, 523 – 531.
118. O.I. Shchegolikhina, A.A. Zhdanov, V.A. Igonin, Yu.E. Ovchinnikov, V.E. Shklover, Yu.T. Struchkov, Synthesis and structure of unusual skeletal cylindrical nickel cyclohexasiloxanates, *Organometallic chemistry in the USSR*, **1991**, 4, 39 – 44.
119. A. Cornia, A.C. Fabretti, D. Gatteschi, G. Palyi, E. Rentschler, O.I. Shchegolikhina, A.A. Zhdanov, Molecule-Based Magnets: Ferro- and Antiferromagnetic Interactions in Nickel(II) Cyclohexasiloxanolate Sandwich Complexes, *Inorganic Chemistry*, **1995**, 34, 5383 – 5387.
120. V.A. Igonin, S.V. Lindeman, K.A. Potekhin, V.E. Shklover, Y.T. Struchkov, O.I. Shchegolikhina, A.A. Zhdanov, I.V. Razumovskaya, The structure of sandwich complexes of Ni with macrocyclic 12-membered cis-hexaphenylcyclohexasiloxanolate ligands, *Organometallic chemistry in the USSR*, **1991**, 790 – 795.
121. J. Ribas, M. Monfort, R. Costa, X. Solans, The first ferromagnetic tetranuclear nickel(II) complex with a μ -azido bridge. Structure and magnetic properties of [Ni₄(μ -N₃)₄(2-oxo-1,3-diaminopropane)₂(2-hydroxo-1,3-diaminopropane)₂](ClO₄)₂, *Inorganic Chemistry*, **1993**, 32, 695 – 699.
122. A. Cornia, A.C. Fabretti, G. Gavioli, C. Zucchi, M. Pizzotti, A. Vizi-Orosz, O.I. Shchegolikhina, Y.A. Pozdnyakova, G. Pályi, Heterobimetallic Cyclosiloxanolate Sandwich Clusters: Na{[η ⁶-(PhSiO₂)₆]₂[Fe(OR)]₂Ni₄(μ ⁶-Cl)} (R = H, Me), *Journal Cluster Science*, **1998**, 9, 295 – 319.
123. G. Gavioli, R. Battistuzzi, P. Santi, C. Zucchi, G. Pályi, R. Ugo, A. Vizi-Orosz, O.I. Shchegolikhina, Y.A. Pozdnyakova, S.V. Lindeman, A.A. Zhdanov, Bimetallic siloxane cluster of higher valent transition metals: Na{[η ⁶-(PhSiO₂)₆]₂Co₂Ni₄(μ -Cl)}, *Journal Organometallic Chemistry*, **1995**, 485, 257 – 266.
124. F.J. Feher, J.F. Walzer, Antiferromagnetic exchange in an isomorphous series of siloxy-bridged early-transition-metal dimers: comparisons of antiferromagnetic exchange interactions in isomorphous d₁-d₁, d₁-d₂, d₂-d₂, and d₂-d₃ exchange-coupled dimers, *Inorganic Chemistry*, **1990**, 29, 1604 – 1611.
125. A.N. Bilyachenko, A.I. Yalymov, A.A. Korlyukov, J. Long, J. Larionova, Y. Guari, A.V. Vologzhanina, M. Eskova, E.S. Shubina, M.M. Levitsky, Unusual penta- and hexanuclear Ni(II)-based silsesquioxane polynuclear complexes, *Dalton Transactions*, **2016**, 45, 7320 – 7327.
126. A.N. Bilyachenko, A.I. Yalymov, M.S. Dronova, A.A. Korlyukov, A.V. Vologzhanina, M.A. Es'kova, J. Long, J. Larionova, Y. Guari, P.V. Dorovatovskii, E.S. Shubina, M.M. Levitsky, Unusual penta- and hexanuclear Ni(II)-based silsesquioxane polynuclear complexes, *Inorganic Chemistry*, **2017**, 56, 12751 – 12763.
127. A.A. Korlyukov, A.V. Vologzhanina, M.I. Buzin, N.V. Sergienko, B.G. Zavin, A.M. Muzafarov, Cu(II)-Silsesquioxanes as Secondary Building Units for Construction of Coordination Polymers: A Case Study of Cesium Containing Compounds, *Crystal Growth & Design*, **2016**, 16, 1968 – 1977.
128. R. Duchateau, Incompletely Condensed Silsesquioxanes: Versatile Tools in Developing Silica-Supported Olefin Polymerization Catalysts, *Chemical Reviews*, **2002**, 102, 3525 – 3542.
129. a) V.A. Igonin, S.V. Lindeman, Yu.T. Struchkov, Yu.A. Molodtsova, Ya.A. Pozdnyakova, O.I. Shchegolikhina, A.A. Zhdanov, Crystal structure of the Nd, Gd, and Dy sandwich complexes involving 8 - membered macrocyclic phenylsiloxanolate ligands, *Russian Chemical Bulletin*, **1993**, 42, 176 – 181; b) C. Zucchi O.I. Shchegolikhina, M. Borsari, A. Cornia, G. Gavioli, A.C. Fabretti, E. Rentschler, D. Gatteschi, R. Ugo, R. Psaro, Yu.A. Pozdnyakova, S.V. Lindeman, A.A. Zhdanov, G. Pfilyi, Cyclooligosiloxanolate cluster complexes of transition metals and lanthanides, *Journal of Molecular Catalysis A: Chemical*, **1996**, 107, 313 – 321.

130. O.I. Shchegolikhina, Yu.A. Pozdnyakova, S.V. Lindeman, A.A. Zhdanov, R. Psaro, R. Ugo, G. Gavioli, R. Battistuzzi, M. Borsari, T. Ruffer, C. Zucchi, G. Pfilyi, Cyclosiloxane sandwich complexes of a lanthanide metal: $\text{Na}_6\{[(\text{C}_6\text{H}_5\text{SiO}_2)_8]_{12}\text{Nd}_4(\mu^4\text{-O})\}$, *Journal of Organometallic Chemistry*, **1996**, 514, 29 – 35.
131. V.A. Igonin, S.V. Lindeman, Yu.T. Struchkov, O.L. Shchegolikhina, Yu.A. Molodtsova, Yu.A. Pozdnyakova, A.A. Zhdanov, Crystal structure of the La^{3+} sandwich complex based on 8-membered macrocyclic siloxanolate ligands, *Russian Chemical Bulletin*, **1993**, 42, 168 – 173.
132. F. Libau, *The Structural Chemistry of Silicates*, Springer-Verlag, Berlin, **1988**, pp. 353, ISBN 9783642500763.
133. V. Lorenz, A. Edelmann, S. Gießmann, C.G. Hrib, S. Blaurock, F.T. Edelmann, Disiloxanediolates and Metallasilsesquioxanes of the Rare Earth Elements, *Zeitschrift Für Anorganische Und Allgemeine Chemie*, **2010**, 636, 2172 – 2191.
134. J.D. Lichtenhan, Polyhedral Oligomeric Silsesquioxanes: Building Blocks for Silsesquioxane-Based Polymers and Hybrid Materials, *Comments on Inorganic Chemistry, A Journal of Critical Discussion of the Current Literature*, **1995**, 17, 115 – 130.
135. F.J. Feher, D.A. Newman, J.F. Walzer, Silsesquioxanes as models for silica surfaces, *Journal of the American Chemical Society*, **1989**, 111, 1741 – 1748.
136. a) M. Motevalli, D. Shah, A.C. Sullivan, Oxovanadium(IV) complexes of mercaptocarboxylic acids, *Dalton Transactions*, **1993**, 1849-1855; b) M.B. Hursthouse, M.A. Hossain, M. Motevalli, M. Sanganee, A.C. Sullivan, Synthesis and structure of the unusual dimeric lithium derivative of the tetraphenyldisiloxanediolate dianion, *Journal Organometallic Chemistry*, **1990**, 381, 293 – 297; c) M. Motevalli, D. Shah, A. C. Sullivan, Polymeric chains from $[(\text{Ph}_2\text{SiOLi} \times \text{THF})_2\text{O}]_2$ and linear dicoordinating nitrogen bases. Crystal X-ray structures of $[(\text{Ph}_2\text{SiOLi})_2\text{O} \times \text{THF}]_2 \times 2\text{DABCO}$, $\text{DABCO} = 1,4\text{-diazabicyclo}[2.2.2]\text{octane}$, and $[(\text{Ph}_2\text{SiOLi})_2\text{O} \times \text{THF}]_2 \times 2\{4,4'\text{-bipyridine}\}$, *Journal Organometallic Chemistry*, **1996**, 513, 239 – 246; d) J.J. Carbo, O. Gonzalez del Moral, A. Martin, M. Mena, J.-M. Poblet, C. Santamaria, Construction of Titanasiloxanes by Incorporation of Silanols to the Metal Oxide Model $[\text{Ti}(\eta^5\text{-C}_5\text{Me}_5)(\mu\text{-O})_3(\mu_3\text{-CR})]$: DFT Elucidation of the Reaction Mechanism, *Chemistry - A European Journal*, **2008**, 14, 7930 – 7938; e) L. Postigo, A. B. Vazquez, J. Sanchez-Nieves, P. Royo, E. Herdtweck, Mono- and Dinuclear Cyclopentadienylsiloxo Titanium Complexes: Synthesis, Reactivity, and Catalytic Polymerization Applications, *Organometallics*, **2008**, 27, 5588 – 5597.
137. a) M.A. Hossain, M.B. Hursthouse, A. Ibrahim, M. Mazid, A.C. Sullivan, Cyclic metallasiloxane compounds of Ti(IV) and Zr(IV). X-Ray crystal structures of a *cis*-bis(pyridine) *bis*(cyclosiloxy)titanate and a pyridinelithiated tris(cyclosiloxy)zirconate, *Dalton Transactions*, **1989**, 2347 – 2352; b) M. Motevalli, D. Shah, S.A.A. Shah, A.C. Sullivan, Synthesis and structural characterisation of the cyclosiloxymagnesium compound $[(\text{py})_2\text{Li}]_2\text{-}\mu\text{-Mg}[(\text{Ph}_2\text{SiO})_2\text{O}][(\text{Ph}_2\text{SiO})_3\text{O}]$ having both six- and eight-membered magnesiasiloxane rings, *Journal of the Chemical Society, Chemical Communications*, **1994**, 2427 – 2428.
138. a) M. Lazell, M. Motevalli, S.A.A. Shah, C.K.S. Simon, A.C. Sullivan, Lithium bridged cyclosiloxy-niobium(V) and -tantalum(V) complexes: thermal decomposition, solid-state and solution structural studies, *Dalton Transactions*, **1997**, 3363 – 3366; b) L. King, M. Motevalli, A.C. Sullivan, High oxidation state chromium, molybdenum and tungsten imido metallasiloxanes, *Dalton Transactions*, **1999**, 3225 – 3228; c) L. King, M. Motevalli, A.C. Sullivan, High oxidation state imido metallasiloxanes: synthesis and structural characterisation of novel bis-imido chromium(VI) and molybdenum(VI) compounds, *Dalton Transactions*, **2000**, 1357 – 1362; d) M. Lazell, M. Motevalli, S.A.A. Shah, C.K.S. Simon, A.C. Sullivan, Formation of ring-expanded products from certain combinations of tetraphenyldisiloxanediolates $[(\text{Ph}_2\text{SiOM}')_2\text{O}](\text{M}' = \text{Li or Na})$ and group 4 metal chlorides MCl_4 , *Dalton Transactions*, **1996**, 1449 – 1454.
139. R.W.J.M. Hanssen, R.A. van Santen, H.C.L. Abbenhuis, The dynamic status quo of polyhedral silsesquioxane coordination chemistry, *European Journal of Inorganic Chemistry*, **2004**, 675 – 683.

140. J. Annand, H.C. Aspinall, Lanthanide silsesquioxanes: monomeric and functionalized Complexes, Dalton Transactions, **2000**, 1867 – 1871.
141. V. Lorenz, S. Gießmann, Y.K. Gun'ko, A.K. Fischer, J.W. Gilje, F.T. Edelmann, Fully Metalated Silsesquioxanes: Building Blocks for the Construction of Catalyst Models, Angewandte Chemie International Edition, **2004**, 43, 4603 – 4606.
142. V. Lorenz, A. Fischer, F.T. Edelmann, Silsesquioxane chemistry. Part 10. Silsesquioxane silanolate complexes of samarium and scandium Journal Organometallic Chemistry, **2002**, 647, 245 – 249.
143. P.L. Arnold, A.J. Blake, S.N. Hall, B.D. Ward, C. A. Wilson, functional model for lanthanide doped silicate materials: synthesis of an apically substituted samarium silsesquioxane complex, Dalton Transactions, **2001**, 488 – 491.
144. A.R. Willauer, A.M. Dabrowska, R. Scopelliti, M. Mazzanti, Structure and small molecule activation reactivity of a metallasilsesquioxane of divalent ytterbium, Chemical Communications, **2020**, 56, 8936 – 8939;
145. V. Lorenz, S. Blaurock, H. Gorls, F.T. Edelmann, The First Niobasilsesquioxanes, Organometallics, **2006**, 25, 5922 – 5926.
146. G. Wu, Y. Chen, D.-J. Xu, J.-C. Liu, W. Sun, Z. Shen, Synthesis and molecular structure of a tetrameric neodymium-silsesquioxane cage complex: $\{[(i-C_4H_9)_7(Si_7O_{12})Nd]_4NaCl\}$, Journal of Organometallic Chemistry, **2009**, 694, 1571 – 1574.
147. V. Lorenz, S. Blaurock, C.G. Hrib, F.T. Edelmann, Coupling of Silsesquioxane Cages in the Coordination Sphere of Erbium, European Journal Inorganic Chemistry, **2010**, 2605 – 2608.
148. S. Marchesi, F. Carniato, E. Boccaleri, Synthesis and characterisation of a novel Europium(III)-containing heptaisobutyl-POSS, New Journal Chemistry, **2014**, 38, 2480 – 2485.
149. B.P. Kumar, A.P. Kumar, P.H. Bindu, A.K. Mukherjee, A.S. Patra, Red Light Emission of POSS Triol Chelated with Europium, Asian Journal of Nanoscience and Materials, **2019**, 2, 244 – 256.
150. B.P. Kumar, B.V.D. Kumar, C.M. Raghavan, S.J. Harshavardhan, S.S. Yi, S. Gandhi, J. Jian, J. Kiwan, D.S. Shin, POSS-based luminescent hybrid material for enhanced photo-emitting properties, Journal of Materials Science, **2013**, 48, 7533 – 7539.
151. a) L. Zherlitsyna, N. Auner, M. Bolte, Bis(μ_6 -cis-2,4,6,8,10,12,14,16-octamethylcyclooctasiloxane-2,4,6,8,10,12,14,16-octolato)octakis[(dimethylformamide)copper(II)] dimethylformamide solvate enclosing a pyrazine molecule. Acta Crystallographica Section C: Crystal Structure, **2006**, 62, 199 – 200; b) V. Pashchenko, M. Lang, B. Wolf, L. Zherlitsyna, N. Auner, O.; Shchegolikhina, Y.; Pozdniakova, F.; Schütz, P.; Kopietz, M. Kollar, Structural and magnetic investigations on new molecular quantum rings, Comptes Rendus Chimie, **2007**, 10, 89 – 95; b) L. Zherlitsyna, N. Auner, M. Bolte, Y. Pozdniakova, O. Shchegolikhina, K. Lyssenko, V. Pashchenko, B. Wolf, M. Lang, F. Schütz, Synthesis, Structure and Magnetic Properties of a Novel Hexanuclear Copper Methylsiloxane Complex, European Journal of Inorganic Chemistry, **2007**, 4827 – 4838.
152. L. Zherlitsyna, N. Auner, M. Bolte, Bis(μ_6 -cis- 2,4,6,8,10,12,14,16-octamethylcyclooctasiloxane-2,4,6,8,10,12,14,16-octolato)octakis[(dimethyl-formamide)copper(II)] dimethylformamide solvate enclosing a pyrazine molecule, Acta Crystallographica Section C: Crystal Structure, **2006**, 62, 199 – 200.
153. a) F. A. Cotton, E. V. Dikarev, M. A. Petrukhina, S.-E. Stiriba, Studies of Dirhodium(II) Tetra(trifluoroacetate). 5. Remarkable Examples of the Ambidentate Character of Dimethyl Sulfoxide, Inorganic Chemistry, **2000**, 39, 1748 – 1754; b) Y.-F. Song, H. Abbas, C. Ritchie, N. McMillan, D.-L. Long, N. Gadegaard, L. Cronin, From polyoxometalate building blocks to polymers and materials: the silver connection, Journal of Materials Chemistry, **2007**, 17, 1903 – 1908.
154. Z. Fei, S. Busse, F. T. Edelmann, The first tantalasilsesquioxanes. Journal of the Chemical Society, Dalton Transactions, **2002**, 2587 – 2589.

155. R. Duchateau, T.W. Dijkstra, J.R. Severn, R.A. van Santen, I.V. Korobkov, Synthesis and characterization of tin containing polyhedral oligometallasilsesquioxanes (POMSS), Dalton Transactions, **2004**, 2677 – 2682.
156. R.T. Baker, K.C. Ott, W. Tumas, F. Liu, K.D. John, B.L. Scott, Synthesis and Characterization of Iron Silsesquioxane Phosphane Complexes, Angewandte Chemie International Edition, **2000**, 39, 3127 – 3130.
157. E.A. Quadrelli, J.E. Davies, B.F.G. Johnson, N. Feeder, Molecular insight into the non-innocence of a silica-support: the structure of a platinum – silsesquioxane derivative, Chemical Communications, **2000**, 1031 – 1032.
158. U.N. Nehete, G. Anantharaman, V. Chandrasekhar, R. Murugavel, M.G. Walawalkar, H.W. Roesky, D. Vidovic, J. Magull, K. Samwer, B. Sass, Polyhedral Ferrous and Ferric Siloxanes. Angewandte Chemie International Edition, **2004**, 43, 3832 – 3835.
159. a) E. Lucenti, F.J. Feher, J.W. Ziller, Synthesis and Characterization of Osmium-Containing Silsesquioxanes: High-Yield Routes to $\{\text{Os}_3(\text{CO})_{10}(\mu\text{-H})[(\mu\text{-O})\text{Si}_7\text{O}_{10}(c\text{-C}_6\text{H}_{11})_7]\}$ and the New Clusters $\{\text{Os}_3(\text{CO})_{10}(\mu\text{-H})[(\mu\text{-O})\text{Si}_7\text{O}_9(\text{OH})_2(c\text{-C}_6\text{H}_{11})_7]\}$, $\{[\text{Os}_3(\text{CO})_{10}(\mu\text{-H})]_2(\mu\text{-O})_2\text{Si}_7\text{O}_9(\text{OH})(c\text{-C}_6\text{H}_{11})_7\}$, $\{\text{Os}_3(\text{CO})_{10}(\mu\text{-H})[(\mu\text{-O})\text{Si}_8\text{O}_{11}(\text{OH})(c\text{-C}_6\text{H}_{11})_8]\}$, and $\{[\text{Os}_3(\text{CO})_{10}(\mu\text{-H})]_2(\mu\text{-O})_2\text{Si}_8\text{O}_{11}(c\text{-C}_6\text{H}_{11})_8\}$, Organometallics, **2007**, 26, 75 – 82; b) H. Wessel, C. Rennekamp, S.-D. Waezsada, H.W. Roesky, M.L. Montero, I. Usón, Isostructural Molecular Amino- and Oxoaminoalumosilicates, Organometallics, **1997**, 16, 3243 – 3245; b) F.T. Edelmann, S. Gießmann, A. Fischer, Silsesquioxane Chemistry, 4.: Silsesquioxane Complexes of Titanium(III) and Titanium(IV), Journal of Organometallic Chemistry, **2001**, 620, 80 – 89.
- 160 Y.N. Kononevich, A.A. Anisimov, A.A. Korlyukov, U.S. Tsareva, O.I. Shchegolikhina, A.M. Muzafarov, Synthesis and structures of novel tetra- and pentanuclear copper sandwich-like metallasiloxanes with pyridine ligands, Mendeleev Communications, **2017**, 27, 332 – 334.
161. H.M. Lindemann, M. Schneider, B. Neumann, H.-G. Stammer, A. Stammer, P. Jutzi, Synthesis and Reactivity of Core-Functionalized Polyhedral Titanasiloxanes, Organometallics **2002**, 21, 3009 – 3017.
162. V. Pashchenko, B. Brendel, B. Wolf, M. Lang, K. Lyssenko, O. Shchegolikhina, Y. Molodtsova, L. Zherlitsyna, N. Auner, F. Schütz, M. Kollar, P. Kopietz, N. Harrison, Synthesis, Structure and Magnetic Properties of a Novel Linear CuII-Trimer Complex, Berichte der deutschen chemischen Gesellschaft, **2005**, 22, 4617 – 4625.
163. V.P. Tretyakov, G.P. Zimtseva, E.S. Rudakov, A.V. Bogdanov, Unusual selectivity of alcohol oxidation by oxygen in aqueous alkaline solutions of copper phenanthroline complexes, Reaction Kinetics, Mechanisms and Catalysis, **1982**, 19, 263 – 266.
164. A.N. Bilyachenko, A.I. Yalymov, M.S. Dronova, A.A. Korlyukov, A.V. Vologzhanina, M.A. Es'kova, J. Long, J. Larionova, Y. Guari, P.V. Dorovatovskii, E.S. Shubina, M.M. Levitsky, Family of Polynuclear Nickel Cage-like Phenylsilsesquioxanes; Features of Periodic Networks and Magnetic Properties, Inorganic Chemistry, **2017**, 56, 12751 – 12763.
165. A.I. Yalymov, A.N. Bilyachenko, M.M. Levitsky, A.A. Korlyukov, V.N. Khrustalev, L.S. Shul'pina, P.V. Dorovatovskii, M.A. Es'kova, F. Lamaty, X. Bantreil, B. VILLEMEJEANNE, J. Martinez, E.S. Shubina, Y.N. Kozlov, G.B. Shul'pin, High Catalytic Activity of Heterometallic (Fe_6Na_7 and Fe_6Na_6) Cage Silsesquioxanes in Oxidations with Peroxides, Catalysts, **2017**, 7, 101 – 119.
166. a) H.C.L. Abbenhuis, R.A. van Santen, A.D. Burrows, M.T. Palmer, H. Kooijman, M. Lutz A. L. Spek, Synthesis and structural characterisation of platinum silsesquioxane complexes, Chemistry Communication, **1998**, 2627 – 2628; b) N. Mintcheva, M. Tanabe, K. Osakada, Synthesis and Characterization of Platinasilsesquioxane Complexes and Their Reaction with Arylboronic Acid, Organometallics, **2011**, 30, 187 – 190.
167. A. Lee, J. Xiao, F. J. Feher, New Approach in the Synthesis of Hybrid Polymers Grafted with Polyhedral Oligomeric Silsesquioxane and Their Physical and Viscoelastic Properties, Macromolecules, **2005**, 38, 438 – 444.

168. G. Anantharaman, H. W. Roesky, H.-G. Schmidt, M. Noltemeyer, J. Pinkas, Synthesis and X-ray Crystal Structure of $[(\text{THF})\text{Zn}(\text{O}_2(\text{OH})\text{SiR})_4]$ ($\text{R} = (2,6\text{-}i\text{-Pr}_2\text{C}_6\text{H}_3)\text{N}(\text{SiMe}_3)$): Enroute to Larger Aggregates, *Inorganic Chemistry*, **2003**, 42, 970 – 973.
169. U.N. Nehete, G. Anantharaman, V. Chandrasekhar, R. Murugavel, M.G. Walawalkar, H.W. Roesky, D. Vidovic, J. Magull, K. Samwer, B. Sass, Polyhedral ferrous and ferric siloxanes, *Angewandte Chemie International Edition*, **2004**, 116, 3920 – 3923.
170. A.N. Bilyachenko, M.S. Dronova, A.A. Korlyukov, M.M. Levitsky, M.Yu. Antipin, B.G. Zavin, Cage-like manganesephenylsiloxane with an unusual structure, *Russian Chemical Bulletin*, **2011**, 60, 1762 – 1765.
171. M.M. Levitsky, A.N. Bilyachenko, E.S. Shubina. Cagelike metallagermanates and metallagermoxanes: Synthesis, structures and functional properties, *Coordination Chemistry Reviews*, **2019**, 386, 209 – 239.
172. M.T. Pope, A. Müller, *Polyoxometalate Chemistry: An Old Field with New Dimensions in Several Disciplines*, *Angewandte Chemie International Edition*, **1991**, 30, 34 – 48.
173. H. Furukawa, K.E. Cordova, M. O’Keeffe, O. M. Yaghi, The Chemistry and Applications of Metal-Organic Frameworks, *Science*, **2013**, 341, 1230444 – 1230459.
174. H. He, G.-J. Cao, S.-T. Z. Heng, G.-Y. Yang, Lanthanide Germanate Cluster Organic Frameworks Constructed from $\{\text{Ln}_8\text{Ge}_{12}\}$ or $\{\text{Ln}_{11}\text{Ge}_{12}\}$ Cage Cluster Building Blocks, *Journal of the American Chemical Society*, **2009**, 131, 15588 – 15589.
175. A.N. Kulakova, E.E. Sedykh, M.M. Levitsky, P.V. Dorovatovskii, V.N. Khrustalev, L.S. Shul’pina, E.S. Shubina, Y.N. Kozlov, N.S. Ikonnikov, A.N. Bilyachenko, G.B. Shul’pin, The first tris-heteroleptic copper cage, ligated by germsesquioxanes, 2,20-bipyridines and 3,5-dimethylpyrazolates. Synthesis, structure and unique catalytic activity in oxidation of alkanes and alcohols with peroxides, *Journal of Organometallic Chemistry*, **2019**, 899, 120911 – 120918.
176. A.P. Sadimenko, S.S. Basson, *Organometallic complexes of heterocycles II. Complexes of pyrazoles*, *Coordination Chemistry Reviews*, **1996**, 147, 247 – 297.
177. a) A. Shilov, E.G. Shul’pin, Activation of the C–H bond by metal complexes, *Russian Chemical Reviews*, **1990**, 59, 853 – 867; б) A.M. Kirillov, G.B. Shul’pin, Pyrazinecarboxylic acid and analogs: Highly efficient co-catalysts in the metal-complex-catalyzed oxidation of organic compounds, *Coordination Chemistry Reviews*, **2013**, 257, 732 – 754.
178. a) F. d’Acunzo, P. Baiocco, M. Fabbrini, C. Galli, P. Gentili, A Mechanistic Survey of the Oxidation of Alcohols and Ethers with the Enzyme Laccase and Its Mediation by TEMPO, *European Journal of Organic Chemistry*, **2002**, 24, 4195 – 4201; б) L. Que Jr., W. B. Tolman, *Angewandte Chemie International Edition*, **2002**, 41, 1114 – 1137; в) C. Gerdemann, C. Eicken, B. Krebs, The Crystal Structure of Catechol Oxidase: New Insight into the Function of Type-3 Copper Proteins, *Accounts of Chemical Research*, **2002**, 35, 183 – 191.
179. a) J.A.R. Salvador, J.H. Clark, The allylic oxidation of unsaturated steroids by tert-butyl hydroperoxide using surface functionalised silica supported metal catalysts, *Green Chemistry*, **2002**, 4, 352 – 356; б) J. Le Bras, J. Muzart, Selective copper-catalyzed allylic oxidations using a 1/1 ratio of cycloalkene and tert-butylperbenzoate, *Journal of Molecular Catalysis A: Chemical*, **2002**, 185, 113 – 117; в) G.B. Shul’pin, J. Gradinaru, Y.N. Kozlov, Alkane hydroperoxidation with peroxides catalysed by copper complexes, *Organic and Biomolecular Chemistry*, **2003**, 1, 3611 – 3617; г) E.A. Lewis, W.B. Tolman, Reactivity of Dioxygen–Copper Systems, *Chemical Reviews*, **2004**, 104, 1047 – 1076.
180. G.B. Shul’pin, Metal-catalyzed hydrocarbon oxidations, *Comptes Rendus Chimie*, **2003**, 6, 163 – 178.
181. A.E. Shilov, G.B. Shul’pin, Activation of C–H Bonds by Metal Complexes. *Chemistry Reviews*, **1997**, 97, 2879 – 2932.

182. S. Hazra, L.M.D.R.S. Martins, M.F.C. Guedes da Silva, A.J.L. Pombeiro, Sulfonated Schiff base dimeric and polymeric copper(II) complexes: Temperature dependent synthesis, crystal structure and catalytic alcohol oxidation studies, *Inorganic Chimica Acta*, **2017**, 455, 549 – 556.
183. a) A.E. Shilov, G.B. Shul'pin, Activation and Catalytic Reactions of Saturated Hydrocarbons in the Presence of Metal Complexes, Kluwer Academic Publishers: New York, **2002**, pp 548, ISBN 9780792361015; б) E.T. Denisov, I.B. Afanasev, Oxidation and Antioxidants in Organic Chemistry and Biology; Taylor & Francis: Boca Raton, FL, **2005**, pp. 1024, ISBN 9780824753566; в) D.S. Nesterov, E.N. Chygorin, V.N. Kokozay, V.V. Bon, R. Boca, Y.N. Kozlov, L.S. Shulpina, J. Jezierska, A. Ozarowski, A.J.L. Pombeiro, G.B. Shul'pin, Heterometallic Co^{II}₄Fe^{III}₂ Schiff Base Complex: Structure, Electron Paramagnetic Resonance, and Alkane Oxidation Catalytic Activity. *Inorganic Chemistry*, **2012**, 51, 9110 – 9122.
184. V.A. Igonin, S.V. Lindeman, Yu.T. Struchkov, O.I. Shchegolikhina, A.A. Zhdanov, Polymetalloorganosiloxanates - a novel class of the organosilicon metal complexes, *Acta Crystallographica Section A: Foundations of Crystallography*, **1993**, 49, 207 – 207.
185. a) Y.-F. Song, H. Abbas, C. Ritchie, N. McMillian, D.-L. Long, N. Gadegaard, L. Cronin, From polyoxometalate building blocks to polymers and materials: the silver connection, *Journal of Materials Chemistry*, **2007**, 17, 1903 – 1908; б) T. Hasell, J.L. Culshaw, S.Y. Chong, M. Schmidtman, M.A. Little, K.E. Jelfs, E.O. Pyzer-Knapp, H. Shepherd, D.J. Adams, G.M. Day, A.I. Cooper, Controlling the Crystallization of Porous Organic Cages: Molecular Analogs of Isorecticular Frameworks Using Shape-Specific Directing Solvents, *Journal of the American Chemical Society*, **2014**, 136, 1438 – 1448.
186. M.S. Dronova, PhD thesis, Moscow, **2013**.
187. M.M. Levitsky, A.N. Bilyachenko, Modern concepts and methods in the chemistry of polyhedral metallasiloxanes, *Coordination Chemistry Reviews*, **2016**, 306, 235 – 269.
188. M.M. Levitsky, B.G. Zavin, A.N. Bilyachenko, Chemistry of metallasiloxanes. Current trends and new concepts, *Russian Chemical Reviews*, **2007**, 76, 847 – 866.
189. M.-L. Wind, B. Braun-Cula, F. Schax, C. Herwig, C. Limberg, A Polysiloxide Complex with two Chromium(III) η²-Superoxo Moieties, *Israel Journal of Chemistry*, **2019**, 59, 1 – 5.
190. G.S. Astakhov, M.M. Levitsky, A.A. Korlyukov, L.S. Shul'pina, E.S. Shubina, N.S. Ikonnikov, A.V. Vologzhanina, A.N. Bilyachenko, P.V. Dorovatovskii, Y.N. Kozlov, G.B. Shul'pin, New Cu₄Na₄- and Cu₅-Based Phenylsilsesquioxanes. Synthesis via Complexation with 1,10-Phenanthroline, Structures and High Catalytic Activity in Alkane Oxidations with Peroxides in Acetonitrile, *Catalysts*, **2019**, 9, 701 – 719.
191. A.A. Korlyukov, A.V. Vologzhanina, M.I. Buzin, N.V. Sergienko, B.G. Zavin, A.M. Muzafarov, Cu(II)-Silsesquioxanes as Secondary Building Units for Construction of Coordination Polymers: A Case Study of Cesium-Containing Compounds, *Crystal Growth & Design*, **2016**, 16, 1968 – 1977.
192. M.S. Dronova, A.N. Bilyachenko, A.D. Kirilin, E.S. Shubina, M.M. Levitsky, Quantum-chemical analysis of the structure formation of framework organosiloxanes and organometallic siloxanes, *Tonkiye khimicheskiye tekhnologii*, **2013**, 8, 49 – 54.
193. B. Bleaney, K.D. Bowers, Anomalous Paramagnetism of Copper Acetate. *Proceedings of the Royal Society of London. Series A. Mathematical and Physical Sciences*, **1952**, 214, 451 – 465.
194. D.L. Lewis, K.T. McGregor, W.E. Hatfield, D.J. Hodgson, Preparation and structural and magnetic characterization of beta-di-u-hydroxo-bis [2-(2-dimethylaminoethyl)-pyridine]dicopper(II) perchlorate, *Inorganic Chemistry*, **1974**, 13, 1013 – 1019.
- 195 V.H. Crawford, H.W. Richardson, J.R. Wasson, D.J. Hodgson, W.E. Hatfield, Relation between the singlet-triplet splitting and the copper-oxygen-copper bridge angle in hydroxo-bridged copper dimers, *Inorganic Chemistry*, **1976**, 15, 2107 – 2110.
196. A.N. Bilyachenko, M.M. Levitsky, A.A. Korlyukov, V.N. Khrustalev, Y.V. Zubavichus, L.S. Shul'pina, E.S. Shubina, A.V. Vologzhanina, G.B. Shul'pin, Heptanuclear Cage Cu^{II}-Silsesquioxanes:

- Synthesis, Structure and Catalytic Activity, *European Journal of Inorganic Chemistry*, **2018**, 22, 2505 – 2511.
197. G.S. Astakhov, A.N. Bilyachenko, M.M. Levitsky, A.A. Korlyukov, Y.V. Zubavichus, P.V. Dorovatovskii, V.N. Khrustalev, A.V. Vologzhanina, E.S. Shubina, Tridecanuclear $\text{Cu}^{\text{II}}_{11}\text{Na}_2$ Cage-like Silsesquioxanes, *Crystal Growth & Design*, **2018**, 18, 5377 – 5384.
198. a) R. Sakamoto, S. Katagiri, H. Maeda, H. Nishihara, Bis(terpyridine) metal complex wires: Excellent long-range electron transfer ability and controllable intrawire redox conduction on silicon electrode, *Coordination Chemistry Reviews*, **2013**, 257, 1493 – 1506; b) G. Schwarz, I. Haßlauer, D. G. Kurth, From terpyridine-based assemblies to metallo-supramolecular polyelectrolytes (MEPEs), *Advances in Colloid and Interface Science*, **2014**, 207, 107 – 120.
199. a) Y.K. Gun'ko, R. Reilly, F.T. Edelmann, H.-G. Schmidt, The First Ce^{IV} Metallasilsesquioxane Complex: $[\text{Ce}\{(c\text{-C}_6\text{H}_{11})_8\text{Si}_8\text{O}_{13}\}_2(\text{py})_3]$, *Angewandte Chemie International Edition*, **2001**, 40, 1279 – 1281; b) S. Gießmann, V. Lorenz, P. Liebing, L. Hilfert, A. Fischera, Frank T. Edelmann, Synthesis and structural study of new metallasilsesquioxanes of potassium and uranium, *Dalton Transactions*, **2017**, 46, 2415 – 2419.
200. E.P. Tishkova, L.A. Kudryavtseva, A.E. Arbuzov, Reactions of esters of tetracoordinated phosphorus acids with nucleophilic reagents in highly organized media, *Russian Chemical Bulletin*, **1996**, 45, 284 – 298.
201. A.N. Kulakova, A.N. Bilyachenko, A.A. Korlyukov, J. Long, M.M. Levitsky, E.S. Shubina, Y. Guari, J. Larionova, New Ni_4Na_2 -Phenylgermsesquioxane Architecture: Synthesis, Structure and Slow Dynamic Behaviour, *Dalton Transactions*, **2018**, 47, 6893 – 6897.
202. S. Banerjee, M. Nandy, S. Sen, S. Mandal, G.M. Rosair, A.M.Z. Slawin, C.J. Gomez Garcia, J.M. Clemente-Juan, E. Zangrando, N. Guidolin, S. Mitra, Isolation of four new $\text{Co}^{\text{II}}/\text{Co}^{\text{III}}$ and Ni^{II} complexes with a pentadentate Schiff base ligand: syntheses, structural descriptions and magnetic studies, *Dalton Transaction*, **2011**, 40, 1652 – 1661.
203. a) D.N. Woodruff, R.E.P. Winpenny, R.A. Layfield, Lanthanide Single-Molecule Magnets, *Chemical Reviews*, **2013**, 113, 5110 – 5148; b) R.A. Layfield, M. Murugesu, Lanthanides and actinides in molecular magnetism, John Wiley & Sons, **2015**, pp. 336, ISBN 9783527335268.
204. J.-C. G. Bunzli, V.K. Pecharsky, Handbook on the Physics and Chemistry of Rare Earths: Including Actinides, Elsevier, **2016**, pp. 141, ISBN 9780471968856.
205. H. Masakazu, T. Shinsuke, Y. Takashi, U. Keiji, U. Masafumi, M. Hideyuki, Synthesis and Structures of the First Titanium(IV) Complexes with Cyclic Tetrasiloxide Ligands: Incomplete and Complete Cage Titanosiloxanes, *Chemistry Letters*, **2005**, 34, 1542 – 1543.
206. C.Y. Chow, H. Bolvin, V.E. Campbell, R. Guillot, J.W. Kampf, W. Wernsdorfer, F. Gendron, J. Autschbach, V.L. Pecoraro, T. Mallah, Assessing the exchange coupling in binuclear lanthanide(III) complexes and the slow relaxation of the magnetization in the antiferromagnetically coupled Dy_2 derivative, *Chemical Science*, **2015**, 6, 4148 – 4159.
207. a) K. Binnemans, Lanthanides and Actinides in Ionic Liquids, *Chemical Reviews*, **2007**, 107, 2592 – 2614; b) P. Hänninen, H. Härmä, Berlin Heidelberg: Berlin, Heidelberg, Springer Science & Business Media, **2011**, 7, 1 – 45.
208. W.T. Carnall, P.R. Fields, K. Rajnak, Electronic Energy Levels of the Trivalent Lanthanide Aquo Ions. III. Tb^{3+} , *The Journal of Chemical Physics*, **1968**, 49, 4450 – 4455.
209. S.V. Eliseeva, J.-C.G. Bunzli, Lanthanide luminescence for functional materials and biosciences, *Chemical Society Reviews*, **2010**, 39, 189 – 227.